# 8. ANALYSIS OF DESIGN EVENTS

In previous chapters of this SAR, the features of the standardized NUHOMS® system which are important to safety have been identified and discussed. The purpose of this chapter is to present the engineering analyses for normal and off-normal operating conditions, and to establish and qualify the system for a range of credible and hypothetical accidents. As stated in Chapter 1, the analyses presented in this section are applicable to the standard length 24P and 52B canisters. An evaluation of the long cavity 24P canister, for the same design criteria, is provided in Appendix H and J. Appendices K and L provide the evaluation for the NUHOMS®-61BT DSC and -24PT2 DSC, respectively. Evaluations for other canisters and modules may be included as additional appendices at a later time.

In accordance with NRC Regulatory Guide 3.48 (8.1), the design events identified by ANSI/ANS 57.9-1984, (8.2) form the basis for the accident analyses performed for the standardized NUHOMS® system. Four categories of design events are defined. Design event Types I and II cover normal and off-normal events and are addressed in Section 8.1. Design event Types III and IV cover a range of postulated accident events and are addressed in Section 8.2. These events provide a means of establishing that the NUHOMS® system design satisfies the applicable operational and safety acceptance criteria as delineated herein.

It is important to note that, given the generic nature of this SAR, the majority of the analyses presented throughout this chapter are based on bounding conservative assumptions and methodologies, with the objective of establishing upper bound values for the responses of the primary components and structures of the standardized NUHOMS® system for the design basis events. Because of the conservative approach adopted herein, the reported temperatures and stresses in this chapter envelope the actual temperatures or states of stress for the various operating and postulated accident conditions. More rigorous and detailed analyses and/or more realistic assumptions and loading conditions would result in temperatures and states of stress which are significantly lower than the reported values.

## 8.1 Normal and Off-Normal Operations

Normal operating design conditions consist of a set of events that occur regularly, or frequently, in the course of normal operation of the NUHOMS® system. These normal operating conditions are addressed in Section 8.1.1. Off-normal operating design conditions are events that could occur with moderate frequency, possibly once during any calendar year of operation. These off-normal operating conditions are addressed in Section 8.1.2. The thermal-hydraulic, structural, and radiological analyses associated with these events are presented in the sections which follow.

## 8.1.1 Normal Operation Structural Analysis

Table 8.1-1 shows the normal operating loads for which the NUHOMS® safety-related components are designed. The table also lists the individual NUHOMS® components which are affected by each loading. The magnitude and characteristics of each load are described in Section 8.1.1.1.

The method of analysis and the analytical results for each load are described in Sections 8.1.1.2 through 8.1.1.9. The mechanical properties of materials employed in the structural analysis of the NUHOMS® system components are presented in Table 8.1-3.

### 8.1.1.1 Normal Operating Loads

The normal operating loads for the NUHOMS® system components are:

1. Dead Weight Loads
2. Design Basis Internal and External Pressure Loads
3. Design Basis Thermal Loads
4. Operational Handling Loads
5. Design Basis Live Loads

These loads are described in detail in the following paragraphs.

#### A. Dead Weight Loads

Table 8.1-4 and Table 8.1-5 show the weights of various components of the NUHOMS® system. The dead weight of the component materials is determined based on nominal component dimensions.

A density value of 0.283 pound per cubic inch for carbon steel, 0.285 pound per cubic inch for stainless steel, 0.408 pound per cubic inch for lead shielding, and 0.064 pound per cubic inch for solid neutron shielding material are used in the dead weight calculations.

A nominal concrete density of 140 to 145 pounds per cubic foot is conservatively selected as a design basis for the shielding and thermal evaluations. A maximum nominal density of 150 pounds per cubic foot is conservatively assumed for the structural evaluation of the HSM.

B. Design Basis Internal and External Pressure

The maximum internal pressures for the NUHOMS®-24P DSC for normal, off-normal, and accident operating conditions are shown in Table 8.1-6. The maximum DSC internal pressure during normal, off-normal and accident conditions is based on failure of 1%, 10%, and 100% of the fuel rods, respectively. 100% of the fuel rod fill gas and 30% of the fission gases are assumed to be released in the DSC cavity from the failed fuel rods. The DSC internal pressure for normal operating conditions is a maximum of 21.7 psia (7.0 psig) for the seasonal normal operating temperature range of 0°F to 100°F. This pressure corresponds to the DSC in the transfer cask at 100°F ambient condition which bounds the DSC in the HSM storage case at 100°F ambient. The DSC internal pressure for off-normal operating conditions is a maximum of 24.8 psia (10.1 psig) over a seasonal off-normal temperature range of -40°F to 125°F. This pressure corresponds to the DSC in the transfer cask at 100°F ambient condition which bounds the DSC in the HSM storage case or in the transfer cask (with sunshade protection) at the maximum ambient temperature of 125°F. The transfer cask is required to have a sunshade for solar insolation protection whenever the ambient temperature exceeds 100°F. The maximum DSC internal pressure for postulated accident conditions is a maximum of 73.4 psia (58.7 psig) over a seasonal temperature range of -40°F to 125°F. The bounding design basis accident pressure is determined by assuming cladding failure in 100% of the spent fuel rods stored in the DSC. The cladding failure is assumed to release all the fuel rod fill gas and 30% of the fission gas generated in PWR fuel assemblies conservatively irradiated to 50,000 MWD/MTU (72-1004 CoC only allows storage of assemblies up to 45,000 MWD/MTU). This postulated worst case condition is included in the design basis for the NUHOMS®-24P DSC as a conservative means of providing overpressure protection for the DSC containment boundary. For normal operating conditions, the gas inside the DSC is assumed to be brought to thermodynamic equilibrium with the maximum normal ambient temperature of 100°F. These calculations are repeated for the NUHOMS®-52B DSC with the results listed in Table 8.1-7. Similar assumptions are made for off-normal and accident conditions to determine the DSC internal pressure occurring with a gas temperature at an extreme ambient temperature of 125°F. The effects of postulated accident pressures are described in Section 8.2. A value of 11 psig is used as the design pressure in the normal and off-normal stress analyses (Service Levels A and B). A conservative value of 41 psig is used in the Service Level C stress analyses. The calculated pressures for this level C condition are equal to the maximum off-normal pressures presented in Table 8.1-6 and Table 8.1-7. A Service Level D case is considered, in which it is postulated that the maximum ambient temperature of 125°F is reached in conjunction with 100% failure of the fuel cladding, and the vents in the HSM are blocked. The pressures calculated for this condition are equal to the maximum accident pressures presented in Table 8.1-6 and Table 8.1-7.

The limiting external pressure load on the DSC shell include hydrostatic pressure of water in the annulus between the DSC and the transfer cask plus a pressure of 14.7 psi during the vacuum drying step of the DSC fuel loading operations.

Maximum 24P DSC internal pressures for Normal, Off-Normal and Accident conditions when storing fuel with BPRAs are presented in Appendix J.

C. Design Basis Thermal Loads

The NUHOMS® transfer cask, DSC, and HSM are subjected to the thermal expansion loads associated with normal operating conditions. The range of average daily ambient temperatures used for the design of the transfer cask, DSC, and HSM for normal operating conditions is 0°F to 100°F. The normal operating seasonal average daily ambient temperature fluctuates from 0°F minimum (winter) to 100°F maximum (summer) and is conservatively assumed to occur for a sufficient duration to establish steady state conditions for the transfer cask, DSC and HSM. These minimum and maximum steady-state long-term ambient design temperatures, envelop the 24 hour average seasonal ambient temperature at any location within the contiguous United States (8.46).

The long-term average normal ambient temperature for the 50 year design life of the system is assumed to be 70°F. This base case average ambient temperature bounds practically all reactor sites within the United States (8.27). Exceptions should be addressed on site specific basis by the licensee as necessary.

The range of ambient temperature cases analyzed are further defined in Section 8.1.3. The resulting temperature distributions in the HSM, DSC and transfer cask are determined by performing thermal analyses for these ambient conditions. The thermal analyses, described in Section 8.1.3, provide temperature distributions for the HSM, DSC, and transfer cask such as those shown in Table 8.1-17, Table 8.1-22b through Table 8.1-29a and Figure 8.1-1 through Figure 8.1-12. These temperature distributions are developed for the range of normal ambient temperatures specified above and are applicable to any size HSM array. The corresponding HSM structural analysis results for thermal loads are applicable to HSM arrays ranging in size from a single stand-alone module to a single row of side-by-side modules or a double row of back-to-back side-by-side modules of unrestricted length.

Figure 8.1-1 and Figure 8.1-3 show the temperature distribution around the circumference of the DSC (when in storage in an HSM) for the base case 70°F lifetime average ambient temperature. The maximum temperatures of the centermost fuel rods for each fuel assembly for the DSC are also shown. The analysis and HEATING7 (8.5) results for the 70°F ambient temperature base case are discussed in Section 8.1.3. The DSC and fuel assembly temperature distributions during storage in an HSM are also evaluated for the minimum average daily (winter) and maximum average daily (summer) ambient conditions. The resulting temperature distribution for the 100°F ambient temperature case are shown in Figure 8.1-2 and Figure 8.1-4. The fuel assembly temperatures for the minimum average daily (winter) conditions are enveloped by this case and are, therefore, not evaluated further.

Figure 8.1-5 and Figure 8.1-6 show the temperature distribution in a spacer disk located mid-length along the axis of the DSC for the 100°F ambient temperature case. This temperature distribution is determined by averaging the temperatures from a two-dimensional HEATING7 calculation of the heat transfer across a spacer disk (steel assumed to be between the guide sleeves and DSC shell) and the higher temperatures of the helium on either side of the spacer

disk (from the analysis results with helium assumed to be between the guide sleeves and the DSC shell). This accounts for the effects of helium heating the surfaces of the spacer disk.

Figure 8.1-7 through Figure 8.1-10 show the temperatures at various locations in the 24P and 52B HSMs for the 70°F and 100°F normal operating ambient temperature cases, respectively. The temperature distributions shown are derived from two dimensional HEATING7 analyses described in Section 8.1.3.

The maximum calculated temperatures for the various structural sections of the HSM for normal operating conditions are summarized in Table 8.1-24 and Table 8.1-25. A more detailed tabulation of the HSM thermal results used for the structural design of the HSM is shown in Table 8.1-17. The HSM reinforced concrete design is controlled by these thermal gradients.

The effect of DSCs being emplaced at varying locations throughout an HSM array are represented by the single module analysis presented herein since the prefabricated HSMs which make up HSM arrays are free-standing units. The appropriate peak temperatures and thermal gradients from Table 8.1-17 are applied to the HSM analytical model shown in Figure 8.1-21 and the resulting forces and moments calculated.

Figure 8.1-11 shows the temperature distribution in the NUHOMS® standardized transfer cask during transfer of a loaded DSC for normal operating conditions. This distribution conservatively assumes a constant 100°F ambient temperature with solar heating of the transfer cask outer surface. Similarly, Figure 8.1-12 shows the transfer cask temperature distribution with a constant ambient temperature of 0°F. Solar heat loads are conservatively neglected for this case. The DSC is assumed to remain in the transfer cask for a sufficient length of time to reach steady state conditions. Tables 8.1-28 and 8.1-29 present a summary of the thermal analysis results for the NUHOMS® -24P and -52B DSCs within the standardized cask. Similar analyses were performed for a DSC that is inside the OS197 transfer cask. The temperatures at key locations are shown in Table 8.1-29a.

The temperature distributions derived from the three normal operating cases (0°F, 70°F, 100°F) are considered in the structural analysis of the DSC, HSM and transfer cask discussed in Sections 8.1.1.2 through 8.1.1.9. The temperature distributions for each component are used to determine the effects of thermal stresses and thermal cycling on the NUHOMS® components. These results are also used to evaluate the effects of creep on the HSM reinforced concrete.

The thermophysical properties of materials used in the thermal and stress analyses of the NUHOMS® system components are presented in Table 8.1-8 and Table 8.1-9.

D. Operational Handling Loads

There are two categories of handling loads: (1) inertial loads associated with on-site handling and transporting the DSC between the fuel handling/loading area and the HSM, and (2) loads associated with loading the DSC into (and unloading the DSC from) the HSM.

Loads associated with handling the DSC are ± 1.0g in the axial, transverse and vertical directions applied separately, as well as ± 0.5g in the axial, transverse, and vertical directions applied simultaneously.

The most significant operational loading condition for the NUHOMS® system components is sliding of the DSC from/to the transfer cask into/out of the HSM during the DSC insertion/extraction process. Sliding is achieved by the push/pull forces induced by the hydraulic ram system. These forces are applied to the grapple ring assembly which is an integral part of the DSC bottom end assembly. The forces induced by the ram system are reacted by friction forces which develop between the sliding surfaces of the DSC, the transfer cask, and HSM support rails.

Based on the surface finish and the contact angle of the DSC support rails inside the HSM described in Chapter 4, a bounding coefficient of friction is conservatively assumed to be 0.25. Therefore, the nominal ram load required to slide the DSC under normal operating conditions is approximately 29,580 lbs, calculated as follows:

$$P = \frac{0.25\,W}{\cos\theta} = 0.29\,W = 0.29(102{,}000\text{ lbs}) = 29{,}580\text{ lbs} \qquad (8.1\text{-}1)$$

Where:

P = Push/Pull Load

W = Loaded DSC Weight ≈ 102,000 lbs

θ = 30 degrees, Angle of the Canister Support Rail

However, the DSC bottom cover plate and grapple ring assembly are conservatively designed to withstand a normal operating insertion force equal to 80,000 pounds and a normal operating extraction force equal to 60,000 pounds. The fully loaded DSC weight is conservatively assumed to be 102,000 pounds. To insure retrievability for a postulated jammed DSC condition, the ram is sized with a capacity for an enveloping load of 80,000 pounds, as described in Section 8.1.2. These loads also bound the friction forces postulated to develop between the sliding surfaces of the DSC and transfer cask during worst case off-normal conditions.

E. Design Basis Live Loads

As discussed in Section 3.2.4, a live load of 200 pounds per square foot is conservatively selected to envelope all postulated live loads acting on the HSM, including the effects of snow and ice. Live loads which may act on the transfer cask are negligible, as discussed in Section 3.2.4.

8.1.1.2 Dry Shielded Canister Analysis

The Standardized NUHOMS®-24P and NUHOMS®-52B DSC shell assemblies are analyzed for the normal, off-normal and postulated accident load conditions using two basic ANSYS (8.48) finite element models: a top-end half-length model of the DSC shell assembly and a bottom-end half-length model of the DSC shell assembly. A 90° (one-quarter) cross sectional segment of the DSC is used to analyze axisymmetric loads, and a 180° (one-half) cross sectional segment is used to analyze non-axisymmetric loads. The 24P and 52B DSC shell assemblies include the DSC shell, top and bottom outer and inner cover plates, top and bottom shield plugs, grapple ring and grapple ring support, support ring, and all the associated welds. These components and their interfaces are modeled using 3-D solid and gap elements. Typical models of the DSC shell assembly are shown in Figure 8.1-14a and Figure 8.1-14b, for the top and bottom halves of the DSC shell assembly, respectively.

The above described models are used to evaluate stresses in the NUHOMS®-24P and NUHOMS®-52B DSCs due to:

1. Dead Weight

2. Design Basis Normal Operating Internal and External Pressure Loads

3. Normal Operating Thermal Loads

4. Normal Operation Handling Loads

The methodology used to evaluate the effects of these normal loads is addressed in the following paragraphs. Table 8.1-10 and Table 8.1-11 summarize the resulting stresses for normal operating loads.

A. DSC Dead Load Analysis

Dead load analyses of the DSC are performed for both vertical and horizontal positions of the DSC. In the vertical position, the DSC shell supports its own empty weight and the entire weight of the top end components. When inside the Transfer Cask, the weight of the fuel and the bottom end components is transferred to the Transfer Cask by bearing through the inner cover plate, shield plug and outer bottom cover plate. When in the horizontal position, the DSC is in the Transfer Cask or in the HSM. In this position, the DSC shell assembly end components and the internal basket assembly bear against the DSC shell. The DSC shell assembly is supported by two cask rails located at ± 18.5° (when in the Transfer Cask) and ± 30° (when in the HSM) from the bottom centerline of the DSC. This is shown schematically in Figure 8.1-13.

Dead load stresses are obtained from static analyses performed using the ANSYS finite element models described above. Both, the top-end half and bottom-end half models are analyzed for a

1g load, using the appropriate finite element model and boundary conditions, for horizontal and vertical configurations. For the horizontal dead load analyses, the DSC is conservatively assumed to be supported on one rail. In addition, the fuel-loaded spacer discs of the basket assembly bear on the inner surface of the DSC shell. DSC shell stresses in the region of the spacer discs resulting from the bearing load and from local deformations at the cask rails are evaluated using the ANSYS model described in Section 8.1.1.3. The DSC shell assembly components are evaluated for primary membrane and membrane plus bending stress and for primary plus secondary stress. Enveloping maximum stress intensities are summarized in Table 8.1-10 for the NUHOMS®-24P DSC and Table 8.1-11 for the NUHOMS®-52B DSC.

B. DSC Normal Operating Design Basis Pressure Analysis

The DSC shell assembly analytical models shown in Figure 8.1-14a and Figure 8.1-14b are used for the normal operating design pressure analyses. The design basis internal pressures are shown in Table 8.1-6 and Table 8.1-7. A bounding internal pressure of 10 psig is conservatively applied to the analytical model as uniform internal pressure loadings and the DSC stresses calculated. Two loading distribution cases are considered; one with the inner cover plates pressurized and one with the outer cover plates pressurized. The inner pressure boundary, defined by the DSC shell, the inner bottom cover plate, the inner top cover plate and the associated welds, is evaluated for the 10 psig normal operating internal pressure. The inner top cover plate is also evaluated without the outer top cover plate in place for the draining blowdown pressure of 20 psig. This load case controls over the helium leak test pressure of 12 psig. A strongback is installed to support the inner top cover plate for this pressure load case. A separate ANSYS (8.48) finite element model, which incorporates the strongback structure, is used for these analyses. The resulting maximum stress intensities are reported in Table 8.1-10 and Table 8.1-11.

C. DSC Normal Operating Thermal Stress Analysis

The thermal analysis of the DSC for the various conditions, as presented in Section 8.1.3 provide temperature distributions along the axial, tangential, and radial directions of the DSC, along with maximum and minimum DSC component temperatures. These temperature distributions are imposed onto the DSC shell assembly ANSYS stress analysis models shown in Figure 8.1-14a and Figure 8.1-14b for thermal stress evaluation. Maximum component temperatures are used to determine material properties and stress allowables used in the stress analysis. DSC shell assembly materials are all SA 240 Type 304 stainless steel with the exception of the shield plugs, which are made of A-36 carbon steel. However, because these dissimilar materials are not mechanically fastened, allowing free differential thermal growth, the thermal stresses in the DSC shell components are due entirely to thermal gradients. The results of the thermal analysis show that for the range of normal operating ambient temperature conditions, the thermal gradients are primarily along the axial and tangential directions of the DSC and that no significant thermal gradients exist through the wall of the DSC. Stresses resulting from thermal gradients are classified as secondary stresses and are evaluated for Service Level A and B conditions. Maximum stress intensities resulting from the thermal stress analyses are summarized in Table 8.1-10 for the NUHOMS®-24P DSC and Table 8.1-11 for the NUHOMS®-52B DSC.

The gaps between the support rods and the DSC cavity and between the spacer discs and the DSC shell are evaluated for possible interference due to thermal expansion. There is sufficient space provided in the axial direction between the internal basket assembly and the inner surfaces of the DSC shell assembly for free thermal expansion. Similarly, sufficient radial gap is provided between the spacer disks and inside of the DSC shell to permit free thermal expansion. This design feature also acts to minimize the effects of thermal cycling and fatigue on the DSC.

D. DSC Operational Handling Load Analysis

To load the DSC into the HSM, the DSC is pushed out of the transfer cask using a hydraulic ram. The applied force from the hydraulic ram, specified in Section 8.1.1.1, is applied to the center of the DSC outer bottom cover plate at the center of the grapple ring assembly. The ANSYS finite element model shown in Figure 8.1-14b is used to calculate the stresses in the DSC shell assembly. In the analysis, the ram load is applied to the cover plate in the form of two arcs, assuming that the load is concentrated at the barrel diameter, excluding the cutouts for extension of the grapple arms.

To unload the HSM, the DSC is pulled using grapples which fit into the grapple ring. For analysis of grapple pull loading, the 180° ANSYS finite element model of the bottom half DSC assembly is refined in the area of the grapple assembly and outer cover plate, as shown in Figure 8.1-15. The stresses in the DSC outer bottom cover plate and grapple ring resulting from the DSC retrieval load distribution are evaluated using the model shown in Figure 8.1-15. The load is applied to the grapple ring plate nodes corresponding to the contact area between the ram grapple arms and the grapple ring plate. Several submodels of the DSC grapple assembly were analyzed to identify primary stresses alone and in combination with secondary stresses under DSC unloading operations.

The controlling stresses from these analyses are tabulated in Table 8.1-10 and Table 8.1-11.

E. Evaluation of the Results

The maximum calculated DSC shell stresses induced by normal operating load conditions are shown in Table 8.1-10 and Table 8.1-11. The calculated stresses for each load case are combined in accordance with the load combinations presented in Table 3.2-6. The resulting stresses for the controlling load combinations are reported in Section 8.2.10 with the ASME Code allowable stresses.

8.1.1.3 DSC Internal Basket Analysis

The DSC internal basket assembly can be utilized to store various types of spent fuel assemblies. As discussed in Section 3.1.1, the physical parameters selected for this generic analysis conservatively envelope those of other assembly types. The weight of each spent fuel assembly is transferred to the spacer disks by the guide sleeves for PWR fuel and by the channels for BWR fuel for any load applied perpendicular to the DSC axis. The support rods do not bear any

normal operation loads during storage in the HSM except for their own weights. The stresses induced by the weights of these components are evaluated by simple beam theory and found to be negligible. The normal operating loads which induce stresses in the spacer disks are the dead weight loads and differential thermal expansion effects. These effects are evaluated using the analysis models described below.

Two basic models are developed for the basket assembly: models for loading in the plane of the spacer discs, and models for loading out of the plane of the spacer discs. The in-plane models are used for horizontal deadweight, thermal, and side drop analyses presented in Section 8.2.5. The out-of-plane models are used for vertical deadweight, handling, seismic, and end drop analyses.

A. DSC Internals Dead Weight Analysis

The spacer disk dead weight stresses are calculated for the vertical and horizontal orientations inside the transfer cask and for the horizontal orientation inside the HSM. Vertical deadweight evaluation of the basket assembly addresses a DSC in the transfer cask. The weight of the fuel is assumed to be distributed over the area of DSC inner cover plate. The spacer disc is evaluated for out-of-plane gravity loads resulting from its own inertial load and, as appropriate, the inertial load of related basket components (the oversleeves for the 24P basket; the spacer sleeves, poison sheets, and poison sheet support bars for the 52B basket design). Support rods are evaluated for self weight and interaction loads with spacer discs and sleeves.

For horizontal loading, the basket assembly supports its self weight plus the weight of the fuel. Loads are transmitted through the spacer discs to the DSC shell and then to the support rails (centered at ± 18.5° and ± 30° from the bottom center of the DSC in the transfer cask and the HSM, respectively). Flexibility of the DSC shell is considered in determining the circumferential distribution of load under the spacer disc. The effect of the support rails on the spacer discs stresses and load distribution is considered in the evaluation of the spacer discs.

The spacer disk horizontal dead weight stresses inside the transfer cask are calculated using the analytical models described in Section 8.2.5.2. The spacer disk horizontal dead weight stresses are obtained from the analysis load step corresponding to the applied 1g dead weight load.

The NUHOMS®-24P spacer disc vertical dead weight stresses are calculated by factoring the results from the NUHOMS®-24P spacer disc 75g end drop linear elastic static analysis described in Section 8.2.5.2.C (v) by 1/75.

The NUHOMS®-52B spacer disc vertical dead weight stresses are calculated using the analytical model described in Section 8.2.5.2.C (vi). The dead weight stresses are obtained from the analysis load step corresponding to the applied 1g vertical dead weight load.

The spacer disc dead weight stress intensities while inside the HSM are calculated using the analytical models described in Section 8.2.5.2. The model boundary conditions are modified to

reflect the support conditions provided by the DSC support rails. Linear elastic static analyses are performed for the 1g horizontal dead weight loads.

The controlling spacer disc dead weight stress intensities from the analyses described above are reported in Table 8.1-10 and Table 8.1-11, respectively.

Under normal conditions in the vertical orientation, the support rods provide longitudinal support for the spacer discs. The support rods are evaluated for compressive loads resulting from self weight of the basket assembly. Thermal stresses in the support rods are not significant since the axial temperature distribution of the DSC shell is relatively constant over the region where the spacer discs are located and there is no appreciable differential thermal expansion between spacer discs. For the NUHOMS®-52B support rods the effect of preload is considered in the stress calculations.

B. DSC Internals Thermal Stress Analysis

The effects of axial and radial thermal expansion are evaluated for the DSC internal basket components. The ANSYS (8.48) models as shown in Figure 8.1-16 and Figure 8.1-17 are used for thermal stress analyses of the spacer disc for the NUHOMS®-24P and NUHOMS®-52B baskets, respectively.

A typical temperature distribution (corresponding to 100°F ambient temperature) obtained from the heat transfer analyses is shown in Figure 8.1-5. These temperature distributions are mapped as temperature nodal loads onto the spacer disc structural models. A static analysis is then performed to determine the thermal stresses. The maximum stresses determined from the thermal stress analyses are summarized in Table 8.1-10. A similar analysis is performed for the NUHOMS®-52B DSC spacer disc using the temperature distributions corresponding to the design basis ambient air temperature conditions described in Section 8.1.3. A typical temperature distribution for the 52B DSC is shown in Figure 8.1-6. The maximum stresses determined from the thermal stress analyses are shown in Table 8.1-11.

As described in Section 8.1.1.2, Paragraph C, adequate space exists in the cavity of the DSC, between the spent fuel assemblies and the shield plug assemblies, for free thermal expansion. To verify that adequate provision for free axial expansion of the spent fuel assemblies and other internal components of the basket are included, the differential expansion of each DSC component is calculated. The effect of thermal expansion and irradiation growth on both BWR and PWR fuel assemblies and the DSC cavity is evaluated for various ambient temperatures. The -40°F ambient condition for PWR fuel inside the 24P DSC provides the worst case for differential thermal growth between the fuel assemblies and the DSC cavity. A simplified 2-D, cylindrical HEATING7 model of the fuel assemblies is constructed with a heat generation of 1.0 kW. The fuel assembly is modeled as consisting of 4 distinct regions: (1) a stainless steel nozzle region which is 12.62" long (2) a plenum region of zircaloy which is 9.13" long (3) a low power density region of the active fuel (40" long) and (d) a high power density region of the active fuel (104" long). The resulting average temperatures for these 4 regions are 400 °F, 450 °F, 550 °F, and 662 °F respectively. The calculated average temperature of the 24P DSC shell for the -40°F ambient condition is 141 °F.

The following equation is used to determine the length of a PWR fuel assembly for the -40°F ambient case:

$$L_H = (L_{Z1}\alpha_{Z1}\Delta T_1 + L_{Z2}\alpha_{Z2}\Delta T_2 + L_{Z3}\alpha_{Z3}\Delta T_3 + L_S\alpha_S\Delta T_S) + L_T \qquad (8.1\text{-}2)$$

Where for the design basis PWR fuel:

$L_H$ = Hot length of spent fuel assembly, in.

$L_{Zn}$ = Length of Zircaloy guide tube segments defined as follows:

$L_{z1}$ = 9.13 in. (plenum region)

$L_{z2}$ = 40 in.(low power density region)

$L_{z3}$ = 104 in. (high power density region)

$L_S$ = Length of stainless steel per fuel assembly (Nozzle region)
= 12.62 in.

$\alpha_Z$ = Zircaloy coefficient of thermal expansion
= 3.5E-6 in./in.°F. (8.65)

$\alpha_s$ = Stainless steel coefficient of thermal expansion
is 9.19E-6 in./in.°F at 400 °F. (8.3)

$\Delta T_n$ = $T_{n(hot)} - 70°F$

$\Delta T_1$ = 450° - 70° = 380°F

$\Delta T_2$ = 550° - 70° = 480°F

$\Delta T_3$ = 662° - 70° = 592°F

$\Delta T_S$ = 400° - 70° = 330°F

$L_T$ = Total length of fuel assembly at room temperature
= 165.75 in.

Therefore:

$L_H$ = 166.083 in.

The nominal length of the DSC cavity at room temperature is 167.00 inches. The minimum length of the DSC cavity ($L_H$) at 141°F is:

$$L_H = L_c \alpha \Delta T + L_c \quad (8.1\text{-}3)$$

Where:

$L_c$ = 166.94 in., Minimum DSC length at room temperature

$\Delta T$ = 141° - 70° = 71°F

$\alpha$ = 8.65E-6 in./in.°F at 141°F (8.3)

Therefore:

$L_H$ = 167.043 in.

Therefore the clearance available for irradiation growth at hot conditions is the difference between the minimum hot DSC cavity length and the hot fuel assembly length or 0.960 inch (167.043"-166.083").

Taking thermal expansion of Zircaloy into consideration, the minimum cold clearance available to accommodate irradiation growth of PWR fuel is 0.958 inch.

A similar calculation for BWR spent fuel assemblies demonstrates that the minimum available clearance to accommodate irradiation growth is 1.014 inch.

Potential interference due to differential thermal expansion between the DSC cavity and the support rods are evaluated. In the 24P (standard and long cavity designs) and the 52B designs, the nominal gap between the DSC cavity and the support rods is 0.53 inches. Differential expansion occurs between the stainless steel DSC and support rods. Interference evaluations are performed for both, the DSC in the HSM and the DSC in the transfer cask under normal and off normal design basis ambient temperature conditions. Using an approach that includes support rod and DSC tolerances, the closest gap occurs during the 100° HSM load condition, which yields a gap of 0.074 inches for the 24P DSC. Similarly, a gap of 0.09 inches is calculated for the 52B DSC.

The nominal radial gap between the shell and spacer disc is 0.44 inches for both the 24P and the 52B DSCs. The resulting radial growth obtained is 0.236 inches for the 24P DSC and 0.243 inches for the 52B DSC. These evaluations, which included the effect of fabrication tolerances, show that the gaps between the DSC shell cavity and support rods, and between DSC shell and the spacer discs do not close due to differential thermal expansion.

C. DSC Internals Handling Stress Analysis

The NUHOMS-24P and –52B handling model is a full symmetry version of the entire basket assembly, as shown in Figure 8.1-18a. Only inertia loads, resulting from on-site handling and transport of the loaded DSC, concurrent with a 1g gravity load are applied to this model.

D. Evaluation of the Results

The maximum calculated DSC stresses in the spacer discs induced by normal operating load conditions are shown in Table 8.1-10 and Table 8.1-11. The calculated stresses for each applicable load case are combined in accordance with the load combinations presented in Table 3.2-6. The resulting stresses for the controlling load combinations are reported in Section 8.2.10 with the ASME Code allowable stresses.

8.1.1.4 DSC Support Structure Analysis

The general description of the DSC support structure inside the HSM is provided in previous sections. The DSC support structure is shown in Figures 4.2-6 and 4.2-7. The DSC support rails are supported vertically and horizontally by three moment resisting braced frames anchored to the HSM floor and side wall. The DSC support structure design uses bolted and welded connection details. Normal operating condition loads on the DSC support structure consist of the DSC dead weight, the support structure dead weight, and the DSC operational handling loads. The resulting friction loading which develops between the sliding surfaces of the DSC shell and the DSC support rails is transferred axially by the support rails to the HSM front wall.

The various components of the DSC support structure are subjected to normal operating loads including dead weight, thermal, and operational handling loads. A linear elastic beam model of the assembly is utilized to evaluate axial, shear, and bending stresses in the DSC support structure members. The geometry for the analytical model is shown in Figure 8.1-20. The support structure portion of the model consists of 137 nodes and 139 beam elements. Rigid members are used to approximate the connection between the support rails and the cross member support beams to maintain the geometric relationship between these members for load transfer. The DSC support structure analytical model is incorporated into the HSM analytical model discussed in Section 8.1.1.5.

A. DSC Support Structure Dead Weight Analysis

For the dead weight analysis, the total weight of the DSC is applied to the support rails. The dead weight of the DSC support structure is also included in this analysis.

B. DSC Support Structure Operational Handling Analysis

For the NUHOMS® system operational handling loads, a sliding force of 29,580 pounds is applied axially to the DSC support rails to account for the sliding friction between the DSC shell and the support rails.

C. DSC Support Structure Thermal Analysis

The thermal stress analysis of the DSC support structure considers the differential growth of the steel components relative to the floor, front and sidewalls to which the support structure is attached. In addition, the effect of temperature gradient in support steel components is also considered. Thermal stress evaluation of the steel components is performed considering the variation of elastic modulus and thermal expansion coefficient of steel and concrete with temperature.

D. Evaluation of DSC Support Structure Results

The results of the DSC support structure analysis are tabulated in Table 8.1-14. Maximum normal operating loads calculated for the DSC support structure end connections are listed in Table 8.1-15. The maximum calculated DSC support structure deflections for normal and off-normal operating loads are shown in Table 8.1-16. Specific information on the DSC support structure seismic loads can be found in Section 8.2.3. Additional details of the DSC support structure analysis are presented in Section 8.2.10 using the aforementioned design load analysis results.

8.1.1.5 HSM Loads Analysis

As discussed in Chapter 4, the NUHOMS® modular storage system has the flexibility of arranging prefabricated modules in arrays of single or double module rows. The exact number of HSMs in an array is dependent on plant specific needs and economic trade-offs and can range in size from a single stand-alone HSM to multiple arrays of HSMs.

In order to qualify the design for a range of NUHOMS® ISFSI applications, a single free-standing HSM is evaluated. The HSM structural analyses includes an evaluation of normal operating, off-normal, and postulated accident loads for the HSM. The frame and shear wall action of the HSM floor, walls and roof slab are considered to be the primary structural system for transverse loads. The structural analysis of an individual module provides a conservative methodology for evaluating the response of the HSM structural elements under various static and dynamic loads for any HSM array configured in accordance with Section 4.1.1.

The HSM side walls and roof slab thicknesses are established on the basis of radiological shielding requirements. As such, all other thickness requirements such as the minimum barrier thickness requirements for tornado generated missiles specified by NUREG-0800, Section 3.5.3 (8.19) are bounded. The ultimate strength method is used to evaluate stresses in the HSM

reinforced concrete walls, roof, and floor. The HSM reinforcement is designed to meet the minimum and maximum reinforcement requirements of ACI 349-85 (8.20). The available design strength exceeds that required for the factored design loads specified in Section 3.2. The reinforcement layout for the prefabricated HSMs is shown on Figure 8.1-19 and the Appendix E drawings. HSM construction details such as construction joints and reinforcing bar splices will be detailed on the construction drawings.

The HSM structural analysis is applicable to ISFSIs ranging in size from a single stand-alone module up to an array of unlimited size. The reinforced concrete HSM is evaluated assuming frame and shear wall behavior using the analytical models shown in Figure 8.1-21 through Figure 8.1-24. The reinforced concrete portion of the HSM model shown in Figure 8.1-21 and Figure 8.1-22 consists of 214 nodes and 215 plate elements. The DSC support structure model shown in Figure 8.1-20 is also incorporated into the HSM model. The analytical model of the HSM base unit, for thermal stress analysis shown in Figure 8.1-23 consists of solid brick elements representing the HSM floor, side wall, front wall, and rear wall. This analytical model does not include the DSC support structure, HSM door, or roof. The HSM roof analytical model shown in Figure 8.1-24 also consists of solid brick elements.

The various normal operating loads are applied to the analytical models and the HSM internal forces and moments calculated by performing a linear elastic finite element analysis. The HSM finite element model results are applicable to both a side-by-side single module row or a back-to-back side-by-side double module row arrangements. The analysis shows that the single HSM provides the governing case for load combinations containing tornado wind and missile loads, seismic loads and flooding conditions. The postulated response investigated for each of these cases is the potential for sliding or overturning of the single free-standing HSM which envelopes that of an HSM array. The analysis also shows that thermal loads control the reinforcement requirements for the HSM walls, roof, and floor. A description of the individual loads and load analyses are provided in the following sections.

The HSM analytical model used for the analysis of a single, free-standing HSM for the bounding environmental loads (design basis tornado, earthquake, and flooding effects) is shown in Figure 8.1-21 and Figure 8.1-22. The load inputs for this analysis are described in Sections 8.2.2 through 8.2.4. The HSM base unit and roof models shown in Figure 8.1-23 and Figure 8.1-24, respectively, are used for the thermal analysis of the HSM. The load inputs for this analysis are described in Section 8.1.1.5, Paragraph C, Section 8.1.2.2, Paragraph A, and Section 8.2.7.2. The remaining HSM loads such as dead loads, and live loads are also evaluated using the analytical model shown in Figure 8.1-21 and Figure 8.1-22. The results of these analyses are summarized in Table 8.1-19, 8.2-3, and 8.2-18. The resulting design analysis of the HSM to determine the reinforcement requirements is presented in Section 8.1.1.5, Paragraph E.

A. HSM Dead Load and Live Load Analyses

The dead weight of the HSM plus the loaded DSC and the DSC support structure weights are applied to the analytical model shown in Figure 8.1-21 and Figure 8.1-22 which represents a single free-standing prefabricated HSM. The resulting calculated maximum dead load shears

and moments are tabulated in Table 8.1-19. A live load of 200 psf is applied to the HSM roof to conservatively envelope all postulated live loads, including snow and ice. The resulting calculated maximum live load shears and moments are tabulated in Table 8.1-19.

B. Concrete Creep and Shrinkage Analyses

ACI 349-85 Section 9.2.2 states that "where the effects of... creep or shrinkage may be significant, they shall be included with the dead load...". Since creep is mainly dependent on elastic strain due to dead loads, the loading contribution from creep is minimal as the dead loads are small in relation to the capacity of the HSM frame and shear walls formed by the walls, roof and floor. The creep strain is conservatively calculated using the ultimate creep strain value suggested by Wang and Salmon (8.21).

$$\varepsilon'_c = C_u \varepsilon_c \qquad (8.1\text{-}4)$$

Where:

$\varepsilon'_c$ = Creep strain in./in.

$C_u$ = Ultimate creep strain or ratio of creep to initial strain from dead weight
= 2.35

$\varepsilon_c$ = Initial strain from dead weight
= 3E-5 in./in. (approximate value)

Therefore:

$\varepsilon'_c$ = 4.65E-5 in./in.

Shrinkage of the HSM concrete is conservatively calculated using an ultimate shrinkage strain value suggested by Wang and Salmon. Additionally, since shrinkage is significantly affected by the surface area to volume ratio, the ultimate shrinkage strain value is reduced according to the method recommended by Fintel (8.22). The combined shrinkage strain is:

$$\varepsilon_s = \varepsilon_{sh\mu} \alpha \qquad (8.1\text{-}5)$$

Where:

$\varepsilon_s$ = Shrinkage strain (in./in.)

$\varepsilon_{sh\mu}$ = Ultimate shrinkage strain = 8E-4 in./in.

$\alpha$ = Volume to surface area reduction = 0.5 (conservative)

Therefore:

$\varepsilon_s$ = 4E-4 in./in.

For determination of moments and shears in the HSM due to creep and shrinkage, the total strain is converted to an axial change in length across the roof of a prefabricated HSM.

$$\Delta L = L(\varepsilon_s + \varepsilon'_c)$$

Where:

$\Delta L$ = Axial length change (in.)

L = Length from center to center of HSM walls = 98 in.

$\varepsilon_s$ = 4E-4 in./in.

$\varepsilon'_c$ = 4.65E-5 in./in.

The resulting change in length of the HSM roof slab, $\Delta L$ = 0.044 inch.

Shortening due to creep and shrinkage occurs gradually over a period of time, and the effects are lessened by plastic creep flow and microcracking of the members. Ambient humidity also acts to reduce the effects of creep and shrinkage. The PCI design handbook (8.23) suggests that the calculated creep and shrinkage shortening values be reduced by a factor of three to five for design. Also, creep and shrinkage forces act opposite to those of thermal expansion forces for the HSM. Hence, it is conservative to neglect creep and shrinkage effects. Therefore, creep and shrinkage are not considered further for the HSM design.

C. HSM Thermal Loads Analysis

To evaluate the effects of thermal loads on the HSM, heat transfer analyses for a range of normal ambient temperatures are performed and the limiting thermal gradients and temperature values at various locations in the HSM determined. The thermal results for the NUHOMS®-24P HSM are bounding and are used for all thermal load analyses. A more detailed description of the heat transfer analyses is provided in Section 8.1.3. Structural analyses of the HSM for the maximum calculated floor, wall and roof temperature loads listed in Table 8.1-17 are performed for the HSM using the analytical models shown in Figure 8.1-23 and Figure 8.1-24. The results of these

analyses are summarized in Table 8.1-19. The basis for the HSM thermal analysis is discussed further in the following paragraphs.

ACI 349-85, Appendix A, provides a general methodology for designing reinforced concrete structures subjected to thermal loads. The commentary to this Appendix, Section A.3.3, defines a range of approaches utilized in the analysis of thermal loads. One approach accounts the self-relieving nature of the thermal loads (relief is obtained by the occurrence of thermal cracking when the concrete modulus of rupture is reached). For the thermal analysis of the HSM for normal operating conditions, the thermal loads are calculated for the cracked cross sections of the HSM walls, roof and floor.

To account for the seasonal effects of ambient temperature fluctuations on the outside surface of the HSM, an average daily ambient temperature range of 0°F (winter) to 100°F (summer) is considered in the heat transfer analysis for normal operating conditions. Analyses are performed for ambient temperatures of 70°F and 100°F to determine the limiting design conditions for the HSM. For the HSM roof slab the results of the HSM heat transfer analysis for normal operating conditions for a life time average ambient temperature of 70°F and with solar heat flux effects included are shown in Figure 8.1-7. For the HSM roof slab the results indicate a maximum local inside surface temperature of 164°F. Maximum thermal gradients of 50°F for the HSM roof slab and 29°F for the HSM side walls are also calculated.

The results of the heat transfer analysis for the 100°F ambient temperature case (maximum average summer temperature), with a solar heat flux (62 Btu/hr. ft.$^2$) indicates a maximum local inside surface temperature of 201°F as shown Figure 8.1-8. The thermal gradients through the concrete thickness are 59°F for the roof slab and 32°F for the HSM side walls. The results of the thermal analysis for normal operating conditions are tabulated in Table 8.1-24. The HSM concrete temperatures associated with the extreme ambient condition of 125°F, and the postulated accident condition of a total ventilation air inlet and outlet blockage are also evaluated, as discussed in subsequent SAR sections. The maximum local concrete surface temperature of the HSM for this short duration condition is 479°F.

For conservatism and consistency with the philosophy of the ACI 349-85, Section A.4.3, the strength properties of the concrete and reinforcing steel used in the HSM structural analysis are taken at the postulated temperature range for each load case. For all normal operating load cases the concrete and reinforcing properties are assumed to be equal to the specified values ($f'_c$ = 5000 psi for concrete and $f_y$ = 57,000 psi for rebar). For the 125°F extreme ambient blocked vent accident case the material properties are assumed to be equal to those specified in Table 8.1-3 at 479°F i.e., $f'_c$ = 4500 psi and $f_y$ = 51,000 psi. The use of material properties at 479°F is conservative since the average concrete temperatures calculated are well below this value even for short term conditions which may result from postulated accident events such as blockage of the HSM vents. Temperature dependent mechanical properties of concrete and reinforcing steel utilized for the HSM are presented in Table 8.1-3.

The adverse effects on reinforced concrete in relation to its strength properties, its deterioration and subsequent spalling and crack formation due to sustained elevated temperatures is discussed

in detail in Appendix D and is summarized in the following paragraphs. As concluded in Appendix D, and based on the criteria specified by ACI 349-85 and tests performed in recent years, no adverse effect on reinforced concrete strength, particularly in terms of concrete deterioration and spalling is anticipated for the range of HSM concrete temperatures calculated. The effect of elevated short and long term temperatures on normal concrete structures are discussed further in the following paragraphs.

The effects of elevated short and long term temperatures on concrete structures has been the subject of much research in the U.S. and European communities. The findings of these studies and tests have been reported in a number of publications. A review of some reports, particularly references (8.11), (8.22), and (8.24) show that the physical, chemical, and mechanical properties of concrete are not significantly affected at temperatures below 212°F. When heated beyond 212°F, unsealed concrete begins to lose its internal free moisture, causing loss of weight and shrinkage at higher temperatures. As this process continues the chemically bonded water within the cement paste is released which further accelerates the loss of weight and volume. The chemical and physical change in concrete affects its mechanical properties. Mechanical properties primarily affected by long-term sustained temperatures above 212°F are modulus of elasticity, compressive strength, tensile strength and the Poisson ratio. Data on these properties for normal Portland cement concrete as a function of temperature are extracted from various publications.

Figure 8.1-25 gives a comparison of strength losses with sustained high temperatures. Figure 8.1-26 shows the strength behavior of three types of aggregate commonly used. As can be observed from these curves, the compressive strength of concrete for a short duration temperature rise is unaffected. However, long-term heating at temperatures above 250°F reduces the compressive strength of the concrete. For the operating temperature range of the NUHOMS® HSM shown in Table 8.1-17, no loss in compressive strength results. During a postulated blocked vent accident the HSM concrete is heated beyond the normal range in localized areas for a short period of time. The concrete strength properties used in analysis of the off-normal and accident conditions are reduced accordingly to reflect the results of these findings.

In Figure 8.1-27 and Figure 8.1-28, the effects on modulus of elasticity of Portland cement concrete exposed to short and long term elevated temperatures are shown. These figures indicate substantial loss of elastic modulus at temperatures beyond 400°F. No substantial loss in properties is expected to occur for temperatures below 200°F which bounds the long term average normal operating temperature conditions for the HSM. The modulus of elasticity determines the flexural rigidity of the structure, and substantial loss of modulus of elasticity will cause excessive flexural deflections in long span members. Since the NUHOMS® concrete roof slab is a deep, short span member, flexural deflections are negligible. Furthermore, the decrease in modulus of elasticity decreases the calculated concrete thermal stresses. Other effects of the mechanical properties of concrete (i.e., reduction in tensile strength, creep, and shrinkage due to elevated temperatures) are investigated and found to have an insignificant effect on the design of the HSM.

Table 8.1-24 shows that the maximum HSM temperature for the life time average ambient temperature of 70°F does not exceed the ACI limit of 200°F for local area temperatures. The average HSM temperature for this condition does not exceed 150°F. As discussed above no reduction in concrete strength results from a short term temperature rise such as would occur for maximum and extreme ambient temperature conditions, or blockage of the HSM vents. Even for a sustained temperature increase of up to 250°F, the resulting reduction in concrete strength is minimal. As can be seen from Table 8.1-24, the HSM concrete temperatures are less than or equal to 250°F for all cases but the enveloping blocked vent case, which is postulated to occur for a period of 5 days or less.

Coupled with the conservative reductions in concrete material strength used in the HSM design calculations for the 125°F off-normal and accident conditions, the design criteria utilized is adequate to ensure that the NUHOMS® HSM will perform its intended safety function for all design conditions.

D. Radiation Effects on HSM Concrete

The accumulated neutron flux over the 50 year service life of the HSM is estimated to be 1.7E14 neutrons/cm$^2$. From the study by Hilsdorf, Kropp, and Koch (8.25), the compressive strength and modulus of elasticity of concrete is not affected by a neutron flux of this magnitude.

The gamma energy flux deposited in the HSM concrete is 1.7E9 MeV/cm$^2$-sec. or 3.0E-4 watt/cm$^2$. According to ANSI/ANS-6.4-1977 (8.26), the temperature rise in concrete due to this level of radiation is negligible. Thus, radiation effects on concrete strength are not evaluated further for the HSM design.

E. HSM Design Analysis

For comparison with the normal operating condition loads factored to include the ACI Codes strength reduction factors the flexural and shear strength capacities for the various HSM concrete sections are calculated using the ultimate strength method of ACI 349-85.

Conservatively ignoring the contribution of the compression reinforcing, the ultimate moment capacity of a typical 12 inch wide section of the HSM wall, roof, or floor for normal operating load combinations is:

$$M_u = \phi A_s f_y \left( d - \frac{A_s f_y}{1.7 f_c' b} \right) \qquad (8.1\text{-}6)$$

Where:

$M_u$ = Ultimate moment capacity k-in./ft.

b = 12 in., Width of section

| | | |
|---|---|---|
| d | = | Depth of the section minus rebar cover (see Appendix E drawings) |
| $\phi$ | = | 0.9, Flexural reduction factor |
| $f'_c$ | = | 5000 psi, Design compressive strength of concrete at 201°F |
| $A_s$ | = | Area of tensile reinforcing steel (see Appendix E drawings) |
| $f_y$ | = | 57,000 psi, Rebar design strength at 201°F |

Therefore:

| | | |
|---|---|---|
| $M_u$ | = | 1753 k-in./ft. for the 3'-0" thick roof slab |
| | = | 881 k-in./ft. for the 2'-6" thick front wall |
| | = | 694 k-in./ft. for the 1'-6" thick side walls |
| | = | 305 k-in./ft. for the 1'-0" thick rear wall |
| | = | 206 k-in./ft. for the 1'-0" thick floor slab |
| | = | 531 k-in./ft. for the 2'-0" thick shield walls |

The ultimate out of plane shear capacity of the HSM concrete for the normal operating loading combination without shear reinforcement for a typical 12 inch wide strip is:

$$\phi V_c = 2\phi \sqrt{f'_c}\ bd \qquad (8.1\text{-}7)$$

Where all parameters are as defined previously except:

| | | |
|---|---|---|
| $\phi$ | = | 0.85; Shear reduction factor |

Therefore:

| | | |
|---|---|---|
| $\phi V_c$ | = | 42.5 k/ft. for the 3'-0" thick roof slab |
| | = | 40.5 k/ft. for the 2'-6" thick front wall |
| | = | 22.9 k/ft. for the 1'-6" side walls |
| | = | 14.3 k/ft. for the 1'-0" rear wall |
| | = | 13.5 k/ft. for the 1'-0" thick floor slab |
| | = | 31.2 k/ft. for the 2'-0" thick end shield walls |

The thicker roof and front wall sections qualify as deep flexural members and the allowable shear capacity ($V_c$) may be calculated in accordance with Section 11.8.6 of ACI 349 using the formula:

$$V_c = \left(3.5 - 2.5\frac{M_u}{V_u\, d}\right)\left(1.9\sqrt{f'_c} + 2500\,\rho_w\frac{V_u\, d}{M_u}\right) b_w\, d \qquad (8.1\text{-}8)$$

but not to exceed

$$6\sqrt{f'_c}\; b_w\, d$$

8.1.1.6 HSM Door Analyses

The access opening for transferring the DSC into and out of the HSM is protected by a shielded door. The standard door (used in HSM Model 102) is a thick reinforced concrete door with a steel plate at the rear. The standard door design provides for increased shielding compared to the alternate door (used in HSM Model 80). The alternate door is a steel door with a core of concrete shielding material. Both doors are recessed into the HSM front wall and bear against the concrete docking flange as shown in Appendix E drawings. The door is attached to the front wall by four embedded studs with threaded nuts.

Standard Door Analysis: The weight of the 24 inch thick reinforced concrete door (with ½ inch thick steel plate at the rear) is 11.2 kips. The door is designed conservatively for a maximum pressure of 10 psi which envelops the equivalent pressure load due to seismic and tornado wind pressure. The maximum moment and shear forces due to the enveloping load are 26.4 kip-in/ft and 1.98 kips/ft, respectively. These computed moments and shear forces are significantly less than the bending capacity (1451.2 kips-in/ft) and the shear capacity (18.3 kips/ft) of the door.

Alternate Door Analysis: For normal system operation, the door assembly is only subjected to the dead weight which is transmitted by bearing directly into the HSM front wall, and handling loads resulting from installation and removal of the door during DSC transfer operations.

The concrete bearing strength required to support a bearing load on the frame from the door weight of 6556 pounds is a small fraction of the ACI 349 (Section 10.15) permissible concrete bearing strength of $\phi[0.85\, f'_c\, A_1] = 0.7\,[0.85 \times 5 \times 6 \times 80.63] = 1440$ kips. The embedded anchors for the HSM door frame are designed in accordance with ACI 349-85, Appendix B. The governing design load combination for the HSM door embedded anchors is the dead load plus tornado wind load combination. The dead load consists of the weight of the door. The wind load consists of the uniform suction acting on the door. The wind load produces shear and tension on the anchors. The maximum stress in the door subjected to the tornado wind pressure drop load is 3.17 ksi, which is much less than the allowable stress of 33 ksi. The maximum stress in the door due to seismic load is 30.2 ksi, which is less than the allowable stress of 39.4 ksi. The maximum tensile load in the anchors is 18.1 kips which is less than the allowable tension load of 106.0 kips.

8.1.1.7 HSM Heat Shield Analysis

The design of the HSM heat shield assembly is shown in Figure 4.2-7 and on the drawings in Appendix E. The heat shield acts to reduce the HSM concrete temperatures due to the heat rejected by the spent fuel assemblies during normal operating conditions, off-normal conditions, and postulated accident conditions. The only loading that the heat shield assembly is subjected to during normal operation is its own dead weight. Since over-size holes are used at the bolted connections to the HSM no thermal expansion loads are experienced by the heat shield.

The only loading that the HSM heat shield assembly experiences during off normal conditions or a postulated accident is the inertia force associated with a seismic event. The heat shield, studs and the support embedments are analyzed for normal, off-normal, and accident loads. The heat shield is conservatively analyzed as a series of simply supported beams with a span equal to the distance between two adjacent bolts in the longitudinal direction. Also, instead of performing a frequency analysis of the side wall heat shield plates to establish the dynamic amplification factor (DLF) the maximum DLF of 4.25 for 2% damping is selected from the design response spectra curve.

Using these conservative assumptions, the maximum bending stress in the plates obtained for dead weight and seismic load is 5.4 ksi, which is well within the allowable limit of 26.8 ksi, at an operating temperature of 270°F. Maximum axial and bending stresses in the studs are 2.1 ksi and 32.8 ksi, which give an interaction ratio of 0.92. The maximum shear stress in the studs is 0.5 ksi which is less than the allowable shear stress of 18 ksi. The calculated stresses demonstrate that the heat shield is capable of withstanding any normal, off-normal, or postulated accident condition.

8.1.1.8 HSM Axial Retainer for DSC

The design of the HSM axial retainer for the DSC is shown on the drawings in Appendix E. Additional details are provided in Section 8.2.3.2.

8.1.1.9 On-Site Transfer Cask Analysis

The on-site transfer cask is evaluated for normal operating condition loads including:

1. Dead Weight Load
2. Thermal Loads
3. Handling Loads

The NUHOMS® transfer cask is shown in Figure 1.3-6 and on the drawings contained in Appendix E. The transfer cask to be used by a utility may be of the design documented in Appendix E, or any other previously NRC reviewed and approved design such as the transfer cask designs documented in the NUHOMS®-24P Topical Report [4.13], the Oconee Nuclear Station ISFSI Safety Analysis Report [4.16], and the Calvert Cliffs ISFSI Safety Analysis Report [4.17], provided that it is demonstrated prior to use that the limiting conditions of use as described in the COC can be met. Three transfer casks, the standardized, OS197, and OS197H

transfer casks are discussed in this SAR. Table 8.1-20, Table 8.1-20a, and Table 8.1.20b summarize the calculated stresses for the normal operating loads for the standardized, OS197, and OS197H transfer casks, respectively. The methodology used to evaluate the transfer cask for the effects of normal operating loads is described in the following paragraphs. The analytical results and comparisons with the acceptance criteria defined in Section 3.2 are also presented in this section.

A. Transfer Cask Dead Weight Analysis

The effects of dead weight for a loaded transfer cask are evaluated for two cases. The first case evaluated is for the transfer cask hanging vertically by the two lifting trunnions, and loaded with its maximum payload. A maximum wet payload of 91,804 pounds is used in the analysis of the standardized cask, while a load of 101,250 pounds and 126,000 pounds is used for the OS197 and OS197H transfer casks, respectively.

The second dead weight load case evaluated for the transfer cask includes the loaded transfer cask resting in a horizontal position on the support skid transport trailer. In this orientation, the weight of the cask is shared between the lower support trunnions and the upper lifting trunnions resting in the pillow block supports of the support skid. The maximum dead load stresses are shown in Table 8.1-20, Table 8.1-20a, and Table 8.1-20b for the standardized, OS197, and OS197H transfer casks, respectively. The local stresses around the trunnions are included in the normal handling load case described in Paragraph B.

B. Transfer Cask Normal Handling Loads Analysis

The major components of the transfer cask affected by the normal handling loads are the structural shell including the top and bottom cover plates, the upper and lower trunnions, the upper trunnion assembly insert plates, and the structural shell local to the trunnions. As described for the dead weight analysis, there are two normal operating cask handling cases which form the design basis for the transfer cask. These cases are illustrated in Figure 8.1-30 and are summarized as follows:

(i) The transfer cask is oriented in the vertical position, loaded to its maximum estimated weight of 200,000 lbs, 208,500 lbs and 250,000 lbs for the standardized, OS197, and OS197H transfer casks, respectively, hanging by the upper lifting trunnions, and present in an area of the plant which requires conformance with the requirements of NUREG-0612. Accordingly, the allowable design stresses for the upper trunnions and their attachment welds are restricted to the smaller of one sixth of the material yield strength, or one tenth of the material ultimate strength for critical lifts. Allowable stresses for the remaining transfer cask components including the lower support trunnions are governed by the requirements of the ASME Code. The cask handling load is assumed to be shared equally between the two upper trunnions. An additional load factor of 15% is conservatively applied to account for the inertial effects of crane hoist motions in accordance with CMAA #70 recommendations. The transfer cask is designed so that the cask lifting yoke engages the outer most portion of the upper trunnion assembly. During

the heaviest lift from the fuel pool, the cask/DSC contains water, the DSC top shield plug is in place, and the DSC and cask top cover plates are removed. For this condition the maximum ANSI N14.6 design load for the two upper trunnions of the standardized cask due to a vertical lift is conservatively assumed to be 100 kips per trunnion plus the 15% allowance, or 115 kips, acting vertically, with a moment arm measured from the center of the yoke lifting hook to the middle surface of the transfer cask structural shell. For the OS197 and OS197H transfer casks, the maximum load considered for the vertical lift per trunnion is 120 kips and 144 kips, respectively.

The maximum calculated upper trunnion stress for the standardized transfer cask under this load case is 5.5 ksi at the junction between the trunnion shoulder and the trunnion sleeve attached to the structural shell plate. This compares with the ANSI N14.6 allowable stress of 13.5 ksi for the trunnion material. The maximum weld stress is 6.7 ksi. The ANSI N14.6 allowable weld stress is 8.0 ksi. The maximum calculated stress intensity in the lower trunnion is 9.5 ksi, and the maximum weld stress is 12.6 ksi. These stresses compare with the ASME Code allowable value of 20 ksi.

For the critical lift of the OS197 transfer cask, the limiting stress occurs at the junction between the trunnion shoulder and the trunnion sleeve weld. The maximum weld stress ratio is 0.98 based on a stress of 5.08 ksi versus an allowable of 5.21 ksi.

The upper trunnion assembly of the OS197H cask is designed to accommodate a lifted load of 250,000 lbs. The limiting stress occurs in the upper trunnion sleeve. The maximum trunnion sleeve stress ratio is 0.87 based on a stress of 3.34 ksi versus an allowable of 3.82 ksi.

The maximum stress in the standardized transfer cask structural shell occurs in the thickened plate at the junction with the upper trunnion sleeves. Stresses in the structural shell are calculated using the WRC Bulletin No. 107 (8.54) method for the standardized transfer cask and an ANSYS finite element analysis for the OS197 and OS197H transfer casks. The maximum calculated stress intensity in the standardized transfer cask structural shell is 42.6 ksi compared with an ASME Code allowable stress intensity value of 67.5 ksi. For the OS197 the maximum calculated stress intensity in the cask structural shell for the critical lift combinations using finite element analysis is 19.6 ksi (23.5 ksi for the OS197H) versus an allowable of 60 ksi.

(ii) During transport of the DSC from the plant's fuel/reactor building to the ISFSI, the transfer cask is oriented in a horizontal position, and is firmly secured to the support skid/transport trailer. During this operation the cask/DSC is loaded with fuel with the DSC top shield plug and the DSC and cask top cover plates in place. The resulting trunnion loads are developed by taking the summation of moments about a horizontal axis to account for the fact that the upper trunnions are closer to the horizontal center of gravity of the cask and thus carry a greater part of the total cask weight compared with the lower support trunnions. The transfer cask is supported in pillow block supports at two locations; the lower support trunnions near the bottom end of the cask, and the lifting

upper trunnions supports near the top end of the cask. The allowable stresses for the on-site transfer load cases are governed by the ASME Code. For the standardized cask the maximum postulated ASME Code upper lifting trunnion load is 118 kips while the critical load for the structural shell plate is a combination of the 58 kips dead load acting vertically, plus a postulated lateral load of ± 1g or 116 kips acting radial to the shell. The loads from this case envelope the design basis transport operation loads of ± 0.5g simultaneously applied in three directions to account for vibratory motion loads and start/stop loads which may occur during transport. The design loads for the lower support trunnion are developed in a similar manner.

The OS197 transfer cask upper lifting trunnions are evaluated for a combined vertical and dead weight handling loads of 146.3 kips and a radial load of 146.3 kips (163.8 kips each for the OS197H). The lower trunnions are evaluated for 112.5 kips each for the radial and axial directions and 112.5 kips for the combined effects of vertical and dead weight loading (126 kips each for the OS197H).

During transfer of a DSC from the transfer cask to and from the HSM, the transfer cask is restrained to the HSM to prevent any relative motion. The restraint device functions by firmly securing the transfer cask lifting trunnions to embedded anchor points in the HSM front wall. The maximum load exerted on the transfer cask lifting trunnions is equal to the maximum hydraulic ram load, or 80 kips. This load magnitude is much less than the design basis handling loads described above and is therefore enveloped by the calculated stresses reported for that case. During transfer, the cask rail welds are loaded in shear by the friction of the sliding DSC. At an assumed shear of 80 kips, the stress on the rail welds is 5.8 ksi compared to an allowable value of 9.4 ksi.

For the standardized cask, the maximum calculated upper lifting trunnion stress intensity for the transport load case is 5.7 ksi and occurs at the junction of the sleeve to the cask shell. This compares with an ASME Code allowable stress of 33.8 ksi. The maximum calculated weld stress intensity is 7.1 ksi compared with an ASME Code allowable stress, of 45 ksi. The maximum calculated lower support trunnion stress intensity is 9.5 ksi compared to the ASME Code allowable of 20 ksi. The maximum weld stress intensity is 12.6 ksi and the maximum cask structural shell stress intensity is 42.6 ksi compared with ASME Code allowable values of 20.0 ksi and 67.5 ksi respectively.

For the OS197 transfer cask the maximum calculated upper lifiting trunnion stress for the transport case is 6.46 ksi at the junction of the shoulder of the trunnion and the trunnion sleeve (7.23 ksi for the OS197H). This compares with an ASME allowable stress of 45.0 ksi. The maximum calculated weld stress is 3.56 ksi (3.98 ksi for the OS197H) versus an ASME allowable of 11.25 ksi. The maximum lower trunnion stress for the transport case is 9.41 ksi (10.53 ksi for the OS197H) compared to an allowable of 22.9 ksi. The maximum weld stress for this load case is 8.21 ksi (9.20 ksi for the OS197H) versus an allowable of 11.45 ksi. The maximum OS197 cask structural shell stress intensity is 41.4 (46.8 ksi for the OS197H) ksi compared with an allowable of 60 ksi.

C. Transfer Cask Normal Operating Thermal Stress Analysis

The heat transfer analyses of the transfer cask are presented in Section 8.1.3. Analyses are performed for the normal operating ambient temperature range of 0°F to 100°F to establish the through wall thermal gradients. Results for the standardized cask are shown in Figure 8.1-11 and Figure 8.1-12. Similar analyses are also performed for the OS197 transfer cask and OS197H transfer cask. The resulting gradients are used in the structural evaluation of the cask. A circumferential temperature gradient is also calculated with the transfer cask secured to the support skid/transport trailer. This gradient includes heat input due to solar heat flux.

The nominal room temperature gaps, of 0.5 inch axially and 0.375 inch radially, between the DSC and the transfer cask inner cavity are established to ensure that for the worst case tolerance buildup and differential temperatures that the DSC will slide in/out of the transfer cask without binding. Thermal stresses due to the differential expansion of the dissimilar materials; namely stainless steel, carbon steel, lead, and neutron shielding material, are evaluated. The analyses for the normal operating thermal loads are summarized in the paragraphs which follow.

Calculations for the combined effect of the worst case radial thermal gradients, and the circumferential temperature variation, are performed using the combined transfer cask/DSC axisymmetric finite element ANSYS models shown on Figures 8.2-9 and 8.2-10 and described in Section 8.2.5.2, Paragraph B (i). In addition, the ANSYS models are also used to evaluate the effects of differential expansion of the dissimilar materials. The temperatures associated with the radial and axial thermal gradients are input to the analytical model as discrete element temperatures and the resulting induced thermal stresses calculated. Transfer cask stresses due to axial growth of the cask are minimized by the design of the support skid pillow block support system.

The results of these analyses for the standardized cask are shown in Table 8.1-20. Similar analyses are performed for the OS197 and OS197H transfer casks. The structural analysis results for the OS197 and OS197H transfer casks under thermal loading are shown in Table 8.1-20a and Table 8.1-20b, respectively.

D. Transfer Cask Analysis Results Comparisons

The results of the transfer cask analyses for normal operating loads are combined to obtain stresses for the associated load combinations which are compared to the appropriate allowable stresses, as discussed in Section 8.2.10.

8.1.2 Off-Normal Load Structural Analysis

Table 8.1-2 shows the off-normal operating loads for which the NUHOMS® safety-related components are designed. This section describes the design basis off-normal events for the NUHOMS® system and presents analyses which demonstrate the adequacy of the design safety features of a NUHOMS® system.

For an operating NUHOMS® system, off-normal events could occur during fuel loading, cask handling, trailer towing, canister transfer and other operational events. Two off-normal events are defined which bound the range of off-normal conditions. The limiting off-normal events are defined as a jammed DSC during loading or unloading from the HSM and the extreme ambient temperatures of -40°F (winter) and +125°F (summer). These events envelope the range of expected off-normal structural loads and temperatures acting on the DSC, transfer cask, and HSM.

8.1.2.1 Jammed DSC During Transfer

The interfacing dimensions of the top end of the transfer cask and the HSM access opening sleeve are specified so that docking of the transfer cask with the HSM is not possible should gross misalignments between the transfer cask and HSM exist. Furthermore, beveled lead-ins are provided on the ends of the transfer cask, DSC, and DSC support rails to minimize the possibility of a jammed DSC during transfer. Nevertheless, it is postulated that if the transfer cask is not accurately aligned with respect to the HSM, the DSC binds or becomes jammed during transfer operations. Based on the dimensions of the DSC, transfer cask, and HSM, the maximum misalignment of the sliding surfaces is limited by operating procedures to 1/8 inch or less. Assuming a worst case misalignment in positioning and docking the transfer cask with the HSM access opening sleeve, the maximum possible misalignment which would permit transfer of the DSC to occur is 1/4 inch. Although unlikely, any greater misalignment may cause axial sticking and/or a rotation of the DSC to occur which may result in a binding condition.

A. Detection of the Event

When a jam of the DSC occurs during transfer the hydraulic pressure in the ram begins to increase. The maximum ram push/pull forces are limited to a maximum load equal to 80,000 lb. Override controls are available to the operator to increase the ram force up to its maximum design load, equal to 80,000 lb, or to interrupt the transfer operation at any time.

B. Axial Sticking of the DSC

The DSC has beveled lead-ins on each end which are designed to avoid binding or sticking on small (≤ 1/4 inch) obstacles. The transfer cask and the DSC support rails inside the HSM are also designed with lead-ins to minimize binding or obstruction during DSC transfer. The off-normal handling load event postulated to occur assumes that the leading edge of the DSC becomes jammed against some immovable feature because of gross misalignment of the transfer cask.

During the transfer operation, the force exerted on the transfer cask and the DSC by the hydraulic ram is that required to first overcome static, then sliding friction of the DSC and the transfer cask or DSC support rail sliding surfaces. If motion is prevented, the hydraulic pressure increases, thereby increasing the force on the DSC until the system pressure limit is reached. This limit is controlled so that adequate force is available to overcome variations in surface finish, etc., but is sufficiently low to ensure that component damage does not occur.

For off-normal loads, the DSC bottom cover plate and the grapple ring assembly are subjected to a maximum ram push/ grapple pull force of 80,000 pounds. The method of analysis for off-normal loads is the same as that described for normal loads in Sections 8.1.1.1 and 8.1.1.2.

For the postulated loading condition as illustrated in Figure 8.1-31, it is conservatively assumed that the force created by the jammed DSC condition produces a force-couple of magnitude F x R, where: F is the imposed force of 80,000 pounds and R is 33.625 inches, the outside radius of the DSC shell. Thus, a moment of 2690 in.-kip is produced in the DSC shell. The gross section modulus available to resist this bending moment is 2165 $in.^3$. Thus, the DSC shell stress due to the 2690 in.-kip moments is:

$$S_{mx} = \frac{M}{S} \qquad (8.1\text{-}9)$$

Where:

M = 2690 in.-kip, Bending moment

S = 2165 $in.^3$, DSC section modulus

Therefore:

$S_{mx}$ = 1.24 ksi

This magnitude of stress is negligible when compared to the allowable membrane stress of 18.7 ksi. The results of the off-normal analyses are reported in Table 8.1-10 for the NUHOMS®-24P, and Table 8.1-11 for the NUHOMS®-52B.

For a jammed DSC, the 80,000 pound ram load is postulated to be reacted by a DSC support rail inside the HSM at the most critical location. At the same time, a concentrated force of one fourth of the DSC weight is assumed to act vertically at mid span of the DSC support rail member. The results of this analysis are reported in Table 8.1-10, Table 8.1-11, and Table 8.1-14.

C. Binding of the DSC

If axial alignment within system operating specifications is not achieved, it may be possible to pinch the DSC shell as shown in Figure 8.1-32. The pinching force acting on the DSC shell and the transfer cask inner liner is directly proportional to the angle of rotation. The maximum possible inclination angle established by various conservative geometric and operational assumptions is less than one degree. If this angle is conservatively assumed to be one degree, then the pinching force is taken as the product of the maximum ram loading of 80,000 pounds and the sine of the angle, or 1,400 pounds. This force is assumed to be distributed around the circumference of the DSC shell and either the transfer cask or HSM sleeve as a cosine distribution.

The 1,400 pound load is conservatively assumed to be applied as a point load at a location away from the ends of the cask or DSC. The resulting maximum stresses are given by Table 31, Case 9a of Roark (8.16) as:

Membrane stress:

$$\sigma = \frac{0.4P}{t^2}$$

Bending stress:

$$\sigma' = \frac{2.4P}{t^2}$$

Therefore, the maximum stress is:

$$\sigma + \sigma' = \frac{2.8P}{t^2}$$

For the DSC shell, t = 0.625 inch. For the cask inner liner, t = 0.5 inch. Substituting for t and P equal to 1400 pounds, the maximum extreme fiber stresses in the DSC shell and cask inner liner are 10.0 ksi and 15.7 ksi respectively. The DSC handling stress is enveloped by the handling stresses described in Chapter 8 of this SAR and deemed acceptable. The 15.7 ksi stress in the cask inner liner is acceptable as compared against the Level A/B allowable of 32.6 ksi for membrane plus bending.

The tangential component of ram loading under the assumed condition is less than the force of the jammed condition calculated previously in Paragraph B and as such is not considered further. The stresses on the DSC are given in Table 8.1-10 and Table 8.1-11, and for the DSC support assembly inside the HSM for the jammed condition are reported in Table 8.1-14.

D. Consequences of Jammed DSC

In both scenarios for a jammed DSC, the stress on the DSC shell and transfer cask inner liner are demonstrated to be much less than the ASME Code allowable stress. Therefore, permanent deformation of the DSC shell and cask inner liner does not occur. There is no potential for breach of the DSC containment pressure boundary and therefore, no potential for release of radioactive material.

E. Corrective Action

In both cases, the required corrective action is to reverse the direction of the force being applied to the DSC by the ram, and return the DSC to its previous position. Since no permanent deformation of the DSC or transfer cask inner liner occurs, the sliding transfer of the DSC to its previous position

is unimpeded. The transfer cask alignment is then rechecked, and the cask repositioned as necessary before attempts at transfer are renewed.

8.1.2.2 Off-Normal Thermal Loads Analysis

As described previously, the NUHOMS® system is designed for use at all reactor sites within the continental United States. Therefore, off-normal ambient temperatures of -40°F (extreme winter) and 125°F (extreme summer) are conservatively chosen. In addition, even though these extreme temperatures would likely occur for a short period of time, it is conservatively assumed that these temperatures occur for a sufficient duration to produce steady state temperature distributions in each of the affected NUHOMS® components. Each licensee should verify that this range of ambient temperatures envelopes the design basis ambient temperatures for the ISFSI site. The NUHOMS® system components affected by the postulated extreme ambient temperatures are the transfer cask and DSC during transfer from the plant's fuel/reactor building to the ISFSI site, and the HSM during storage of a DSC.

The thermal stresses in the various NUHOMS® system components due to the off-normal temperatures are calculated in the same manner as described for the normal operating thermal loads. A description of these methods is provided in Sections 8.1.1.2 for the DSC shell, 8.1.1.3 for the DSC internals, and 8.1.1.8 for the on-site transfer cask.

A. HSM Off-Normal Thermal Load Analysis

As described in Section 8.1.3.1, the maximum HSM temperatures are calculated for the off-normal extreme ambient temperature of 125°F. The resulting maximum HSM concrete temperature calculated for off-normal conditions is 241°F. The maximum calculated temperature gradient is 55°F for the HSM roof and 34°F for the HSM side walls. These values are comparable to the maximum temperature gradients calculated for the 100°F normal operating ambient temperature. The short duration peak concrete temperature meets the ACI 349-85 limit of 350°F. Since the ultimate shear and moment capacities for each module concrete section are the same for off-normal and accident conditions (see Section 8.2.7), the maximum calculated shear forces and bending moments resulting from either case are conservatively used for design.

The DSC Support Steel is analyzed for thermal stresses due to growth differential between the steel and the concrete structure.

B. DSC Off-Normal Thermal Stress Analysis

The off-normal thermal gradients and maximum temperatures for -40°F and 125°F ambient air are developed for the DSC resting in the cavity of transfer cask as described in Section 8.1.3.3. The 100°F case with solar insolation bounds the 125°F case without solar. Therefore, the 100°F results are used. The maximum off-normal calculated surface temperature for the DSC shell is 355°F for an extreme ambient temperature of 100°F. The corresponding internal pressure for the DSC is shown in Table 8.1-6.

The off-normal thermal gradients and maximum temperatures are also developed for the DSC resting in the HSM, as described in Section 8.1.3.2. The maximum off-normal surface temperature calculated for the DSC shell is 382°F for an extreme ambient air temperature of 125°F.

There may be restrictions for onsite transfer and handling of the DSC under these extreme temperature conditions. Refer to Technical Specifications 1.2.13 and 1.2.14 of the NUHOMS® COC.

C. Transfer Cask Off-Normal Thermal Stress Analysis

As described in Section 8.1.3.3 the maximum temperatures and associated through wall thermal gradients are calculated for a loaded on-site transfer cask for a maximum ambient temperature range of -40°F and 125°F. The temperature gradient for the 125°F ambient temperature case includes a sun screen that allows no solar heat flux on the cask. For the standardized cask the bounding 100°F case with solar insolation results in a maximum calculated temperature of 235°F on the exterior of the transfer cask and a maximum through wall temperature gradient of 61°F for the bounding postulated off-normal cases.

For the OS197 transfer cask, the maximum calculated temperature on the cask exterior is 251°F for the 125°F ambient temperature case with no solar heat flux.

The results of the off-normal thermal analyses shown in Table 8.1-10, Table 8.1-11, Table 8.1-21, and Table 8.1-21a and Table 8.1-21b for each of the NUHOMS® system components are combined with the appropriate results from other analyses for the associated load combinations. The resulting stresses and comparisons with allowable stresses are discussed in Section 8.2.10.

There may be restrictions for onsite handling of the transfer cask with a loaded DSC under these extreme temperature conditions. Refer to Technical Specifications 1.2.13 and 1.2.14 of the NUHOMS® COC.

## 8.1.3 Thermal Hydraulic Analysis

This section of the SAR describes the thermal analysis of the NUHOMS® HSM, DSC and transfer cask. The analytical models of the HSM, the DSC and the transfer cask are described and the calculation results summarized. The thermophysical properties of the NUHOMS® system components used in the thermal analysis are listed in Table 8.1-8 and Table 8.1-9. The following evaluations are performed for the NUHOMS® system:

1. Thermal Analysis of the HSM

2. Thermal Analysis of the DSC in the HSM

3. Thermal Analysis of the DSC in the Transfer Cask

The NUHOMS® components are evaluated for a range of design basis ambient temperatures as follows:

A. Normal Operating Conditions: The system components are evaluated for average ambient temperatures in the range of 0°F minimum (winter) to 100°F maximum (summer). Ambient temperatures within this range are assumed to occur for a sufficient duration to cause a steady-state temperature distribution in the NUHOMS® system components. For the evaluation of thermal cycling and material properties, fluctuations in the ambient temperature from winter to summer conditions are assumed to occur once per year for the HSM, and six times per year for the transfer cask. The lifetime average ambient temperature for the 50 year service life is taken as 70°F. The "stress-free" temperature for material properties is also assumed to be 70°F.

B. Off Normal and Accident Conditions: The system components are evaluated for the extreme ambient temperatures of -40°F (winter) and 125°F (summer). Should these extreme conditions ever occur, they would be expected to last for a very short duration of time. Nevertheless, these ambient temperatures are conservatively assumed to occur for a sufficient duration to cause a steady-state temperature distribution in the NUHOMS® system components (a few hours for the transfer cask, several days for the HSM). In addition, for postulated accident conditions the HSM ventilation inlet and outlet openings are assumed to be completely blocked for a five day period concurrent with the extreme ambient conditions (125°F) as described in Section 8.2.7.

### 8.1.3.1 Thermal Hydraulics of the HSM

#### A. Principles of HSM Cooling System

The HSM is cooled by a natural draft of air entering through the air inlet openings located in the lower side walls of the HSM, and exiting through air outlet openings located in the upper side walls of the HSM. Cooler air at the prevailing ambient conditions is drawn into the HSM. The cooler air flows from the bottom of the HSM along the outer DSC surface where it is warmed by the decay heat of the spent fuel inside the DSC. The warmed air flows along the ceiling of the HSM and exits through the air outlet openings. The HSM vent geometries and flow paths for ventilation air are illustrated in Figure 8.1-34 and Figure 8.1-35 and on the drawings contained in Appendix E.

The HSM roof and side walls are the primary concrete surface conducting heat to the outside environment. For analytical purposes, an HSM centered in a group of HSMs, each loaded with a DSC, is assumed. For the thermal analysis of an interior HSM with no DSC present in the adjacent HSMs, the outer surface of the wall is assumed to be exposed to the prevailing ambient conditions. For the thermal analyses of a single free-standing HSM, or an HSM at the end of a multiple module array, a shield wall is modeled, the outer surface of which is assumed to be exposed to the prevailing ambient conditions. The ISFSI basemat is in contact with soil, which is assumed to be at a constant temperature at a combined depth of eleven feet. Air infiltration and heat radiation from the HSM access opening door is conservatively neglected.

The temperature difference ($\Delta T$) and distribution, and the height difference ($\Delta h$) between the HSM vent inlets and outlets creates a "stack effect," to drive air through the HSM. The ventilation air has sufficient velocity to provide adequate cooling for the DSC so that the spent fuel cladding temperature remains below acceptable limits. The ventilation flow paths inside the HSM are designed so that the pressure difference due to the stack effect ($\Delta P_s$) are greater than the pressure losses due to friction, vent area changes and flow direction changes ($\Delta P_f$).

The pressure loss due to friction is calculated by summing the individual losses ($K/A^2$, where K is the loss coefficient and A is the flow area) through the air inlet openings, the air outlet openings, and the flow paths through the HSM. Standard loss coefficients for entrances, exits, screens, elbows, slots, friction, flow over cylinders, flow between parallel plates, flowpath expansions and contractions are taken from References 8.28 and 8.44. The pressure drop due to the flow losses is determined by:

$$\Delta P_f = \frac{\dot{m}^2}{2 g_c \bar{\rho}} \sum_i \frac{K_i}{A_i^2} 1 \qquad (8.1\text{-}10)$$

Where:

$\dot{m}$ = Mass flow rate (lbm/ sec)

$g_c$ = Gravitational constant

$\bar{\rho}$ = Average density(lbm/ $ft^3$)

The pressure drop from the stack effect is calculated as follows:

$$\Delta P_S = \frac{g \rho_s \Delta T_{avg} h}{g_c T_s} \qquad (8.1\text{-}11)$$

Where:

$\Delta T_{avg}$ = Stack average temperature difference (°R)

h = Height (ft.)

g = Local acceleration due to Gravity = $g_c$

$T_s$ = Stack average temperature (°R)

$\rho_s$ = Stack average density ($lbm/ft^3$)

The above equations are solved iteratively to determine values of $\Delta T_{avg}$ and $\dot{m}$ at specific values of ($K/A^2$) for $\Delta P_f \leq \Delta P_s$. This flow rate calculation conservatively accounted for possible flow separation at the center of the DSC which then flows toward the HSM side wall outlet vents. Based on this analysis, the geometry of the flow areas for the HSM are established as shown on

the drawings in Appendix E. Using the calculated values of $\dot{m}$, the HSM bulk air temperatures surrounding the DSC are determined assuming isotropic heat flow from the DSC surface and integrating the energy equation around the DSC. The natural circulation cooling flow over the DSC surface for the standardized NUHOMS® system design is substantially higher (approximately three times) than the NUHOMS®-07P design due to the increased capacity of the HSM vents and the increased driving force of the DSC. The results of this analysis are shown in Table 8.1-21b, Table 8.1-22 (PWR) and Table 8.1-23 (BWR) for a range of ambient conditions.

The resulting bulk air temperatures for the range of ambient conditions are used in the subsequent HSM analyses to calculate the temperatures throughout the HSM and DSC shell. In the HSM HEATING7 model, the Boundary Type 1 (surface-to-boundary) is used to describe the natural circulation heat transfer between the DSC and the adjacent cooling air at the bulk air temperatures. The DSC temperatures are used as boundary conditions to determine the temperature distributions for the DSC internals and the spent fuel assembly regions. These calculations are described in the following paragraphs.

A metal heat shield is placed around the upper half of the DSC to shield the HSM walls and roof from thermal radiation effects. The location and geometry of the heat shield is shown in Figure 4.2-7 and on the HSM drawings contained in Appendix E. The heat shield protects the HSM concrete walls and ceiling from direct thermal radiation emanating from the DSC surface and significantly increases the combined surface area for convection cooling inside the HSM. The concrete walls and ceiling are subjected to thermal radiation from the back side of the heat shield, however, the radiation is emanated at substantially lower temperatures than the direct thermal radiation from the DSC surface.

B. Computer Program:

The HEATING7 computer program is used for the heat transfer analysis of the DSC. The HEATING7 program is known as "The HEATING Program," where HEATING is an acronym for "Heat Engineering and Transfer In Nine Geometries." HEATING7 is designed to be a functional module within the SCALE system of computer programs (8.15) for performing standardized analysis for licensing evaluations of nuclear systems. Thus its features are designed to perform thermal analyses on problems arising in licensing evaluations, and its input format is designed to be compatible with that of other functional modules within the SCALE system. HEATING7 may also be used as a stand-alone heat conduction code.

HEATING7 solves steady-state and/or transient heat conduction problems in one-, two-, or three-dimensional Cartesian or cylindrical coordinates or in one-dimensional spherical coordinates. The thermal conductivity, density, and specific heat may be both spatially and temperature-dependent. In addition, the thermal conductivity may be anisotropic. Selected materials may undergo a change of phase for transient calculations involving one of the explicit procedures specified. The heat generation rates may be dependent on time, temperature and position. Boundary temperatures may be dependent on time and position. Boundary conditions which may be applied along surfaces of an analytical model include specified temperatures or any combination of prescribed heat flux, forced convection, natural convection, and radiation.

Models are also available to simulate the thermal fin efficiency of certain finned surfaces. In addition, one may specify radiative heat transfer across gaps or regions which are embedded in the model. The boundary condition parameters may be time- and/or temperature-dependent. The mesh spacing may be variable along each axis.

The HEATING7 thermal calculations performed for the DSC employed the optional direct solution technique of the program. This technique generally required from three to eight iterations per calculation to obtain results with a convergence of better than 0.1% on the temperatures at each node in the analytical model.

For the DSC thermal calculations one hundred percent of the heat is conservatively assumed to be generated in the active fuel length of the spent fuel rods with no heat generation in the remaining portion of the fuel rods or the non-fuel bearing components. This conservative approach provides bounding values of spent fuel cladding temperatures for storage. The amount of heat rejected to the HSM concrete by the spent fuel due to direct gamma radiation or neutron emission is a very small fraction of the total heat generated by fission product decay.

The ANSYS computer code (8.67) is also used for the thermal analysis of the DSC shell inside the HSM and HSM concrete structure. ANSYS is a comprehensive thermal, structural, and fluid flow analysis package. The capabilities of ANSYS for performing thermal analysis of the HSM and DSC are similar to HEATING7 program. ANSYS has additional capabilities in modeling cylindrical structures inside rectangular structures similar to DSC inside the HSM. It is a finite element code capable of solving steady state and transient thermal analysis problems in one, two, or three dimensions. It has been successfully used in the past to perform thermal analyses for NRC licensed storage systems such as the TN-32 PWR Spent Fuel Storage (8.68).

It is a capable of modeling heat transfer via a combination of conduction, radiation and both natural and forced convection. Material properties defined in ANSYS may be dependent on temperature and position, and may be anisotropic. Similarly, heat generation within the model may be dependent on time, location and/or temperature. Boundary conditions can be applied to surfaces within the model and include specified temperatures, heat flux, natural or forced convection and radiation to the ambient environment. Radiation heat transfer between entities within the model may be represented by one-dimensional heat transfer links or by three-dimensional radiation superelements whose radiation view factors are calculated by ANSYS. The ANSYS solid modeling preprocessor allows model dimensions to be defined parametrically, allowing the user to easily study the impact of dimensional changes.

C. Thermal Model of the HSM

The ANSYS model of DSC inside the HSM is shown in Figure 8.1-36 and Figure 8.1-36a. The ANSYS model is a two-dimensional model that represents the center cross section of a HSM module at an axial location of maximum decay heat power during storage operation. Radiation from the surface of the HSM is only modeled from the roof using SURF151 elements. The emissivity of the concrete surface is 0.9. The heat flux due to solar insolation is also applied to the roof surface using SURF151 elements. The decay heat from the fuel assemblies is applied on

the inner surface of the DSC using SURF151 elements. The heat decay from the fuel assemblies is applied on the inner surface of the DSC using SURF151 elements.

ANSYS models of the HSM have been generated for both the NUHOMS®-24P and NUHOMS®-52B designs, differing only in the DSC decay heat, DSC length, and the bulk air temperatures. A bounding decay heat power level for 40,000 MWD/MTU, 4.0% initial enrichment PWR fuel with a base case 5 year cooling time of 1 kW/PWR assembly (resulting in a total of 24 kW/DSC) is used for the NUHOMS®-24P design. A heat flux of 284.3 BTU/hr-ft.$^2$ (0.0329 BTU/min.-in.$^2$) is determined by distributing the total decay heat power of 24 kW over the entire internal surface area of the DSC. The heat rejection through the fuel assembly end fittings and the DSC shield plugs and cover plates are included. Similarly, a decay heat of 19.2 kW/DSC is used for the NUHOMS®-52B design.

The soil below the ISFSI basemat is modeled as a seven foot thick region with a constant temperature boundary at the edge of this region. Sufficient mesh refinement is used in the HSM analytical model to obtain accurate temperature distributions through the thickness of the HSM walls, roof, and floor slab.

The thermal analysis of a typical HSM is performed for a loaded DSC located in the interior of a multiple module array with a DSC present in the two adjacent HSMs. The HSM roof and side walls are modeled, the outer surfaces of which are assumed to be exposed to the prevailing ambient conditions. For summer ambient conditions, a solar heat flux of 62 BTU/hr.-ft.$^2$ for normal conditions, and 123 BTU/hr.-ft.$^2$ for off-normal and accident conditions, is conservatively applied to the roof surface. The enveloping solar heat flux of 123 Btu/hr-ft$^2$°F for the extreme off-normal case is based on Reference 8.59. It is calculated for the worst case location in the contiguous United States using the maximum day long solar irradiation value specified for a horizontal surface in the worst month with the maximum clearness correction. Similarly, the solar heat flux of 62 Btu/hr-ft$^2$°F for the normal case is an enveloping value for the southeastern United States and is approximately half of the extreme off-normal value. Solar heat loads are conservatively neglected for the HSM thermal analysis for winter ambient conditions for normal, off-normal and accident conditions.

For the PWR HSM thermal analysis, a value of 0.0329 Btu/Min-in$^2$ is calculated for the decay heat flux through the DSC shell using the DSC shell assembly internal surface area. Use of the DSC shell assembly internal surface area, including the end covers, and exclusion of the 1.08 axial peaking factor for the HSM thermal analysis is based on the test data contained in Reference 7.10. The reference test data for cylindrical casks shows that the measured surface temperature profiles are relatively flat over the entire length, indicating that the heat flux is nearly uniform over the surface and axial peaking is not affecting the surface temperatures distribution. One reason for the relatively flat temperature profiles is the high thermal conductivity of the DSC shell material and relatively open design of the DSC basket assembly. The resulting heat flux is therefore more representative of the manner in which heat is actually rejected to the HSM air space by the DSC. The active fuel length of 144 inches and the peaking factor of 1.08 are conservatively used in the thermal analysis of the DSC internals for the evaluation of local effects such as the peak fuel clad temperature. The outer surface of the DSC shell dissipates heat to the HSM through both

convection and radiation. The air surrounding the DSC is modeled as a void and only radiation and convection mechanism for heat transfer from all HSM interior surfaces and the DSC outer surface is considered.

Convection heat transfer from the DSC and HSM surfaces is modeled by inputting a constant air temperature for the void regions between the DSC and HSM. These temperatures are also used to calculate the heat transfer coefficients for these regions. The bulk air temperatures used for each ambient temperature case are shown in Table 8.1-22 (PWR) and Table 8.1-23 (BWR). With these temperatures and the equations for the heat transfer coefficients described below, the ANSYS program calculates the temperatures of the DSC exterior surface and the HSM interior and exterior surfaces.

The spent fuel assembly decay heat is removed from the DSC outer surface through convection. A heat transfer coefficient $h_{hor\text{-}cyl}$ is used which corresponds to the heat transfer coefficient for natural circulation of air over a horizontal cylinder. Horizontal slab surfaces with convection on their lower surface, such as the HSM ceiling, are assumed to be cooled by natural convection with a heat transfer coefficient of $h_{ceil}$. Horizontal surfaces with convection on their upper surfaces, such as the HSM roof outer surface, are assumed to be cooled by natural convection with a heat transfer coefficient of $h_{plate}$.

Both sides of the metal heat shield and the HSM concrete walls are assumed to be cooled by air with a heat transfer coefficient of $h_{wall}$. Radiation heat transfer is modeled between the DSC outer surface and heat shield, between the DSC outer surface and the HSM floor, and between the heat shield and the HSM concrete walls and ceiling. The external surface of the HSM roof is assumed to be cooled by external air with a heat transfer coefficient of $h_{plate}$, and by radiation cooling to ambient air. The formulas used for the calculation of the heat transfer coefficients for natural convection are as follows [all in BTU/(hr. ft.$^2$ °F)] (8.28):

$$h_{can} = 0.22\,(\Delta T)^{1/3} \qquad (8.1\text{-}12)$$

$$h_{hor\text{-}cyl} = 0.18\,(\Delta T)^{1/3} \qquad (8.1\text{-}12A)$$

$$h_{ceil} = 0.12\,(\Delta T/L)^{1/4} \qquad (8.1\text{-}13)$$

$$h_{plate} = 0.22\,(\Delta T)^{1/3} \qquad (8.1\text{-}14)$$

$$h_{wall} = 0.19\,(\Delta T)^{1/3} \qquad (8.1\text{-}15)$$

Where:

$\Delta T = T_{surface} - T_{air}$

L = Characteristic length

The value of characteristic length (L) is assumed to be the median length of 57.6 inches.

The heat transfer coefficients are used by ANSYS following each iteration using the resulting average temperature of the corresponding surface node. A sufficient number of iterations are performed until a stable convergence is achieved. The remaining thermal-hydraulic parameters used in the HSM heat transfer calculations are given in Table 8.1-8 and Table 8.1-9.

The results of the ANSYS analysis for the HSM are in the form of temperature distribution profiles. The resulting temperature profile shows the steady state temperature distribution on the outer surface of the DSC.

The calculated HSM wall and roof temperature gradients are used in the reinforced concrete structural analysis for long term thermal loads which occur during normal operating conditions, and the short term thermal loads occurring during off-normal and postulated accident conditions. The HSM thermal analysis results are also used to obtain steady state temperature distributions for the outer surface of the DSC for the range of design basis ambient conditions. These steady state surface temperatures are used as a temperature boundary condition for the DSC model, described in Section 8.1.3.2.

D. Description of the Cases Evaluated for the HSM

The HSM thermal analyses are performed for the design basis ambient air temperatures defined in Section 8.1.3. These include a total of four cases with ambient air entering and/or surrounding the HSM at the following temperatures:

1. 70°F (lifetime average) and 100°F (maximum summer average) for normal operating conditions which can be expected to occur for long periods of time (PWR and BWR),

2. 125°F (extreme summer maximum) for off-normal conditions which can be expected to occur for short periods of time (PWR and BWR), and

3. 125°F extreme ambient temperatures with the HSM inlet and outlet vents postulated to be blocked for a period of five days as described in Section 8.2.7 (PWR is bounding). This design basis condition is designated as an accident condition assumed to occur once in service life of the ISFSI.

The results of these calculations are summarized in Table 8.1-24 (PWR) and Table 8.1-25 (BWR) which shows that the highest temperature regions for the DSC occur on its top surface. The maximum temperature at this location is 399°F (for PWR 125°F extreme ambient temperature). Similarly the HSM ceiling maximum temperature above the DSC is 241°F. During normal operation, the maximum temperature at the top of the DSC is 374°F (for 100°F ambient temperature). During normal operation, the maximum HSM temperature is 201°F (for 100°F ambient case). The HSM normal operation ventilation outlet air maximum temperature is 200°F (for 100°F ambient case).

The DSC shell temperatures used in the DSC internals analyses described in Section 8.1.3.2 are approximately 20°F lower than the maximum DSC shell temperatures reported above. This is justified based on the conservative methodology used in Section 8.1.3.2 for DSC internals temperature distribution calculation. The analyses used a two-dimensional model of the DSC basket that did not take credit for radial conduction heat transfer through the spacer discs.

### 8.1.3.2 Thermal Analysis of the DSC Inside the HSM

For the DSC thermal analyses, the internal basket assembly of the DSC is modeled in detail using HEATING7 code. A worse case, two-dimensional slice of the DSC and fuel cross sections is modeled. Heat transfer effects along the axis of the DSC (third dimension) are conservatively neglected. The DSC is assumed to be cooled through natural convection with the DSC surface specified as a temperature boundary condition equal to that calculated in the HSM thermal analysis. The fuel region inside the DSC is modeled as heat source equal to 1.08 times the nominal decay heat power of 1.0 kW/assembly for PWR fuel and 0.37 kW/assembly for BWR fuel.

The steady state outer surface temperatures for the DSC resting inside the HSM are calculated in the HSM thermal analysis, described in Section 8.1.3.1. The results for each HSM analysis case are used to obtain average DSC surface temperatures for each region in the analytical model representing the DSC cylindrical shell. These surface temperatures are used as boundary conditions for the DSC thermal analysis and are assumed to remain constant.

#### 8.1.3.2.1 NUHOMS®-24P DSC Inside HSM

##### A. Thermal Model of the NUHOMS®-24P DSC

The HEATING7 computer program is used to perform the thermal analysis of the DSC internal basket assembly and spent fuel assembly regions. The analytical model of the DSC contains 115 regions and is shown in Figure 8.1-38, with the individual regions indicated by number. The model includes 12 regions inside the guide sleeves for the spent fuel assemblies, 48 regions for the guide sleeves, 35 regions for the space between the adjacent guide sleeves and the DSC shell, and 20 regions for the DSC shell. The space between the guide sleeves and DSC shell are assumed to be filled with helium. In order to facilitate the thermal stress analysis of the DSC spacer disks, a similar model of the DSC is used with steel in the spaces between the guide sleeves and the DSC shell.

The heat generated in the fuel region is assumed to be transferred to the guide sleeves and through the guide sleeve walls by conduction. For the narrow gaps between adjacent guide sleeves, heat transfer is assumed to occur through conduction and radiation. Convection is conservatively neglected as the Grashof number which corresponds to convection between two parallel plates in an enclosed space is small for the DSC basket geometry. In the physical system, macroscopic convection in these regions and conduction in the axial direction would provide an additional mechanism for heat removal from the DSC, however, these are conservatively neglected. For the space between the horizontal and vertical surfaces of the outer

guide sleeve and the DSC shell, heat is assumed to be transferred through conduction and radiation. Any convection heat transfer in this region is conservatively neglected. Heat transfer through the DSC shell is achieved by conduction.

The base case 5 year cooled PWR fuel decay heat power of 1 kW for each spent fuel assembly is applied as a heat flux uniformly distributed over the fuel regions inside the guide sleeves. The resulting volumetric heat density, including a peaking factor of 1.08, which was applied over the active fuel length of 144 inches is 5.39E-3 Btu/min.-in.$^3$.

An effective thermal conductivity for the fuel region inside the DSC guide sleeve is determined to account for the different materials ($UO_2$, zircaloy and helium) and to include the combined effects of radiation, conduction, and convection. Appendix B describes the derivation of the effective thermal conductivity used to model the fuel region. Effective thermal conductivities are developed for the condition with a vacuum inside the DSC during the drying and helium backfilling operations as shown in Appendix B. A thermal emissivity of 0.587 was used for the radiation between all stainless steel surfaces (8.8).

The resulting calculated temperature profiles for the DSC are used for the evaluation of fuel cladding temperatures, helium temperatures, guide sleeve temperatures, and other DSC internal component temperatures. These temperatures are also used to evaluate the thermal stresses in the DSC shell and the spacer discs.

The maximum DSC shell temperature under all normal, off-normal or accident conditions is 640°F as reported in Table 8.1-26. This maximum temperature occurs on the DSC shell surface at mid-length of the DSC. The temperature at the ends of the DSC for this condition is at least 100°F lower than the maximum DSC shell temperature.

B. Evaluation of NUHOMS®-24P DSC inside the HSM

The DSC and fuel assembly heat transfer analyses with the DSC inside the HSM are performed for the design basis ambient air temperature cases defined in Section 8.1.3. These include a total of four cases corresponding to ambient air entering the HSM at:

1. 70°F and 100°F for normal operating conditions,

2. 125°F for off-normal conditions, and

3. 125°F ambient conditions with the HSM inlet and outlet vents blocked for 5 days as described in Section 8.2.7.

Since the principal cases of interest are those which maximize the fuel cladding temperatures, the DSC thermal analyses are limited to evaluating summer ambient conditions as described in Section 8.1.3.1. From these analysis results, key temperatures are extracted and summarized in

Table 8.1-26. The results obtained from the HEATING7 analysis are in the form of temperature profiles for the DSC cross-section.

The back wall of the HSM facing the DSC top end does not require a heat shield. As noted above, the maximum temperature of the DSC shield plugs is substantially less than the DSC shell at mid-length. In addition, ventilation air flows in the gap between the DSC and the HSM back wall acts to cool the concrete and DSC end assembly. The resulting HSM back wall temperatures are bounded by the HSM side wall and/or ceiling concrete temperatures. The maximum temperature of the HSM back wall concrete is less than 150°F for the 100°F ambient case which is well within acceptable limits.

From the 70°F ambient temperature profile in Figure 8.1-40 for the DSC, it can be observed that the maximum temperatures occur for the fuel regions in the centermost guide sleeves just above the horizontal center line of the DSC. The maximum temperature occurs slightly above the midplane because the lower half of DSC shell is at a lower temperature than is the upper half. Also the DSC temperature distribution is not symmetric for the fuel assemblies located further from the central region of the DSC.

For the fuel assemblies located towards the outer edge of the DSC (i.e., fuel assemblies #1, 6, 7, 10, 11, and 12 in Figure 8.1-1), the boundary temperature is higher than the central region. The reason for this temperature distribution is that the heat flow is from the fuel assemblies/guide sleeves located in the center of the DSC to the fuel assemblies/guide sleeves located on the perimeter of the DSC. Heat is then removed from the DSC outer surface by natural convection and radiation. As a result, the outer-most fuel assemblies experience temperatures which are far below the bounding fuel clad temperature for the central fuel assemblies with the guide sleeve temperatures elevated above those of the corresponding fuel assemblies.

The fuel assemblies located toward the center of the DSC (i.e., fuel assemblies #3 and #4 in Figure 8.1-1) show temperature profiles with peak temperatures at the center fuel region. This type of temperature distribution can also be observed in the test results and was predicted by the COBRA-SFS Code as documented in Reference 7.10. As shown in Figure 5-29 of the reference report, the temperature distribution for the central fuel assembly is symmetrical with the maximum temperature occurring at the center. For the fuel assemblies located on the boundary of the DSC basket there is less symmetry.

For variations in ambient air temperatures for normal operating conditions, the maximum calculated fuel clad temperatures for the base case 5 year cooled PWR fuel varies from 700°F (371°C) for 70°F ambient air, to 711°F (377°C) for 100°F ambient air. The maximum cladding temperature of 700°F (371°C), corresponding to 70°F lifetime average ambient temperature, is below the design basis initial storage temperature limit of 724°F (384°C) defined in Section 3.3.7.1 for long term dry storage. For extreme ambient conditions, or short term operating conditions, the maximum fuel cladding temperature ranges from 720°F (382°C) to 909°F (487°C). These values are well below the short term temperature limit of 1058°F (570°C) defined in Section 3.3.7.1. Plots of maximum fuel cladding temperature versus DSC shell

temperature are shown in Figure 8.1-45. The corresponding DSC internal pressures are listed in Table 8.1-6.

8.1.3.2.2 NUHOMS®-52B DSC Inside HSM

A. Thermal Model of the NUHOMS®-52B DSC

The HEATING7 computer program is used to perform the thermal analysis of the NUHOMS®-52B DSC internal basket assembly and spent fuel regions in the same manner as that performed for the NUHOMS®-24P DSC as described in Section 8.1.3.2.1. The analytical model of the DSC contains 278 regions and is shown in Figure 8.1-39, with the individual regions indicated by number. The model includes 26 regions inside the fuel channels for the spent fuel assemblies, 104 regions for the channels, 85 regions for the space between the adjacent channels and the DSC shell, 43 regions for neutron absorber plates, and 20 regions for the DSC shell.

The base case 5 year cooled BWR fuel decay heat power of 0.37 kW for each fuel assembly is applied as a heat flux uniformly distributed over the fuel regions inside the fuel channels. The resulting volumetric heat density, including a peaking factor of 1.08, which is applied over the active fuel length of 142.24 inches is 5.70E-3 Btu/min.-in.$^3$. The remaining aspects of the NUHOMS®-52B DSC thermal model are described in Section 8.1.3.2.2.

The maximum NUHOMS®-52B DSC shell temperature under all normal, off-normal or accident conditions is 640°F as reported in Table 8.1-27.

B. Evaluation of NUHOMS®-52B DSC inside the HSM

The NUHOMS®-52B and fuel assembly heat transfer analyses with the DSC inside the HSM is performed in the same manner for the same ambient conditions as that for the NUHOMS®-24P DSC as described in Section 8.1.3.2.1. The results from these analyses are summarized in Table 8.1-27. The corresponding HEATING7 temperature profile for the 70°F ambient case is shown in Figure 8.1-41.

The distribution of fuel cladding temperatures for the 70°F and 100°F ambient cases are shown in Figure 8.1-3 and Figure 8.1-4. The maximum calculated fuel cladding temperatures for the base case 5 year cooled BWR fuel varies from 725°F (385°C), for 70 ambient air to 735°F (391°C), for 100°F ambient air. The maximum cladding temperature of 725°F (385°C), corresponding to the 70°F lifetime average ambient temperature, is below the design basis initial storage temperature limit of 790°F (421°C) defined in Section 3.3.7.1 for long term dry storage. For extreme ambient conditions or short term operating conditions, the maximum fuel cladding temperature ranges from 734°F (395°C) to 988°F (531°C). These values are less than the short term temperature limit of 1058°F (570°C) defined in Section 3.3.7.1. Plots of maximum fuel cladding temperature versus DSC shell temperature are shown in Figure 8.1-46. The corresponding DSC internal pressures are listed in Table 8.1-7.

8.1.3.3 Thermal Analysis of the DSC Inside the Transfer Cask

8.1.3.3.1 NUHOMS®-24P DSC Inside Transfer Cask

A. NUHOMS®-24P DSC in Cask During Transport

The cylindrical transfer cask and DSC shell are modeled as long composite cylinders with the cross section configuration shown in Figure 8.1-42. Full contact between all cask materials (steel, lead, and solid neutron shield) is assumed. When the transfer cask is in the horizontal position, the DSC outer surface is assumed to be in contact with the transfer cask inner liner. Two separate models are developed to determine the radial and circumferential temperature distribution at various composite regions of the transfer cask. The first model is for the bottom half of the transfer cask cross-section where the DSC outer surface is assumed to be in contact with the transfer cask inner liner. The second model is for the top half of the transfer cask cross-section with the gap between the DSC outer surface and the top region of the transfer cask inner liner at its maximum value.

The transfer cask is evaluated for a range of ambient temperatures including the normal, off-normal, and postulated accident conditions which are described in Section 8.1.3.1. The ambient conditions include:

1. 0°F to 100°F for normal operating conditions, and

2. -40°F and 125°F for off-normal and accident conditions.

The total decay heat power for the base case 5 year cooled PWR spent fuel assemblies of 24 kW/DSC is uniformly distributed over the inner cavity surface area of the DSC. The solar heat flux is conservatively neglected for winter ambient conditions to maximize the transfer cask through wall temperature gradient.

The temperatures of the DSC shell outer surface, through the wall thickness of the transfer cask, and the transfer cask outer surface are determined by performing a heat balance analysis for the applied decay heat power and the ambient air conditions, including the effects of solar heating as applicable. The enveloping solar heat flux of 62 Btu/hr.-ft.$^2$°F for the normal case (8.59) is used. A steady state heat balance analysis is performed to determine the temperatures at which the heat flow equals the convection and radiation heat loss from the outer surface of the transfer cask as follows (8.8):

$$\dot{Q} = \left[0.18\left(T_{out} - T_{air}\right)^{4/3} + 0.1714x10^{-8}\,\varepsilon\ldots\left(T_{out}^4 - T_{air}^4\right)\right]A_o \qquad (8.1\text{-}16)$$

Where:

$\varepsilon$ = 0.587 (for cask emissivity)

$0.1714 \times 10^{-8}$ = Stefan-Boltzmann constant

$A_o$ = Cask outer surface area, including ends

$T_{out}$ = Cask outer surface temperature

The conduction heat transfer from the transfer cask outer surface is conservatively neglected. Equation (8.1-16) is solved iteratively for each ambient air condition to obtain

$$\Delta T = T_{out} - T_{air}$$

To obtain the surface temperatures, $T_{in}$, on the inner liner of the transfer cask the steady state heat transfer relationship for a composite cylinder is used (8.57).

$$(T_{in} - T_{out}) = \frac{\dot{Q}}{2\pi L} \sum_{n=1}^{n} \frac{\ln\left(\frac{r_n + 1}{r_n}\right)}{K_n} \qquad (8.1\text{-}17)$$

Where: $r_1$, $r_2$, $r_3$ $r_4$, $r_5$, $r_6$ and $r_7$ are the radii for the regions through the cask wall as shown in Figure 8.1-42.

In the top half model of the transfer cask shown in Figure 8.1-42, to calculate the DSC outer surface temperature ($T_{DSC}$), conduction, convection and radiation heat transfer from the DSC inner surface through the DSC shell and the air gap to the transfer cask inner liner are evaluated. The heat loss through the gap is calculated using the 0.75 inch maximum air gap.

$$\dot{Q} = \frac{0.1714 \times 10^{-8} A_{DSC}\left(T_{DSC}^4 - T_{in}^4\right)}{1/\varepsilon_1 + \frac{r_1}{r_2}(1/\varepsilon_2 - 1)} + \frac{K_e 2\pi L}{\ln\left(\frac{r_2}{r_1}\right)} (T_{DSC} - T_{in}) \qquad (8.1\text{-}18)$$

Where:

$\varepsilon_2$ = 0.587 = $\varepsilon_1$ for stainless steel surfaces

$r_1$ = Outside radius of DSC

$r_2$ = Inside radius of the cask

$A_{DSC}$ = DSC outside total surface area = $2\pi r_1 L + 2\pi r_1$

$K_e$ = Temperature dependent effective thermal conductivity

The $K_e$ is evaluated at the average fluid temperature in the gap.

An iterative solution of equation 8.1-18 provides the DSC outer surface temperature value ($T_{DSC}$) for the top half of the DSC.

For the bottom half model of the transfer cask shown in Figure 8.1-42, complete contact between the DSC outer surface and the lower region of the transfer cask inner liner is assumed. Equation 8.1-17 is then used to determine the DSC outer surface temperature value ($T_{DSC}$) for the bottom half of the DSC.

An analysis is performed for normal, off-normal, and accident summer ambient conditions, including the effect of a solar heat flux applied to the cask outer surface for the base case 5 year cooled PWR fuel. The resulting through wall thermal gradients for the transfer cask for the normal and off-normal conditions are summarized in Table 8.1-28 for the standardized cask and Table 8.1-29a for the OS197 cask. As discussed previously, the 125°F ambient case does not include any solar heat flux and is therefore bounded by the 100°F case for the standardized cask. Also, as discussed in Section 8.2.5.3, complete loss of neutron shield for the solid neutron shield material is not a credible event. Therefore, the 125°F off-normal and accident thermal cases are bounded by the 100°F case and are not considered further. For the case of a liquid neutron shield (OS197 Cask), a complete loss of neutron shield was evaluated. The results are discussed in Section 8.2.5.3. The OS197 Cask was also evaluated for the 125°F ambient case without solar heat flux. The resulting temperature gradients were used to perform a thermal stress analysis of the transfer cask as discussed in 8.1.1.9.

The resulting temperatures for the DSC outer surface are used as temperature boundary conditions for the heat transfer analyses of the DSC internals to confirm that short term fuel clad temperatures during transport from the plant's fuel handling building to the HSM remain below 570°C. The analytical models and the methodology used to perform the heat transfer analyses to determine the temperatures of the DSC internals and the fuel cladding are discussed in Section 8.1.3.2.

B. NUHOMS®-24P DSC in Cask During Draining and Drying

The methodology used to evaluate the heat transfer effects which occur during transport of the DSC (inside the transfer cask) from the plant's fuel handling building to the ISFSI, where the DSC is transferred for storage, are discussed in the previous paragraphs. Other conditions during the NUHOMS® system operations also result in heat transfer effects on the system components. These include placement of the DSC and transfer cask in the plant's fuel pool, loading of spent fuel into the DSC, seal welding of the DSC, draining and vacuum drying of the DSC, and backfilling the DSC with helium. Of these conditions, vacuum drying is the most severe since heat conduction in the cavity of the DSC filled with helium is minimized.

For the DSC inside the transfer cask, increased temperature conditions are encountered during the vacuum drying process. An analysis of the transfer cask and DSC is performed to determine the temperature distribution and the maximum fuel cladding temperature for this condition. The analytical methods used for this analysis are similar to those discussed in Sections 8.1.3.2 and 8.1.3.3. The cask and DSC are oriented vertically for this operation and the DSC cavity is dried

by pulling a vacuum. The resulting through wall thermal gradients in the transfer cask are bounded by those calculated in Section 8.1.3.3 and as such are not evaluated further. The maximum fuel cladding temperature calculated for this condition is 909°F (487°C) which is well below the 570°C short term temperature limit.

8.1.3.3.2 NUHOMS®-52B DSC Inside Transfer Cask

A. NUHOMS®-52B DSC in Cask During Transport

The thermal analysis of the NUHOMS®-52B DSC inside the transfer cask is performed using the same methodology for the same conditions as that for the NUHOMS®-24P DSC described in Section 8.1.3.3.1. The resulting through wall thermal gradients for the standardized transfer cask for the normal and off-normal conditions are summarized in Table 8.1-29. The thermal analysis results for the NUHOMS®-52B DSC inside the OS197 are enveloped by the results for the NUHOMS®-24P DSC which are presented in Table 8.1-29a.

B. NUHOMS®-52B DSC in Cask During Draining and Drying

The thermal analysis of the NUHOMS®-52B DSC internals for the increased temperature conditions which occur during vacuum drying is performed in the same manner as that for the NUHOMS®-24P DSC described in Section 8.1.3.3.1. The resulting maximum fuel cladding temperature for this condition is 988°F (531°C) which is within the short term temperature range of 1058°F (570°C) defined in Section 3.3.7.1.

**Table 8.1-1**
**NUHOMS® Normal Operating Loading Identification**

| Load Type | Affected Component | | | | |
|---|---|---|---|---|---|
| | DSC Shell Assembly | DSC Internals | DSC Support Structure | Reinforced Concrete HSM | On-site Transfer Cask |
| Dead Weight | X | X | X | X | X |
| Internal/External Pressure | X | | | | |
| Normal Thermal | X | X | X | X | X |
| Normal Handling | X | X | X | X | X |
| Live Loads | | | | X | X |

**Table 8.1-2**
**NUHOMS® Off-Normal Operating Loading Identification**

| Load Type | Affected Component | | | | |
|---|---|---|---|---|---|
| | DSC Shell Assembly | DSC Internals | DSC Support Structure | Reinforced Concrete HSM | On-site Transfer Cask |
| Dead Weight | X | X | X | X | X |
| Internal/External Pressure | X | | | | |
| Off-Normal Thermal | X | X | X | X | X |
| Off-Normal Handling | X | X | X | X | X |

**Table 8.1-3**
**Mechanical Properties of Materials**

| Material | Temperature (°F) | Stress Properties[1] (ksi) | | | Elastic Modulus[1] (x1.0E3 ksi) (E) | Average Coefficient of Thermal Expansion[1] ($x10^{-6}$ in./in.-°F) |
|---|---|---|---|---|---|---|
| | | Stress Intensity ($S_m$) | Yield Strength ($S_y$) | Ultimate Strength ($S_u$) | | |
| Stainless Steel ASME SA240 Type 304 | 70 | - | 30.0 | 75.0 | 28.3 | -- |
| | 100 | 20.0 | 30.0 | 75.0 | -- | 8.55 |
| | 200 | 20.0 | 25.0 | 71.0 | 27.6 | 8.79 |
| | 400 | 18.7 | 20.7 | 64.4 | 26.5 | 9.19 |
| | 500 | 17.5 | 19.4 | 63.5 | 25.8 | 9.37 |
| | 600 | 16.4 | 18.2 | 63.5 | 25.3 | 9.53 |
| | 700 | 16.0 | 17.7 | 63.5 | 24.8 | 9.69 |
| Stainless Steel ASME SA479 Type XM-19[10] | -100 | 33.3 | 55.0 | 100.0 | 29.1 | -- |
| | -20 | 33.3 | 55.0 | 100.0 | -- | -- |
| | 70 | -- | -- | -- | 28.3 | -- |
| | 100 | 33.3 | 55.0 | 100.0 | -- | 8.30 |
| | 200 | 33.2 | 47.0 | 99.5 | 27.6 | 8.48 |
| | 400 | 30.2 | 40.8 | 90.7 | 26.5 | 8.79 |
| | 500 | 29.7 | 38.8 | 89.1 | 25.8 | 8.92 |
| | 600 | 29.2 | 37.3 | 87.8 | 25.3 | 9.03 |
| | 700 | 28.8 | 36.3 | 86.5 | 24.8 | 9.15 |

**Table 8.1-3**
**Mechanical Properties of Materials**

(continued)

| Material | Tempera-ture (°F) | Stress Properties[1] (ksi) | | | Elastic Modulus[1] (x1.0E3 ksi) (E) | Average Coefficient of Thermal Expansion[1] ($x10^{-6}$ in./in.-°F) |
|---|---|---|---|---|---|---|
| | | Stress Intensity ($S_m$) | Yield Strength ($S_y$) | Ultimate Strength ($S_u$) | | |
| Carbon[7] Steel ASTM A36 | 70 | - | 36.0 | 58.0 | 29.5 | -- |
| | 100 | 19.3 | 36.0 | 58.0 | - | 5.53 |
| | 200 | 19.3 | 32.8 | 58.0 | 28.8 | 5.89 |
| | 400 | 19.3 | 30.8 | 58.0 | 27.7 | 6.61 |
| | 500 | 19.3 | 29.1 | 58.0 | 27.3 | 6.91 |
| | 600 | 17.7 | 26.6 | 58.0 | 26.7 | 7.17 |
| | 700 | 17.3 | 25.9 | 58.0 | 25.5 | 7.41 |
| Carbon[8][9] Steel ASME SA516 Grade 70 | 70 | 23.3 | 38.0 | 70.0 | 29.5 | -- |
| | 100 | 23.3 | 38.0 | 70.0 | -- | 5.53 |
| | 200 | 23.1 | 34.6 | 70.0 | 28.8 | 5.89 |
| | 400 | 21.7 | 32.6 | 70.0 | 27.7 | 6.61 |
| | 500 | 20.5 | 30.7 | 70.0 | 27.3 | 6.91 |
| | 600 | 18.7 | 28.1 | 70.0 | 26.7 | 7.17 |
| | 700 | 18.3 | 27.4 | 70.0 | 25.5 | 7.41 |

**Table 8.1-3**
**Mechanical Properties of Materials**

(continued)

| Material | Tempera-ture (°F) | Stress Properties[1] (ksi) | | | Elastic Modulus[1] (x1.0E3 ksi) (E) | Average Coefficient of Thermal Expansion[1] ($x10^{-6}$ in./in.-°F) |
|---|---|---|---|---|---|---|
| | | Stress Intensity ($S_m$) | Yield Strength ($S_y$) | Ultimate Strength ($S_u$) | | |
| Precipitation Hardened Steel ASME SA564 Type 630[11] | 70 | -- | -- | -- | 28.3 | -- |
| | 100 | 46.7 | 115.0 | 140.0 | -- | 5.89 |
| | 200 | 46.7 | 106.3 | 140.0 | 27.6 | 5.90 |
| | 400 | 45.5 | 98.3 | 136.3 | 26.5 | 5.91 |
| | 500 | 44.4 | 95.2 | 133.2 | 25.8 | 5.91 |
| | 600 | 43.8 | 92.8 | 131.4 | 25.3 | 5.93 |
| | 700 | -- | -- | -- | 24.8 | 5.94 |
| Carbon Steel ASME SA537 Class 2[8] Plate $2^1/_2$" < t < 4" | 70 | -- | -- | -- | 29.5 | -- |
| | 100 | 25.0 | 55.0 | 75.0 | -- | 5.53 |
| | 200 | 25.0 | 50.5 | 75.0 | 28.8 | 5.89 |
| | 400 | 24.7 | 45.8 | 74.4 | 27.7 | 6.61 |
| | 500 | 24.7 | 43.7 | 74.4 | 27.3 | 6.91 |
| | 600 | 24.7 | 43.0 | 74.4 | 26.7 | 7.17 |
| | 700 | 24.3 | 40.8 | 72.9 | 25.5 | 7.41 |

**Table 8.1-3**
**Mechanical Properties of Materials**

(continued)

| Material | Tempera-ture (°F) | Stress Properties[1] (ksi) | | | Elastic Modulus[1] (x1.0E3 ksi) (E) | Average Coefficient of Thermal Expansion[1] ($x10^{-6}$ in./in.-°F) |
|---|---|---|---|---|---|---|
| | | Stress Intensity ($S_m$) | Yield Strength ($S_y$) | Ultimate Strength ($S_u$) | | |
| Transfer Cask[5] Lifting Trunnions SA564 Type 630[9] | 70 | 45.0 | 105.0 | 135.0 | 28.3 | -- |
| | 100 | 45.0 | 105.0 | 135.0 | 28.1 | 5.89 |
| | 200 | 45.0 | 97.1 | 135.0 | 27.6 | 5.90 |
| | 400 | 43.8 | 89.8 | 131.4 | 26.5 | 5.91 |
| | 500 | 42.8 | 87.0 | 128.5 | 25.8 | 5.91 |
| | 600 | 42.1 | 87.7 | 126.7 | 25.3 | 5.93 |
| Cask Lifting Trunnion Sleeves[9] SA508 Class 3A | 70 | 30.0 | 65.0 | 90.0 | 29.2 | -- |
| | 100 | 30.0 | 65.0 | 90.0 | 29.0 | 6.50 |
| | 200 | 30.0 | 61.8 | 90.0 | 28.5 | 6.67 |
| | 400 | 30.0 | 59.0 | 90.0 | 27.4 | 7.07 |
| | 500 | 30.0 | 58.0 | 90.0 | 27.0 | 7.25 |
| | 600 | 30.0 | 57.1 | 90.0 | 26.4 | 7.42 |
| OS197 Lifting Trunnion Sleeves SA182 Type F304N | 70 | 23.3 | 35.0 | 80.0 | 28.3 | -- |
| | 100 | 23.3 | 35.0 | 80.0 | -- | 8.55 |
| | 200 | 23.3 | 28.7 | 80.0 | 27.6 | 8.79 |
| | 400 | 20.3 | 22.5 | 73.2 | 26.5 | 9.19 |
| | 500 | 18.8 | 20.9 | 71.2 | 25.8 | 9.37 |
| | 600 | 17.8 | 19.8 | 69.7 | 25.3 | 9.53 |

**Table 8.1-3**
**Mechanical Properties of Materials**

(continued)

| Material | Temperature (°F) | 28 Day Compressive Strength (ksi) | Modulus of Elasticity (1.0E3 ksi) |
|---|---|---|---|
| Concrete Normal Wt.[2] 5000 psi Strength | 100 | 5.0 | 4.0 |
| | 200 | 5.0 | 3.6 |
| | 300 | 4.8 | 3.3 |
| | 400 | 4.5 | 3.0 |
| | 500 | 4.5 | 2.9 |

| Material | Temperature (°F) | Yield Strength (ksi) | Modulus of Elasticity (1.0E3 ksi) |
|---|---|---|---|
| Reinforcing Steel[2] ASTM A615 Grade 60 | 100 | 60.0 | 29.0 |
| | 200 | 57.0 | 28.4 |
| | 300 | 54.0 | 27.8 |
| | 400 | 51.0 | 27.3 |
| | 500 | 51.0 | 27.0 |

| Solid Neutron Shielding Material[4] | Poisson Ratio | Compressive Strength (ksi) | Modulus of Elasticity (1.0E3 ksi) |
|---|---|---|---|
| BISCo NS-3 | 0.2 | 3.9 | 0.16 |

**Table 8.1-3**
**Mechanical Properties of Materials**

(continued)

| Material | Temperature (°F) | Allowable Stress Values for Class 2[1] Components (S) (ksi) | Yield Strength[1] (ksi) |
|---|---|---|---|
| Structural Bolting Material ASTM A325 | 100 | 20.2 | 81.0 |
| | 200 | 20.2 | 73.9 |
| | 400 | 20.2 | 69.3 |
| Transfer Cask Bolting Materials ASME SA-193 Grade B7 | -40 | 25.0 | 105.0 |
| | +70 | 25.0 | 105.0 |
| | +100 | 25.0 | 98.0 |
| | +200 | 25.0 | 94.1 |
| | +400 | 25.0 | 91.5 |
| | +500 | 25.0 | 88.5 |
| | +600 | 25.0 | 85.3 |

| Material | Yield Strength (ksi) | Tensile Strength (ksi) | Modulus of Elasticity ($1x10^6$ psi) | Coefficient of Linear Expansion ($x10^{-6}$ in./in.-°F) | Approximate Melting Point (°F) |
|---|---|---|---|---|---|
| Chemical Lead | 1.9 | 2.5 | 2 | 16.4 | 621 |

| Material | Stress Properties (ksi) | | Charpy V-Notch Energy (ft-lb) |
|---|---|---|---|
| | Yield Strength ($S_y$) | Ultimate Strength ($S_u$) | |
| Borated Stainless Steel Neutron Absorber Material ASTM A887 Type 304 B3 Grade A or B | 30.0 | 75.0 | 10 |

**Table 8.1-3**
**Mechanical Properties of Materials**

(concluded)

(1) Steel data and thermal expansion coefficients are obtained from ASME Boiler and Pressure Vessel Code, Section III-1 Appendices. (8.3)

(2) Concrete and reinforcing steel data were obtained from Handbook of Concrete Engineering, by Mark Fintel. (8.22)

(3) Lead data was obtained from CRC Handbook of Tables for Applied Engineering Science, 2nd Edition, pp. 111 and 118. (8.4)

(4) Data obtained from manufacturers published information.

(5) Age hardened at 1150°F in accordance with notes of ASME Code, Appendix I, Table I-1.1, I-2.1 and I-3.1.

(6) Deleted

(7) Allowable stress intensity values ($S_m$) and the yield strength ($S_y$) for ASTM A36 steel are given in Table I-11.1 and Table I-13.1, respectively, of the ASME Boiler and Pressure Vessel Code, Section III, Division 1, Appendix I.

(8) Carbon steel DSC basket materials shall be impact tested in accordance with ASME Code Subsection NF Article NF-2300. Impact test temperature is -20°F.

(9) Carbon steel transfer cask structural shell, trunnion sleeves, and trunnion materials shall be impact tested in accordance with ASME Code Subsection NC Article NC-2300. The lowest service temperature is 0°F.

(10) ASME SA479 Type XM-19 material is age hardened/annealed at 1925°F to 1975°F.

(11) ASME SA564 Type 630 material for 52B Support Rods and Spacer Sleeves is age hardened at 1100°F. Support rod material shall be impact tested in accordance with ASME Code, Section II. Impact Test temperature is –20°F.

**Table 8.1-4**
**Estimated NUHOMS®-24P Component Weights**

| | Component Description | Calculated Weight (Pounds) |
|---|---|---|
| 1. | Dry Shielded Canister Shell Assembly | 15,778 |
| 2. | DSC Top Shield Plug | 7,859 |
| 3. | DSC Internal Basket Assembly | 12,189 |
| 4. | DSC Inner and Outer Top Cover Plates | 1,934 |
| 5. | 24 PWR Spent Fuel Assemblies | ≤40,368[4] |
| 6. | Weight of Water in DSC Cavity | 14,843 |
| | Total Wet DSC Loaded Weight (w/o DSC inner and outer top cover plates.) | 91,038 |
| | Total Dry DSC Loaded Weight (w/ DSC inner and outer top cover plates.) | 78,129 |
| 7. | Standardized Transfer Cask Empty Weight | 107,091[1][3] |
| 8. | Standardized Transfer Cask Max. Loaded Weight | 193,642[2][5] |
| 9. | HSM Single Module Weight, Model 80 (empty) | 243,000 |
| 10. | HSM Single Module Weight, Model 102 (empty) | 248,000 |

(1) Includes weight of cask top cover plate assembly.
(2) Weight includes: DSC dry weight plus fuel, plus water in DSC and cask less DSC and cask top cover plate assemblies.
(3) The as-built empty weight for the OS197 transfer cask is 111,250 lbs, including neutron shield water.
(4) The standard design DSC fuel assembly weight of 1,682 lbs/assembly is used.
(5) The maximum loaded weight for the OS197 transfer cask without DSC and OS197 top cover plates is 199,372 lbs.

**Table 8.1-5**
**Estimated NUHOMS®-52B Component Weights**

| | Component Description | Calculated Weigh (Pounds) |
|---|---|---|
| 1. | Dry Shielded Canister Shell Assembly | 15,658 |
| 2. | DSC Top Shield Plug | 7,621 |
| 3. | DSC Internal Basket Assembly | 12,012 |
| 4. | DSC Inner and Outer Top Cover Plates | 1,934 |
| 5. | 52 BWR Spent Fuel Assemblies | ≤37,700 |
| 6. | Weight of Water in DSC Cavity | 16,211 |
| | Total Wet DSC Loaded Weight (w/o DSC inner and outer top cover plates.) | 89,202 |
| | Total Dry DSC Loaded Weight (w/ DSC inner and outer top cover plates.) | 74,925 |
| 7. | Standardized Transfer Cask Empty Weight (w/collar) | 113,501[(1)(3)] |
| 8. | Standardized Transfer Cask Max. Loaded Weight | 198,294[(2)(4)] |
| 9. | HSM Single Module Weight, Model 80 (empty) | 252,000 |
| 10. | HSM Single Module Weight, Model 102 (empty) | 257,000 |

(1) Includes weight of cask top cover plate assembly.
(2) Weight includes: DSC dry weight plus fuel, plus water in DSC and cask less DSC and cask top cover plate assemblies.
(3) The as-built empty weight of the OS197 transfer cask is 111,250 pounds, including water in the neutron shield.
(4) The maximum loaded weight for the OS197 transfer cask without DSC and cask top cover plates is 196,197 lb.

**Table 8.1-6**
**NUHOMS®-24P DSC Operating and Accident Pressures[5] (w/o BPRAs)**

| Operating Condition | Limiting Case Description | Max DSC Pressure[4] (psia) | Max Total DSC Pressure (psia) | Design Basis Pressure (psia) |
|---|---|---|---|---|
| Normal | DSC in Cask, 100°F | 21.4 | 21.7[1] | 24.7 |
| Off-Normal | DSC in Cask, 100°F | 21.4 | 24.8[2] | 24.7 |
| Accident | Blocked HSM vents, 125°F | 26.8 | 73.4[3] | 74.7 |

(1) Normal operating total pressure with 1% of fuel rod cladding failure.
(2) Off-normal operating total pressure with 10% of fuel rod cladding failure. The calculated pressure exceeds the design basis pressure by 0.1 psig. This is acceptable based on paragraph NB-3223(a) of ASME Section III, Subsection NB.
(3) Enveloping accident total pressure with 100% of fuel rod cladding failure.
(4) Total DSC internal pressure without any fuel rod cladding failure.
(5) Maximum 24P DSC internal pressures for Normal, Off-Normal and Accident conditions when storing fuel with BPRAs are presented in Appendix J.

**Table 8.1-7**
**NUHOMS®-52B DSC Operating and Accident Pressures**

| Operating Condition | Limiting Case Description | Max DSC Pressure[4] (psia) | Max Total DSC Pressure (psia) | Design Basis Pressure (psia) |
|---|---|---|---|---|
| Normal | DSC in Cask, 100°F | 21.0 | 21.1[1] | 24.7 |
| Off-Normal | DSC in Cask, 100°F | 21.0 | 22.8[2] | 24.7 |
| Accident | Blocked HSM vents, 125°F | 24.7 | 45.8[3] | 74.7 |

(1) Normal operating total pressure with 1% of fuel rod cladding failure.
(2) Off-normal operating total pressure with 10% of fuel rod cladding failure
(3) Enveloping accident total pressure with 100% of fuel rod cladding failure.
(4) Total DSC internal pressure without any fuel rod cladding failure.

**Table 8.1-8**
**Thermophysical Properties of Materials**

| Material | Effective Thermal Conduct. (k) (Btu/h-ft-°F) | Density (lb./ft.$^3$) | Specific Heat ($C_P$) (Btu/lb.-°F) | Emissivity (e) Fraction |
|---|---|---|---|---|
| Carbon Steel | Table 8.1-9 Ref [8.3] | 490 Ref [8.57] | 0.11 Ref [8.57] | 0.21[(1)] $0.21 \leq e \leq 1.0$[(2)] Ref [8.66] |
| Concrete | Table 8.1-9 Ref [8.11] | 140 Ref [8.11] | 0.25 Ref [8.7] | 0.9 Ref [8.11] |
| Stainless Steel | Table 8.1-9 Ref [8.3] | 493 Ref [8.56] | Table 8.1-9 Ref [8.4] | 0.587 Ref [8.8] |
| Lead | Table 8.1-9 Ref [8.57] | 705 Ref [8.57] | 0.03 Ref [8.57] | -- |
| Soil | 0.5 Ref [8.28] | 112.5 Ref [8.28] | 0.225 Ref [8.28] | -- |
| BISCo NS-3 | 0.488 Ref [8.63] | 110.0 Ref [8.63] | -- -- | -- -- |

(1) Galvanized Carbon Steel
(2) Painted galvanized carbon steel surface

**Table 8.1-9**
**Temperature Dependent Thermophysical Properties**

| Temperature (°F) | Density (lb./cu.ft.) | Specific Heat (Btu/lb.-°F) | Thermal Conductivity (Btu/h-ft.-°F) |
|---|---|---|---|
| Stainless Steel | | | |
| -60 | | 0.100 | 7.7 |
| 140 | | 0.115 | 8.95 |
| 640 | 493 | 0.135 | 11.50 |
| 1000 | | 0.143 | 13.20 |
| 1640 | | 0.156 | 15.6 |
| Carbon Steel | | | |
| 100 | 490 | 0.11 | 23.9 |
| 200 | | | 24.4 |
| 500 | | | 23.1 |
| 1000 | | | 20.0 |
| Lead | | | |
| 32 | 708 | 0.03 | 20.10 |
| 212 | | | 19.00 |
| 572 | | | 18.00 |
| Concrete | | | |
| 100 | 140 | 0.25 | 1.17 |
| 200 | | | 1.14 |
| 500 | | | 1.04 |
| 1000 | | | 0.80 |
| Helium (8.7) | | | |
| 45 | 0.01116 | 1.24 | 0.0831 |
| 80 | 0.01016 | 1.24 | 0.0866 |
| 260 | 0.00762 | 1.24 | 0.1037 |
| 350 | 0.00685 | 1.24 | 0.11252 |
| 495 | 0.00578 | 1.24 | 0.1283 |
| 1520 | 0.00277 | 1.24 | 0.2248 |
| Zircaloy (8.64) | | | |
| 100 | | | 6.82 |
| 400 | | | 7.11 |
| 800 | - | - | 7.64 |
| 1000 | | | 7.96 |
| 1100 | | | 8.13 |

**Table 8.1-9**
**Temperature Dependent Thermophysical Properties**

(concluded)

| Temperature °F | Density (lb./cu. ft.) ρ | Viscosity (sq. ft./s) υ | Specific Heat (Btu/lb.-°F) ($C_p$) | Thermal Conductivity (Btu/h-ft.-°F) k | Prandtl Number Pr |
|---|---|---|---|---|---|
| Air (8.57) | | | | | |
| 0 | 0.086 | 0.00013 | 0.239 | 0.0133 | 0.73 |
| 32 | 0.081 | 0.000145 | 0.240 | 0.0140 | 0.72 |
| 100 | 0.071 | 0.000180 | 0.240 | 0.0154 | 0.72 |
| 200 | 0.060 | 0.000239 | 0.241 | 0.0174 | 0.72 |
| 300 | 0.052 | 0.000306 | 0.243 | 0.0193 | 0.71 |
| 400 | 0.046 | 0.000378 | 0.245 | 0.0212 | 0.689 |
| 500 | 0.0412 | 0.000455 | 0.247 | 0.0231 | 0.683 |
| 1000 | 0.0271 | 0.000917 | 0.262 | 0.0319 | 0.713 |

**Table 8.1-10**
**Maximum NUHOMS®-24P DSC Stresses for Normal and Off-Normal Loads**

| DSC Components | Stress Type | Maximum Stress Intensity (ksi)[1] | | | |
|---|---|---|---|---|---|
| | | Dead Weight | Internal Pressure [2] | Thermal [2] | Handling [2] |
| DSC Shell | Primary Membrane | 2.63 | 1.71 | N/A | 12.10 |
| | Membrane + Bending | 3.04 | 3.71 | N/A | 17.21 |
| | Primary + Secondary[5] | 2.74 | 14.71[6] | 32.19 | 19.69 |
| Inner Top Cover Plate | Primary Membrane | 0.76 | 1.18[6] | N/A | 1.81 |
| | Membrane + Bending | 2.19 | 12.07[6] | N/A | 2.05 |
| | Primary + Secondary[5] | 2.10 | 15.19[6] | 24.88 | 2.06 |
| Outer Top Cover Plate | Primary Membrane | 1.20 | 2.27 | N/A | 0.16 |
| | Membrane + Bending | 1.85 | 7.76 | N/A | 0.39 |
| | Primary + Secondary [5] | 1.27 | 6.94 | 23.85 | 0.36 |

See End of Table for Notes.

**Table 8.1-10**
**Maximum NUHOMS®-24P DSC Stresses for Normal and Off-Normal Loads**

(concluded)

| DSC Components | Stress Type | Maximum Stress Intensity (ksi)[1] | | | |
|---|---|---|---|---|---|
| | | Dead Weight | Internal Pressure [2] | Thermal [2] | Handling [2] |
| Inner Bottom Cover Plate | Primary Membrane | 0.71 | 0.36[6] | N/A | 15.66 |
| | Membrane + Bending | 0.83 | 0.92[6] | N/A | 25.49 |
| | Primary + Secondary[5] | 0.82 | 13.2 [6] | 27.99 | 25.49[3] |
| Outer Bottom Cover Plate | Primary Membrane | 0.71 | 0.45 | N/A | 16.87 |
| | Membrane + Bending | 1.21 | 0.81 | N/A | 31.13 |
| | Primary + Secondary[5] | 1.13 | 5.81[6] | 30.27 | 31.13[3] |
| Spacer Disk | Primary Membrane | 1.95 | Note 7 | N/A | 8.84[4] |
| | Membrane + Bending | 2.71 | Note 7 | N/A | 12.43[4] |
| | Primary + Secondary | 2.71 | Note 7 | 47.77 | 54.14[3][4] |

(1) Values shown are maximum irrespective of location.
(2) Envelope of Normal and Off-Normal conditions.
(3) Includes thermal loads.
(4) Includes deadweight loads.
(5) Per Note 2 of Table NB3217-1, the stress at the intersection between a shell and a flat head may be classified as secondary (Q) if the bending moment at the edge is not required to maintain the bending stresses in the middle of the head within acceptable limits. Thus, the primary plus secondary stresses were computed in a finite element model that assumed moment-transferring connections, whereas the primary membrane and bending stresses were computed assuming pinned connections. All thermal stresses are classified as secondary.
(6) These stresses are due to Service Level A 20 psig blow down pressure. A strongback is applied to the inner top cover plate.
(7) The DSC internal structures are not affected by pressure loads.

**Table 8.1-11**
**Maximum NUHOMS®-52B DSC Stresses for Normal and Off-Normal Loads**

| DSC Components | Stress Type | Maximum Stress Intensity(ksi)[1] | | | |
|---|---|---|---|---|---|
| | | Dead Weight | Internal Pressure [2] | Thermal [2] | Handling [2] |
| DSC Shell | Primary Membrane | 2.63 | 1.55 | N/A | 12.10 |
| | Membrane + Bending | 3.04 | 3.37 | N/A | 17.21 |
| | Primary + Secondary | 2.74 | 14.71[6] | 30.70 | 19.88 |
| Inner Top Cover Plate | Primary Membrane | 0.76 | 1.18[6] | N/A | 1.48 |
| | Membrane + Bending | 2.19 | 12.07[6] | N/A | 1.70 |
| | Primary + Secondary[5] | 2.10 | 15.19[6] | 27.04 | 1.71 |
| Outer Top Cover Plate | Primary Membrane | 1.20 | 2.06 | N/A | 0.16 |
| | Membrane + Bending | 1.85 | 7.05 | N/A | 0.40 |
| | Primary + Secondary[5] | 1.27 | 6.31 | 25.34 | 0.34 |

See End of Table for Notes.

**Table 8.1-11**
**Maximum NUHOMS®-52B DSC Stresses for Normal and Off-Normal Loads**

(concluded)

| DSC Components | Stress Type | Maximum Stress Intensity(ksi)[1] | | | |
|---|---|---|---|---|---|
| | | Dead Weight | Internal Pressure[2] | Thermal[2] | Normal Handling[2] |
| Inner Bottom Cover Plate | Primary Membrane | 0.71 | 0.36[6] | N/A | 13.76 |
| | Membrane + Bending | 0.83 | 0.92[6] | N/A | 22.38 |
| | Primary + Secondary | 0.82 | 13.2[6] | 27.43 | 22.38[3] |
| Outer Bottom Cover Plate | Primary Membrane | 0.71 | 0.41 | N/A | 12.65 |
| | Membrane + Bending | 1.21 | 0.74 | N/A | 23.35 |
| | Primary + Secondary | 1.13 | 5.81[6] | 28.99 | 23.35[3] |
| Spacer Disk | Primary Membrane | 1.50 | Note 7 | N/A | 9.7 |
| | Membrane + Bending | 2.38 | Note 7 | N/A | 28.36 |
| | Primary + Secondary | 2.38 | Note 7 | 82.7 | 28.36 |

(1) Values shown are maximum irrespective of location.
(2) Envelop of Normal and Off-Normal conditions.
(3) Includes Thermal loads
(4) Not Used
(5) Per Note 2 of Table NB3217-1, the stress at the intersection between a shell and a flat head may be classified as secondary (Q) if the bending moment at the edge is not required to maintain the bending stresses in the middle of the head within acceptable limits. Thus, the primary plus secondary stresses were computed in a finite element model that assumed moment transferring connections, whereas the primary membrane and bending stresses were computed assuming pinned connections. All thermal stresses are classified as secondary.
(6) These stresses are due to Service Level A 20 psig blow down pressure. A strongback is applied to the inner top cover plate.
(7) The DSC internal structures are not affected by pressure loads.

**Table 8.1-12**

**Deleted**

**Table 8.1-13**

**Deleted**

**Table 8.1-14**
**Maximum DSC Support Structure Stresses for Normal and Off-Normal Loads**

| Component | Load Type | Calculated Stress[1] | | |
|---|---|---|---|---|
| | | Axial (ksi) | Bending (ksi)[2] | Shear (ksi)[3] |
| Support Rail | Dead Weight | 0.35 | 1.76 | 2.93 |
| | Normal DSC Handling Loads | 0.89 | 0.12 | 0.03 |
| | Off-Normal DSC Handling Loads | 6.53 | 9.29 | 3.71 |
| | Normal Thermal | 0.52 | 11.19 | 1.26 |
| | Off-Normal Thermal | 0.53 | 10.23 | 1.17 |
| Cross Beam | Dead Weight | 0.27 | 1.60 | 6.89 |
| | Normal DSC Handling Loads | 0.02 | 0.08 | 0.02 |
| | Off-Normal DSC Handling Loads | 0.12 | 6.10 | 6.48 |
| | Normal Thermal | 1.08 | 6.74 | 1.27 |
| | Off-Normal Thermal | 0.96 | 6.45 | 1.26 |
| Support Column | Dead Weight | 3.14 | 0.30 | 0.03 |
| | Normal DSC Handling Loads | 0.01 | 0.07 | 0.01 |
| | Off-Normal DSC Handling Loads | 2.90 | 3.90 | 0.22 |
| | Normal Thermal | 0.56 | 3.85 | 0.43 |
| | Off-Normal Thermal | 0.51 | 3.91 | 0.43 |
| Lateral Brace | Dead Weight | 0.04 | 0.00 | 0.00 |
| | Normal DSC Handling Load | 0.05 | 0.00 | 0.00 |
| | Off-Normal DSC Handling Loads | 0.44 | 0.00 | 0.00 |
| | Normal Thermal | 3.45 | 0.18 | 0.00 |
| | Off-Normal Thermal | 3.14 | 0.18 | 0.00 |

(1) Maximum stresses reported irrespective of location.
(2) Maximum bending stress for either direction of bending.
(3) Maximum shear stress for either direction of shear.

**Table 8.1-15**
**Maximum[1] Normal and Off-Normal Loads for DSC Support Structure End Connections**

| Loading | Support Column | | | Lateral Brace | | |
|---|---|---|---|---|---|---|
| | Axial (k) | Shear[2] (k) | Bending[3] (in. k) | Axial (k) | Shear[2] (k) | Bending[3] (in. k) |
| Dead Weight (including DSC) | 20.6 | 0.07 | 2.60 | 0.2 | 0.0 | 0.0 |
| Normal DSC Handling Loads | 0.04 | 0.03 | 1.40 | 0.2 | 0.0 | 0.0 |
| Off-Normal DSC Handling Loads | 19.0 | 0.80 | 35.4 | 1.9 | 0.0 | 0.0 |

(1) Maximum loads reported irrespective of location.
(2) Maximum shear for either direction of shear.
(3) Maximum bending for either direction of bending.

**Table 8.1-16**
**Maximum DSC Support Structure Vertical Displacements**
**for Normal and Off-Normal Loads**

| Components | Load Type | Maximum Vertical Displacements (in.) |
|---|---|---|
| Cross Beam | Dead Weight $DW_s + DW_c$ | .005 |
| | Normal DSC Handling Loads $DW_s + DW_c + HL_n$ | .005 |
| | Off-Normal DSC Handling Loads $HL_o$ | .007 |
| Support Rails | Dead Weight $DW_s + DW_c$ | .007 |
| | Normal DSC Handling Loads $DW_s + DW_c + HL_n$ | .007 |
| | Off-Normal DSC Handling Loads $HL_o$ | 0.04 |

**Table 8.1-17**
**Thermal Load Case Definitions for HSM Structural Analysis**

| Thermal Condition | Case No | Ambient Temp. (°F) | Maximum Inner Surface Temperature (°F) | | | Maximum Outer Surface Temperature (°F) | | | Maximum Thermal Gradient[3] (°F) | | |
|---|---|---|---|---|---|---|---|---|---|---|---|
| | | | Roof | Wall | Floor | Roof | Wall | Floor[1] | Roof | Wall | Floor[1] |
| Normal Operating ($T_o$) | 1<br>2<br>3[2] | 70<br>100<br>0 | 164<br>201 | 137<br>172 | 139<br>172 | 114<br>142 | 118<br>152 | 125<br>155 | 50<br>59 | 29<br>32 | 14<br>17 |
| Off-Normal ($T_a$) | 1<br>2 | 125<br>-40 | 241<br>11 | 203<br>7 | 199<br>10 | 186<br>–26 | 181<br>–7 | 180<br>5 | 55<br>37 | 34<br>14 | 25<br>4 |
| Accident ($T_a$) | 1[4]<br>2 | 125<br>-40 | 441<br>250 | 414<br>237 | 479<br>295 | 240<br>54 | 312<br>138 | 361<br>174 | 201<br>196 | 102<br>99 | 118<br>121 |

1. The floor outside temperature and maximum gradient are reported for the one foot thick HSM floor.
2. The gradients are lower for the 70°F ambient case than the 100°F ambient case. These gradients will be even lower for the 0°F ambient case. Therefore, the 0°F is not considered further in this analysis for concrete.
3. Based on maximum gradient at any cross-section.
4. The reported value corresponds to an accident duration of 120 hours. This value bounds the analysis results corresponding to the licensing basis transient of 40 hours (COC Technical Specification 1.3.1).
5. A description of the various thermal conditions follows.

**Table 8.1-17**

**Thermal Load Case Definitions for HSM Structural Analysis**

(concluded)

Normal Conditions

1. Interior module with 70°F ambient temperature, 18 inch side walls open to ambient, vents open, solar heat flux of 62.0 Btu/hr-ft$^2$

2. Interior module with 100°F ambient temperature, 18 inch side walls open to ambient, vents open, solar heat flux of 62.0 Btu/hr-ft$^2$

3. Interior module with 0°F ambient temperature, 18 inch side walls open to ambient, vents open, solar heat flux neglected (not used)

Off-Normal Conditions

1. Interior module with 125°F ambient temperature, 18 inch side walls open to ambient, vents open, solar heat flux of 123 Btu/hr-ft.$^2$

2. Interior module with -40°F ambient temperature, 18 inch side walls open to ambient, vents open, neglect solar heat flux (not used)

Accident Conditions

1. Interior module with 125°F ambient temperature, 18 inch side walls open to ambient, all inlet and outlet openings in the side walls blocked for 120 hours, solar heat flux of 123 Btu/hr-ft$^2$

2. Interior module with -40°F ambient temperature, 18 inch side walls open to ambient, all inlet and outlet openings in the side walls blocked for 120 hours, solar heat flux neglected (not used)

**Table 8.1-18**

**Deleted**

**Table 8.1-19**
**Maximum HSM Reinforced Concrete Bending Moments and Shear Forces for Normal and Off-Normal Loads**

| Structural Section | Force Component[2] | HSM Internal Forces (kip/ft., in.-k/ft.)[1] | | | |
|---|---|---|---|---|---|
| | | Dead Weight | Live Loads | Normal[3] Thermal | Off-Normal[3] Thermal |
| Floor Slab | Shear | 0.11 | 1.2 | 1.1 | 1.5 |
| | Moment | 0.54 | 6.6 | 11.2 | 14.6 |
| Side Wall | Shear | 0.32 | 3.1 | 3.6 | 4.6 |
| | Moment | 22.6 | 34.7 | 101.9 | 118.9 |
| Front Wall | Shear | 0.96 | 10.8 | 6.4 | 6.1 |
| | Moment | 154.9 | 125.5 | 190.1 | 190.1 |
| Rear Wall | Shear | 0.32 | 0.3 | 3.4 | 3.1 |
| | Moment | 0.54 | 2.3 | 62.5 | 56.3 |
| Roof Slab | Shear | 2.6 | 1.1 | 1.0 | 0.6 |
| | Moment | 33.4 | 14.8 | 120.8 | 33.3 |

(1) Maximum loads reported irrespective of location.
(2) Out-of-plane shears and moments.
(3) Maximum moments based on cracked section properties.

**Table 8.1-20**
**Maximum Standardized Transfer Cask Stresses for Normal Loads**

| Transfer Cask Components | Stress Type | Load Type | | |
|---|---|---|---|---|
| | | Stress (ksi)[1] | | |
| | | Dead Weight | Thermal | Normal Handling |
| Transfer Cask Structural Shell | Primary Membrane | 0.7 | N/A | 0.5 |
| | Membrane + Bending | 0.9 | N/A | 4.1 |
| | Primary + Secondary | 0.9 | 18.4 | 42.6 |
| Top Cover Plate | Primary Membrane | 0.2 | N/A | N/A |
| | Membrane + Bending | 0.6 | N/A | 6.9 |
| | Primary + Secondary | 0.6 | 13.1 | 6.9 |
| Bottom End Assembly | Primary Membrane | 0.5 | N/A | N/A |
| | Membrane + Bending | 1.3 | N/A | 15.4 |
| | Primary + Secondary | 1.4 | 21.4 | 15.4 |
| Transfer Cask Collar for BWR DSC | Primary Membrane | 0.2 | N/A | 0.0 |
| | Membrane + Bending | 0.2 | N/A | 0.0 |
| | Primary + Secondary | 0.5 | 15.8 | 0.0 |

(1) Values shown are maximum irrespective of location.

**Table 8.1-20a**

**Maximum OS197 Transfer Cask Stresses for Normal Loads**

| Transfer Cask Components | Stress Type | Load Type | | |
|---|---|---|---|---|
| | | Stress (ksi)[1] | | |
| | | Dead Weight | Thermal | Normal Handling |
| Transfer Cask Structural Shell | Primary Membrane | 0.92 | N/A | 1.85 |
| | Membrane + Bending | 7.0 [2] | N/A | 14.0 [2] |
| | Primary + Secondary | 7.0 [2] | 9.9 | 14.0 [2] |
| Top Cover Plate | Primary Membrane | 0.0 | N/A | 0.56 |
| | Membrane + Bending | 0.23 | N/A | 4.2 |
| | Primary + Secondary | 0.23 | 3.0 | 4.2 |
| Bottom End Assembly | Primary Membrane | 0.45 | N/A | 0.56 |
| | Membrane + Bending | 6.3 | N/A | 7.2 |
| | Primary + Secondary | 6.3 | 6.0 | 7.2 |

(1) Values shown are maximum irrespective of location.
(2) Stresses in the transfer cask structural shell for these loads are governed by the local stresses at the trunnion interface. Stresses shown are for locations remote from the trunnions.

**Table 8.1-20b**
**Maximum OS197H Transfer Cask Stresses for Normal Loads**

| Transfer Cask Components | Stress Type | Load Type | | |
|---|---|---|---|---|
| | | Stress (ksi)[1] | | |
| | | Dead Weight | Thermal | Normal Handling |
| Transfer Cask Structural Shell | Primary Membrane | 1.0 | N/A | 2.1 |
| | Membrane + Bending | 7.5 [2] | N/A | 14.9 [2] |
| | Primary + Secondary | 7.5 [2] | 9.9 | 14.9 [2] |
| Top Cover Plate | Primary Membrane | <0.01 | N/A | 0.7 |
| | Membrane + Bending | 0.2 | N/A | 5.3 |
| | Primary + Secondary | 0.2 | 3.0 | 5.3 |
| Bottom End Assembly | Primary Membrane | 1.0 | N/A | 1.2 |
| | Membrane + Bending | 6.2 | N/A | 8.6 |
| | Primary + Secondary | 6.2 | 6.0 | 8.6 |

(1) Values shown are maximum irrespective of location.
(2) Stresses in the transfer cask structural shell for these loads are governed by the local stresses at the trunnion interface. Stresses shown are for locations remote from the trunnions.

**Table 8.1-21**
**Maximum Standardized Transfer Cask Stresses for Off-Normal Operating Loads**

| DSC Components | Stress Type | Load Type | |
|---|---|---|---|
| | | Stress (ksi)[1] | |
| | | Seismic[2] | Thermal |
| Transfer Cask Structural Shell | Primary Membrane | 0.5 | N/A |
| | Membrane + Bending | 4.1 | N/A |
| | Primary + Secondary | N/A | 18.4 |
| Top Cover Plate | Primary Membrane | 0.0 | N/A |
| | Membrane + Bending | 6.9 | N/A |
| | Primary + Secondary | N/A | 13.1 |
| Bottom End Assembly | Primary Membrane | 0.0 | N/A |
| | Membrane + Bending | 15.4 | N/A |
| | Primary + Secondary | N/A | 21.4 |
| Transfer Cask Collar for BWR DSC | Primary Membrane | 0.0 | N/A |
| | Membrane + Bending | 0.0 | N/A |
| | Primary + Secondary | N/A | 15.8 |

(1) Values shown are maximum irrespective of location.

(2) Seismic stresses are taken to be equal to the handling load stresses, since handling loads govern over seismic loads.

**Table 8.1-21a**
**Maximum OS197 Transfer Cask Stresses for Off-Normal Operating Loads**

| Transfer Cask Components | Stress Type | Load Type | |
|---|---|---|---|
| | | Stress (ksi)[1] | |
| | | Seismic[2] | Thermal |
| Transfer Cask Structural Shell | Primary Membrane | 1.58 | N/A |
| | Membrane + Bending | 13.6[3] | N/A |
| | Primary + Secondary | N/A | 10.2 |
| Top Cover Plate | Primary Membrane | 0.0 | N/A |
| | Membrane + Bending | 0.34 | N/A |
| | Primary + Secondary | N/A | 5.9 |
| Bottom End Assembly | Primary Membrane | 0.56 | N/A |
| | Membrane + Bending | 8.2 | N/A |
| | Primary + Secondary | N/A | 5.5 |

(1) Values shown are maximum irrespective of location.

(2) Seismic stresses are based on 1.31g in two horizontal directions occurring simultaneously with 0.84g vertical.

(3) Stresses in the transfer cask structural shell for these loads are governed by the local stresses at the trunnion interface. Stresses shown are at locations remote from the trunnions.

**Table 8.1-21b**
**Maximum OS197H Transfer Cask Stresses for Off-Normal Operating Loads**

| Transfer Cask Components | Stress Type | Load Type | |
|---|---|---|---|
| | | Stress (ksi)[1] | |
| | | Seismic[2] | Thermal |
| Transfer Cask Structural Shell | Primary Membrane | 1.8 | N/A |
| | Membrane + Bending | 13.7 [3] | N/A |
| | Primary + Secondary | N/A | 10.2 |
| Top Cover Plate | Primary Membrane | <0.01 | N/A |
| | Membrane + Bending | 0.44 | N/A |
| | Primary + Secondary | N/A | 5.9 |
| Bottom End Assembly | Primary Membrane | 1.74 | N/A |
| | Membrane + Bending | 13.7 | N/A |
| | Primary + Secondary | N/A | 5.5 |

(1) Values shown are maximum irrespective of location.

(2) Seismic stresses are based on 1.31g in two horizontal directions occurring simultaneously with 0.84g vertical.

(3) Stresses in the transfer cask structural shell for these loads are governed by the local stresses at the trunnion interface. Stresses shown are at locations remote from the trunnions.

**Table 8.1-22**
**NUHOMS®-24P HSM Bulk Air Temperature**

| HSM Inlet Air Temperature (°F) | Temperatures in Regions (°F) | | | | | | | | |
|---|---|---|---|---|---|---|---|---|---|
| | 92 | 87 | 81 | 76 | 71 | 66 | 61 | 55 | 49 |
| -40 | -38 | -30 | -21 | -12 | -2 | 7 | 16 | 26 | 35 |
| 0 | 2 | 11 | 21 | 31 | 41 | 51 | 62 | 72 | 82 |
| 70 | 72 | 82 | 94 | 106 | 118 | 129 | 141 | 153 | 165 |
| 100 | 102 | 113 | 125 | 138 | 150 | 163 | 175 | 188 | 200 |
| 125 | 127 | 138 | 151 | 164 | 177 | 191 | 204 | 216 | 230 |

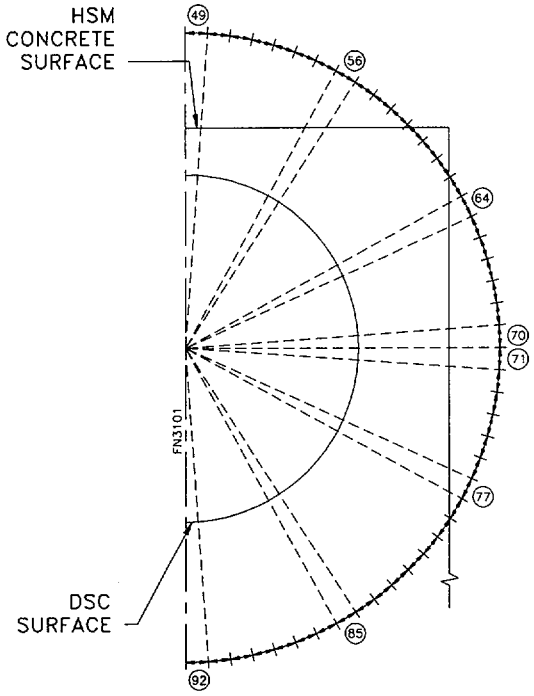


**Bulk Air Temperature Regions in HEATING7 HSM Model**

**Table 8.1-23**
**NUHOMS®-52B HSM Bulk Air Temperature**

| HSM Inlet Air Temperature (°F) | Temperatures in Regions (°F) | | | | | | | | |
|---|---|---|---|---|---|---|---|---|---|
| | 92 | 87 | 81 | 76 | 71 | 66 | 61 | 55 | 49 |
| -40 | -39 | -32 | -24 | -16 | -8 | 0 | 8 | 16 | 24 |
| 0 | 2 | 9 | 18 | 26 | 35 | 44 | 53 | 61 | 70 |
| 70 | 72 | 80 | 90 | 100 | 111 | 121 | 131 | 141 | 151 |
| 100 | 102 | 111 | 121 | 132 | 143 | 154 | 164 | 175 | 186 |
| 125 | 127 | 136 | 147 | 159 | 170 | 181 | 192 | 203 | 215 |

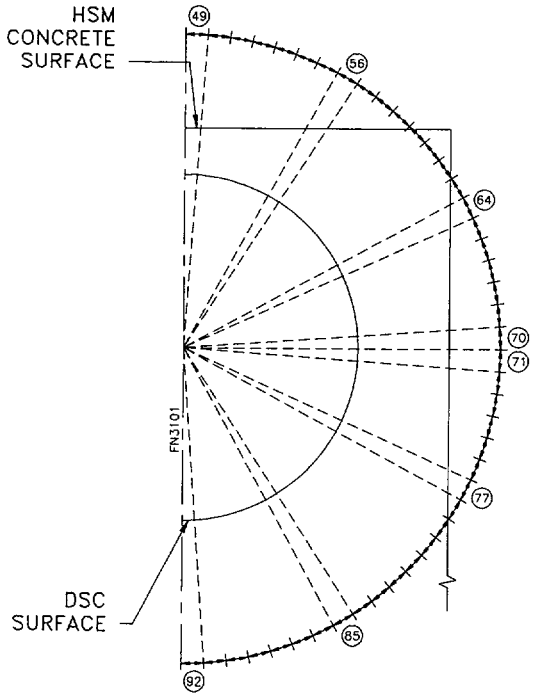


**Bulk Air Temperature Regions in HEATING7 HSM Model**

**Table 8.1-24**
**NUHOMS®-24P HSM Thermal Analysis Results Summary**

| Case | HSM Air Temperature (°F) | | Maximum DSC Outer Surface Temperature (°F) | | | Maximum Concrete Temperature (°F) | | | |
|---|---|---|---|---|---|---|---|---|---|
| | In | Out | Bottom | Side | Top | Roof | | Side Wall | Floor |
| | | | | | | Inside | Outside | | |
| 1 | 70 | 165 | 248 | 311 | 345 | 164 | 114 | 137 | 139 |
| 2 | 100 | 200 | 273 | 339 | 374 | 201 | 142 | 172 | 172 |
| 3 | 125 | 230 | 295 | 362 | 399 | 241 | 186 | 203 | 199 |
| 4 | N/A (All HSM vents plugged for 40 hours with outside air at 125°F) | | 485 | 599 | 640 | 441(1) | 240(1) | 414(1) | 479(1) |

(1) The reported value corresponds to an accident duration of 120 hours. This value bounds the analysis results corresponding to the licensing basis transient of 40 hours (CoC Technical Specification 1.3.1).

**Table 8.1-25**
**NUHOMS®-52B HSM Thermal Analysis Results Summary**

| Case | HSM Air Temperature (°F) | | Maximum DSC Outer Surface Temperature (°F) | | | Maximum Concrete Temperature (°F) | | | |
|---|---|---|---|---|---|---|---|---|---|
| | In | Out | Bottom | Side | Top | Roof | | Side Wall | Floor |
| | | | | | | Inside | Outside | | |
| 1 | 70 | 151 | 214 | 270 | 300 | 150 | 112 | 127 | 128 |
| 2 | 100 | 186 | 239 | 297 | 328 | 185 | 140 | 161 | 160 |
| 3 | 125 | 215 | 261 | 320 | 352 | 224 | 184 | 192 | 187 |
| 4 | N/A(All vents plugged for 40 hours with outside airat 125°F) | | 485 | 599 | 640 | 441(1) | 240(1) | 414(1) | 479(1) |

1. The reported value corresponds to an accident duration of 120 hours. This value bounds the analysis results corresponding to the licensing basis transient of 40 hours (CoC Technical Specification 1.3.1).

**Table 8.1-26**
**NUHOMS®-24P DSC Thermal Analysis Results Summary**

| Case | HSM Vent Air Inlet Temperature (°F) | Max. DSC Shell Temperature (°F) | Max. Fuel Cladding Temperature (°F/°C) | Average Helium Temperature (°F) | Fuel Cladding Acceptance Criteria (°F/°C) |
|---|---|---|---|---|---|
| 1 | 70 | 345 | 700/371 | 420 | 724/384 |
| 2 | 100 | 374 | 711/377 | 435 | 1058/570 |
| 3 | 125 | 399 | 720/382 | 447 | 1058/570 |
| 4 | N/A (HSM Vents plugged for 40 hours with ambient air at 125°F) | 640 | 871/466(1) | 667(1) | 1058/570(1) |
| 5 | N/A (DSC in cask with internal vacuum) | 411 | 909/487 | N/A | 1058/570 |

1. The reported value corresponds to an accident duration of 120 hours. This value bounds the analysis results corresponding to the licensing basis transient of 40 hours (CoC Technical Specification 1.3.1).

**Table 8.1-27**
**NUHOMS®-52B DSC Thermal Analysis Results**

| Case | HSM Vent Air Inlet Temperature (°F) | Max. DSC Shell Temperature (°F) | Max. Fuel Cladding Temperature (°F/°C) | Average Helium Temperature (°F) | Fuel Cladding Acceptance Criteria (°F/°C) |
|---|---|---|---|---|---|
| 1 | 70 | 300 | 725/385 | 481 | 790/421 |
| 2 | 100 | 328 | 735/391 | 492 | 790/421 |
| 3 | 125 | 352 | 743/395 | 502 | 1058/570 |
| 4 | N/A (HSM Vents plugged for 40 hours with ambient air at 125°F) | 640 | 905/495[1] | 719[1] | 1058/570[1] |
| 5 | N/A (DSC in cask with internal vacuum) | 358 | 988/531 | N/A | 1058/570 |

1. The reported value corresponds to an accident duration of 120 hours. This value bounds the analysis results corresponding to the licensing basis transient of 40 hours (CoC Technical Specification 1.3.1).

**Table 8.1-28**
**Standardized Transfer Cask with NUHOMS®-24P DSC Thermal Analysis Results Summary**

| Case | Ambient Air Temperature (°F) | Maximum Inner Liner Temperature (°F) | Maximum Exterior Cask Temperature (°F) | Reference |
|---|---|---|---|---|
| 1 | -40 | 162 | 101 | Case 1B |
| 2 | 0 | 194 | 132 | Case 2B |
| 3 | 70 | 273 | 213 | Case 3A |
| 4 | 100 | 296 | 235 | Case 4A |
| 5 | 100 (vacuum in DSC, cask vertical) | 283 | 216 | Case 4D |

**Table 8.1-29**
**Standardized Transfer Cask with NUHOMS®-52B DSC Thermal Analysis Results Summary**

| Case | Ambient Air Temperature (°F) | Maximum Inner Liner Temperature (°F) | Maximum Exterior Cask Temperature (°F) | Reference |
|---|---|---|---|---|
| 1 | -40 | 155 | 97 | Case 1B |
| 2 | 0 | 187 | 128 | Case 2B |
| 3 | 70 | 267 | 209 | Case 3A |
| 4 | 100 | 290 | 232 | Case 4A |
| 5 | 100 (vacuum in DSC, cask vertical) | 245 | 194 | Case 4E |

**Table 8.1-29a**
**OS197 Transfer Cask with NUHOMS®-24P or 52B DSC Thermal Analysis Results Summary**

| Case | Ambient Air Temperature (°F) | Maximum Inner Liner Temperature (°F) | Maximum Exterior Cask Temperature (°F) |
|---|---|---|---|
| 1 | -40 | 145 | 125 |
| 2 | 0 | 175 | 156 |
| 3 | 70 | 239 | 221 |
| 4 | 100 | 261 | 243 |
| 5 | 125 w/o solar | 269 | 251 |
| 6 | 100 (vacuum in DSC, cask vertical) | 248 | 230 |

**Table 8.1-30**
**Thermal Analysis Results Summary for the HSM Support Structure: 24P and 52B Systems**

| Case | Component | Location (in)[3] | $T_1$ (°F)[1] | $T_2$ (°F)[1] | $T_3$ (°F)[1] | T (°F) |
|---|---|---|---|---|---|---|
| -40°F Amb | Nitronic Plate | 60.38 | 140 | 163[4] | 163[4] | |
| | Support Rail Center | 56.68 | 129 | 153 | 151 | |
| | Cross Beam Center | 46.26 | 98 | 133 | 123 | |
| | Support Leg Top | 42.20 | 87 | 121 | 109 | |
| | Support Leg Bottom | 0.00 | -36 | 6 | -36 | |
| | Railing Ends[2] | | | | | 17.7 |
| 100°F Amb | Nitronic Plate | 60.38 | 252 | 280[4] | 280[4] | |
| | Support Rail Center | 56.68 | 244 | 273 | 271 | |
| | Cross Beam Center | 46.26 | 222 | 261 | 251 | |
| | Support Leg Top | 42.20 | 214 | 253 | 240 | |
| | Support Leg Bottom | 0.00 | 125 | 167 | 125 | |
| | Railing Ends[2] | | | | | 145 |
| 125°F Amb | Nitronic Plate | 60.38 | 274 | 301[4] | 301[4] | |
| | Support Rail center | 56.68 | 267 | 294 | 292 | |
| | Cross Beam Center | 46.26 | 247 | 285 | 276 | |
| | Support Leg Top | 42.20 | 239 | 277 | 266 | |
| | Support Leg Bottom | 0.00 | 159 | 194 | 159 | |
| | Railing Ends[2] | | | | | 164 |
| 40 hr blk vent 125°F Amb | Nitronic Plate | 60.38 | 494 | 494 | 494 | |
| | Support Rail center | 56.68 | 487 | 487 | 487 | |
| | Cross Beam Center | 46.26 | 466 | 466 | 466 | |
| | Support Leg Top | 42.20 | 458 | 458 | 458 | |
| | Support Leg Bottom | 0.00 | 375 | 375 | 375 | |
| | Railing Ends[2] | | | | | 462 |

(1) The locations of $T_1$ through $T_3$ are nearest the HSM back wall, the middle of the HSM, and nearest the HSM front wall respectively.
(2) The support structure railing temperature applies to both ends.
(3) The location is measured vertically from the bottom of the support leg base plate.
(4) Temperature taken at surface of DSC at point of contact with Nitronic Plate ($r=33.625$", $\theta=5\pi/6$).

**Table 8.1-30**
**Thermal Analysis Results Summary for the HSM Support Structure: 24P and 52B Systems (continued)**

| Case | Component | Location (in)[3] | $T_1$ (°F)[1] | $T_2$ (°F)[1] | $T_3$ (°F)[1] | T (°F) |
|---|---|---|---|---|---|---|
| 5 dy blk vent 125°F Amb | Nitronic Plate | 60.38 | 568 | 568 | 568 | |
| | Support Rail center | 56.68 | 563 | 563 | 563 | |
| | Cross Beam Center | 46.26 | 547 | 547 | 547 | |
| | Support Leg Top | 42.20 | 541 | 541 | 541 | |
| | Support Leg Bottom | 0.00 | 479 | 479 | 479 | |
| | Railing Ends[2] | | | | | 528 |
| 40 hr blk vent -40°F Amb | Nitronic Plate | 60.38 | 388 | 388 | 388 | |
| | Support Rail center | 56.68 | 376 | 376 | 376 | |
| | Cross Beam Center | 46.26 | 341 | 341 | 341 | |
| | Support Leg Top | 42.20 | 327 | 327 | 327 | |
| | Support Leg Bottom | 0.00 | 186 | 186 | 186 | |
| | Railing Ends[2] | | | | | 349 |
| 5 dy blk vent -40°F Amb | Nitronic Plate | 60.38 | 444 | 444 | 444 | |
| | Support Rail center | 56.68 | 435 | 435 | 435 | |
| | Cross Beam Center | 46.26 | 409 | 409 | 409 | |
| | Support Leg Top | 42.20 | 399 | 399 | 399 | |
| | Support Leg Bottom | 0.00 | 295 | 295 | 295 | |
| | Railing Ends[2] | | | | | 396 |

1) The locations of $T_1$ through $T_3$ are nearest the HSM back wall, the middle of the HSM, and nearest the HSM front wall respectively.
(2) The support structure railing temperature applies to both ends.
(3) The location is measured vertically from the bottom of the support leg base plate.

| FUEL ASSEMBLY ID NUMBER | MAX FUEL CLAD TEMP (°F/°C) |
|---|---|
| 1 | 540/282 |
| 2 | 649/343 |
| 3 | 696/369 |
| 4 | 700/371 |
| 5 | 661/349 |
| 6 | 570/299 |
| 7 | 590/310 |
| 8 | 653/345 |
| 9 | 654/346 |
| 10 | 604/318 |
| 11 | 549/287 |
| 12 | 546/286 |

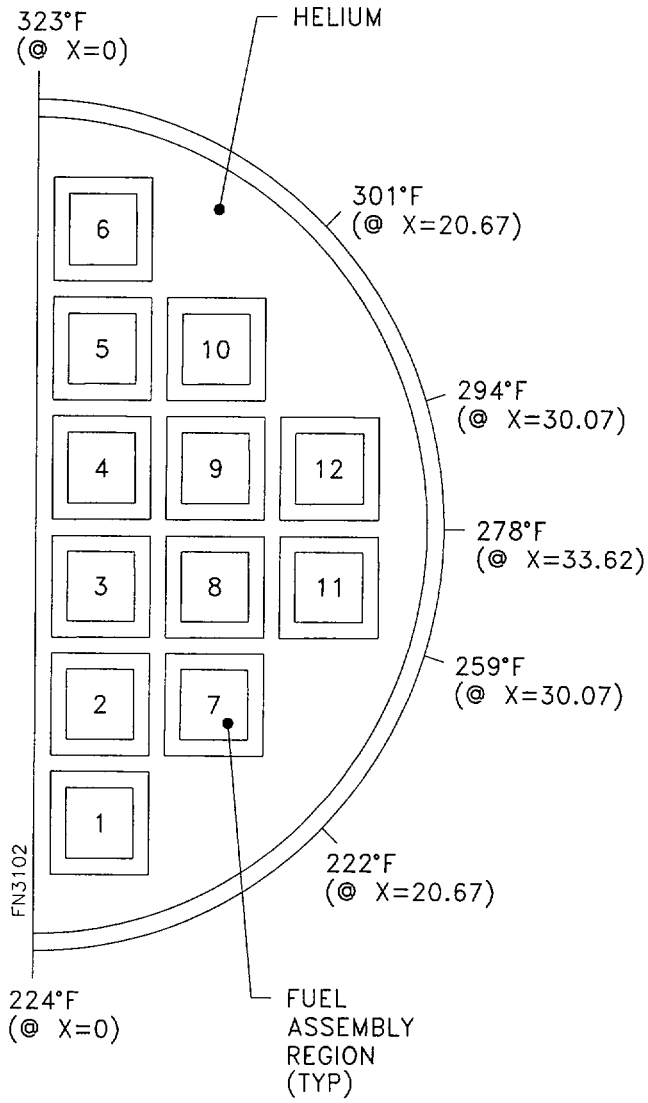


**Figure 8.1-1**
**NUHOMS®-24P DSC Internal Temperature Distribution for 70°F Ambient**

| FUEL ASSEMBLY ID NUMBER | MAX FUEL CLAD TEMP (°F/°C) |
|---|---|
| 1 | 552/289 |
| 2 | 660/347 |
| 3 | 706/374 |
| 4 | 711/377 |
| 5 | 673/356 |
| 6 | 585/307 |
| 7 | 602/317 |
| 8 | 664/351 |
| 9 | 665/352 |
| 10 | 617/325 |
| 11 | 563/295 |
| 12 | 561/294 |

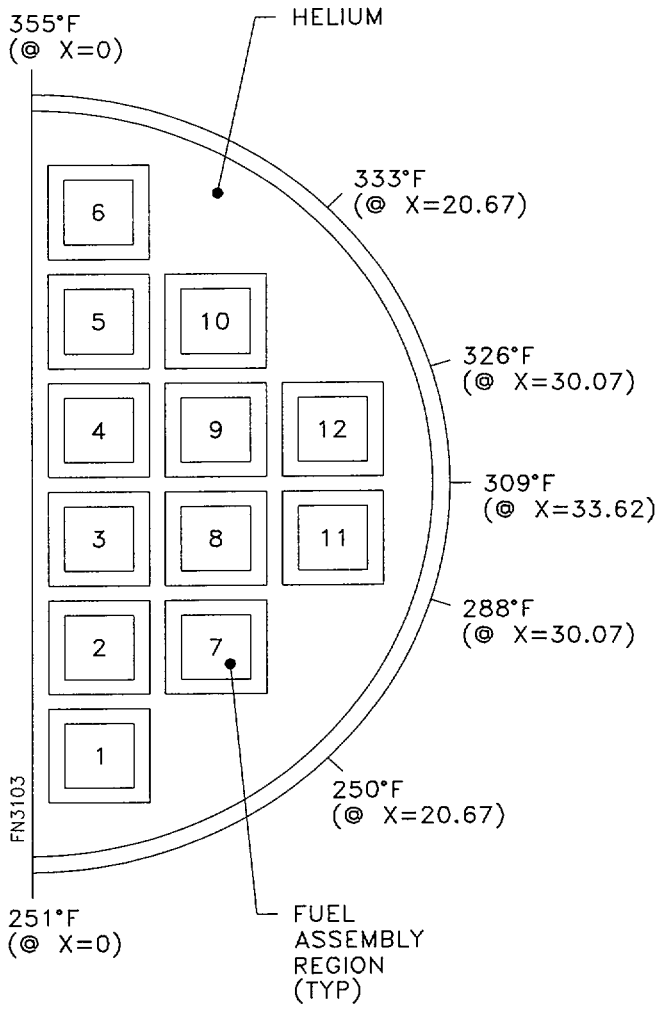


**Figure 8.1-2**
**NUHOMS®-24P DSC Internal Temperature Distribution for 100°F Ambient**

| FUEL ASSEMBLY ID NUMBER | MAX FUEL CLAD TEMP (°F/°C) |
|---|---|
| 1 | 527/275 |
| 2 | 633/334 |
| 3 | 707/375 |
| 4 | 725/385 |
| 5 | 721/383 |
| 6 | 691/366 |
| 7 | 605/318 |
| 8 | 479/248 |
| 9 | 420/216 |
| 10 | 610/321 |
| 11 | 666/352 |
| 12 | 698/370 |
| 13 | 693/367 |
| 14 | 656/347 |
| 15 | 571/299 |
| 16 | 415/213 |
| 17 | 493/256 |
| 18 | 598/314 |
| 19 | 624/329 |
| 20 | 628/331 |
| 21 | 581/305 |
| 22 | 473/245 |
| 23 | 459/237 |
| 24 | 511/266 |
| 25 | 507/264 |
| 26 | 459/237 |

FN663

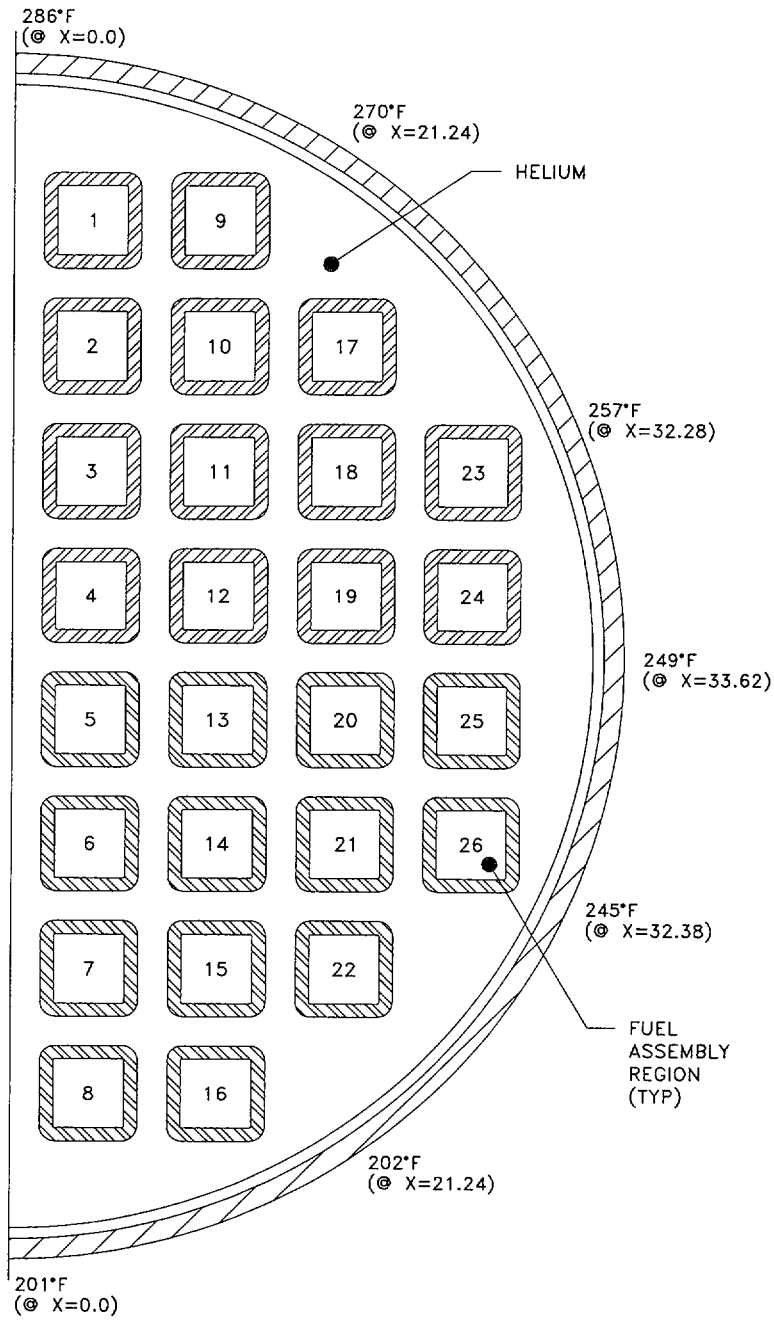


**Figure 8.1-3**
**NUHOMS®-52B DSC Internal Temperature Distribution for 70°F Ambient**

| FUEL ASSEMBLY ID NUMBER | MAX FUEL CLAD TEMP (°F/°C) |
|---|---|
| 1 | 544/284 |
| 2 | 646/341 |
| 3 | 718/381 |
| 4 | 735/391 |
| 5 | 731/388 |
| 6 | 701/372 |
| 7 | 616/324 |
| 8 | 493/256 |
| 9 | 443/228 |
| 10 | 624/329 |
| 11 | 678/359 |
| 12 | 709/376 |
| 13 | 704/373 |
| 14 | 667/353 |
| 15 | 584/307 |
| 16 | 434/223 |
| 17 | 510/266 |
| 18 | 611/322 |
| 19 | 636/336 |
| 20 | 640/338 |
| 21 | 594/312 |
| 22 | 488/253 |
| 23 | 476/247 |
| 24 | 526/274 |
| 25 | 522/272 |
| 26 | 475/246 |

FN664

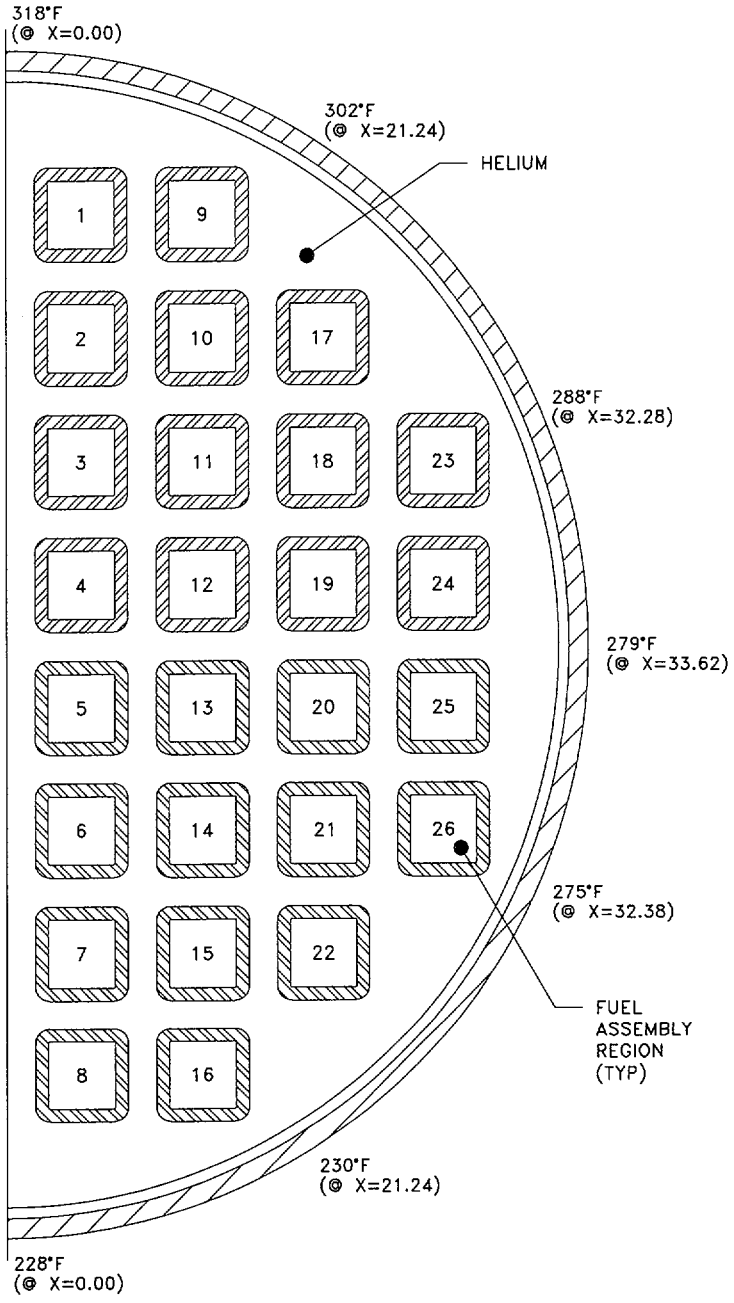


**Figure 8.1-4**
**NUHOMS®-52B DSC Internal Temperature Distribution for 100°F Ambient**

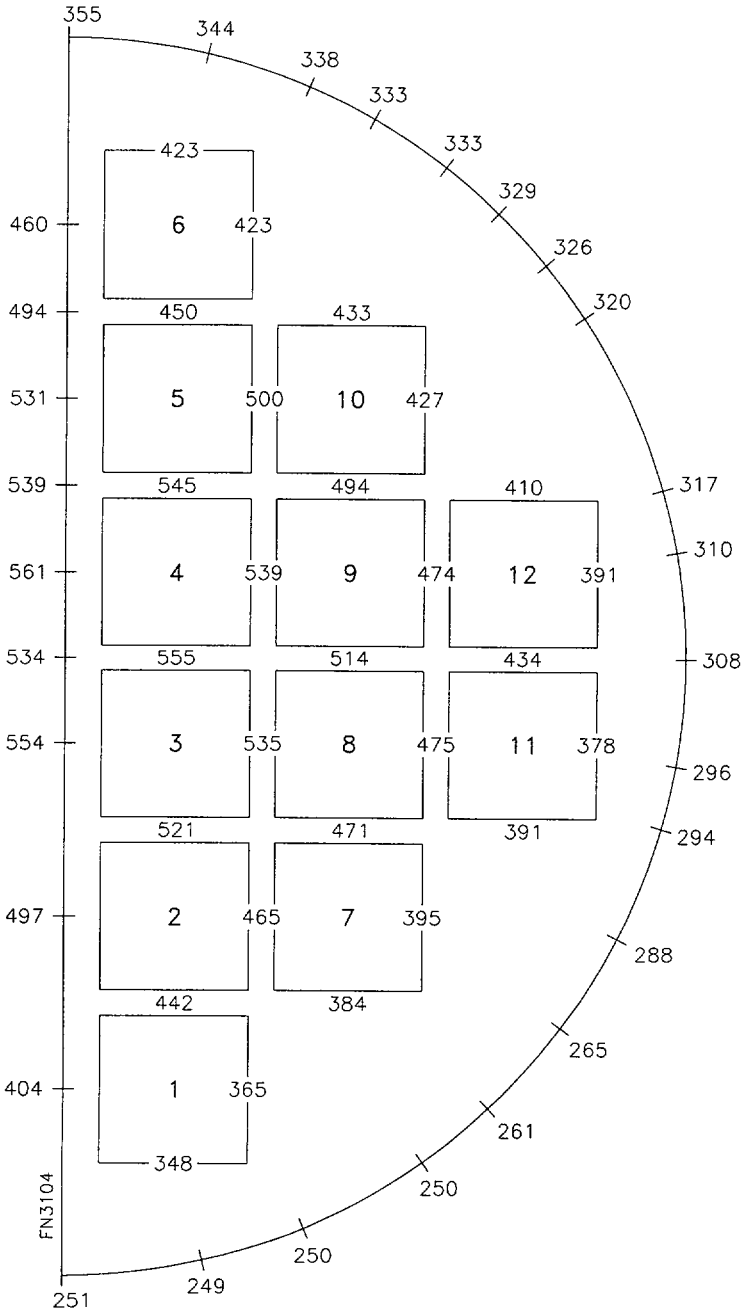


Reference: NUH004.0423, R/2, Figure A-

**Figure 8.1-5**
**NUHOMS®-24P DSC Spacer Disc Temperature Distribution for 100°F Ambient**

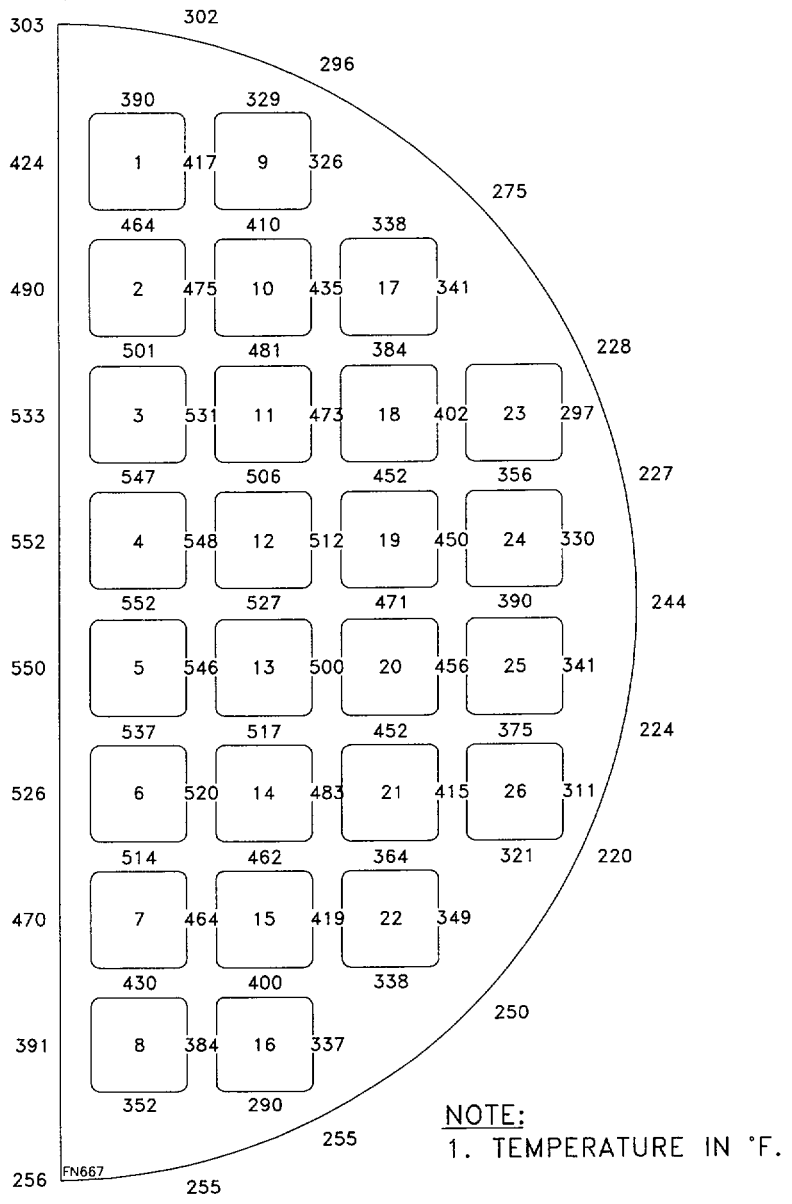


**Figure 8.1-6**
**NUHOMS®-52B DSC Spacer Disk Temperature Distribution for 100°F Ambient**

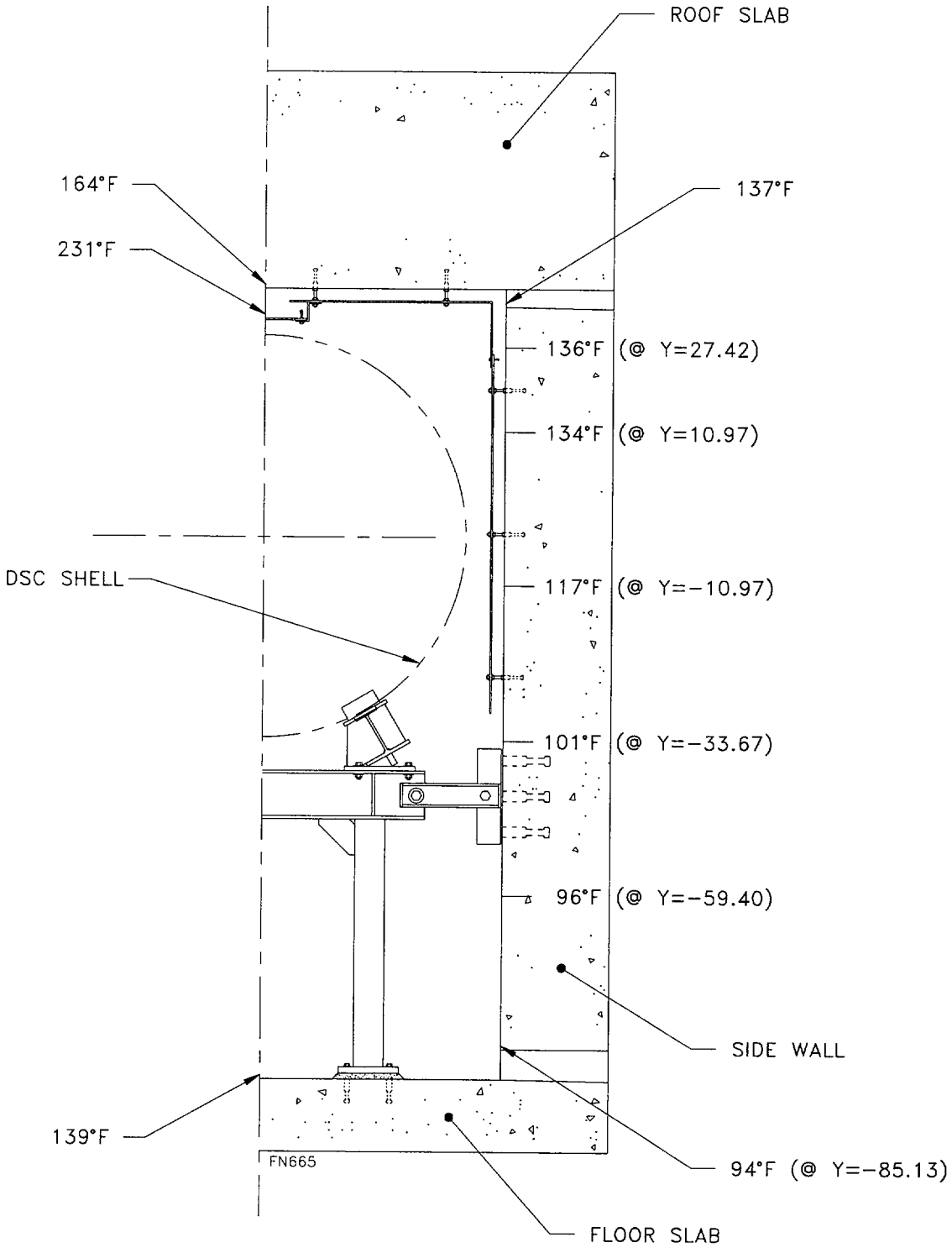


**Figure 8.1-7**
**NUHOMS®-24P HSM Temperature Distribution for 70°F Ambient**

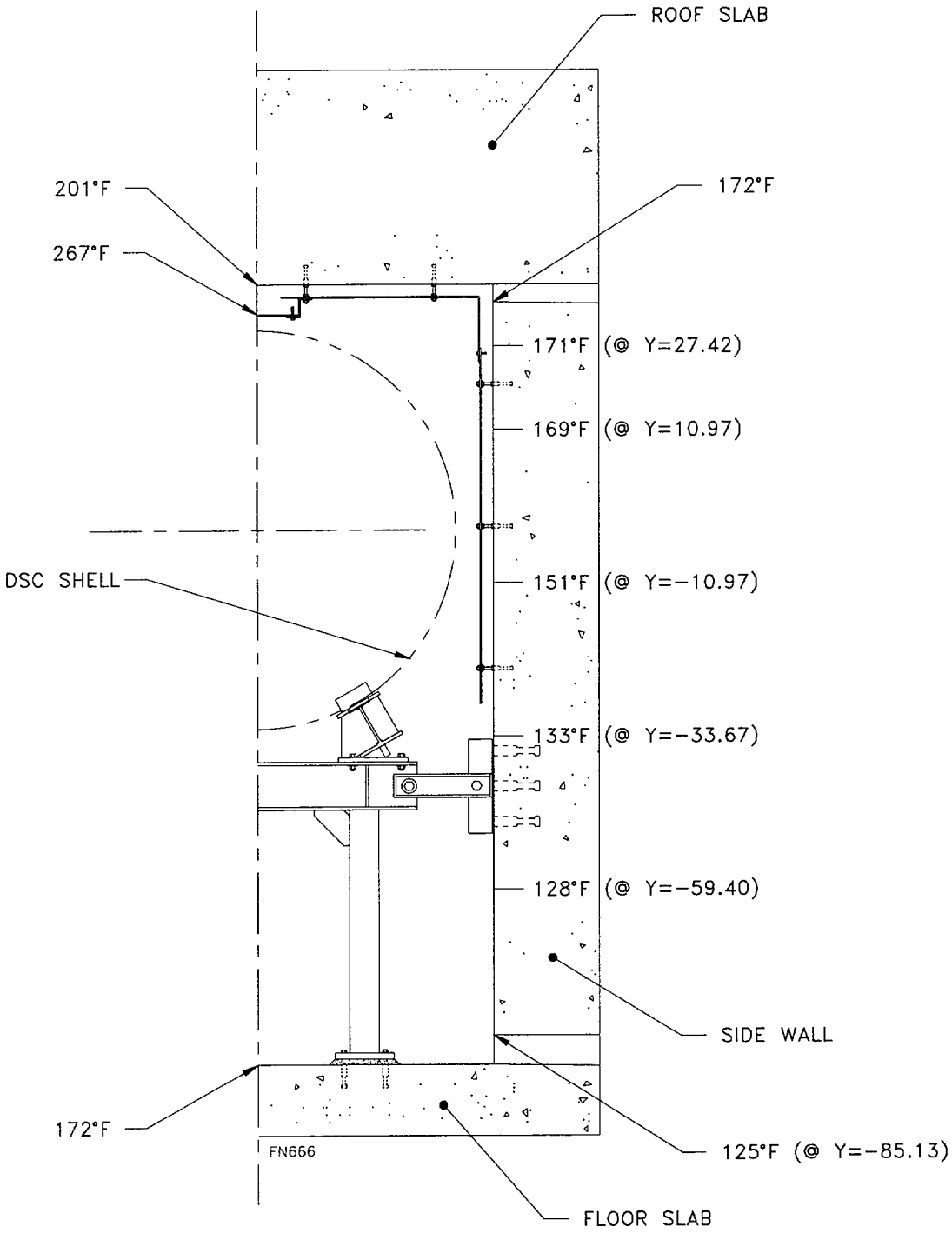


**Figure 8.1-8**
**NUHOMS®-24P HSM Temperature Distribution for 100°F Ambient**

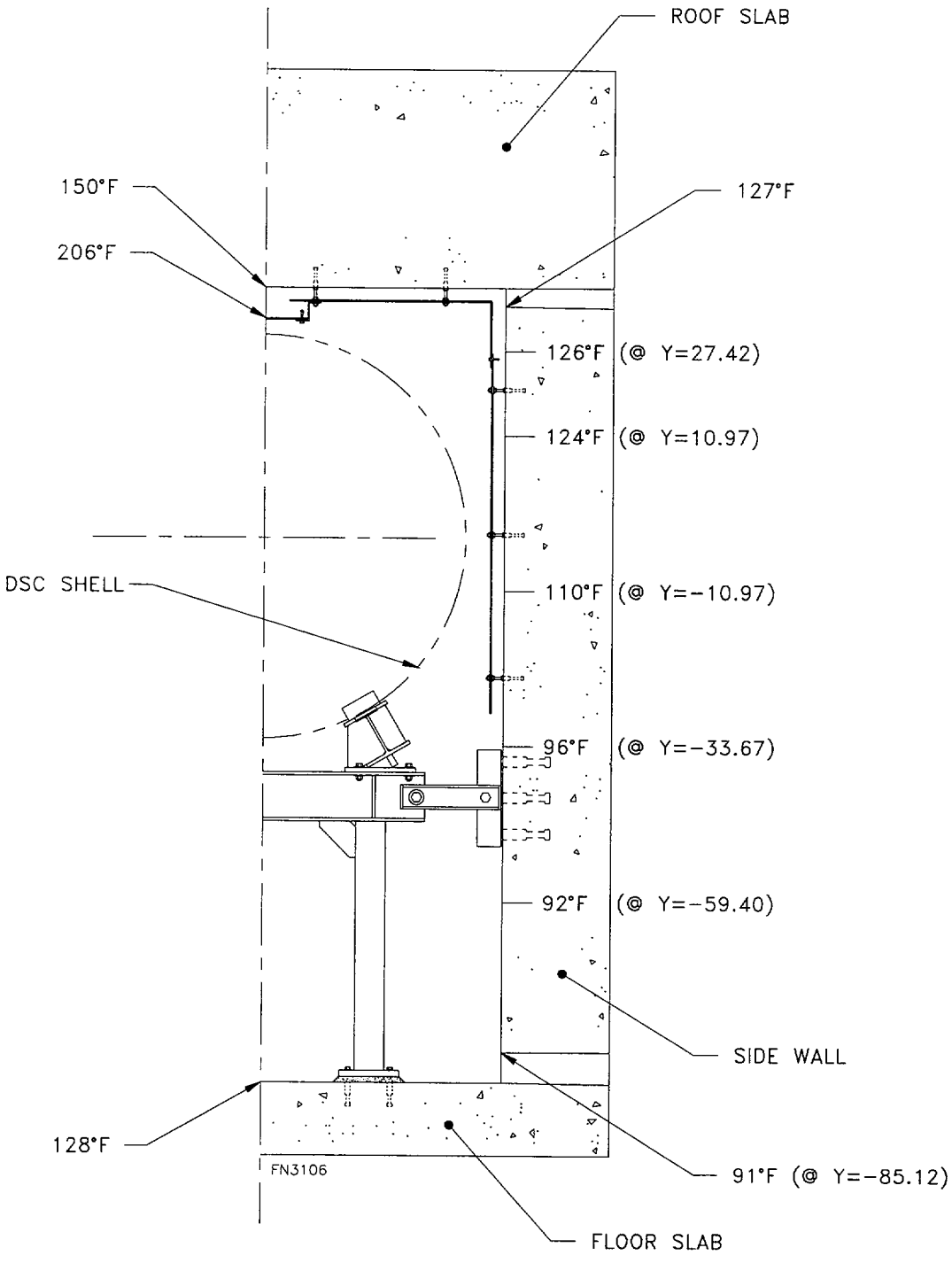


**Figure 8.1-9**
**NUHOMS®-52B HSM Temperature Distribution for 70°F Ambient**

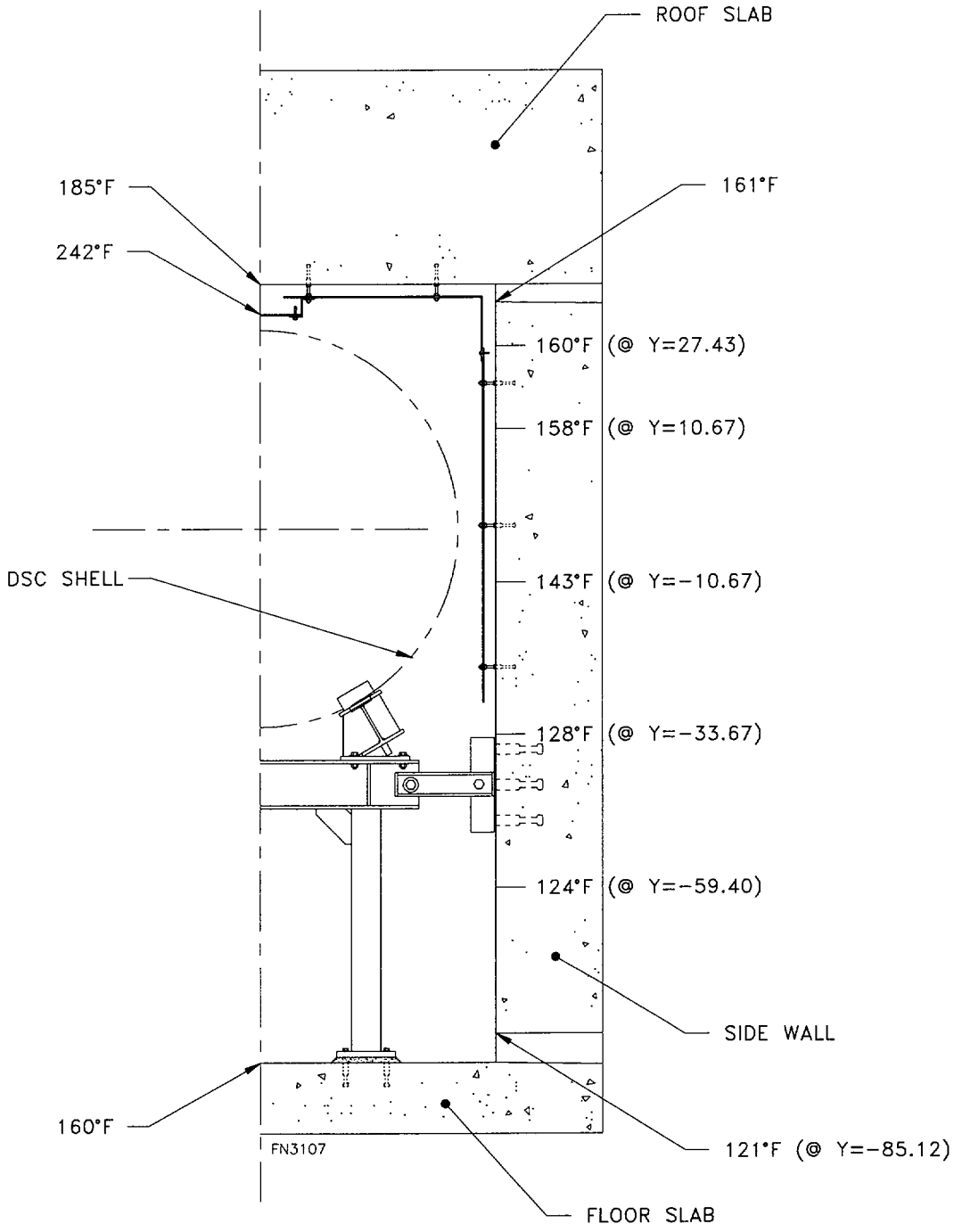


**Figure 8.1-10**
**NUHOMS®-52B HSM Temperature Distribution for 100°F Ambient**

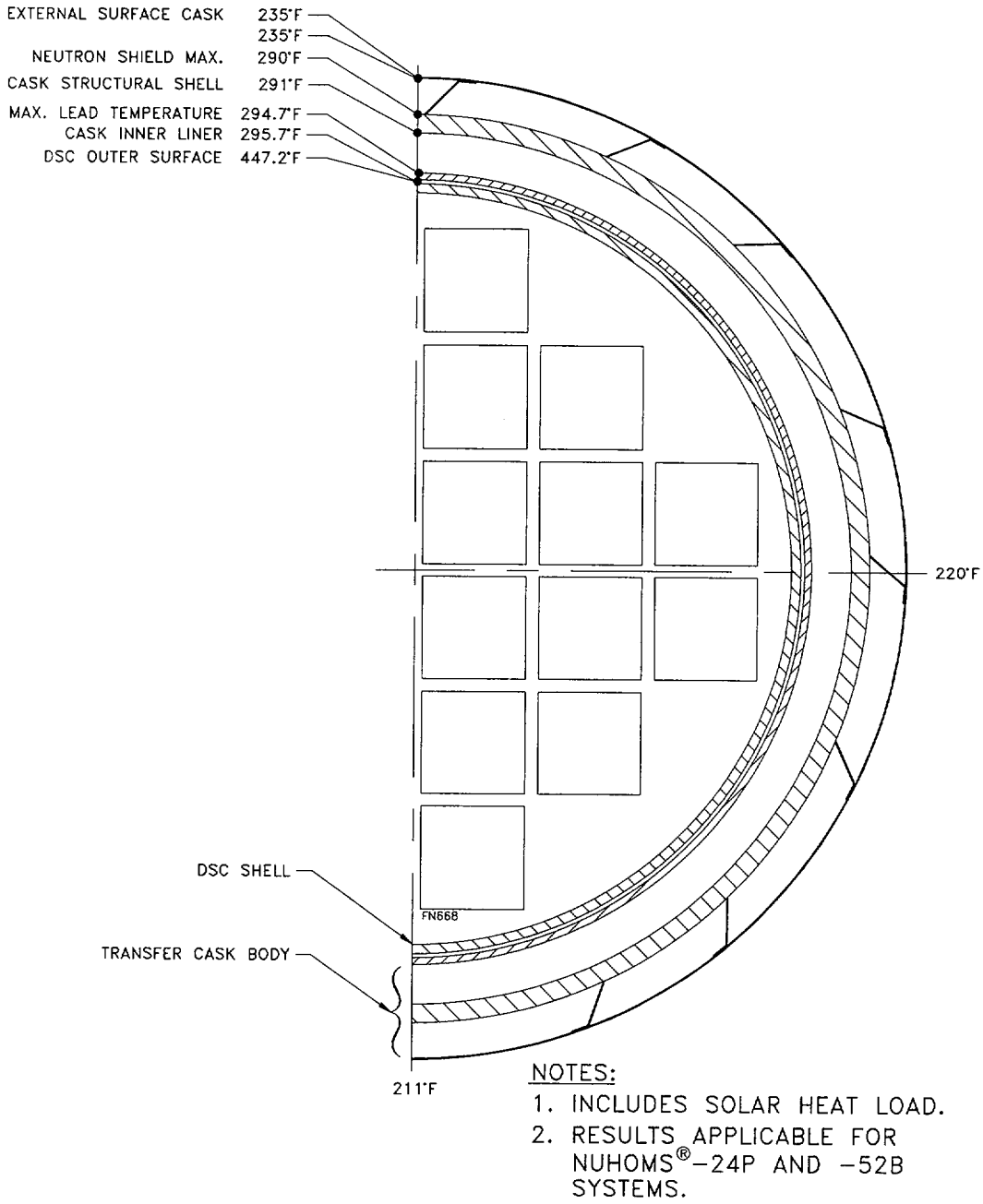


**Figure 8.1-11**
**Standardized Transfer Cask Temperature Distribution for 100°F Ambient**

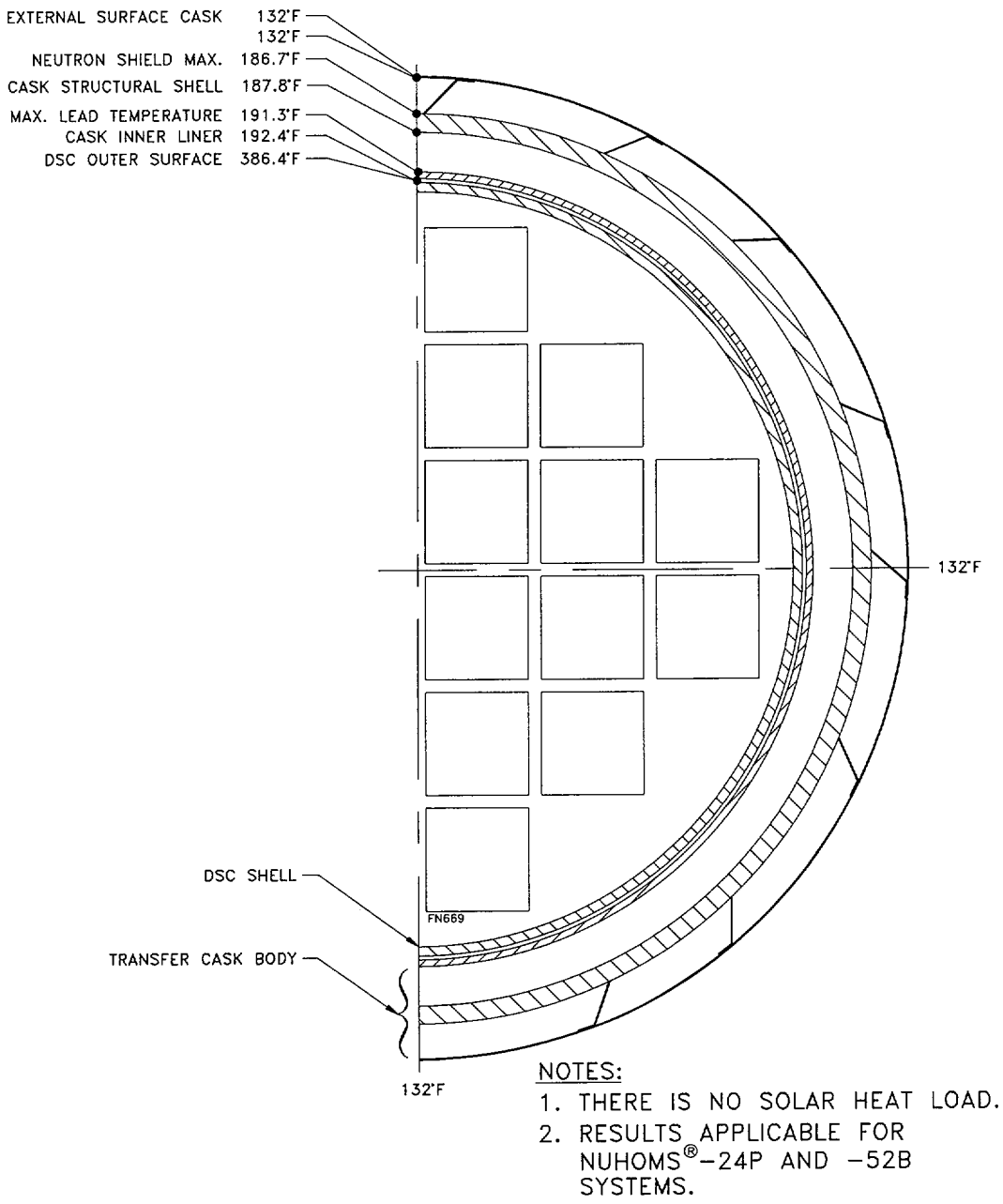


**Figure 8.1-12**
**Standardized Transfer Cask Temperature Distribution for 0°F Ambient**

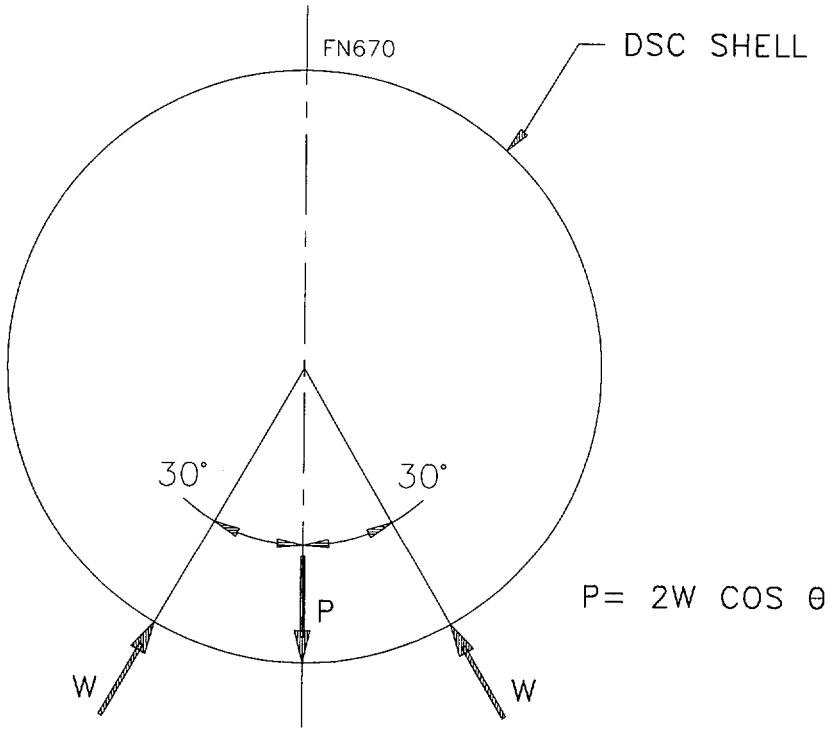


KEY:

P= DEAD WEIGHT OF LOADED DSC.

W= DSC SUPPORT RAIL REACTION.

**Figure 8.1-13**
**DSC Shell Stress Analysis Diagram**

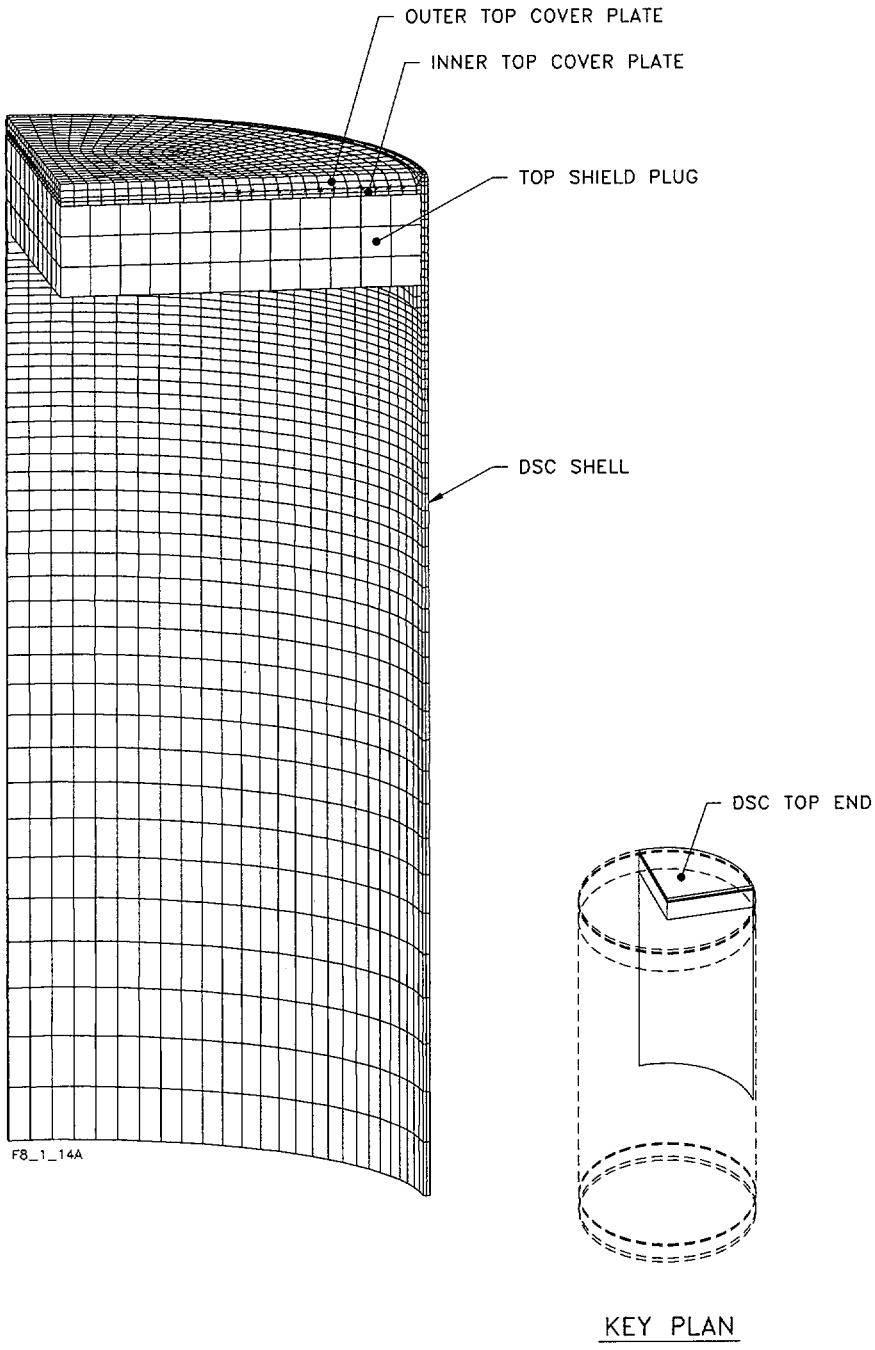


**Figure 8.1-14a**
**DSC Shell Assembly Top End 90° Analytical Model**

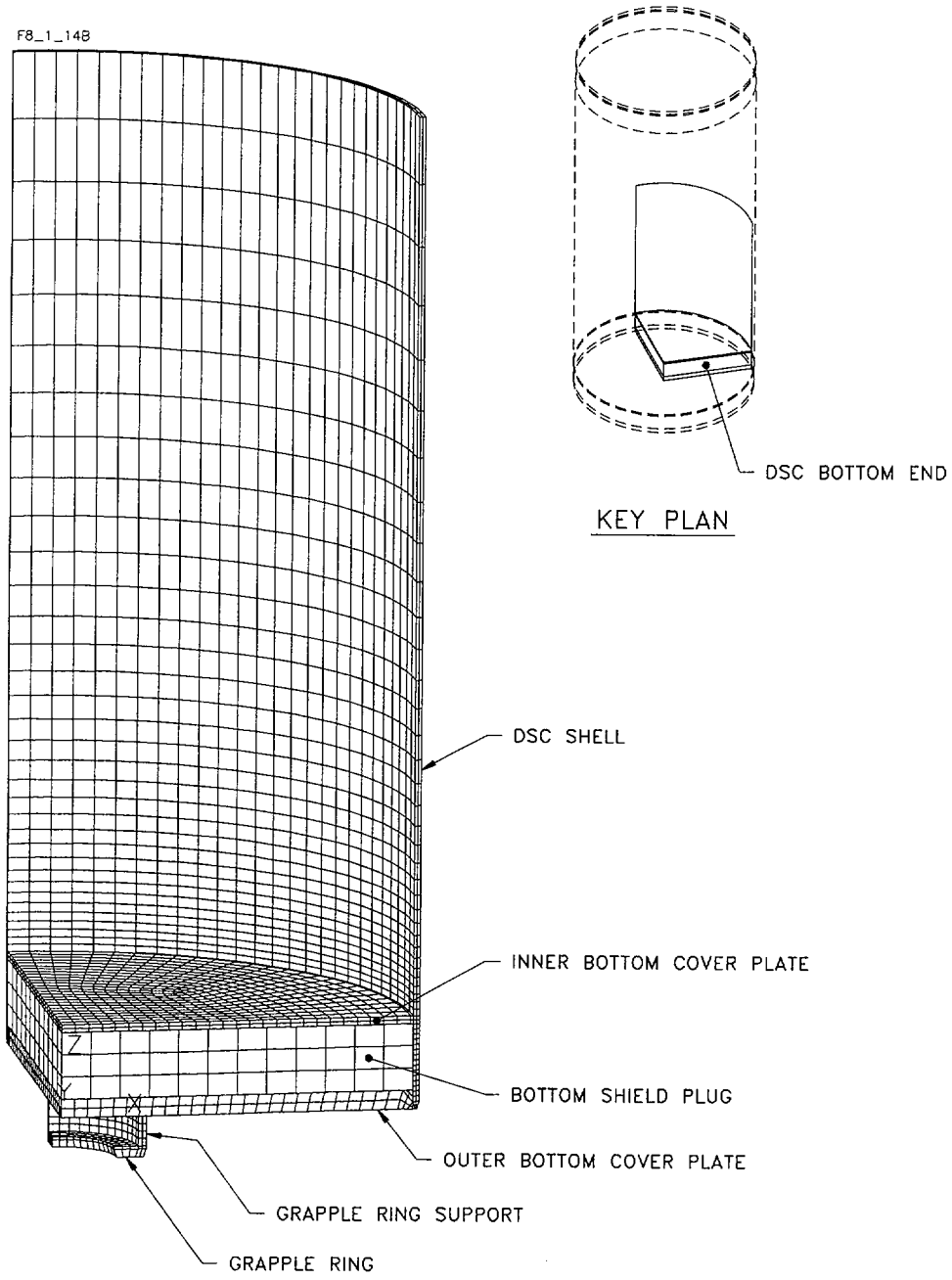


**Figure 8.1-14b**
**DSC Shell Assembly Bottom End 90° Analytical Model**

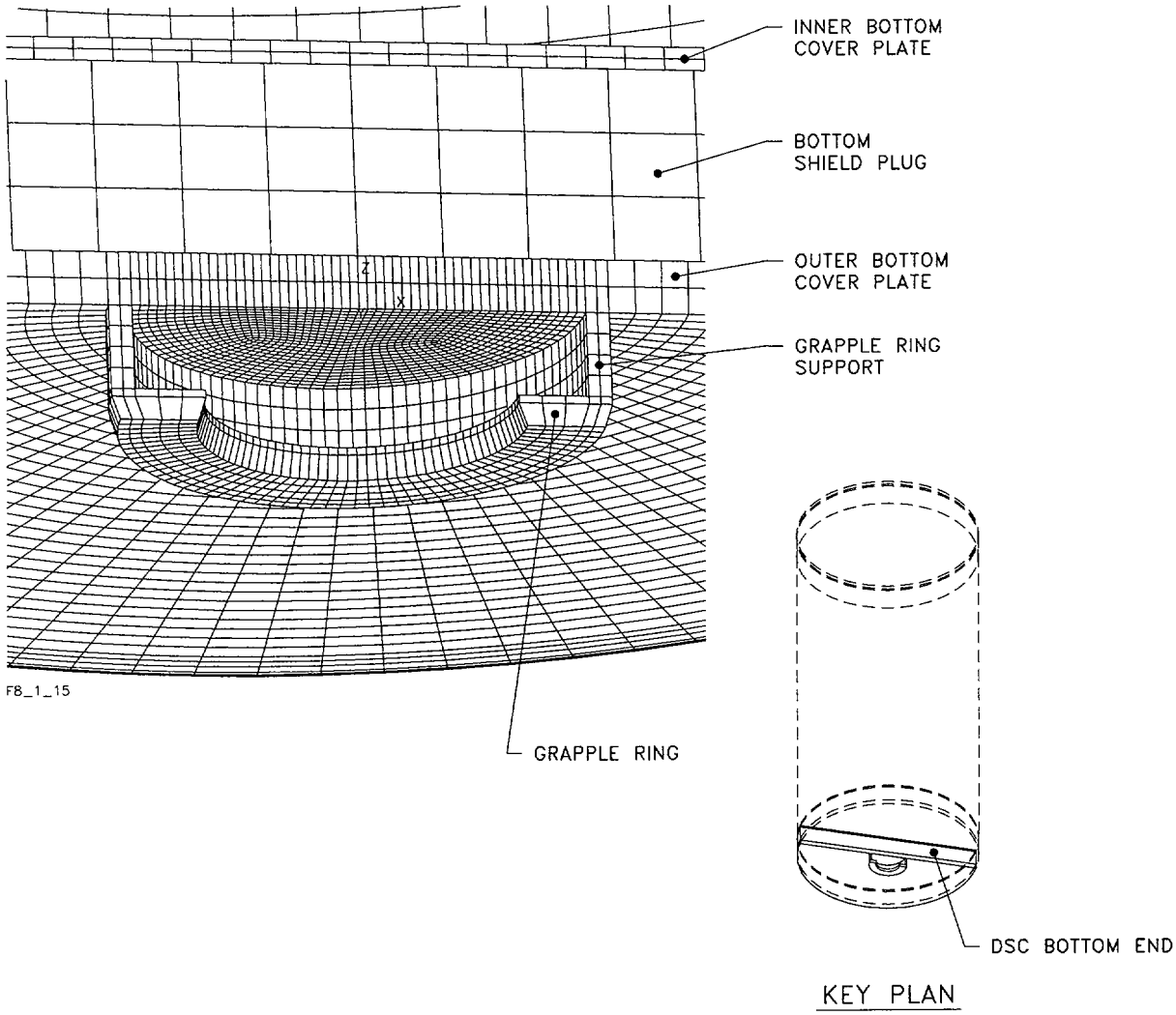


**Figure 8.1-15**
**Partial View of DSC Shell Assembly Bottom End 180° Analytical Model Showing End Plates and Grapple Assembly**

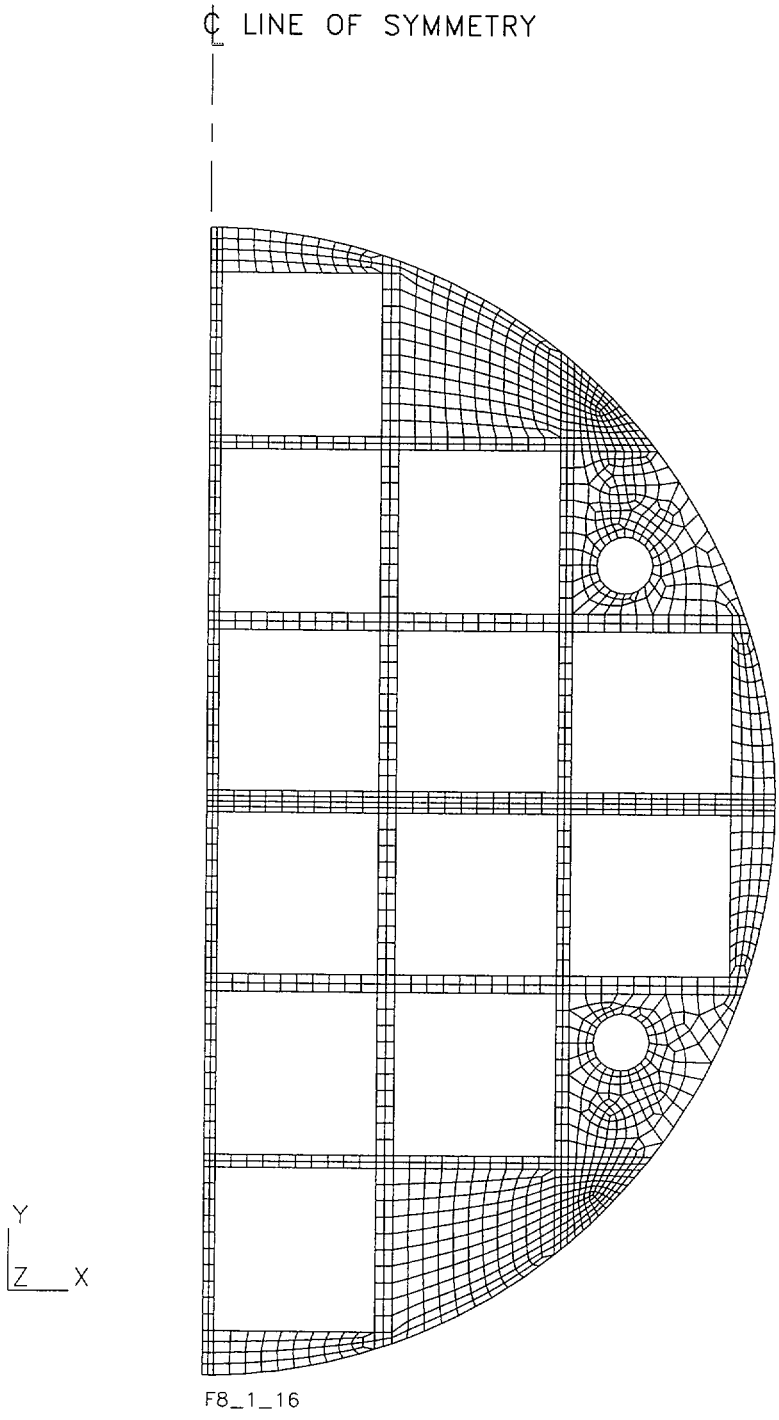


**Figure 8.1-16**
**NUHOMS®-24P DSC Spacer Disk Thermal Model**

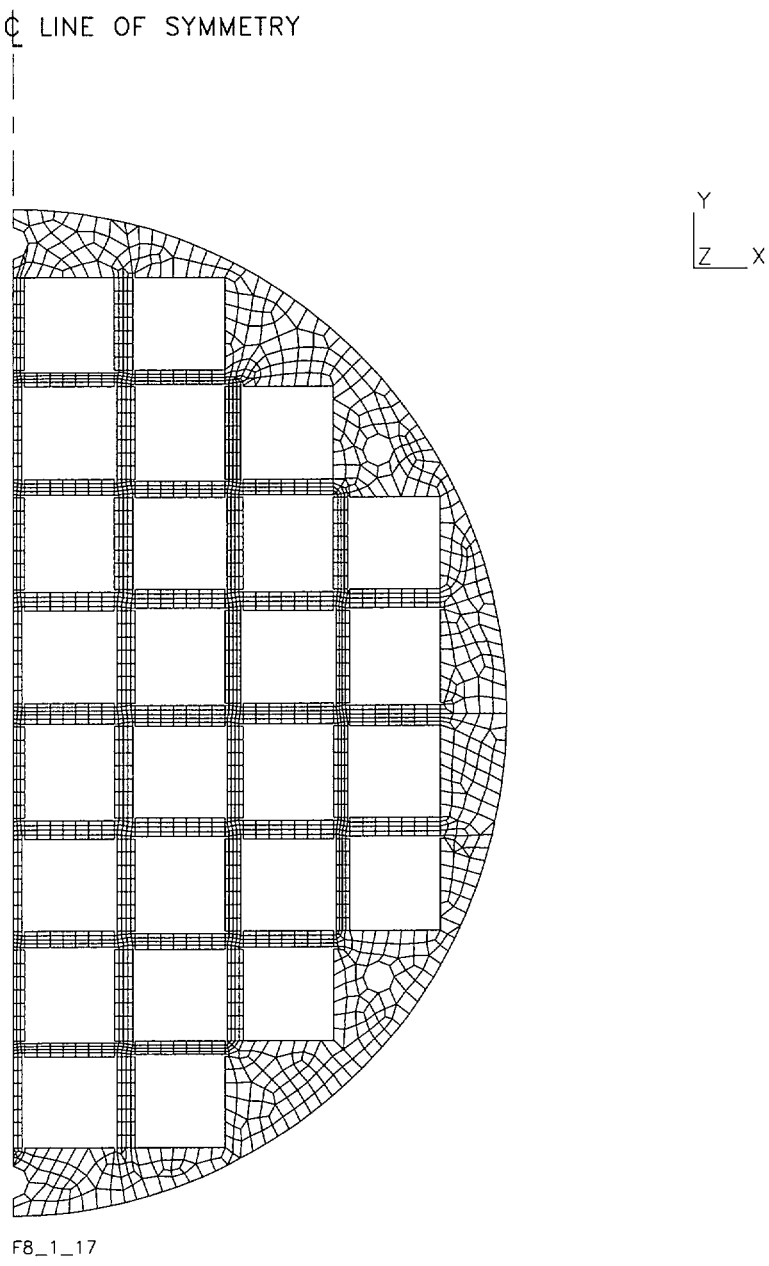


**Figure 8.1-17**
**NUHOMS®-52B DSC Spacer Disk Thermal Model**

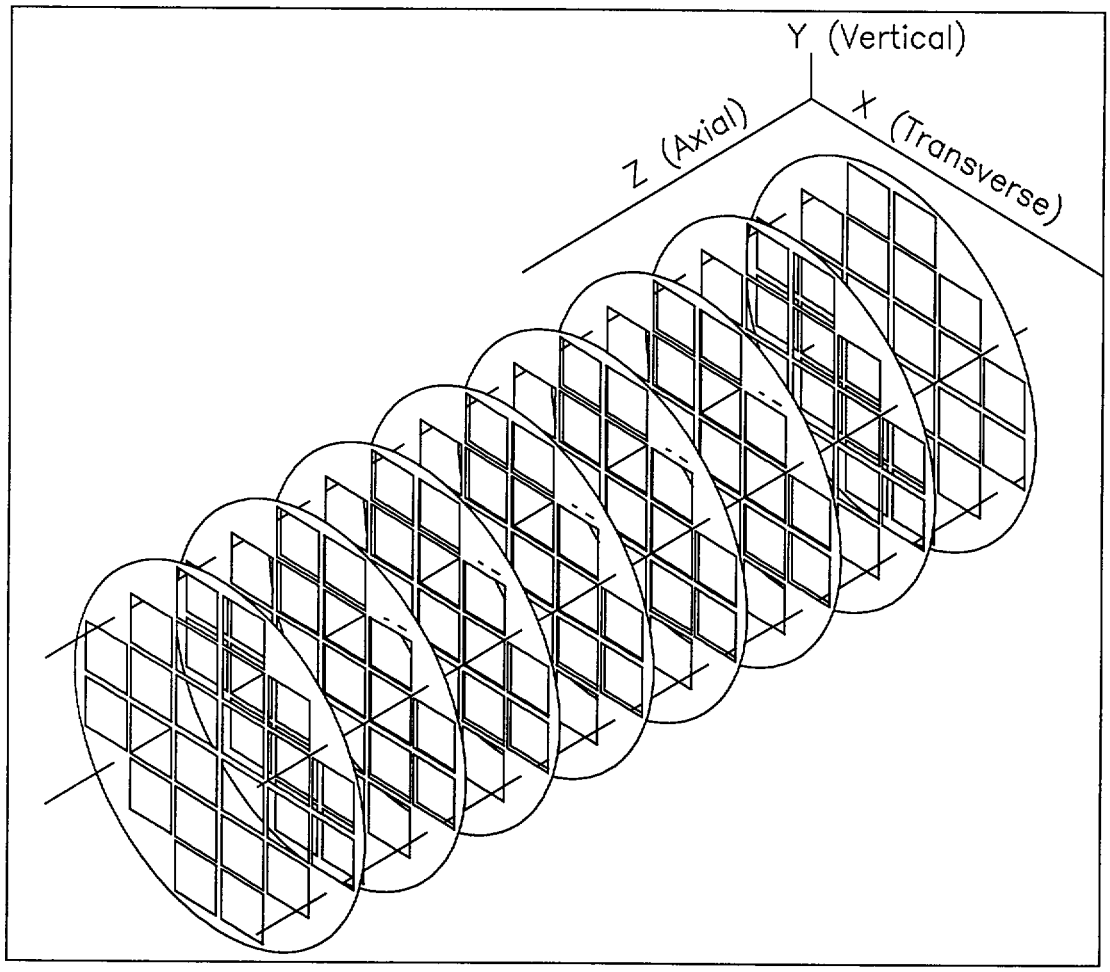


**Figure 8.1-18**
**NUHOMS®-24P DSC Basket Assembly Handling Model**

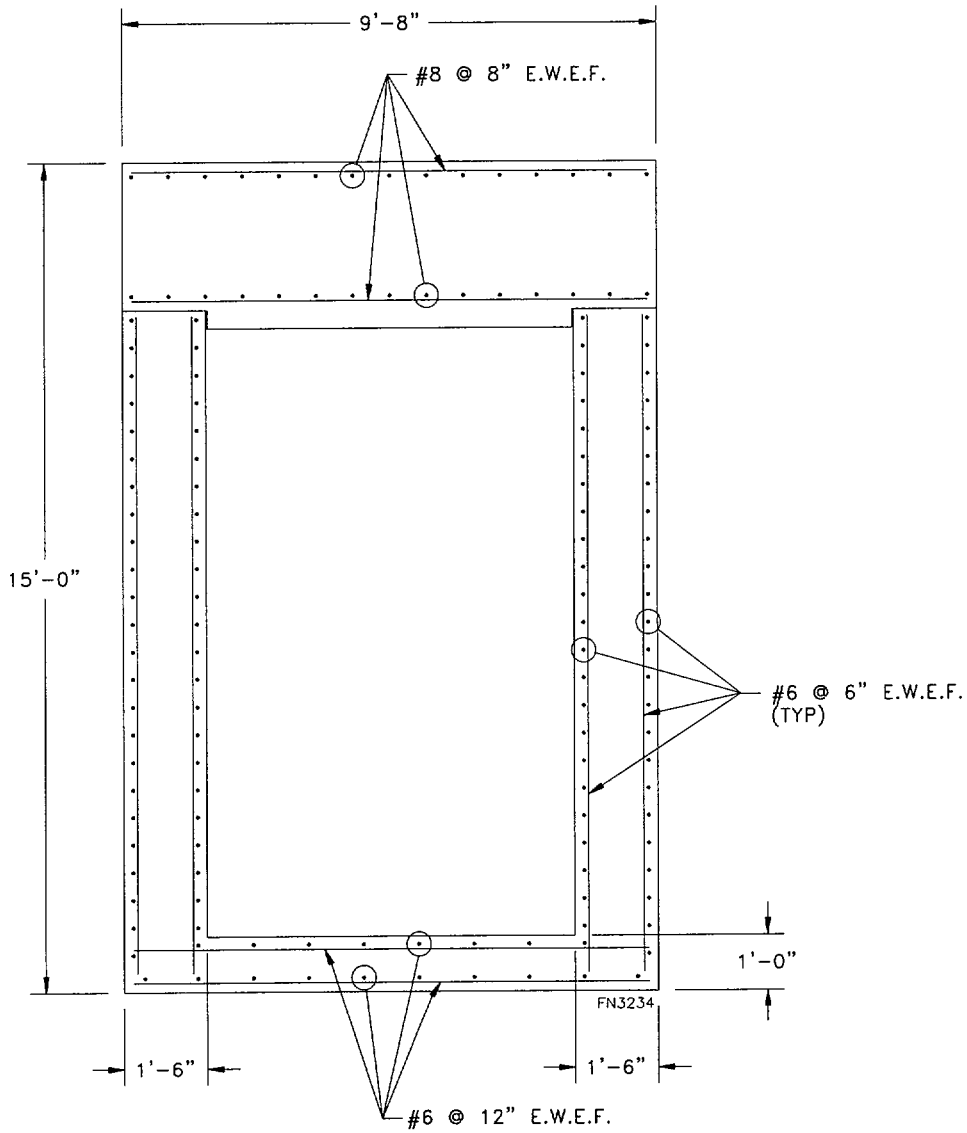


**Figure 8.1-19**
**Typical HSM Reinforcement (Reinforcing bar size and spacing)**

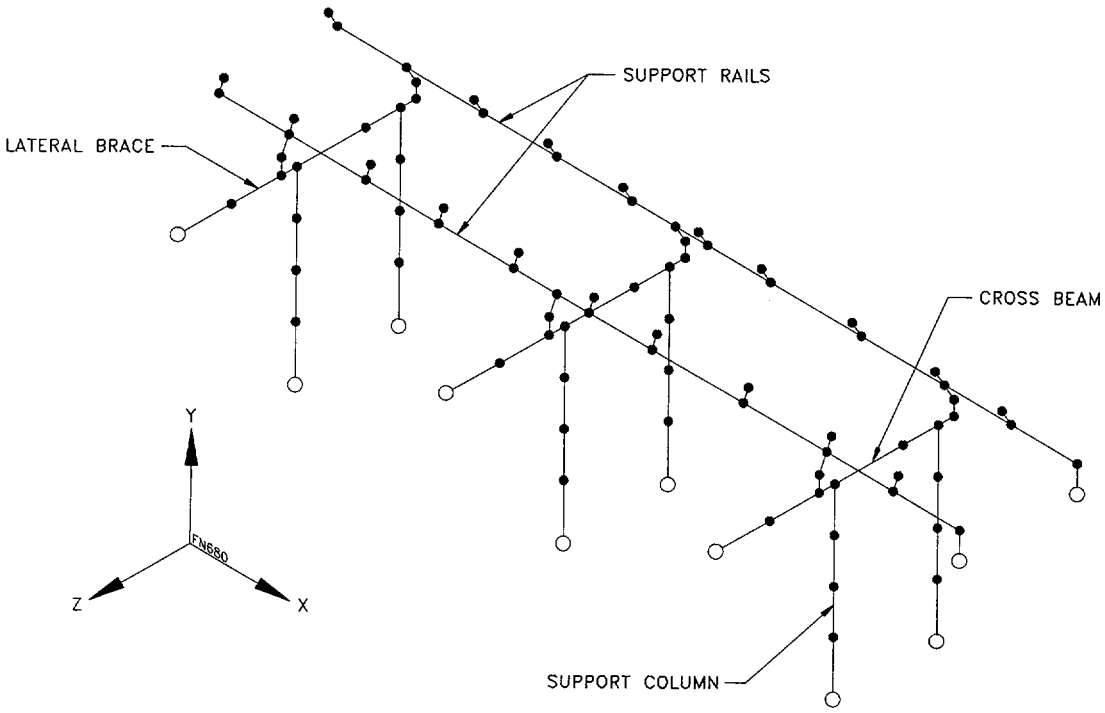


**Figure 8.1-20**
**DSC Support Structure Analytical Model**

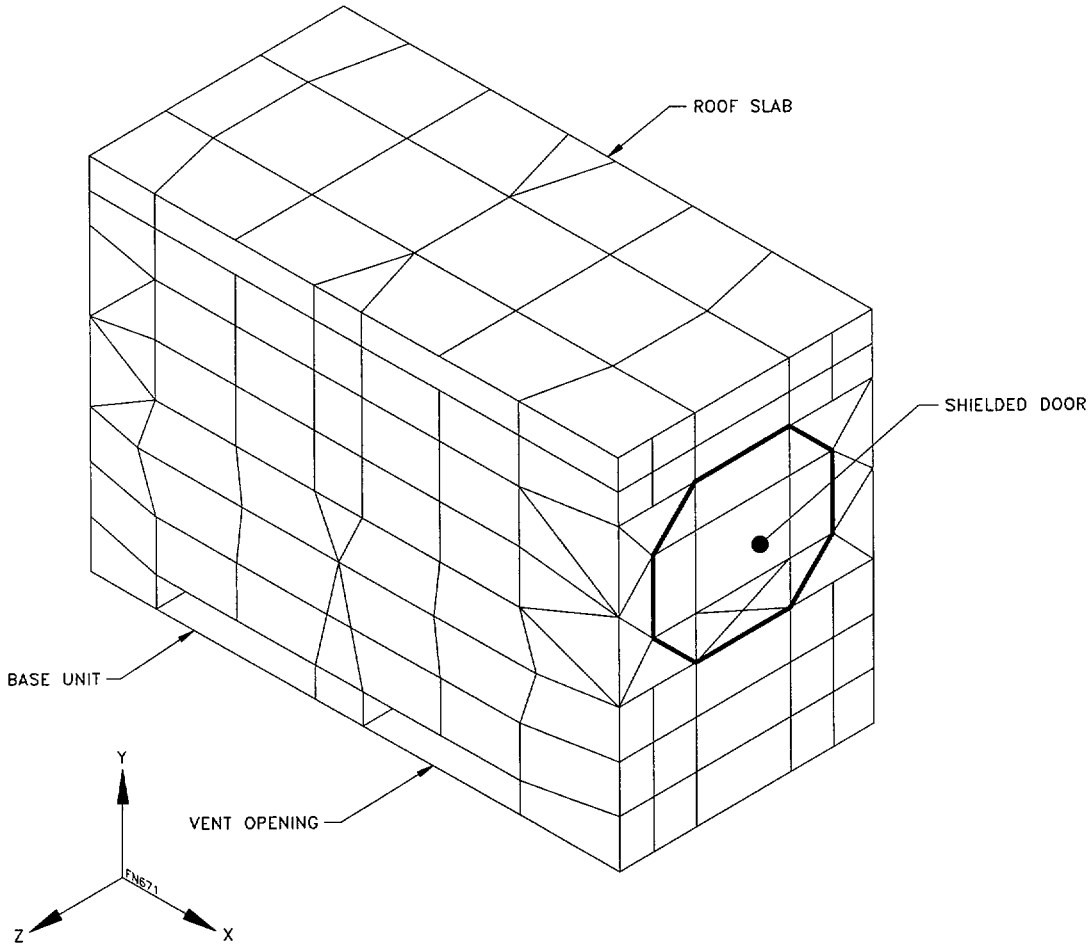


**Figure 8.1-21**
**Prefabricated HSM Analytical Model**

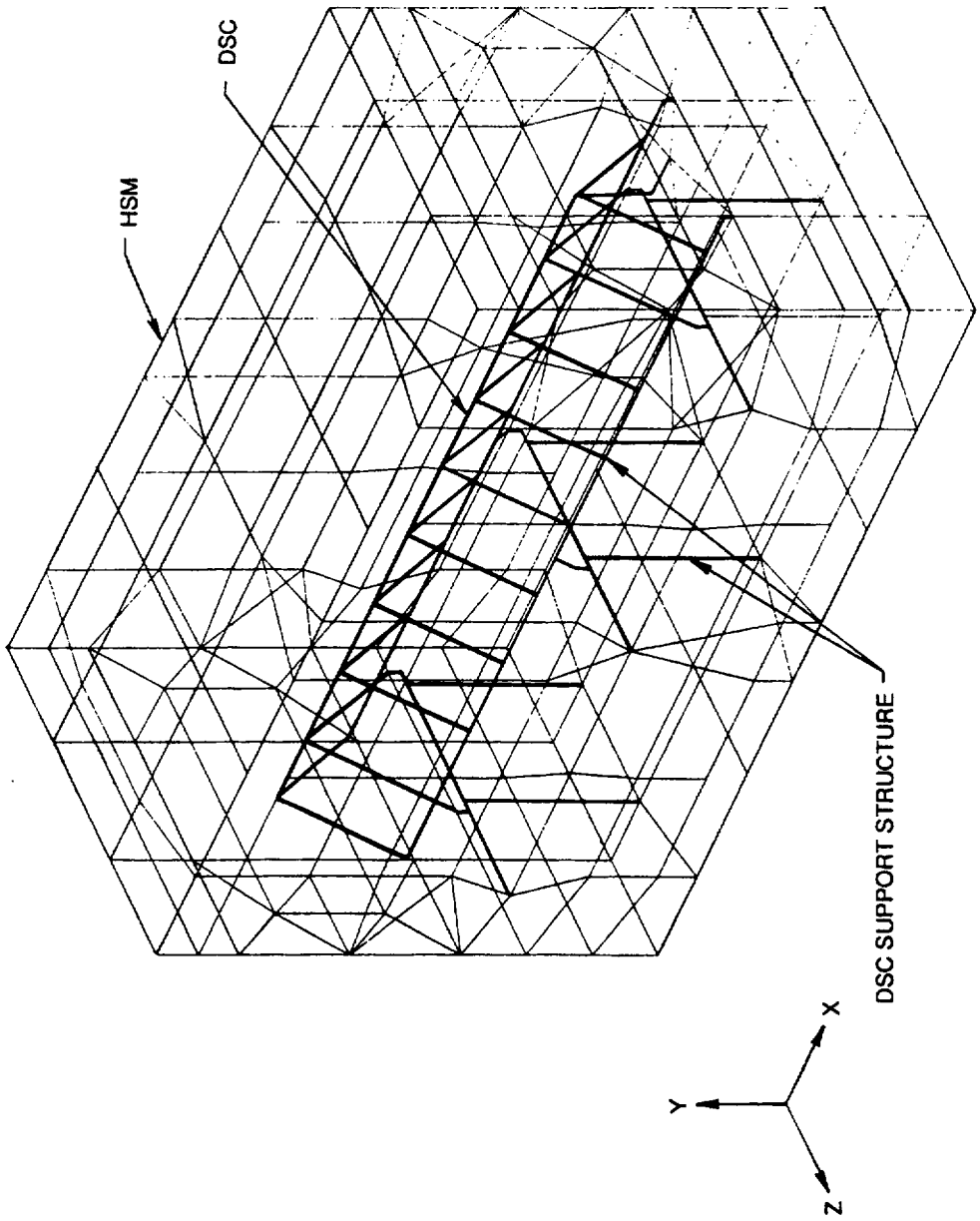


**Figure 8.1-22**
**Analytical Model for HSM, DSC, and DSC Support Structure**

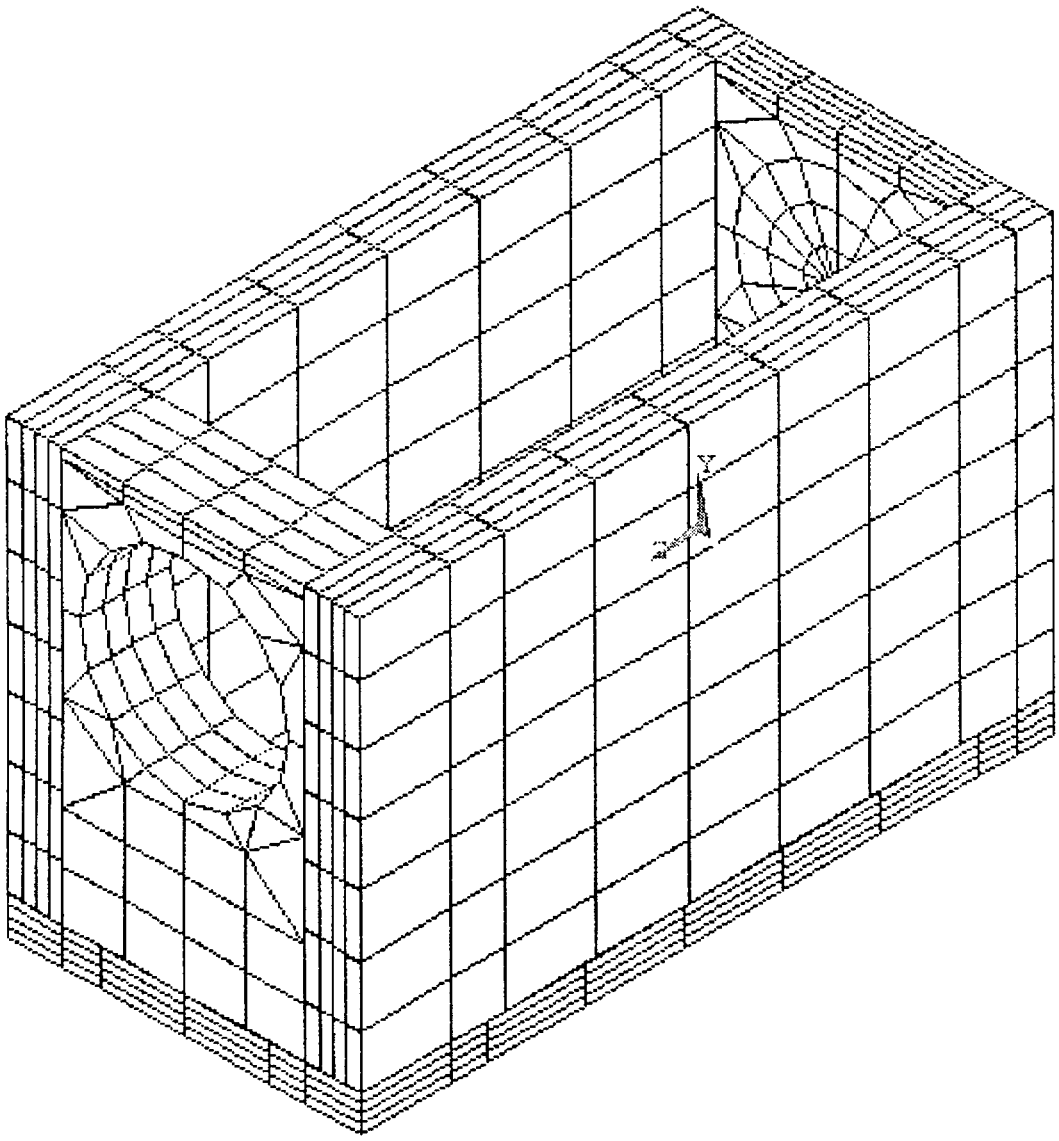

**Figure 8.1-23**
**Analytical Model for HSM Base Unit Thermal Conditions**

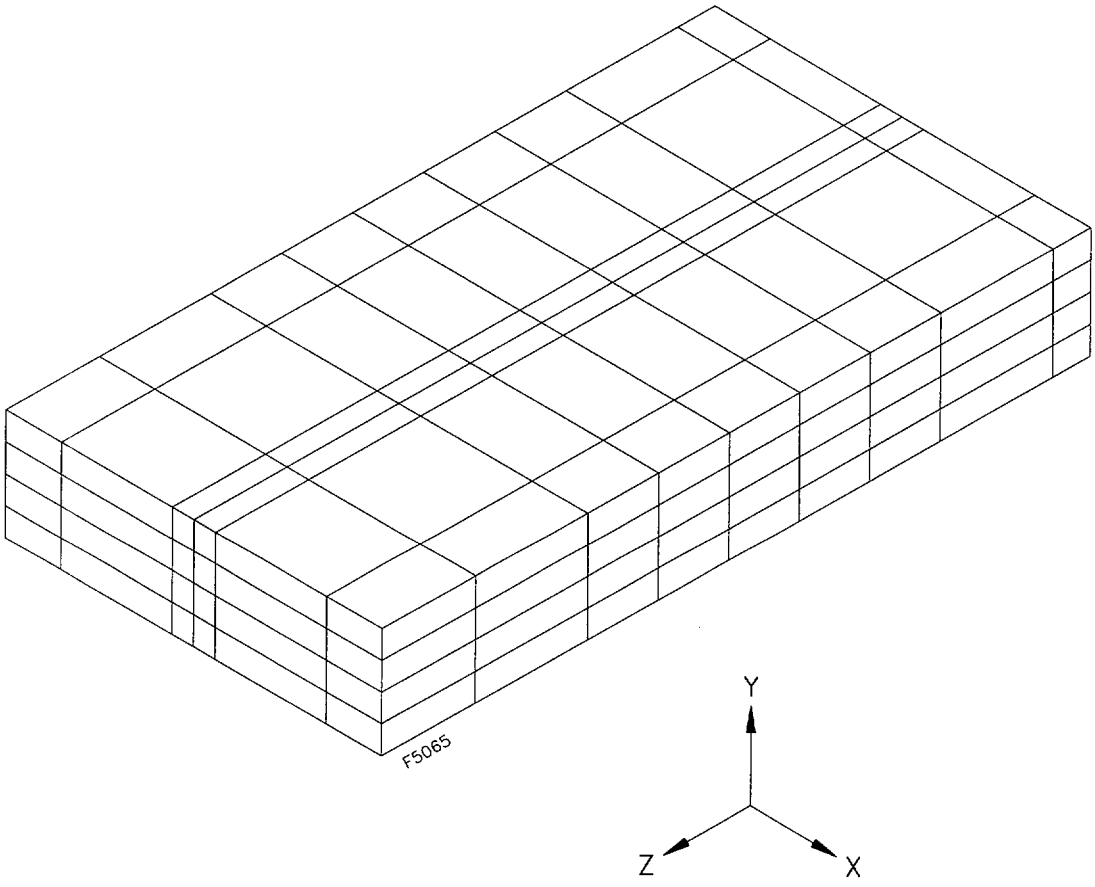


**Figure 8.1-24**
**Analytical Model for HSM Roof Thermal Conditions**

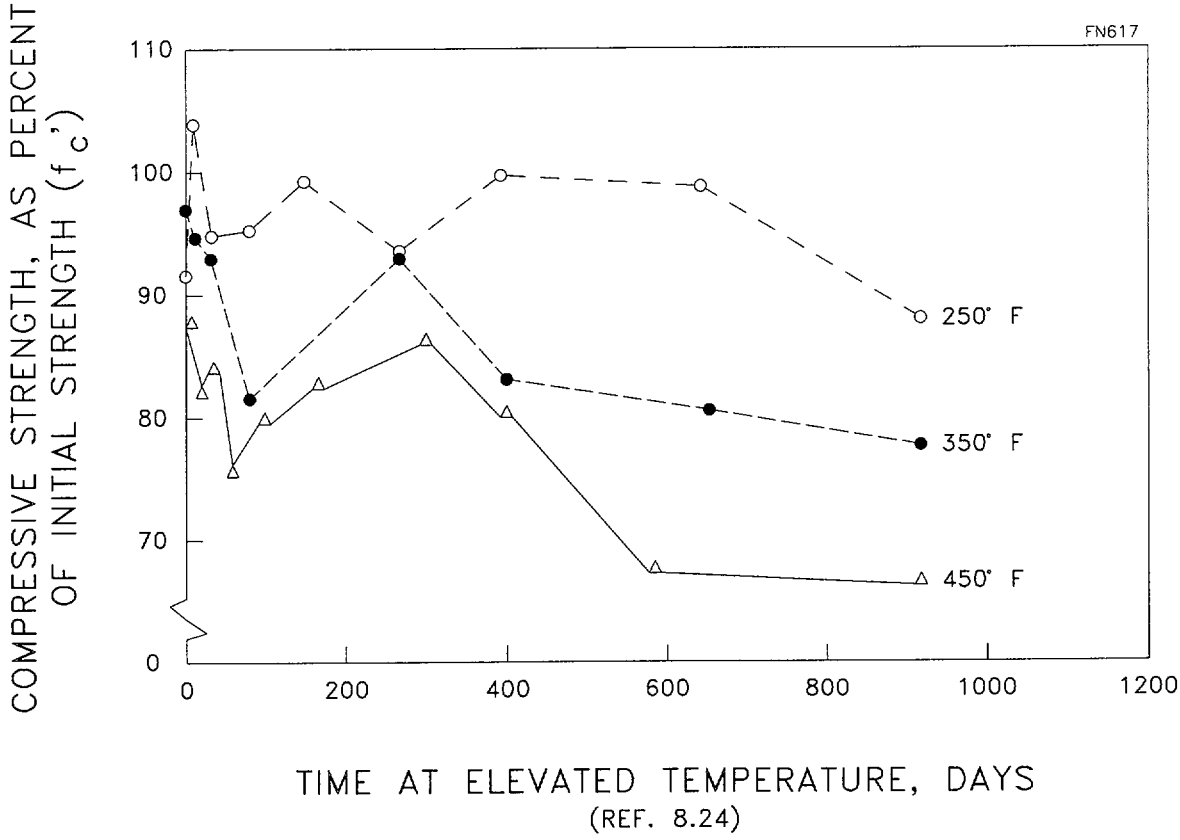


**Figure 8.1-25**
**Variation in Strength of Basalt Aggregate Concrete with Temperature and Length of Exposure**

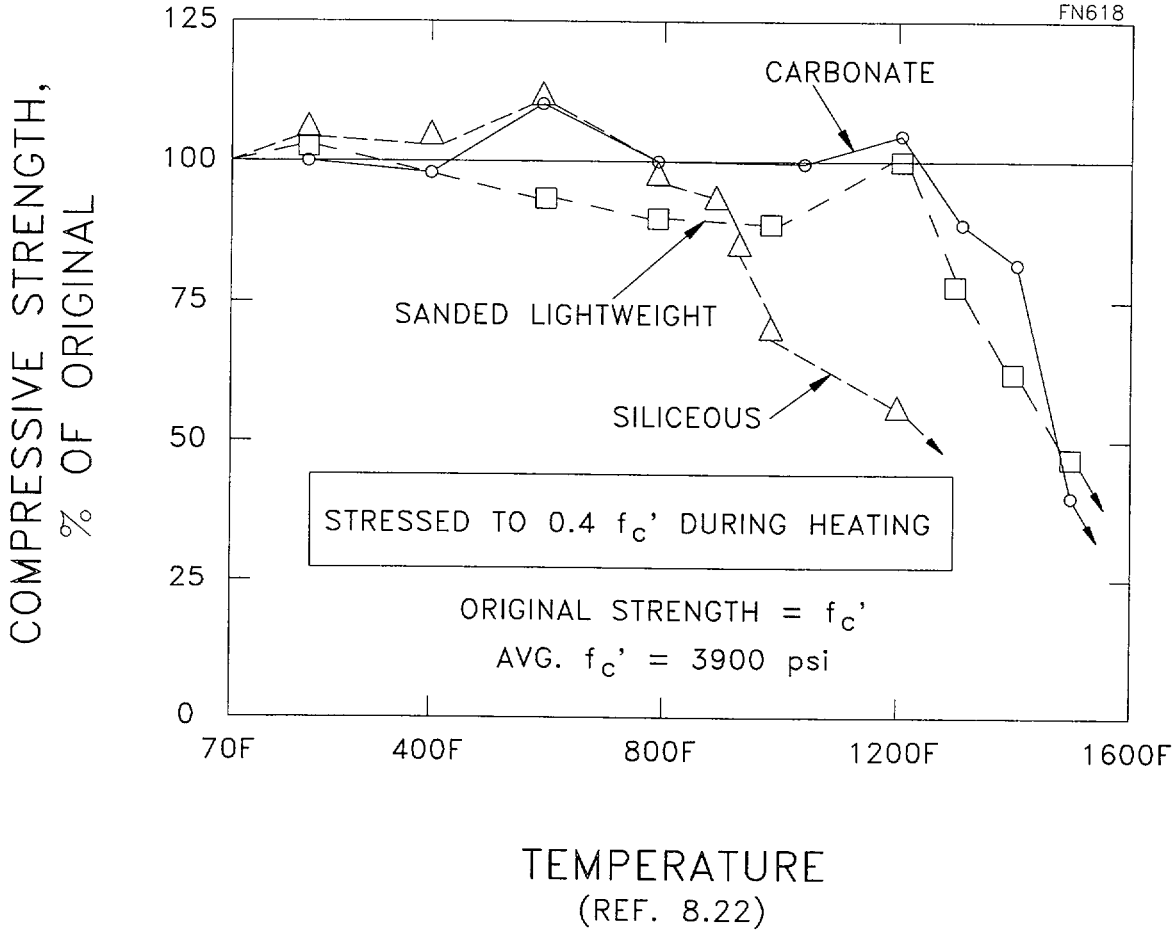


**Figure 8.1-26**
**Compressive Strength of Concrete at High Temperature**

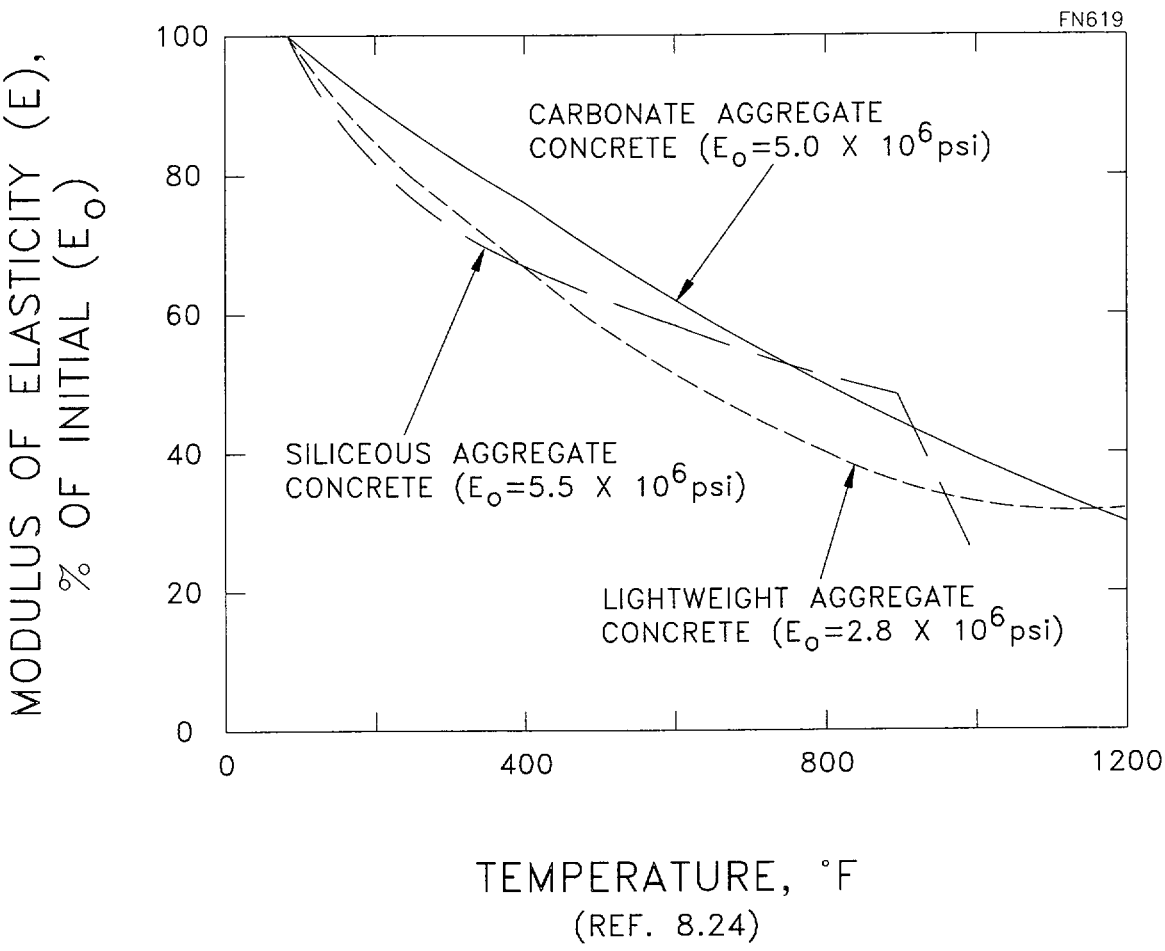


**Figure 8.1-27**
**Modulus of Elasticity of Concrete at High Temperatures**

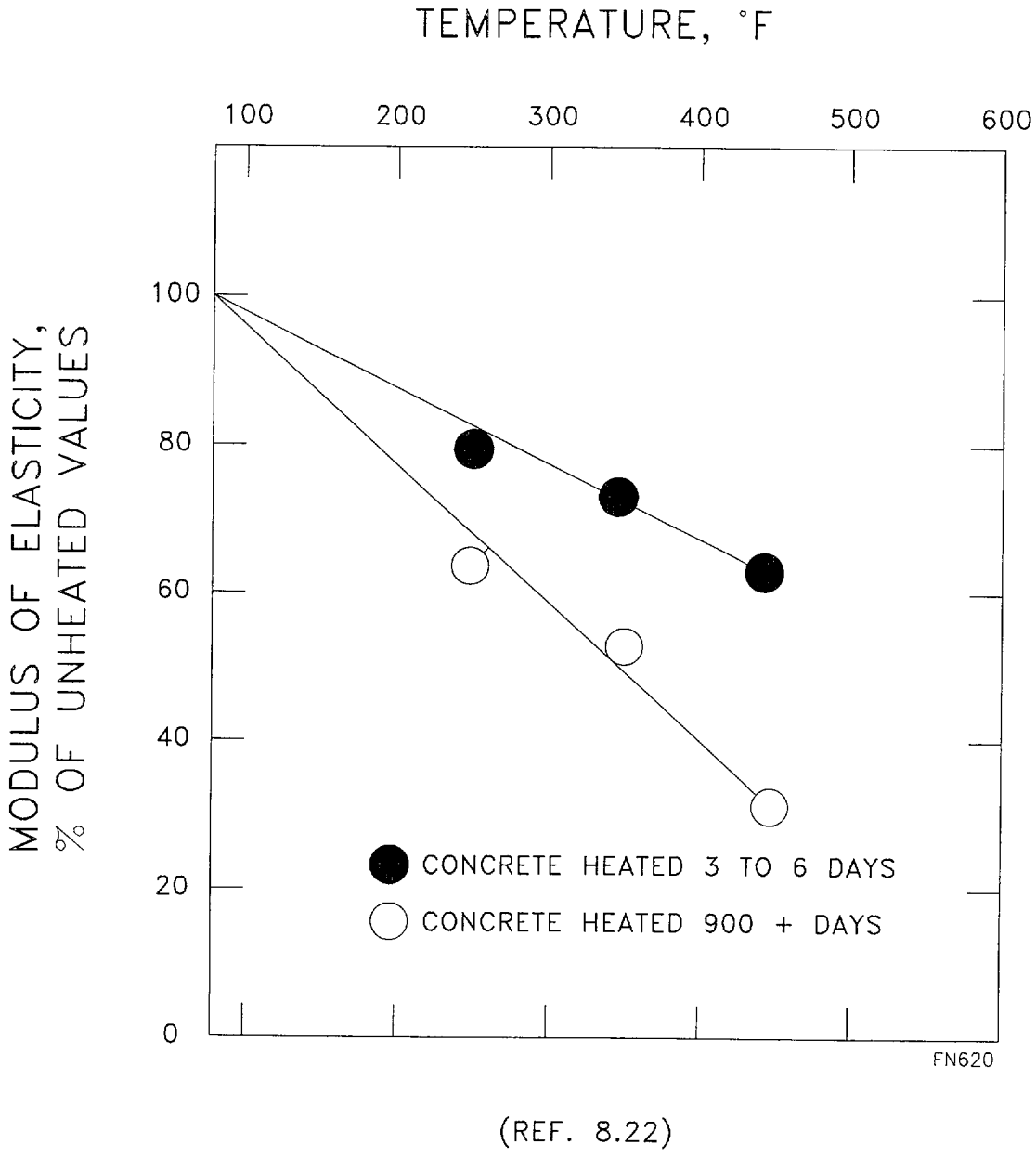


(REF. 8.22)

**Figure 8.1-28**
**Modulus of Elasticity for Portland Cement/Basalt Aggregate Concrete Subjected to Short and Long-Term Heating**

**Figure 8.1-29**

**Deleted**

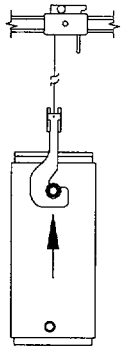

CASE 1: VERTICAL LIFT

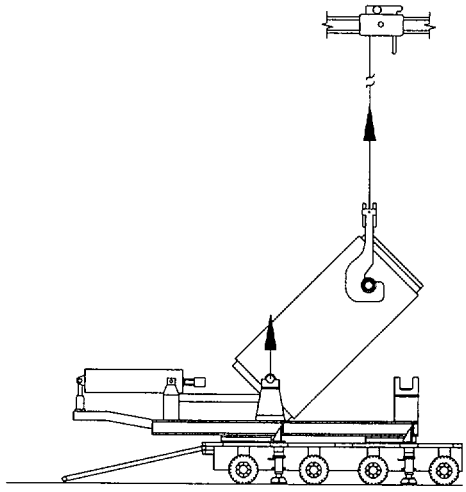

CASE 2: CASK DOWNENDING

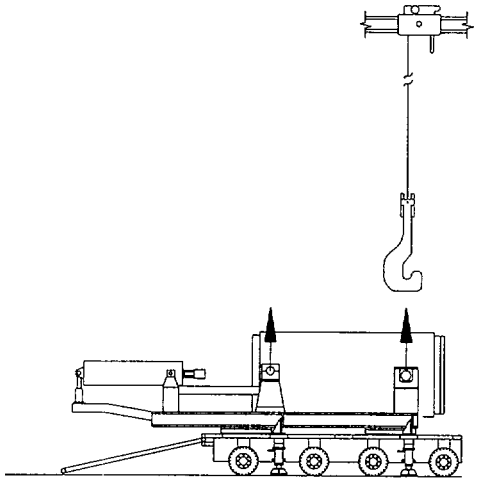

CASE 3: CASK HORIZONTAL ON SKID

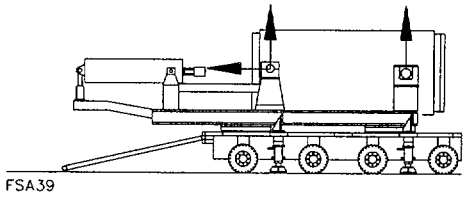


CASE 4: CASK TRANSPORT
(Transverse Loads Not Shown)

**Figure 8.1-30**
**Transfer Cask Handling Loads**

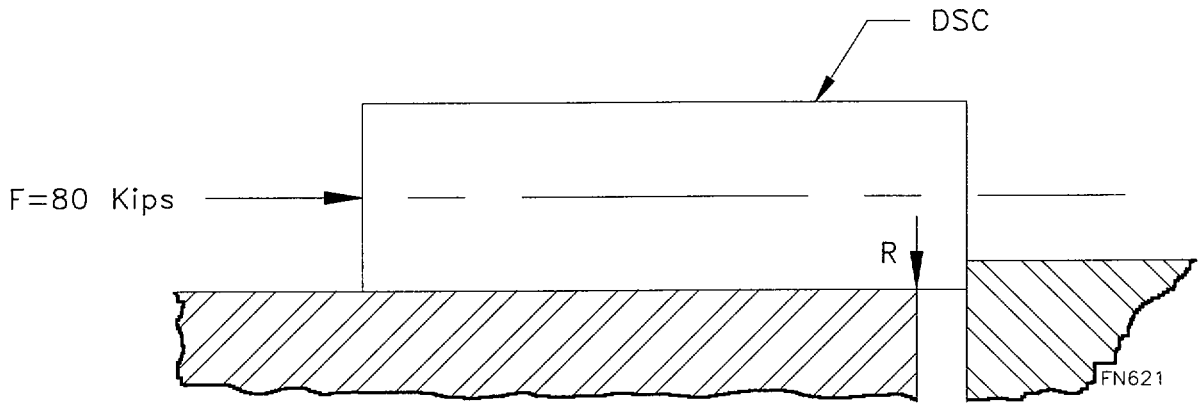


**Figure 8.1-31**
**DSC Axial Jam Condition**

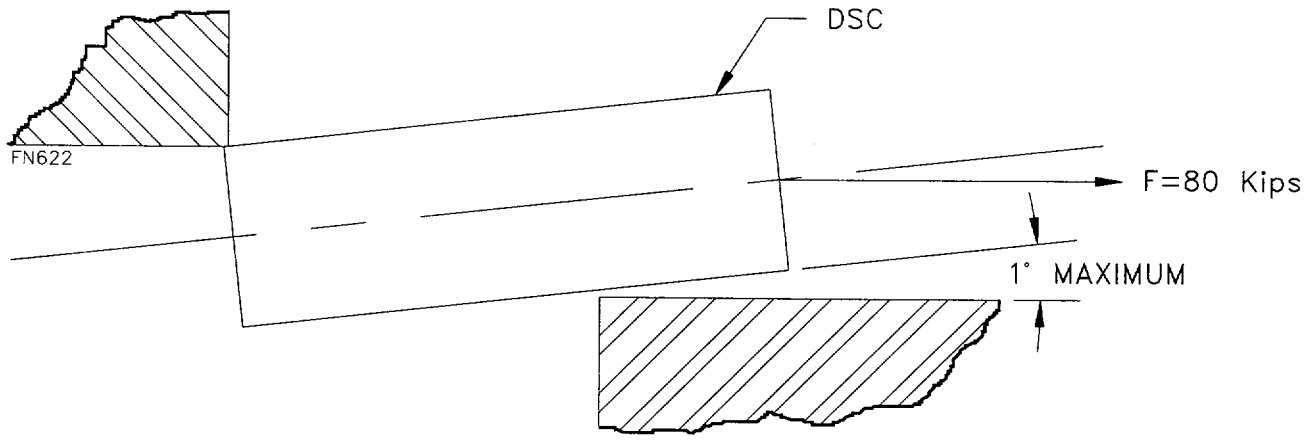


**Figure 8.1-32**
**DSC Binding (Pinching) Condition**

**Figure 8.1-33**

**Deleted**

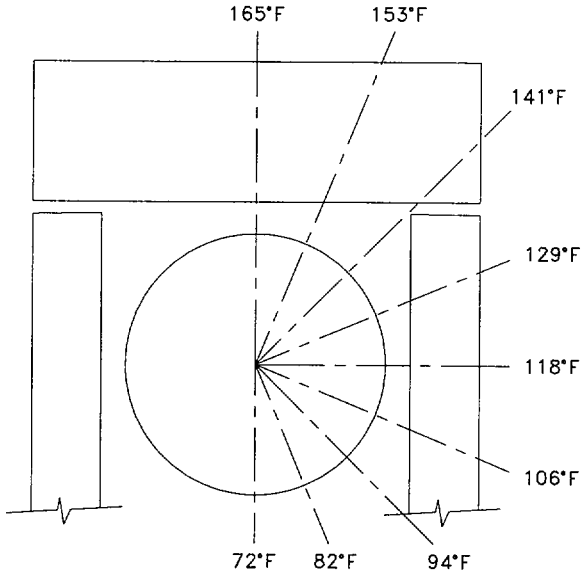


BULK AIR TEMPERATURES INSIDE HSM

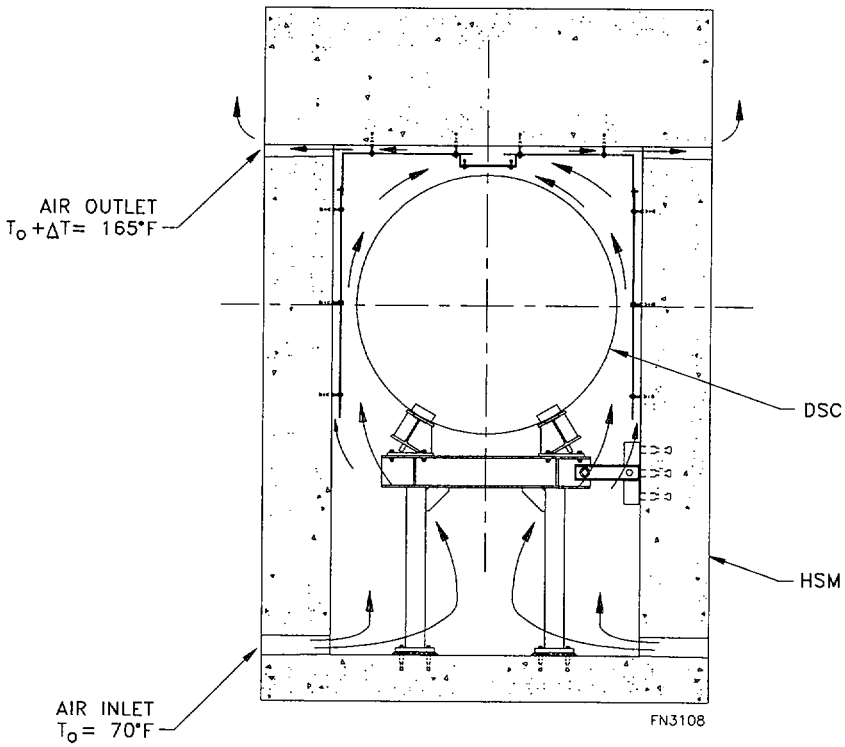


VENTILATION FLOW PATHS

**Figure 8.1-34**
**NUHOMS®-24P HSM Air Temperatures for 70°F Ambient Temperature**

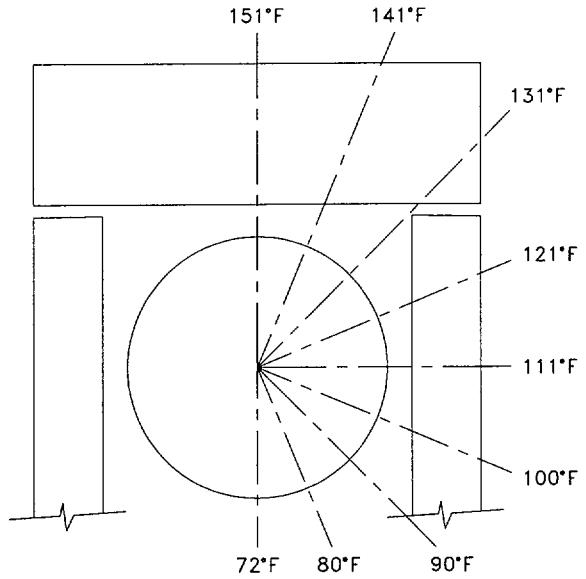


BULK AIR TEMPERATURES INSIDE HSM

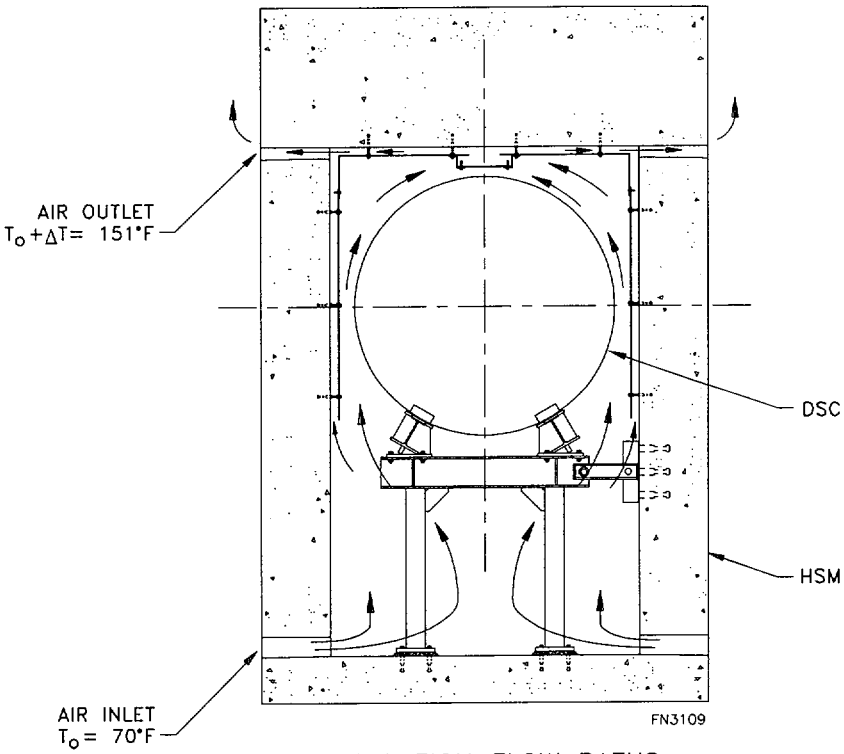


VENTILATION FLOW PATHS

**Figure 8.1-35**
**NUHOMS®-52B HSM Air Temperatures for 70°F Ambient Temperature**

Security-Related Information Figure Withheld Under 10 CFR 2.390.

**Figure 8.1-36**
**Two-Dimensional HSM Model Geometry**

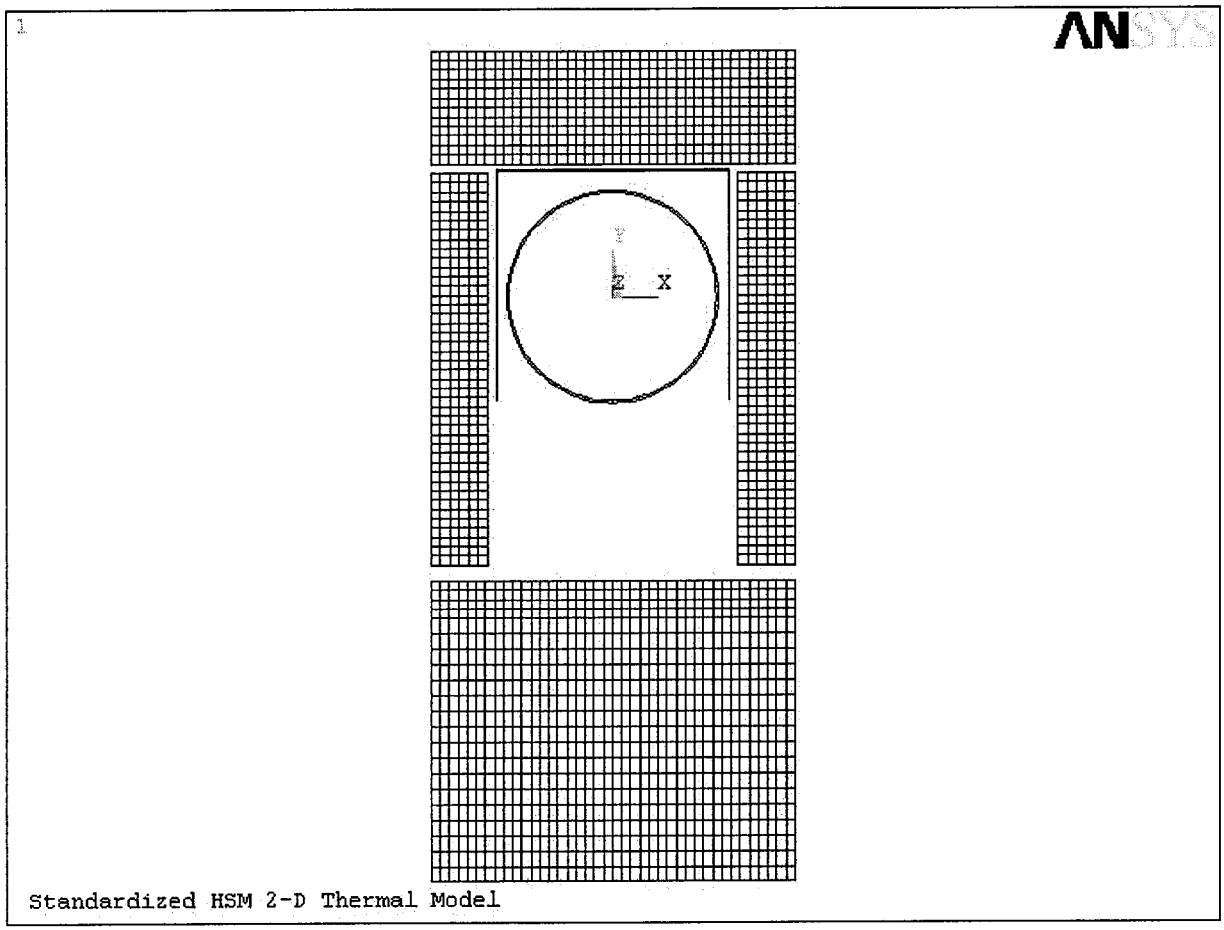


**Figure 8.1-36a**
**ANSYS Model of AHSM**

Figure 8.1-37

**Deleted**

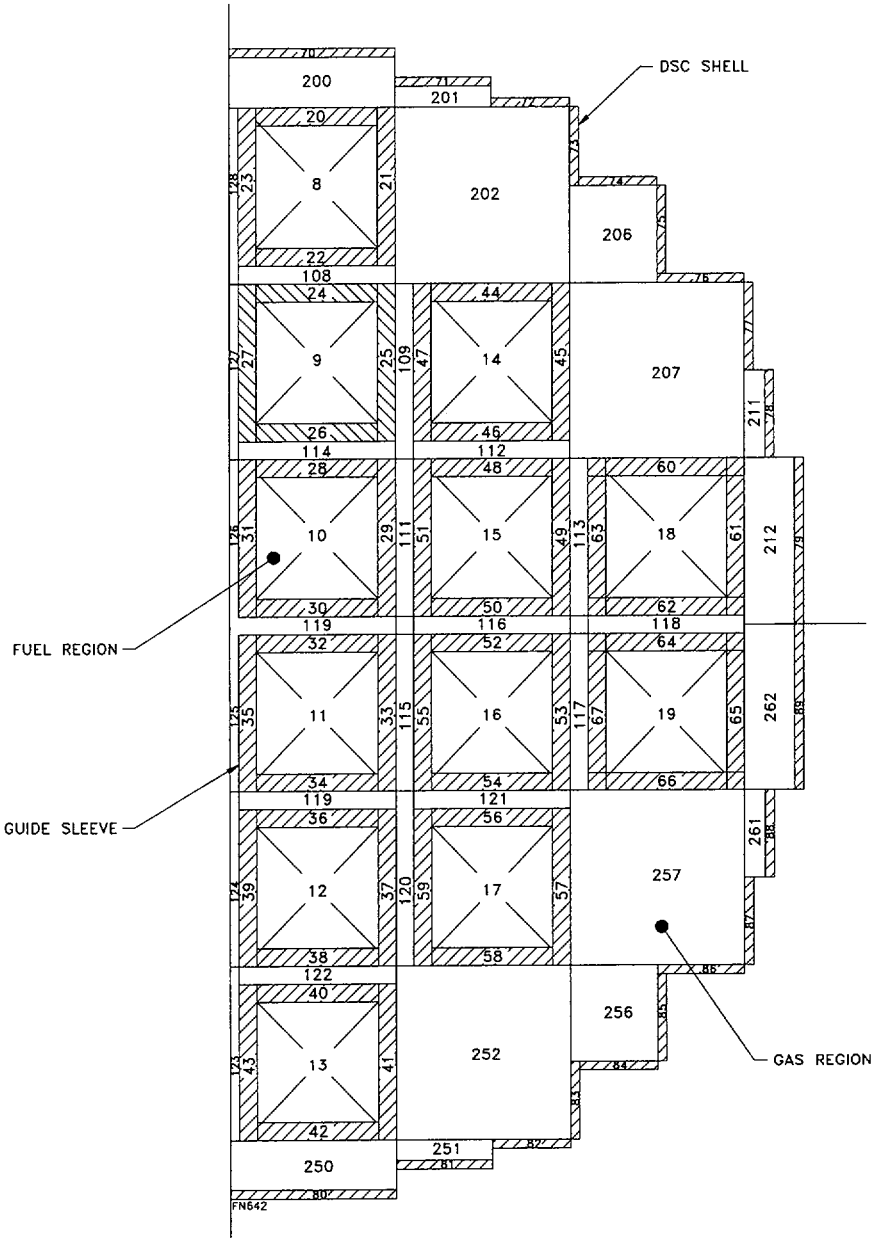


**Figure 8.1-38**
**HEATING7 Model of NUHOMS®-24P DSC**

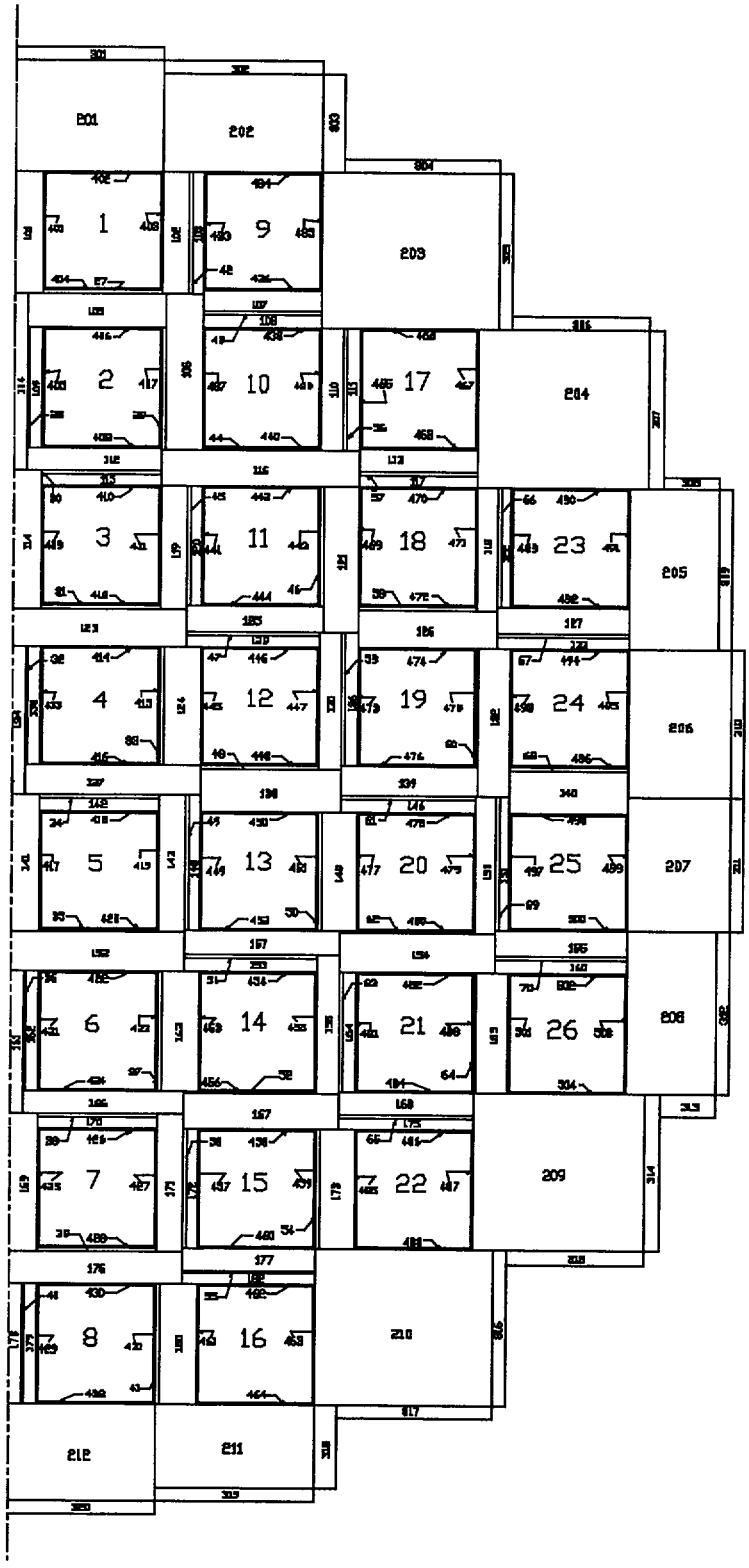


**Figure 8.1-39**
**HEATING7 Model of NUHOMS®-52B DSC**

| | 0.00 | 0.77 | 0.87 | 5.26 | 9.66 | 9.77 | 11.04 | 11.15 | 15.54 | 19.94 | 20.05 | 20.67 | 21.07 | 21.18 |
|---|---|---|---|---|---|---|---|---|---|---|---|---|---|---|
| 33.62 | 323.30 | 323.30 | 323.30 | 323.30 | 323.30 | 323.30 | | | | | | | | |
| 33.00 | 325.39 | 325.30 | 325.29 | 325.03 | 324.28 | 324.28 | | | | | | | | |
| 31.85 | 391.67 | 391.05 | 390.94 | 381.57 | 321.58 | 311.60 | 311.60 | 311.60 | 311.60 | | | | | |
| 31.23 | 427.20 | 425.53 | 425.27 | 412.48 | 339.73 | 315.90 | 313.80 | 313.67 | 311.55 | | | | | |
| 30.70 | 457.86 | 453.84 | 453.34 | 438.65 | 381.74 | 377.05 | 351.85 | 350.18 | 306.00 | 306.00 | 306.00 | | | |
| 30.07 | 498.06 | 486.24 | 485.65 | 469.75 | 434.47 | 433.33 | 393.47 | 391.18 | 310.07 | 306.21 | 304.91 | 301.10 | | |
| 29.97 | 493.69 | 486.00 | 485.95 | 470.04 | 434.74 | 434.52 | 396.41 | 393.66 | 312.91 | 305.13 | 303.61 | 301.10 | | |
| 26.20 | 527.91 | 527.84 | 527.84 | 516.17 | 476.82 | 476.55 | 455.18 | 453.43 | 383.52 | 307.38 | 304.16 | 301.10 | 301.10 | 301.10 |
| 25.57 | 533.80 | 533.88 | 533.89 | 522.76 | 483.57 | 483.30 | 463.95 | 462.35 | 394.89 | 315.38 | 312.78 | 305.77 | 303.67 | 303.22 |
| 21.18 | 571.38 | 569.88 | 569.89 | 562.55 | 529.52 | 529.26 | 522.52 | 521.83 | 475.38 | 397.21 | 393.19 | 383.23 | 376.27 | 374.45 |
| 21.07 | 573.48 | 570.19 | 570.07 | 562.74 | 529.76 | 529.76 | 524.34 | 523.61 | 477.59 | 401.17 | 396.32 | 385.55 | 377.98 | 376.01 |
| 20.67 | 584.87 | 576.62 | 584.77 | 582.73 | 552.11 | 547.36 | 531.68 | 530.60 | 486.17 | 417.49 | 410.39 | 394.64 | 384.49 | 381.93 |
| 20.05 | 611.15 | 617.21 | 617.99 | 613.45 | 591.10 | 590.16 | 541.97 | 541.23 | 499.64 | 449.30 | 447.71 | 408.25 | 393.40 | 390.07 |
| 19.94 | 614.73 | 618.20 | 618.21 | 613.65 | 591.33 | 591.16 | 541.74 | 541.53 | 499.95 | 449.57 | 449.28 | 415.64 | 398.38 | 394.21 |
| 15.54 | 646.22 | 646.71 | 646.72 | 643.31 | 624.01 | 623.85 | 582.95 | 582.81 | 549.86 | 497.03 | 496.69 | 482.25 | 473.04 | 470.67 |
| 11.15 | 645.20 | 658.53 | 658.60 | 661.03 | 643.25 | 643.07 | 603.80 | 603.69 | 580.02 | 536.15 | 535.84 | 523.04 | 514.85 | 512.78 |
| 11.04 | 634.27 | 656.62 | 658.67 | 661.13 | 643.35 | 642.59 | 602.54 | 603.77 | 580.15 | 536.35 | 536.62 | 523.78 | 515.29 | 513.19 |
| 9.77 | 681.34 | 685.91 | 686.69 | 685.51 | 670.89 | 670.51 | 635.81 | 636.97 | 616.93 | 581.84 | 580.79 | 533.16 | 516.35 | 515.95 |
| 9.66 | 684.00 | 686.81 | 686.83 | 685.62 | 671.01 | 670.87 | 637.25 | 637.14 | 617.07 | 582.00 | 581.75 | 539.53 | 516.43 | 516.19 |
| 5.26 | 699.81 | 700.14 | 700.15 | 697.34 | 682.39 | 682.27 | 654.10 | 653.99 | 634.57 | 602.24 | 602.03 | 568.22 | 546.20 | 545.99 |
| 0.87 | 693.84 | 698.44 | 698.46 | 697.32 | 678.78 | 678.60 | 648.70 | 648.65 | 636.45 | 604.98 | 604.72 | 563.36 | 546.41 | 546.24 |
| 0.77 | 689.97 | 697.67 | 698.41 | 697.30 | 678.73 | 676.45 | 645.65 | 648.57 | 636.45 | 604.97 | 603.90 | 551.36 | 544.88 | 546.18 |
| 0.00 | 652.48 | 675.15 | 685.17 | 695.66 | 674.62 | 669.90 | 638.25 | 643.72 | 635.85 | 604.88 | 603.52 | 561.57 | 534.09 | 539.72 |
| -0.77 | 689.09 | 695.27 | 695.82 | 694.98 | 680.86 | 680.63 | 652.13 | 652.77 | 635.94 | 606.29 | 606.39 | 570.48 | 548.16 | 548.76 |
| -0.87 | 693.09 | 695.83 | 695.84 | 694.97 | 680.88 | 680.76 | 652.92 | 652.82 | 635.94 | 606.27 | 606.06 | 571.39 | 549.02 | 548.82 |
| -9.66 | 660.00 | 671.53 | 671.58 | 673.04 | 656.22 | 656.07 | 624.22 | 624.13 | 607.07 | 572.94 | 572.70 | 532.59 | 508.67 | 508.44 |
| -9.77 | 640.91 | 668.99 | 671.42 | 672.93 | 656.07 | 653.89 | 620.87 | 623.91 | 606.92 | 572.76 | 571.61 | 525.84 | 508.57 | 508.16 |
| -11.04 | 648.02 | 648.84 | 649.48 | 648.38 | 630.88 | 630.72 | 589.59 | 590.47 | 566.28 | 522.50 | 522.81 | 511.29 | 503.33 | 501.36 |
| -11.15 | 648.40 | 649.38 | 649.41 | 648.28 | 630.77 | 630.61 | 590.50 | 590.39 | 566.14 | 522.29 | 521.98 | 510.23 | 502.59 | 500.64 |
| -15.54 | 630.87 | 631.28 | 631.29 | 627.74 | 608.66 | 608.51 | 566.67 | 566.53 | 532.22 | 478.42 | 478.10 | 462.80 | 453.08 | 450.58 |
| -19.94 | 585.02 | 595.43 | 595.46 | 593.52 | 573.44 | 573.28 | 522.47 | 522.24 | 475.33 | 422.30 | 422.02 | 383.90 | 364.63 | 359.97 |
| -20.05 | 575.40 | 593.76 | 595.22 | 593.30 | 573.19 | 572.91 | 523.66 | 521.92 | 474.97 | 421.99 | 420.28 | 375.04 | 358.79 | 355.15 |
| -20.67 | 554.63 | 550.25 | 558.02 | 557.75 | 527.48 | 522.29 | 508.64 | 507.53 | 458.20 | 383.49 | 376.26 | 357.52 | 346.04 | 343.15 |
| -21.07 | 544.13 | 539.98 | 540.25 | 534.50 | 500.85 | 500.88 | 498.74 | 498.15 | 447.43 | 362.60 | 357.14 | 345.16 | 336.76 | 334.57 |
| -21.18 | 541.76 | 540.04 | 540.06 | 534.29 | 500.58 | 500.32 | 496.31 | 495.76 | 444.66 | 357.48 | 352.77 | 341.99 | 334.34 | 332.31 |
| -25.57 | 500.17 | 500.23 | 500.23 | 487.91 | 445.16 | 444.88 | 422.45 | 420.58 | 339.90 | 242.81 | 239.51 | 233.60 | 237.10 | 237.82 |
| -26.20 | 493.82 | 493.57 | 493.57 | 480.16 | 436.88 | 436.60 | 411.50 | 409.44 | 324.90 | 231.32 | 227.19 | 223.58 | 236.40 | 236.40 |
| -29.97 | 462.06 | 447.66 | 447.56 | 424.77 | 384.13 | 383.91 | 338.93 | 335.60 | 230.68 | 223.83 | 223.54 | 222.20 | | |
| -30.07 | 471.11 | 448.85 | 447.23 | 424.45 | 383.82 | 382.61 | 335.57 | 332.65 | 226.83 | 223.72 | 223.63 | 222.20 | | |
| -30.70 | 412.84 | 405.14 | 404.16 | 382.97 | 314.39 | 308.44 | 277.61 | 275.54 | 222.20 | 222.20 | 222.20 | | | |
| -31.23 | 369.64 | 366.45 | 365.97 | 347.60 | 258.16 | 226.76 | 224.27 | 224.12 | 221.81 | | | | | |
| -31.85 | 319.96 | 318.82 | 318.63 | 305.25 | 232.78 | 221.70 | 221.70 | 221.70 | 221.70 | | | | | |
| -33.00 | 226.55 | 226.39 | 226.37 | 226.02 | 225.19 | 225.19 | | | | | | | | |
| -33.62 | 224.00 | 224.00 | 224.00 | 224.00 | 224.00 | 224.00 | | | | | | | | |

**Figure 8.1-40**
**NUHOMS®-24P DSC HEATING7 Results for 70°F Ambient**

| Distance | 25.57 | 26.20 | 29.97 | 30.07 | 30.70 | 31.23 | 31.85 | 33.00 | 33.62 |
|---|---|---|---|---|---|---|---|---|---|
| 33.62 | | | | | | | | | |
| 33.00 | | | | | | | | | |
| 31.85 | | | | | | | | | |
| 31.23 | | | | | | | | | |
| 30.70 | | | | | | | | | |
| 30.07 | | | | | | | | | |
| 29.97 | | | | | | | | | |
| 26.20 | 301.10 | | | | | | | | |
| 25.57 | 299.41 | 297.30 | | | | | | | |
| 21.18 | 299.39 | 297.30 | | | | | | | |
| 21.07 | 299.56 | 297.30 | | | | | | | |
| 20.67 | 300.34 | 294.68 | 294.40 | 294.40 | | | | | |
| 20.05 | 306.60 | 297.57 | 294.04 | 292.62 | 288.50 | | | | |
| 19.94 | 309.10 | 300.60 | 292.67 | 291.20 | 288.50 | | | | |
| 15.54 | 384.50 | 372.26 | 295.76 | 292.69 | 288.50 | 285.49 | 285.30 | | |
| 11.15 | 448.25 | 438.73 | 375.92 | 373.44 | 328.02 | 287.47 | 285.30 | | |
| 11.04 | 449.73 | 440.37 | 378.54 | 375.65 | 329.63 | 287.60 | 285.30 | | |
| 9.77 | 467.68 | 460.46 | 414.64 | 413.51 | 353.99 | 289.63 | 285.30 | 280.68 | 279.50 |
| 9.66 | 467.93 | 460.71 | 414.83 | 414.55 | 358.65 | 313.83 | 292.88 | 280.68 | 279.50 |
| 5.26 | 503.99 | 496.97 | 446.97 | 446.67 | 411.72 | 382.09 | 346.83 | 281.33 | 279.50 |
| 0.87 | 511.76 | 505.53 | 460.21 | 459.89 | 423.54 | 392.24 | 354.16 | 281.46 | 279.50 |
| 0.77 | 511.75 | 505.52 | 460.24 | 460.32 | 423.66 | 392.24 | 354.10 | 281.37 | 279.50 |
| 0.00 | 510.72 | 504.53 | 462.25 | 463.69 | 424.13 | 391.83 | 353.33 | 280.46 | 278.40 |
| -0.77 | 510.42 | 503.83 | 456.65 | 456.88 | 420.69 | 389.48 | 351.62 | 279.45 | 277.30 |
| -0.87 | 510.43 | 503.83 | 456.59 | 456.28 | 420.19 | 389.10 | 351.33 | 279.34 | 277.30 |
| -9.66 | 460.60 | 453.34 | 405.94 | 405.68 | 352.22 | 309.51 | 285.16 | 278.36 | 277.30 |
| -9.77 | 460.32 | 453.06 | 405.73 | 404.49 | 344.94 | 271.64 | 266.50 | 278.36 | 277.30 |
| -11.04 | 438.46 | 428.87 | 363.35 | 360.08 | 312.84 | 268.84 | 266.50 | | |
| -11.15 | 436.66 | 426.91 | 360.28 | 357.48 | 310.78 | 268.68 | 266.50 | | |
| -15.54 | 361.05 | 348.60 | 271.14 | 268.00 | 263.90 | 266.53 | 266.50 | | |
| -19.94 | 267.94 | 262.33 | 262.81 | 264.02 | 263.90 | | | | |
| -20.05 | 264.38 | 259.19 | 261.22 | 262.62 | 263.90 | | | | |
| -20.67 | 254.16 | 256.54 | 258.70 | 258.70 | | | | | |
| -21.07 | 242.84 | 236.40 | | | | | | | |
| -21.18 | 240.44 | 236.40 | | | | | | | |
| -25.57 | 236.66 | 236.40 | | | | | | | |
| -26.20 | 236.40 | | | | | | | | |
| -29.97 | | | | | | | | | |
| -30.07 | | | | | | | | | |
| -30.70 | | | | | | | | | |
| -31.23 | | | | | | | | | |
| -31.85 | | | | | | | | | |
| -33.00 | | | | | | | | | |
| -33.62 | | | | | | | | | |

**Figure 8.1-40**
**NUHOMS®-24P DSC HEATING7 Results for 70°F Ambient**
(Sheet 2)

| | 0.00 | 0.60 | 0.73 | 1.31 | 1.39 | 4.04 | 6.69 | 6.77 | 6.90 | 7.95 | 8.08 | 8.65 | 8.73 | 14.02 | 14.10 | 14.25 | 15.15 | 15.28 |
|---|---|---|---|---|---|---|---|---|---|---|---|---|---|---|---|---|---|---|
| 66.83 | 286.30 | 286.30 | 286.30 | 286.30 | 286.30 | 286.30 | 286.30 | 286.30 | | | | | | | | | | |
| 66.20 | 287.60 | 287.69 | 287.74 | 288.06 | 288.10 | 288.04 | 283.28 | 280.60 | 280.60 | 280.60 | 280.60 | 280.60 | 280.60 | 280.60 | 280.60 | | | |
| 65.62 | 304.39 | 304.57 | 304.65 | 305.07 | 305.12 | 303.98 | 284.79 | 282.68 | 282.42 | 281.84 | 281.78 | 281.55 | 281.52 | 278.93 | 276.65 | 275.93 | 271.60 | |
| 61.84 | 400.74 | 404.06 | 405.56 | 414.78 | 415.84 | 422.11 | 403.02 | 401.51 | 398.87 | 379.39 | 376.75 | 364.83 | 363.21 | 280.98 | 276.27 | 276.06 | 271.54 | 269.80 |
| 61.22 | 390.57 | 398.25 | 403.00 | 442.43 | 443.89 | 445.31 | 432.73 | 431.64 | 413.75 | 396.95 | 396.99 | 373.26 | 373.46 | 302.98 | 289.80 | 285.58 | 275.33 | 274.30 |
| 61.14 | 398.58 | 407.14 | 411.91 | 444.20 | 444.29 | 445.66 | 433.09 | 432.92 | 423.61 | 398.13 | 398.01 | 373.77 | 373.65 | 303.26 | 302.79 | 294.71 | 278.83 | 277.50 |
| 58.52 | 487.33 | 488.09 | 488.44 | 490.58 | 490.59 | 487.94 | 475.12 | 474.96 | 470.19 | 433.00 | 432.83 | 402.07 | 401.93 | 346.83 | 346.69 | 345.35 | 338.36 | 337.34 |
| 55.90 | 542.32 | 540.68 | 539.26 | 527.39 | 527.38 | 522.51 | 511.11 | 510.91 | 505.93 | 462.33 | 462.11 | 420.25 | 419.97 | 367.67 | 367.61 | 378.72 | 392.41 | 392.80 |
| 55.82 | 544.95 | 544.54 | 543.76 | 527.87 | 527.72 | 522.80 | 511.48 | 511.36 | 507.64 | 463.26 | 463.06 | 423.06 | 420.01 | 367.69 | 368.34 | 391.64 | 396.55 | 396.32 |
| 55.69 | 549.35 | 551.19 | 552.11 | 528.85 | 528.09 | 523.12 | 511.87 | 511.88 | 510.84 | 464.81 | 464.67 | 500.40 | 530.92 | 473.40 | 436.66 | 416.91 | 403.67 | 402.35 |
| 54.87 | 572.21 | 571.94 | 571.34 | 565.51 | 564.88 | 560.65 | 551.66 | 550.68 | 548.93 | 532.92 | 533.97 | 548.00 | 548.27 | 494.70 | 492.32 | 479.69 | 442.77 | 438.30 |
| 54.73 | 575.97 | 575.98 | 575.45 | 570.92 | 570.46 | 566.68 | 558.40 | 557.37 | 555.46 | 541.11 | 541.66 | 548.49 | 548.41 | 494.88 | 493.04 | 484.17 | 447.96 | 443.57 |
| 54.17 | 591.65 | 594.86 | 594.63 | 592.18 | 592.98 | 591.79 | 587.67 | 587.63 | 587.23 | 569.08 | 568.96 | 574.49 | 574.55 | 530.34 | 526.76 | 495.53 | 466.44 | 466.34 |
| 54.09 | 593.41 | 595.24 | 595.23 | 593.29 | 593.29 | 592.09 | 588.00 | 587.97 | 587.89 | 572.29 | 572.00 | 574.77 | 574.72 | 530.59 | 530.16 | 512.12 | 468.23 | 468.00 |
| 51.44 | 614.61 | 614.74 | 614.74 | 616.53 | 616.55 | 615.84 | 610.50 | 610.40 | 610.31 | 600.26 | 599.00 | 593.73 | 593.65 | 559.20 | 558.97 | 551.65 | 507.84 | 507.60 |
| 48.80 | 630.54 | 629.46 | 629.48 | 632.97 | 632.99 | 632.59 | 627.82 | 627.74 | 627.67 | 625.74 | 623.63 | 610.37 | 610.27 | 580.77 | 580.55 | 574.83 | 532.69 | 532.44 |
| 48.72 | 631.67 | 629.68 | 629.82 | 633.57 | 633.16 | 632.74 | 627.97 | 628.20 | 628.28 | 629.05 | 626.78 | 610.59 | 610.43 | 580.97 | 580.83 | 577.14 | 533.36 | 533.05 |
| 48.56 | 633.98 | 633.04 | 633.27 | 636.59 | 636.80 | 636.64 | 631.01 | 629.32 | 629.69 | 635.75 | 633.25 | 611.20 | 610.64 | 581.19 | 581.19 | 582.24 | 534.72 | 534.03 |
| 47.66 | 650.17 | 648.88 | 648.43 | 658.98 | 659.35 | 660.16 | 655.51 | 655.38 | 652.80 | 644.25 | 642.32 | 631.89 | 630.58 | 598.43 | 596.41 | 592.40 | 556.26 | 551.37 |
| 47.53 | 653.06 | 652.70 | 653.07 | 659.48 | 659.55 | 660.34 | 655.68 | 655.64 | 654.91 | 646.23 | 644.47 | 634.46 | 633.25 | 601.47 | 599.51 | 595.59 | 558.85 | 553.82 |
| 46.95 | 665.83 | 667.20 | 668.16 | 677.19 | 684.62 | 683.77 | 676.25 | 675.48 | 664.92 | 656.44 | 656.38 | 643.74 | 644.01 | 615.89 | 615.57 | 614.71 | 568.43 | 565.43 |
| 46.87 | 667.39 | 668.84 | 669.61 | 674.49 | 684.84 | 683.95 | 676.42 | 676.25 | 670.70 | 657.00 | 656.89 | 644.27 | 644.18 | 616.06 | 615.80 | 615.46 | 574.17 | 570.98 |
| 44.23 | 689.87 | 689.90 | 689.91 | 689.96 | 698.62 | 696.58 | 689.85 | 689.73 | 687.56 | 671.07 | 670.96 | 657.47 | 657.37 | 629.62 | 629.40 | 629.14 | 604.54 | 601.00 |
| 41.58 | 710.79 | 710.17 | 709.80 | 707.35 | 707.20 | 704.61 | 698.74 | 698.63 | 696.93 | 679.70 | 679.58 | 666.27 | 666.16 | 638.18 | 637.91 | 637.62 | 616.86 | 613.50 |
| 41.50 | 711.80 | 711.29 | 710.86 | 707.35 | 707.28 | 704.67 | 698.84 | 698.77 | 697.89 | 679.92 | 679.67 | 666.68 | 666.25 | 638.27 | 637.92 | 637.33 | 617.59 | 614.34 |
| 41.37 | 713.52 | 713.26 | 712.73 | 707.56 | 707.37 | 704.75 | 698.93 | 698.94 | 699.73 | 682.87 | 680.17 | 669.28 | 668.09 | 639.53 | 636.84 | 631.03 | 618.89 | 615.87 |
| 40.31 | 715.89 | 715.90 | 715.79 | 714.91 | 714.81 | 712.40 | 704.35 | 703.49 | 701.96 | 682.71 | 682.39 | 680.55 | 680.28 | 655.85 | 655.36 | 647.44 | 639.56 | 639.33 |
| 40.18 | 716.19 | 716.41 | 716.35 | 715.80 | 715.73 | 713.43 | 705.49 | 704.65 | 703.14 | 682.78 | 682.44 | 680.64 | 680.38 | 655.96 | 655.60 | 651.64 | 639.83 | 639.71 |
| 39.62 | 717.20 | 718.96 | 718.97 | 719.40 | 719.62 | 717.93 | 711.30 | 711.13 | 710.73 | 690.83 | 690.16 | 692.16 | 692.35 | 670.26 | 669.49 | 664.20 | 641.46 | 641.29 |
| 39.54 | 718.00 | 719.09 | 719.09 | 719.69 | 719.70 | 718.01 | 711.38 | 711.24 | 711.10 | 693.23 | 692.43 | 692.54 | 692.45 | 670.37 | 670.18 | 665.48 | 641.67 | 641.50 |
| 36.89 | 722.83 | 722.94 | 722.94 | 723.94 | 723.95 | 722.38 | 715.99 | 715.87 | 715.76 | 704.59 | 703.29 | 698.11 | 698.02 | 676.48 | 676.30 | 672.08 | 646.92 | 646.74 |
| 34.24 | 723.66 | 723.75 | 723.75 | 724.50 | 724.51 | 722.93 | 716.73 | 716.61 | 716.48 | 704.69 | 703.33 | 697.68 | 697.58 | 676.69 | 676.52 | 672.15 | 646.94 | 646.76 |
| 34.16 | 723.63 | 723.74 | 723.74 | 724.44 | 724.49 | 722.91 | 716.72 | 716.59 | 716.39 | 704.50 | 703.28 | 697.59 | 697.53 | 676.66 | 676.49 | 671.86 | 646.92 | 646.49 |
| 34.02 | 723.56 | 723.67 | 723.72 | 724.14 | 724.18 | 722.60 | 716.45 | 716.08 | 715.39 | 704.50 | 703.21 | 697.57 | 697.49 | 676.61 | 676.27 | 671.20 | 646.41 | 643.35 |
| 32.81 | 722.53 | 722.67 | 722.72 | 722.35 | 722.32 | 720.62 | 715.61 | 715.49 | 714.57 | 703.53 | 703.36 | 697.51 | 696.48 | 669.15 | 667.11 | 663.07 | 631.68 | 631.00 |
| 32.68 | 722.34 | 722.43 | 722.45 | 722.31 | 722.31 | 720.61 | 715.60 | 715.39 | 714.25 | 703.44 | 703.37 | 697.69 | 696.11 | 668.99 | 667.13 | 663.44 | 631.62 | 630.98 |
| 32.10 | 721.44 | 721.45 | 721.44 | 721.30 | 721.29 | 719.89 | 714.98 | 714.67 | 713.53 | 702.90 | 702.82 | 693.69 | 693.36 | 669.69 | 669.41 | 669.03 | 642.14 | 638.15 |
| 32.02 | 721.32 | 721.32 | 721.32 | 721.28 | 721.28 | 719.88 | 714.98 | 714.89 | 713.49 | 702.82 | 702.74 | 693.41 | 693.33 | 669.65 | 669.41 | 669.12 | 643.06 | 639.71 |
| 29.38 | 717.07 | 717.34 | 717.47 | 718.31 | 718.31 | 717.14 | 712.26 | 712.17 | 710.65 | 699.18 | 699.10 | 689.89 | 689.82 | 666.37 | 666.15 | 665.89 | 642.89 | 639.62 |
| 26.73 | 702.03 | 703.51 | 704.35 | 710.07 | 710.08 | 709.35 | 704.13 | 704.05 | 701.79 | 691.17 | 691.09 | 683.26 | 683.21 | 659.74 | 659.48 | 659.16 | 623.48 | 620.89 |
| 26.65 | 700.68 | 701.94 | 702.86 | 709.88 | 709.94 | 709.22 | 703.98 | 703.85 | 700.26 | 690.86 | 690.68 | 682.95 | 683.11 | 659.65 | 659.35 | 658.72 | 618.46 | 617.68 |
| 26.52 | 698.32 | 699.12 | 700.13 | 709.49 | 709.79 | 709.09 | 703.82 | 703.42 | 697.28 | 686.45 | 686.60 | 681.94 | 681.49 | 657.74 | 656.57 | 654.08 | 618.29 | 617.61 |
| 25.46 | 695.05 | 695.27 | 695.54 | 697.61 | 697.82 | 696.69 | 688.41 | 687.56 | 686.02 | 671.49 | 671.15 | 668.78 | 668.44 | 645.07 | 644.94 | 644.40 | 620.01 | 615.66 |
| 25.33 | 694.54 | 694.41 | 694.61 | 696.31 | 696.47 | 695.18 | 686.87 | 686.15 | 684.88 | 671.35 | 671.07 | 668.69 | 668.35 | 644.97 | 644.60 | 641.36 | 620.32 | 614.58 |
| 24.77 | 692.54 | 689.90 | 689.90 | 691.42 | 691.13 | 689.03 | 681.23 | 681.11 | 681.18 | 672.37 | 668.99 | 656.96 | 656.46 | 631.75 | 631.23 | 629.11 | 604.18 | 603.74 |
| 24.69 | 691.25 | 689.69 | 689.69 | 691.01 | 691.02 | 688.92 | 681.11 | 680.96 | 680.83 | 670.37 | 667.92 | 656.52 | 656.37 | 631.66 | 631.50 | 628.00 | 603.67 | 603.50 |
| 22.04 | 679.72 | 679.78 | 679.78 | 680.62 | 680.63 | 678.39 | 670.03 | 669.88 | 669.74 | 654.16 | 652.27 | 644.64 | 644.51 | 619.50 | 619.33 | 614.93 | 588.80 | 588.64 |
| 19.39 | 665.94 | 667.41 | 667.41 | 666.65 | 666.65 | 664.25 | 655.76 | 655.59 | 655.38 | 627.02 | 625.68 | 623.82 | 623.69 | 598.51 | 598.35 | 592.28 | 567.59 | 567.42 |
| 19.32 | 664.63 | 667.16 | 667.02 | 665.91 | 666.45 | 664.06 | 655.59 | 655.35 | 654.69 | 623.00 | 622.76 | 623.17 | 623.39 | 598.23 | 597.98 | 588.80 | 566.94 | 566.52 |
| 19.16 | 661.92 | 663.43 | 663.43 | 662.02 | 661.98 | 659.36 | 651.18 | 650.56 | 649.39 | 622.79 | 622.61 | 622.93 | 623.07 | 597.87 | 597.09 | 581.03 | 555.01 | 554.72 |
| 18.27 | 641.56 | 643.99 | 645.05 | 635.43 | 635.03 | 631.15 | 626.05 | 626.20 | 630.34 | 612.57 | 608.63 | 597.25 | 595.81 | 560.92 | 558.12 | 552.49 | 513.08 | 512.20 |
| 18.13 | 637.56 | 638.76 | 638.80 | 634.80 | 634.80 | 630.95 | 625.84 | 625.64 | 624.14 | 608.74 | 604.69 | 592.88 | 591.40 | 556.06 | 553.64 | 548.90 | 512.74 | 512.03 |
| 17.55 | 618.76 | 616.93 | 615.70 | 605.39 | 605.05 | 602.56 | 596.67 | 596.56 | 598.21 | 582.02 | 581.93 | 572.17 | 571.28 | 536.70 | 536.41 | 536.45 | 513.75 | 505.67 |
| 17.47 | 616.41 | 614.31 | 613.11 | 604.86 | 604.84 | 602.37 | 596.48 | 596.40 | 595.81 | 581.37 | 581.29 | 571.10 | 571.03 | 536.43 | 536.13 | 535.83 | 509.33 | 503.20 |
| 14.83 | 579.93 | 580.40 | 580.62 | 582.04 | 582.05 | 580.86 | 574.57 | 574.48 | 572.46 | 557.24 | 557.16 | 545.64 | 545.58 | 508.70 | 508.46 | 508.18 | 472.95 | 467.93 |
| 12.18 | 523.25 | 528.34 | 531.27 | 550.91 | 550.94 | 551.60 | 544.53 | 544.44 | 539.76 | 527.66 | 527.59 | 517.16 | 517.11 | 473.37 | 473.02 | 472.54 | 402.70 | 399.08 |
| 12.10 | 518.40 | 522.74 | 525.90 | 550.42 | 550.58 | 551.28 | 544.18 | 543.97 | 534.41 | 526.71 | 526.60 | 516.21 | 516.85 | 473.07 | 472.18 | 470.16 | 389.20 | 386.16 |
| 11.96 | 509.86 | 512.66 | 516.07 | 549.43 | 550.20 | 550.95 | 543.78 | 543.09 | 523.81 | 511.44 | 514.66 | 509.27 | 508.97 | 460.24 | 445.70 | 451.49 | 391.68 | 389.03 |
| 11.47 | 502.57 | 505.31 | 507.40 | 522.48 | 524.01 | 526.16 | 513.80 | 511.34 | 506.70 | 486.09 | 485.12 | 480.57 | 479.94 | 422.07 | 408.03 | 411.97 | 386.32 | 384.48 |
| 11.14 | 495.48 | 496.09 | 497.31 | 506.68 | 507.71 | 509.26 | 495.62 | 494.06 | 491.32 | 465.55 | 464.90 | 460.55 | 459.91 | 403.85 | 402.99 | 398.77 | 378.60 | 376.92 |
| 11.01 | 492.51 | 491.69 | 492.59 | 500.59 | 501.39 | 502.48 | 488.56 | 487.37 | 485.29 | 465.08 | 464.68 | 460.29 | 459.65 | 403.58 | 402.45 | 393.07 | 374.87 | 373.32 |
| 10.52 | 482.36 | 472.15 | 472.17 | 479.94 | 479.19 | 477.80 | 463.66 | 463.54 | 464.02 | 457.52 | 449.69 | 416.57 | 415.46 | 354.13 | 353.63 | 359.47 | 358.60 | 358.06 |
| 10.44 | 477.53 | 471.49 | 471.50 | 478.85 | 478.89 | 477.52 | 463.35 | 463.15 | 463.00 | 450.54 | 444.97 | 415.42 | 415.23 | 353.89 | 353.67 | 355.57 | 356.04 | 355.61 |
| 7.79 | 437.50 | 437.91 | 437.93 | 442.93 | 442.96 | 441.39 | 427.59 | 427.43 | 427.26 | 397.24 | 393.43 | 377.51 | 377.37 | 311.88 | 311.72 | 309.15 | 295.40 | 293.53 |
| 5.14 | 379.21 | 394.00 | 394.04 | 398.10 | 398.12 | 396.77 | 386.16 | 386.04 | 385.82 | 333.70 | 331.64 | 334.23 | 334.13 | 244.68 | 244.04 | 232.52 | 210.93 | 209.55 |
| 5.07 | 368.31 | 392.69 | 392.86 | 396.63 | 397.73 | 396.42 | 385.82 | 385.50 | 384.14 | 325.13 | 323.45 | 333.23 | 333.87 | 244.28 | 225.12 | 218.91 | 205.33 | 205.00 |
| 4.44 | 363.40 | 366.34 | 366.92 | 369.19 | 369.45 | 368.27 | 350.20 | 348.79 | 346.29 | 320.31 | 318.12 | 311.66 | 310.72 | 212.48 | 205.58 | 205.27 | 198.46 | 202.30 |
| 1.25 | 231.15 | 231.24 | 231.26 | 231.29 | 231.28 | 228.56 | 203.93 | 200.75 | 200.45 | 199.49 | 199.44 | 199.37 | 199.36 | 198.54 | 198.67 | 198.70 | 198.30 | |
| 0.62 | 202.70 | 202.82 | 202.83 | 202.89 | 202.90 | 202.79 | 199.74 | 198.10 | 198.10 | 198.10 | 198.10 | 198.10 | 198.10 | 198.10 | 198.10 | | | |
| 0.00 | 200.90 | 200.90 | 200.90 | 200.90 | 200.90 | 200.90 | 200.90 | 200.90 | | | | | | | | | | |

**Figure 8.1-41**
**NUHOMS®-52B DSC HEATING7 Results for 70°F Ambient**

| Distance | 15.86 | 15.94 | 21.24 | 21.32 | 21.45 | 22.27 | 22.41 | 22.90 | 22.98 | 28.27 | 28.35 | 29.20 | 29.82 | 32.38 | 33.00 | 33.62 |
|---|---|---|---|---|---|---|---|---|---|---|---|---|---|---|---|---|
| 66.83 | | | | | | | | | | | | | | | | |
| 66.20 | | | | | | | | | | | | | | | | |
| 65.62 | | | | | | | | | | | | | | | | |
| 61.84 | 269.80 | 269.80 | 269.80 | 269.80 | 269.80 | 269.80 | | | | | | | | | | |
| 61.22 | 272.08 | 271.83 | 270.73 | 270.60 | 270.37 | 268.33 | 266.75 | 265.80 | | | | | | | | |
| 61.14 | 274.22 | 273.84 | 271.06 | 270.83 | 270.42 | 266.85 | 266.65 | 265.80 | | | | | | | | |
| 58.52 | 332.97 | 332.36 | 284.90 | 283.59 | 281.36 | 266.62 | 266.45 | 265.80 | | | | | | | | |
| 55.90 | 390.91 | 390.52 | 316.55 | 313.18 | 307.37 | 267.26 | 266.98 | 265.80 | | | | | | | | |
| 55.82 | 393.13 | 392.60 | 318.61 | 315.13 | 309.12 | 267.43 | 267.11 | 265.80 | | | | | | | | |
| 55.69 | 396.90 | 396.11 | 322.20 | 318.53 | 312.18 | 267.80 | 267.36 | 265.80 | | | | | | | | |
| 54.87 | 420.26 | 417.99 | 348.60 | 343.68 | 335.06 | 269.48 | 268.78 | 265.80 | | | | | | | | |
| 54.73 | 423.40 | 421.13 | 353.97 | 349.13 | 340.42 | 269.99 | 269.20 | 265.13 | 264.00 | 264.00 | 264.00 | 264.00 | | | | |
| 54.17 | 432.48 | 433.02 | 379.56 | 379.05 | 369.51 | 274.28 | 272.54 | 267.04 | 266.18 | 264.58 | 264.34 | 260.98 | 257.60 | | | |
| 54.09 | 433.53 | 433.36 | 379.79 | 379.51 | 368.44 | 289.26 | 283.09 | 271.25 | 269.62 | 264.83 | 264.49 | 260.16 | 257.60 | | | |
| 51.44 | 469.45 | 469.25 | 408.69 | 408.39 | 403.70 | 375.08 | 370.79 | 356.11 | 353.81 | 277.59 | 276.07 | 259.20 | 257.60 | | | |
| 48.80 | 493.17 | 492.95 | 428.89 | 428.54 | 425.42 | 409.73 | 407.03 | 396.88 | 395.22 | 300.71 | 297.48 | 259.62 | 257.60 | | | |
| 48.72 | 493.97 | 493.13 | 429.02 | 428.28 | 425.05 | 410.98 | 408.32 | 397.99 | 396.30 | 302.27 | 298.94 | 259.64 | 257.60 | | | |
| 48.56 | 507.29 | 500.36 | 431.59 | 419.87 | 424.11 | 413.40 | 410.81 | 400.05 | 398.29 | 305.35 | 301.81 | 259.69 | 257.60 | | | |
| 47.66 | 530.40 | 530.17 | 469.61 | 467.60 | 461.63 | 433.98 | 429.42 | 411.99 | 409.29 | 328.09 | 323.14 | 260.44 | 257.60 | | | |
| 47.53 | 530.75 | 530.38 | 469.83 | 468.32 | 465.45 | 437.01 | 432.49 | 413.15 | 410.43 | 332.62 | 327.72 | 260.58 | 256.74 | 256.70 | | |
| 46.95 | 564.81 | 565.46 | 512.21 | 509.13 | 487.06 | 449.45 | 449.25 | 413.67 | 413.83 | 355.37 | 353.80 | 262.26 | 257.66 | 254.58 | 250.40 | |
| 46.87 | 565.87 | 565.69 | 512.47 | 512.09 | 498.49 | 450.85 | 450.61 | 414.30 | 414.10 | 355.57 | 355.27 | 275.50 | 260.99 | 253.40 | 250.40 | |
| 44.23 | 586.17 | 585.97 | 538.83 | 538.57 | 530.80 | 482.66 | 482.40 | 443.67 | 443.46 | 379.82 | 379.56 | 345.46 | 323.04 | 251.79 | 250.40 | |
| 41.58 | 598.04 | 597.85 | 554.09 | 553.83 | 546.42 | 497.22 | 496.95 | 459.05 | 458.84 | 391.51 | 391.22 | 363.14 | 342.61 | 251.92 | 250.40 | |
| 41.50 | 598.22 | 597.94 | 554.20 | 553.98 | 547.54 | 497.49 | 496.88 | 459.60 | 458.93 | 391.55 | 390.65 | 363.53 | 343.26 | 251.93 | 250.40 | |
| 41.37 | 598.87 | 598.07 | 554.29 | 554.00 | 549.76 | 502.26 | 494.99 | 466.05 | 462.44 | 391.16 | 382.46 | 364.19 | 344.37 | 251.93 | 250.40 | |
| 40.31 | 624.02 | 618.15 | 559.75 | 555.73 | 548.62 | 489.84 | 488.71 | 483.19 | 482.27 | 409.74 | 408.14 | 377.44 | 354.06 | 252.29 | 250.40 | |
| 40.18 | 623.84 | 618.84 | 561.60 | 557.83 | 551.15 | 489.90 | 488.76 | 483.29 | 482.37 | 409.83 | 408.76 | 379.16 | 355.31 | 252.39 | 250.40 | |
| 39.62 | 618.62 | 617.94 | 571.89 | 571.47 | 570.66 | 516.67 | 511.11 | 501.22 | 501.13 | 426.95 | 425.35 | 386.99 | 360.51 | 253.02 | 250.40 | 248.70 |
| 39.54 | 618.19 | 618.01 | 571.98 | 571.64 | 571.26 | 521.67 | 516.03 | 501.51 | 501.24 | 427.04 | 426.65 | 387.95 | 361.20 | 255.95 | 250.44 | 248.70 |
| 36.89 | 623.06 | 622.90 | 578.21 | 577.91 | 577.59 | 539.33 | 533.16 | 510.83 | 510.55 | 434.94 | 434.57 | 400.11 | 374.91 | 274.41 | 250.78 | 248.70 |
| 34.24 | 624.47 | 624.31 | 579.01 | 578.65 | 578.27 | 539.32 | 533.11 | 510.48 | 510.18 | 434.97 | 434.59 | 399.42 | 374.65 | 275.78 | 250.78 | 248.70 |
| 34.16 | 624.63 | 624.32 | 579.01 | 578.52 | 577.64 | 538.90 | 532.97 | 510.51 | 510.14 | 434.93 | 434.39 | 398.97 | 374.43 | 275.76 | 250.76 | 248.70 |
| 34.02 | 626.73 | 624.96 | 577.62 | 572.68 | 563.36 | 537.99 | 532.77 | 511.24 | 510.14 | 434.84 | 433.03 | 398.05 | 374.00 | 275.70 | 250.72 | 248.70 |
| 32.81 | 626.67 | 626.06 | 582.38 | 581.52 | 569.34 | 543.89 | 543.46 | 528.22 | 520.06 | 409.63 | 397.08 | 386.49 | 369.45 | 274.84 | 250.12 | 248.62 |
| 32.68 | 626.68 | 626.08 | 582.41 | 581.65 | 573.43 | 543.78 | 543.59 | 524.68 | 518.41 | 411.24 | 399.12 | 386.96 | 369.40 | 274.76 | 250.00 | 247.90 |
| 32.10 | 628.20 | 627.95 | 587.14 | 586.18 | 579.82 | 543.07 | 542.83 | 507.73 | 506.71 | 427.97 | 426.22 | 392.71 | 370.10 | 274.50 | 249.93 | 247.90 |
| 32.02 | 628.18 | 627.97 | 587.17 | 586.93 | 580.50 | 542.97 | 542.73 | 506.91 | 506.67 | 428.00 | 427.60 | 393.36 | 370.18 | 274.46 | 249.92 | 247.90 |
| 29.38 | 625.95 | 625.74 | 585.63 | 585.40 | 578.89 | 538.66 | 538.41 | 502.19 | 501.97 | 427.89 | 427.53 | 393.93 | 369.48 | 272.26 | 249.81 | 247.90 |
| 26.73 | 614.66 | 614.45 | 574.83 | 574.60 | 567.32 | 527.78 | 527.53 | 493.22 | 493.01 | 419.22 | 418.84 | 380.68 | 354.99 | 250.95 | 246.89 | 247.90 |
| 26.65 | 614.49 | 614.27 | 574.66 | 574.36 | 565.31 | 527.44 | 526.89 | 493.11 | 492.93 | 419.12 | 417.77 | 379.53 | 354.36 | 247.80 | 245.30 | 247.90 |
| 26.52 | 614.39 | 614.09 | 574.46 | 573.68 | 561.26 | 521.38 | 517.48 | 494.10 | 491.24 | 413.81 | 403.07 | 377.48 | 353.30 | 247.54 | 245.30 | |
| 25.46 | 598.88 | 596.76 | 545.26 | 541.37 | 534.48 | 480.85 | 479.68 | 473.80 | 472.82 | 399.38 | 397.92 | 367.91 | 345.13 | 247.03 | 245.30 | |
| 25.33 | 596.21 | 594.04 | 542.62 | 539.14 | 533.00 | 480.61 | 479.58 | 473.71 | 472.74 | 399.33 | 398.14 | 366.72 | 344.08 | 246.99 | 245.30 | |
| 24.77 | 582.04 | 581.23 | 533.95 | 533.59 | 533.32 | 493.03 | 484.36 | 459.44 | 458.75 | 388.97 | 388.00 | 361.24 | 339.64 | 246.87 | 245.30 | |
| 24.69 | 581.22 | 581.07 | 533.79 | 533.44 | 533.10 | 491.82 | 484.58 | 458.97 | 458.68 | 388.92 | 388.62 | 360.54 | 339.01 | 246.85 | 245.30 | |
| 22.04 | 564.88 | 564.74 | 515.64 | 515.35 | 515.05 | 473.29 | 466.68 | 443.07 | 442.82 | 375.35 | 375.10 | 340.27 | 317.52 | 246.61 | 245.30 | |
| 19.39 | 545.01 | 544.87 | 489.26 | 488.87 | 488.42 | 418.97 | 413.63 | 408.06 | 407.85 | 347.50 | 347.22 | 264.09 | 250.23 | 245.97 | 245.30 | |
| 19.32 | 544.38 | 544.68 | 489.03 | 488.10 | 486.47 | 406.50 | 401.88 | 406.91 | 407.53 | 347.27 | 345.69 | 249.86 | 246.71 | 245.85 | 245.30 | |
| 19.16 | 540.63 | 539.29 | 477.30 | 460.89 | 465.50 | 411.72 | 407.66 | 405.32 | 405.05 | 340.07 | 334.84 | 249.18 | 246.60 | 245.79 | | |
| 18.27 | 506.25 | 505.41 | 439.64 | 437.96 | 434.68 | 406.85 | 403.37 | 393.19 | 391.60 | 305.42 | 300.83 | 244.26 | 244.84 | 245.30 | | |
| 18.13 | 506.06 | 505.22 | 439.46 | 437.98 | 431.28 | 404.94 | 401.55 | 391.12 | 389.47 | 301.21 | 296.78 | 242.49 | 236.10 | | | |
| 17.55 | 474.53 | 473.52 | 408.68 | 407.58 | 408.41 | 393.59 | 391.00 | 381.44 | 379.88 | 285.81 | 282.19 | 238.98 | 236.10 | | | |
| 17.47 | 473.61 | 473.35 | 408.54 | 408.21 | 406.52 | 392.08 | 389.55 | 380.07 | 378.52 | 283.93 | 280.41 | 238.62 | 236.10 | | | |
| 14.83 | 446.91 | 446.70 | 384.66 | 384.39 | 379.62 | 350.52 | 346.22 | 331.64 | 329.36 | 255.08 | 253.62 | 237.53 | 236.10 | | | |
| 12.18 | 403.60 | 403.45 | 351.21 | 350.95 | 338.62 | 248.95 | 242.84 | 236.69 | 236.24 | 235.26 | 235.32 | 236.31 | 236.10 | | | |
| 12.10 | 402.09 | 403.08 | 350.94 | 350.57 | 340.04 | 230.19 | 227.83 | 231.00 | 233.08 | 234.61 | 234.68 | 235.87 | 236.10 | | | |
| 11.96 | 397.67 | 398.55 | 342.70 | 337.95 | 328.25 | 227.18 | 226.51 | 229.93 | 232.76 | 234.40 | 234.46 | 235.31 | | | | |
| 11.47 | 383.20 | 383.00 | 314.81 | 308.95 | 298.60 | 216.42 | 215.73 | 210.53 | 233.60 | 233.60 | 233.60 | 233.60 | | | | |
| 11.14 | 373.33 | 372.82 | 298.55 | 293.02 | 283.37 | 211.50 | 210.81 | 205.00 | | | | | | | | |
| 11.01 | 369.36 | 368.79 | 292.59 | 287.26 | 277.99 | 210.15 | 209.52 | 205.00 | | | | | | | | |
| 10.52 | 354.92 | 354.41 | 273.64 | 269.20 | 261.53 | 207.44 | 207.05 | 205.00 | | | | | | | | |
| 10.44 | 352.60 | 352.10 | 270.83 | 266.53 | 259.11 | 207.11 | 206.74 | 205.00 | | | | | | | | |
| 7.79 | 285.92 | 284.89 | 227.46 | 225.92 | 223.28 | 205.91 | 205.72 | 205.00 | | | | | | | | |
| 5.14 | 207.15 | 206.89 | 204.27 | 204.27 | 204.28 | 204.83 | 204.86 | 205.00 | | | | | | | | |
| 5.07 | 204.40 | 204.33 | 203.55 | 203.55 | 203.56 | 203.91 | 204.79 | 205.00 | | | | | | | | |
| 4.44 | 202.30 | 202.30 | 202.30 | 202.30 | 202.30 | 202.30 | | | | | | | | | | |
| 1.25 | | | | | | | | | | | | | | | | |
| 0.62 | | | | | | | | | | | | | | | | |
| 0.00 | | | | | | | | | | | | | | | | |

**Figure 8.1-41**
**NUHOMS®-52B DSC HEATING7 Results for 70°F Ambient**
(Sheet 2)

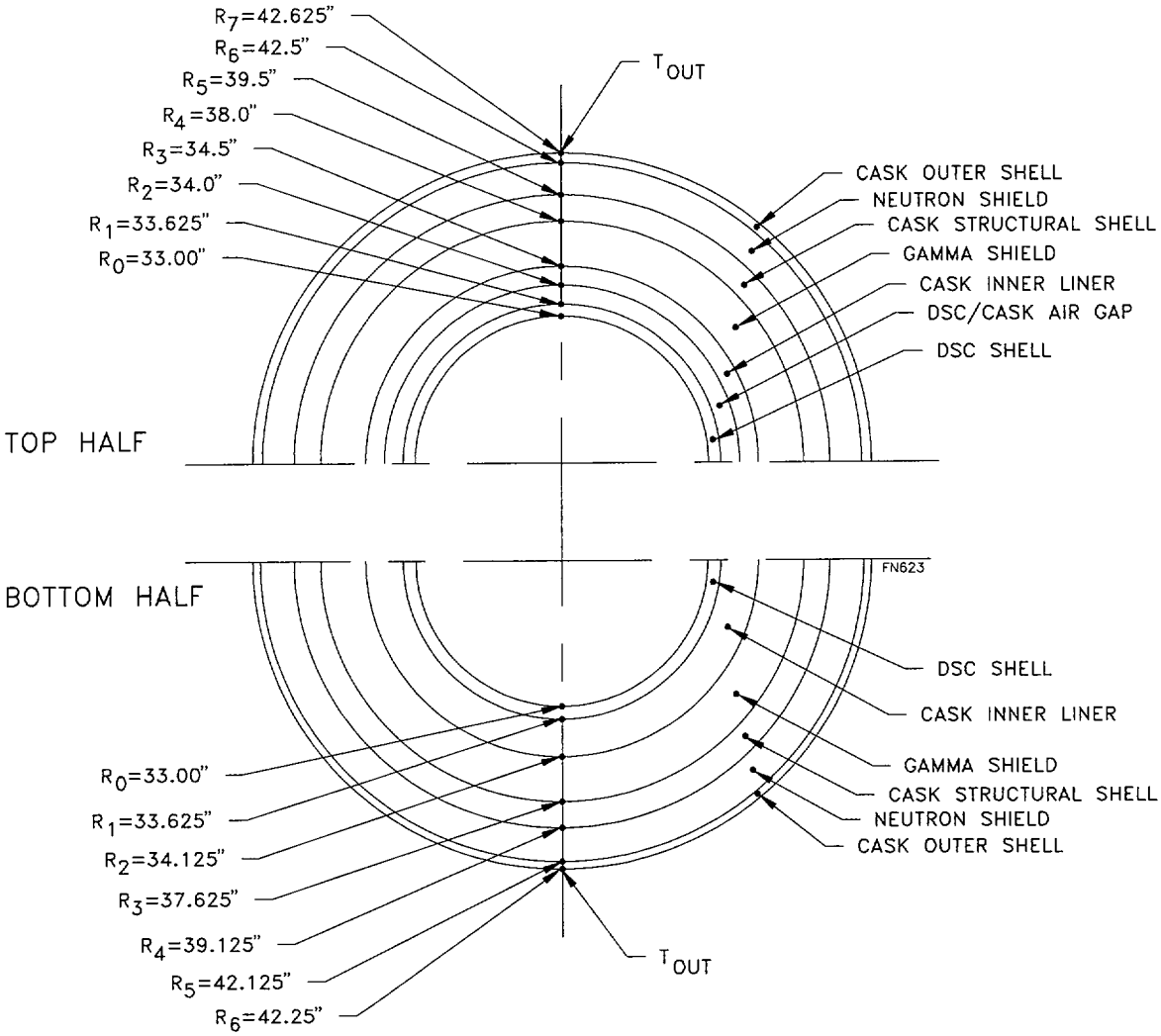


**Figure 8.1-42**
**Transfer Cask Thermal Model for Top and Bottom of the Cask**

**Figure 8.1-43**

**Deleted**

**Figure 8.1-44**

**Deleted**

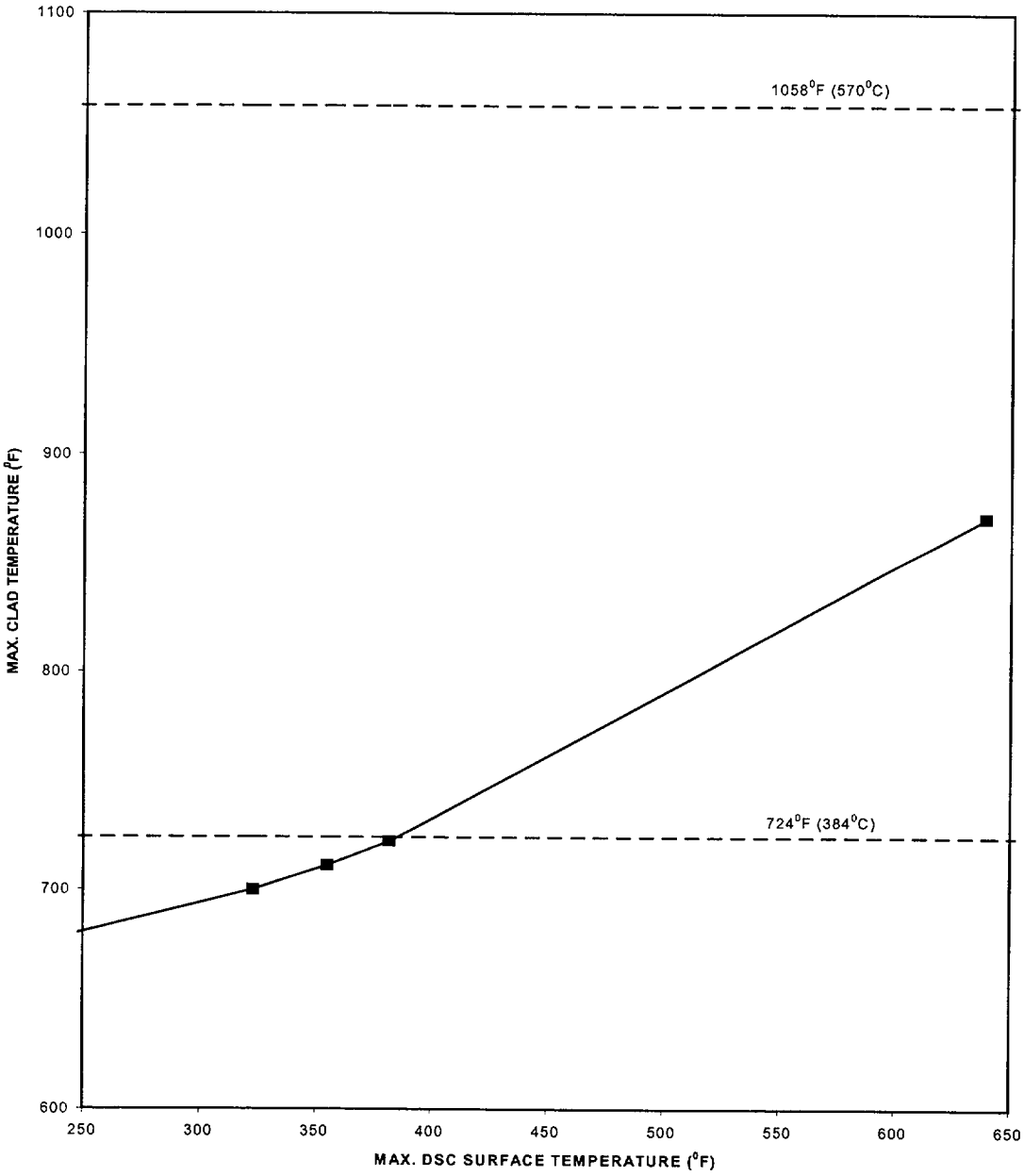


**Figure 8.1-45**
**Maximum Fuel Clad Temperature vs. DSC Surface Temperature for NUHOMS®-24P**

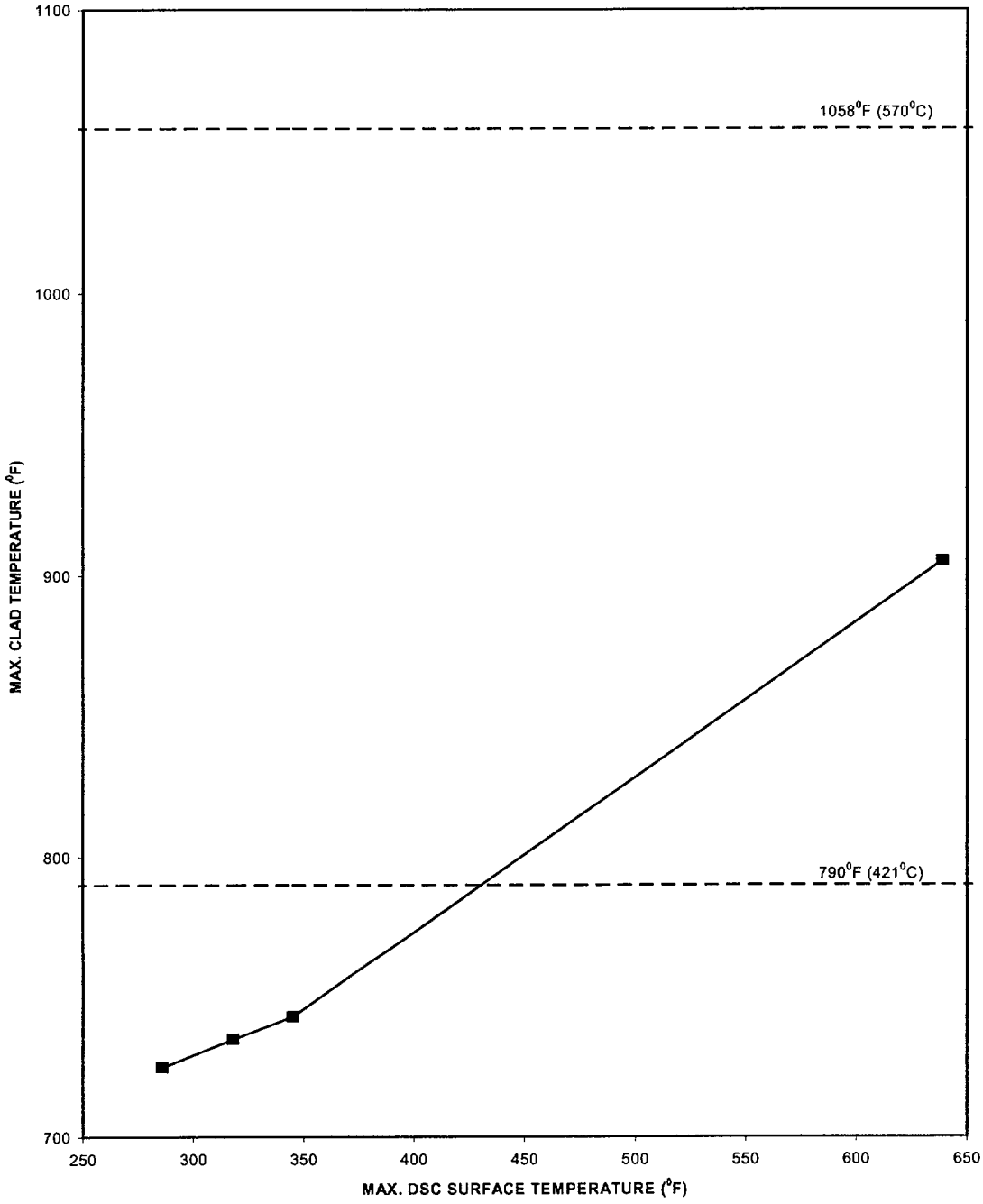


**Figure 8.1-46**
**Maximum Fuel Clad Temperature vs. DSC Surface Temperature for NUHOMS®-52B**

**Figure 8.1-47**

**Deleted**

**Figure 8.1-48**

**Deleted**

**Figure 8.1-49**

**Deleted**

**Figure 8.1-50**

**Deleted**

## 8.2 Accident Analysis

The design basis accident events specified by ANSI/ANS 57.9-1984, and other credible accidents postulated to affect the normal safe operation of the standardized NUHOMS®-24P and NUHOMS®-52B systems are addressed in this SAR section. Appendices K and L provide the evaluation for the NUHOMS®-61BT DSC and -24PT2 DSC, respectively. Analyses are provided for a range of hypothetical accidents, including those with the potential to result in an annual dose greater than 25 mrem outside the owner controlled area in accordance with 10CFR72. The postulated accidents considered in the analysis and the associated NUHOMS® components affected by each accident condition are shown in Table 8.2-1.

In the following sections, each accident condition is analyzed to demonstrate that the requirements of 10CFR72.122 are met and that adequate safety margins exist for the standardized NUHOMS® system design. Radiological calculations are performed to confirm that on-site and off-site dose rates are within acceptable limits. The resulting accident condition stresses in the NUHOMS® system components are evaluated and compared with the applicable code limits set forth in Section 3.2. Where appropriate, these accident condition stresses are combined with those of normal operating loads in accordance with the load combination definitions in Tables 3.2-5, 3.2-6, and 3.2-7. Load combination results for the HSM, DSC, and transfer cask and the evaluation for fatigue effects are presented in Section 8.2.10.

The postulated accident conditions addressed in this SAR section include:

A. Reduced HSM air inlet and outlet shielding.

B. Tornado winds and tornado generated missiles.

C. Design basis earthquake.

D. Design basis flood.

E. Accidental transfer cask drop with loss of neutron shield.

F. Lightning effects.

G. Debris blockage of HSM air inlet and outlet opening.

H. Postulated DSC leakage.

I. Pressurization due to fuel cladding failure within the DSC.

For each postulated condition, the accident cause, the structural, thermal, and radiological consequences, and the recovery measures required to mitigate the accident are presented.

### 8.2.1 Reduced HSM Air Inlet and Outlet Shielding

This postulated accident is the partial loss of shielding for the HSM air inlet and outlet vents provided by the adjacent HSM. All other components of the NUHOMS® system are assumed to be functioning normally.

#### 8.2.1.1 Cause of Accident

An array of free-standing prefabricated HSMs is designed to remain intact for all postulated events. In the unlikely event that large settlements of the ISFSI foundation occur, shifting of adjacent HSMs may occur causing the HSMs to separate. Although adequate means are provided to ensure that the spacing of adjacent HSMs is maintained, for the sake of this conservative generic analysis, it is postulated that an HSM in the middle of the array is separated and now rests against the adjacent HSM side wall. The arrangement is assumed to block the HSM air inlet and outlet openings on the HSM side walls on one side and coincidentally increase the distance between the HSM on the opposite side from 6 inches to 12 inches.

#### 8.2.1.2 Accident Analysis

There are no structural consequences that affect the safe operation of the NUHOMS® system resulting from the separation of the HSMs. The thermal effects of this accident results from the blockage of HSM air inlet and outlet openings on the HSM side walls in contact with each other. This would block the ventilation air flow provided to the HSMs in contact from these inlet and outlet openings. The increase in spacing between the HSM on the opposite side from 6 inches to 12 inches, will reduce the ventilation air flow resistance through the air inlet and outlet openings on these side walls, which will partially compensate the ventilation reduction from the blocked side. However, the effect on the DSC, HSM and fuel temperatures is bounded by the complete blockage of air inlet and outlet openings described in Section 8.2.7. The radiological consequences of this accident are described in the paragraph below.

#### 8.2.1.3 Accident Dose Calculations

The off-site radiological effects that result from a partial loss of adjacent HSM shielding effects is an increase in the air scattered (skyshine) and direct doses from the 12 inch gap between separated HSMs. The air scattered (skyshine) and direct doses are reduced from the gap between HSMs that are in contact with each other. On-site radiological effects result from an increase in direct radiation during recovery operations and increased skyshine radiation. The calculation of these doses during normal conditions is described

in Section 7.3.2.2. Table 8.2-2 shows comparisons of the increased dose rate as a function of distance due to the reduced shielding effects of the adjacent HSM. The dose increase to a person located 100 meters away from the NUHOMS® installation for eight hours a day for five days (estimated recovery time) would be 16 mrem. The increased dose to an off-site person for 24 hours a day for five days located 2000 feet away would be less than 0.1 mrem. Thus, the 10CFR72 requirements for this postulated event are met.

### 8.2.1.4 Recovery

To recover from an accident resulting in a partial loss of adjacent HSM shielding effects, repositioning of the adjacent HSM is required. This can be done using hydraulic jacks or a suitable crane to reposition the affected HSMs. It is estimated that the entire operation could be completed in less than eight hours, of which a mechanic are on the HSM roof for approximately two hours. During this time he receives a dose of less than 2270 mrem. An additional dose to the mechanic and to the crane operator on the ground during this operation will be less than 597 mrem each (assuming an average distance of ten feet from the center of the HSM front wall). Severe foundation settlement requires that the affected HSMs be taken out of service and that repairs to the foundation be made.

## 8.2.2 Tornado Winds/Tornado Missile

### 8.2.2.1 Cause of Accident

In accordance with ANSI-57.9 and 10CFR72.122, the NUHOMS® HSM and transfer cask are designed for tornado effects including tornado wind loads. In addition, the HSM and transfer cask are also designed for tornado missile effects, although not specifically required by ANSI-57.9 and 10CFR72.122. For this conservative generic evaluation, the NUHOMS® system is designed to be located anywhere within the United States. Consequently, the most severe tornado wind loadings specified by NUREG-0800 (8.19) and (8.30) and NRC Regulatory Guide 1.76 (8.31) are selected as a design basis for this postulated accident.

### 8.2.2.2 Accident Analysis

The applicable design parameters for the design basis tornado (DBT) are specified in Section 3.2.1.1. The determination of the tornado wind and tornado missile loads acting on the HSM are detailed in Section 3.2.1.2. The end modules of an array utilize shield walls to resist tornado wind and missile loads. For this conservative generic analysis, the tornado loads are assumed to act on a single free-standing HSM (with two end shield walls and a rear shield wall). This case conservatively envelopes the effects of wind on an HSM array. The transfer cask is also designed for the tornado wind and tornado missile loads defined in Section 3.2.1.2. Thus, the requirements of 10CFR72.122 are met.

A. Effect of DBT Wind Pressure Loads on HSM

As described in Section 3.2.1.2, the maximum DBT generated wind loads are 397 lb./ft.$^2$ and 196 lb./ft.$^2$ on the windward and leeward walls an HSM array. A single stand alone HSM is protected by shield walls on either side and at the rear. For an HSM array, the critical module is on the windward end of the array. This module has an end shield wall to protect the module from tornado missile impacts. The shield wall is also subjected to the 397 lb./ft.$^2$ windward pressure load. The leeward side of the same end module in the array has no appreciable suction load due to the close proximity of the adjacent module. The 196 lb./ft$^2$ suction load is applicable to the shield wall on the opposite end module in the array. For a free standing module the end shield walls are subjected to wind pressure load (397 lb./ft.$^2$ on the shield wall on the windward side) and wind suction load (196 lb./ft.$^2$ on the shield wall on the leeward side). A suction of 357 lb./ft.$^2$ is also applied to the roof of each HSM in the array. For conservatism, the design basis operating wind pressure loads are assumed to be equal to those calculated for the DBT in the formulation of HSM load combination results.

The DBT pressures are applied to the HSM as uniformly distributed loads on the front wall, side walls, rear wall and the roof, . The rigidity of the HSM in the transverse direction (shear wall action of a single HSM) is the primary load transfer mechanism assumed in the analysis. The bending moments and shears at critical locations in the HSM walls and roof are calculated by performing an analysis, using the ANSYS analytical model of the prefabricated HSM. The resulting moments and shears are tabulated in Table 8.2-3 and are included in the formulation of HSM load combination results reported in Section 8.2.10.

An analysis is also performed to evaluate the effects of overturning and sliding of a single, free-standing HSM due to a postulated DBT. For the DBT wind overturning analysis, the overturning moment and the resulting stabilizing moments are calculated. While the weights and overall dimensions of the BWR HSM and PWR HSM are quite similar, the more critical configuration for this analysis is the BWR HSM. The following presents the results of the overturning check for the BWR HSM.

(i) HSM Overturning Analysis

The stabilizing moment ($M_{st}$) for the free standing module with two end shield walls and a rear shield wall is:

$$M_{st} = Wd + W_s (2d + d_s) \qquad (8.2\text{-}1)$$

Where: W = 324 kips, Weight of HSM plus DSC (excluding basemat)

(Conservatively, a lower DSC weight of 72 kips is used.)

| | | | |
|---|---|---|---|
| | $W_s$ | = | 89.3 kips, Weight of end shield wall |
| | d | = | 58 in. (4.83 ft.), Horizontal distance between center of gravity of HSM to the outer edge of the side wall. |
| | $d_s$ | = | 18 in. (1.50 ft.), Horizontal distance from the module to the shield wall center of gravity. |
| Therefore: | $M_{st}$ | = | 30,758 K-in. |

and the overturning moment ($M_{ot}$) for the free standing module with two end shield walls and a rear shield wall due to DBT wind pressure is:

$$M_{ot} = W_1 A_w h/2 + W_3 A_r (d + d_p) \qquad (8.2\text{-}2)$$

| | | | |
|---|---|---|---|
| Where: | $W_1$ | = | (0.397 + 0.196) K/ft.$^2$, Wind load (windward plus leeward) |
| | h | = | 180 in. (15.0 ft.) Wall height |
| | $W_3$ | = | 0.357 K/ft.$^2$, Wind uplift on roof |
| | $A_r$ | = | 241.3 ft.$^2$, Roof area (including shield wall) |
| | $A_w$ | = | 297.5 ft.$^2$, Wall area |
| | $d_p$ | = | 15 in. (1.25 ft.) One-half thickness of shield wall plus 6 inch gap |
| Therefore: | $M_{ot}$ | = | 22,168 K-in. |

Since the overturning moment is smaller than the stabilizing moment, the free-standing HSM will not overturn. The resulting factor of safety against overturning effects for DBT wind loads is 1.38.

The tornado pressure drop of 3 psi is more controlling than the 357 lb./ft.$^2$ DBT negative pressure acting on the HSM door. The pressure drop results in a total load of 18.1 kips on the door, which is reacted by the HSM door frame. The door frame embedded anchors have a tensile load capacity that easily exceeds this total load. All other loads acting on the HSM door assembly envelop DBT negative pressure effects. Therefore DBT negative pressure loads have a negligible effect on the HSM door assembly design.

(ii) HSM Sliding Analysis

To evaluate the potential for sliding of a single, free-standing HSM (One HSM module with two end shield walls and a rear shield wall) the sliding force generated by the postulated DBT wind pressure is compared to the sliding resistance provided by friction between the base of the HSM and the ISFSI basemat. The BWR HSM is the critical configuration presented below.

The force ($F_{sl}$) required to slide a free standing module is:

$$F_{sl} = [W + 2W_s + W_{rs} - 2L(d + T_s + 6)W_3]\mu \qquad (8.2\text{-}3)$$

Where: $\mu$ = 0.6, coefficient of friction (ACI 349-85) (8.20)

W, $W_s$, $W_3$ and d are defined above. The 6" gap between the side wall and the end shield wall is included in the uplift force calculation.

$W_{rs}$ = 66 kips, Weight of rear shield wall

L = 19 ft, Length of HSM side walls

$T_s$ = 2 ft, Thickness of shield wall

Substituting gives:

$$F_{sl} = 278.6 \text{ kips}$$

The sliding force ($F_{hw}$) generated by DBT wind pressure for a single HSM is:

$$F_{hw} = W_1[h\,(L + T_s)]$$

Where: $W_1$, h, L and $T_s$ are as defined above

Substituting gives:

$$F_{hw} = 194.2 \text{ kips}$$

Since the horizontal force generated by the postulated DBT is smaller than the force required to slide the end module in an HSM array, the HSM will not slide. The factor of safety against sliding of the HSM due to DBT wind loads is 1.43.

B. Effects of DBT Wind Pressure Loads on Transfer Cask

The transfer cask design is evaluated for the effects of tornado wind loads in accordance with 10CFR72.122 and ANSI 57.9 criteria. This evaluation is performed for the transfer cask secured horizontally to the transport trailer/skid. Both overall stability and maximum cask stresses are evaluated.

The critical overturning case for the transfer cask stability occurs when the wind loads are applied perpendicular to the cask/skid/trailer.

The stabilizing moment ($M_{st}$) is given by:

$$M_{st} = W_t d$$

Where: $W_t$ = 225 kips, Minimum weight of cask/skid/trailer

$d$ = 66 in., Half wheel base of trailer

Therefore: $M_{st}$ = 14,800 K-in.

Conservatively assuming if the combined cask/skid/trailer has a solid vertical projected area, and ignoring the reduction in total wind pressure due to the open areas and shape factors, the maximum overturning moment ($M_{ot}$) for the cask/skid/trailer due to DBT wind pressure is:

$$M_{ot} = (W_1 + W_2)(A)\, h/2$$

Where: $A$ = 232 ft.$^2$, Combined vertical projected area of cask/skid/trailer

$W_1$ = 0.397 k/ft.$^2$, Wind load windward side

$W_2$ = 0.196 k/ft.$^2$ Wind load leeward side

$h$ = 146 in., Height to top of cask during normal transfer operations

Therefore: $M_{ot}$ = 10,000 k-in.

Since the overturning moment is smaller than the stabilizing moment, the cask/skid/trailer will not overturn. The resulting factor of safety against the overturning effects for DBT wind loads is about 1.5.

The maximum stresses induced in the transfer cask structural shell by DBT wind pressure loads are very conservatively calculated using the correlation presented in Roark (8.16) Table 31 Case 9.c. The wind pressure loads are applied as a line load to the cylindrical shell. Substituting the cask physical dimensions and an equivalent line load of 0.24 k/inch (397 psf x 85.3/144) into the correlation, the maximum calculated shell stress is 3.8 ksi. Similarly, the maximum tornado wind load pressure stresses induced in the top and bottom end plates are calculated using the Roark correlations given in Table 24 Cases 10a and 10b for the simply supported (bolted) top cover and fixed (welded) bottom end plates. The maximum calculated DBT wind pressure stress calculated for these items is 0.5 ksi. Since the resulting DBT transfer cask stresses are a small fraction of the ASME Code Level A allowables, DBT wind loads are not considered further.

The stresses calculated above should be verified by the licensee if the dimensions of the trailer and the skid equipment at the site do not correspond to the value used in this analysis.

C. HSM Missile Impact Analysis

The side walls and roof slab of the reinforced concrete HSM are 18 and 36 inches thick respectively. The side walls of the end HSM in an array are protected from tornado missile impact by 24 inch thick shield walls. The walls and roof are designed to provide adequate biological shielding and easily meet the minimum acceptable barrier thickness requirements for local damage against tornado generated missiles, specified in Table 1 of Section 3.5.3, NUREG-0800. However, in order to demonstrate the adequacy of the HSM design for tornado missiles, a bounding analysis of a free standing module is performed. The items evaluated include the resistance to penetration, scabbing and perforation for a postulated missile impact. For these analyses, a rigid penetration resistant missile consisting of a 280 pound, eight inch diameter blunt nosed hardened steel object is conservatively postulated. The method of analysis is based on the modified NDRC formula as recommended in Section 3.5.3 of NUREG-0800.

The door covering the access opening of the HSM is also evaluated for DBT missile penetration resistance. The door is constructed of steel plate, and is filled with concrete. Missile impact is resisted by the thick steel outer cover plate. The results of this evaluation indicate that the HSM access door provides sufficient capacity to preclude perforation..

The DBT missile penetration resistance analyses for the HSM are presented in the following paragraphs.

(i) Missile Impact Penetration Resistance Analysis

The modified National Defense Research Committee (NDRC) formula from Kennedy, Holmes and Narver (8.32) is used to predict the HSM wall penetration depth for a postulated DBT missile.

$$x = \sqrt{4KNWd^{-0.8}\left[\frac{V}{1000}\right]^{1.8}} \qquad (8.2\text{-}5)$$

When: $\frac{x}{d} = \leq 2.0$

Where:

| | | | |
|---|---|---|---|
| | x | = | Total penetration depth (in.) |
| | d | = | 8 in., Projectile diameter |
| | K | = | $180/\sqrt{f'_c}$, Concrete penetrability factor |
| | | = | 2.55 for $f'_c = 5000$ |
| | N | = | 0.84 (blunt nosed), Projectile shape factor |
| | $f'_c$ | = | 5000 psi, Concrete compressive design strength at 150°F |
| | W | = | Projectile weight = 280 lbm (conservatively assumed) |
| | V | = | Striking velocity = 185.0 ft./s |
| Therefore: | x | = | 4.67 inches |

The perforating thickness, or maximum thickness that the postulated DBT missile will completely penetrate, is calculated using the correlation:

$$\frac{e}{d} = 1.32 + 1.24\left(\frac{x}{d}\right) \text{ for } 1.35 \leq \frac{x}{d} \leq 13.5 \qquad (8.2\text{-}6)$$

$$(e/d) = 3.19\,(x/d) - 0.718\,(x/d)^2 \quad \text{for } x/d \leq 1.35 \qquad (8.2\text{-}7)$$

$x/d = 4.67/8 = 0.584 < 1.35$

Substituting in equation 8.2-7 yields:

$$e = 3.19(0.584) - 0.718(0.584)^2 = 12.95 \text{ in}$$

Therefore; e, the maximum perforation thickness, is conservative.

The minimum thickness necessary to prevent scabbing of material from the rear face of the target is calculated using:

$$\frac{s}{d} = 2.12 + 1.36\left(\frac{x}{d}\right) \text{ for } \left(0.65 \leq \frac{x}{d} \leq 11.8\right) \quad (8.2\text{-}8)$$

$$(s/d) = 7.91\,(x/d) - 5.06\,(x/d)^2 \quad \text{for } (x/d \leq 0.65) \quad (8.2\text{-}9)$$

Using equation 8.2-9 yields:

$$s = 23.1 \text{ in.}$$

Where: $s$ = Scabbing thickness (in.)

Code requirements for nuclear safety related concrete structures (ACI 349-85) require a minimum of 20% additional wall thickness to prevent perforation and scabbing. Scabbing effects control the minimum required wall thickness. Therefore, the minimum wall thickness required to provide adequate protection for the enveloping DBT missile is:

$$1.2s = 27.7 \text{ in.}$$

The specified minimum wall thickness for exterior HSM walls is at least 30 inches including the thickness of the precast shield walls. Consequently, there is adequate protection against local DBT missile impact damage.

The thickness of the end module shield walls (24 inches) may result in some minor scabbing occurring due to the worst case missile impact. Any concrete that is displaced remains within the space between the adjacent module. In the worst possible case, wall debris may block one side of the HSM air inlet or outlet vents. This case is bounded by the blocked inlet and outlet vents case discussed in Section 8.2.7. The combined wall thickness at this location exceeds 36 inches and no possible scabbing of the HSM affects the DSC.

(ii) Local Barrier Impingement Analysis

A composite door comprising a steel plate and concrete is used to cover the HSM access opening after the DSC is in place. The HSM door is analyzed to verify its adequacy for local barrier impingement of a DBT missile. The 280 pound, eight inch diameter artillery shell is used for this calculation as it envelops effects caused by the postulated one inch diameter solid steel sphere. The minimum thickness of a steel plate that can be perforated by the postulated DBT missile is given in the McDonalds, Mehta, and Minor paper (8.33) as:

$$T = \frac{(0.5 M_m V_s^2)^{2/3}}{672\, d_m} = 0.52 \text{ in.} \quad (8.2\text{-}10)$$

Where: $T$ = Perforation thickness (in.)

$M_m$ = Mass of missile $= \frac{W}{g} = 8.7$ lb-sec$^2$/ft

$W$ = Weight = 280 lb. (conservative)

$g$ = 32.2 ft./s$^2$

$V_s$ = Missile strike velocity = 185.0 ft./s

$d_m$ = Diameter of missile = 8 in.

The steel HSM door specified exceeds the minimum required perforation thickness of 0.52 inch by a wide margin.

(iii) Massive Missile Impact Analysis

The HSM stability and potential damage due to impact of the postulated DBT massive missile consisting of a 4000 lb. automobile, 20 sq. ft. frontal area travelling at 195 ft./sec., is evaluated. The massive missile is assumed to impact the shield wall of free standing HSM module. Using the principles of conservation of momentum with a coefficient of restitution of zero, the analysis presented below demonstrates that the free standing module remains stable and the missile energy is dissipated by sliding or slight tipping of the module.

Using conservation of momentum, the missile impact force equals the change in linear (sliding) or angular (overturning) momentum of the HSM. The HSM velocities immediately after impact are:

Sliding:

$$V = \frac{m\ v_i}{M+m} \qquad (8.2\text{-}11)$$

Overturning:

$$\omega_A = \frac{md\ v_i}{md^2 + I_A} \qquad (8.2\text{-}12)$$

Where: $V$ = Initial linear velocity of module after impact

$v_i$ = 195.0 ft./sec., Initial velocity of missile

$\omega_A$ = Initial rotational velocity about point A (Figure 8.2-11)

$m$ = 4000/386.4 = 10.35 lb-sec $^2$/in, Mass of missile

| | | |
|---|---|---|
| M | = | 1471.5 lb-sec $^2$ /in, Mass of loaded HSM plus two shield walls. (Conservatively, a lower DSC weight of 72 kips is used.) |
| d | = | 156 in., CG Elevation of the missile above the basemat. |
| $I_A$ | = | 20,075,643 lb-sec$^2$-in, mass moment of inertia of loaded HSM plus one shield wall about point A |

Substituting and solving for V and $\omega_A$ produces an initial linear velocity of 1.364 ft./sec. and an angular velocity of 0.18 radians/sec.

The actual ratio between HSM sliding and rotation depends on where the missile impacts the shield wall. A low elevation impact produces mainly sliding while a high elevation impact produces mainly rotation.

For an impact at the bottom of the HSM wall, the kinetic energy imparted to the HSM is absorbed by sliding friction between the concrete of the HSM and the basemat. ACI 349-85 (8.20) recommends a coefficient of friction of 0.6. Assuming that the missile impulse load results in sliding of the HSM and equating the kinetic energy to the sliding friction gives:

$$(M + m)\ \mu g\ \Delta = \frac{1}{2}(M + m)\ V^2 \qquad (8.2\text{-}13)$$

Where:

| | | |
|---|---|---|
| $\mu$ | = | 0.6, Coefficient of friction |
| $\Delta$ | = | Linear distance module slides |

M, m, g, and V are as defined above

Substituting gives $\Delta = 0.58$ inch

Therefore, a single free-standing module slides a maximum distance of 5/8 inch due to a low elevation tornado missile impact. In an HSM array, the impact force is transmitted to adjacent HSMs through the spacer channels at the base of each HSM. The total velocity decreases very rapidly with the mass of additional modules. A three module array for example will slide a maximum of 0.12 inch. This assumes that all the energy is absorbed in sliding.

At the opposite extreme, when the massive missile impacts at the top of the shield wall most of the missile energy is absorbed in rotation of the shield wall and HSM. Immediately following missile impact, the support plates holding the top of the shield wall, which are flexible compared with the adjoining concrete, collapse and the shield wall acts as a slab simply supported on two edges. Conservatively neglecting the energy

absorbed in buckling the shield wall support plates and equating the initial kinetic energy of the HSM to the increase in potential energy as the HSM center of gravity rises due to rotation gives:

Loss of Kinetic Energy = Increase in Potential Energy

$$\frac{1}{2} I_A \omega_A^2 = Mgd\left[\cos\left(\beta+\alpha-\frac{\pi}{2}\right) - \cos\beta\right] \quad (8.2\text{-}14)$$

Where:

$\alpha$ and $\beta$ are defined in Figure 8.2-11

M, g, d, $I_A$, and $\omega_A$ are as defined above

Substituting and solving for $\alpha$ shows that the HSM rotates a maximum of 1.12° about the bottom edge opposite the point of impact. Therefore, the HSM and shield wall provide a stable body as tip over does not occur until the c.g. rotates past the edge (point A in Figure 8.2-11) to an angle of more than 30.5°.

The impact force applied to the shield wall by the massive missile and the behavior of the wall is calculated in accordance with Bechtel Topical Report, "Design of Structures for Missile Impact," BC-TOP-9A (8.51).

The maximum force due to the automobile is given by:

$$F = 0.625\ v_i\ m\ g \quad (8.2\text{-}15)$$

Where:

$v_i$, m, and g are defined above.

Substituting for the design basis massive missile parameters, the maximum force due to missile impact is 487.5 kips applied to the end module shield wall. This force is sufficient to buckle the three top support plates provided to stabilize the shield wall. The spacer channel at the base of the module is assumed not to crush. The shield wall then acts as a simply supported slab on the top and bottom edges. For design of the shield wall reinforcement, the missile load is applied at the mid-height of the shield wall and a simple yield line failure is assumed for the full width of the wall.

For a simply supported slab with a hinge at the slab centerline, the required moment capacity is 1155 in-k/ft. The design capacity of the end shield wall is 2109 in-k/ft., which exceeds the required capacity per ACI 349-85 (8.20).

Thus, loss of bending strength of the shield wall due to a tornado missile impact is acceptable and does not affect the safe operation of the HSM. Recovery from this event can be performed in a planned and deliberate manner to replace the shield wall and support plates. This requires temporary shielding during removal and replacement of the wall, or removal of the HSM from service. At no time is there any danger of a release of radioactive materials to the general public.

8.2.2.3 Accident Dose Calculation

Each exposed component of the NUHOMS® system is specifically designed to withstand tornado generated missiles as discussed in the preceding paragraphs. The consequence of reduced shielding effects of adjacent HSMs is presented in Section 8.2.1.

8.2.2.4 Transfer Cask Missile Impact Analysis

The effects of a tornado missile impact on the loaded NUHOMS® transfer cask have been addressed in previous licensing correspondence. These documents are included in Appendix C for ease of reference.

8.2.3 Earthquake

8.2.3.1 Cause of Accident

As discussed in Section 3.2.3, enveloping design basis seismic forces are assumed to act on the NUHOMS® system components. For this conservative generic evaluation, the design response spectra of NRC Regulatory Guide 1.60 (8.35) are selected for the seismic analysis of the NUHOMS® system components.

8.2.3.2 Accident Analysis

As discussed in Section 3.2.3, and shown in Figure 8.2-2, the peak horizontal ground acceleration of 0.25g and the peak vertical ground acceleration of 0.17g are utilized for the design basis seismic analysis of the NUHOMS® components. Based on NRC Reg. Guide 1.61 (8.36), a damping value of three percent is used for the DSC seismic analysis. Similarly, a damping value of seven percent for DSC support steel and concrete is utilized for the HSM. An evaluation of the frequency content of the loaded HSM is performed to determine the dynamic amplification factors associated with the design basis seismic response spectra for the NUHOMS® HSM and DSC. The dominant structural frequencies calculated for a loaded HSM in the lateral direction are 19.1 Hz and 30.4 Hz for the DSC on the support structure and HSM concrete structure, respectively. Table 1 of NRC Regulatory Guide 1.60 requires amplification factors for these structural frequencies, which result in conservative horizontal accelerations of 0.40g. The dominant vertical frequencies of the loaded HSM exceed 33 Hz, corresponding to the zero period acceleration of 0.17g vertical.

The dominant frequencies of the HSM and DSC inside the HSM are determined as part of the response spectra analysis performed using an analytical model identical to that shown in Figure 8.1-22.

A. DSC Seismic Evaluation

As discussed above, the maximum calculated seismic accelerations for the DSC inside the HSM are 0.40g horizontally and 0.17g vertically. An analysis using these seismic loads shows that the DSC will not lift off of the support rails inside the HSM. The resulting stresses in the DSC shell due to vertical and horizontal seismic loads are also determined and included in the appropriate load combinations. The seismic evaluation of the DSC is described in the paragraphs that follow. The DSC support structure is also subjected to the calculated DSC seismic reaction loads as discussed in Paragraph C below.

(i) DSC Natural Frequency Calculation

Two natural frequencies, each associated with a distinct mode of vibration of the DSC are evaluated. These two modes are the DSC shell cross-sectional ovalling mode, and the mode with the DSC shell bending as a beam.

a. DSC Shell Ovalling Mode

The natural frequency for the DSC shell ovalling mode is determined from the Blevins (8.37) correlation as follows.

$$f = \frac{\lambda_i}{2\pi R}\sqrt{\frac{E}{\mu(1-\nu^2)}} \qquad \text{(Blevins, Table 12-1, Case 3)} \qquad (8.2\text{-}16)$$

Where:

$R$ = 33.31 in., DSC mean radius

$E$ = 26.5E6 psi, Youngs Modulus

$\upsilon$ = 0.3, Poisson's ratio

$$\lambda_i = 0.289\,\frac{t}{R}\,\frac{i(i^2-1)}{\sqrt{1+i^2}} \qquad (8.2\text{-}17)$$

$t$ = 0.625 in., Thickness of DSC shell

$\mu$ = 0.288/g, Steel mass density

The lowest natural frequency corresponds to the case when i = 2.

Hence: $\lambda_2$ = 0.0146 sec.

Substituting gives: f = 13.8 Hertz

The resulting spectral accelerations in the horizontal and vertical directions for this DSC ovalling frequency are 1.0g and 0.68g.

b. DSC Beam Bending Mode

The DSC shell is conservatively assumed to be simply supported at the two ends of the DSC. The beam bending mode natural frequency of the DSC was calculated from the Blevins correlation:

$$f_i = \frac{\lambda_i^2}{2\pi L^2}\sqrt{\frac{EI}{m}} \quad \text{(Blevins, Table 8.1, Case 5)} \qquad (8.2\text{-}18)$$

E = 26.5E6 psi, Young's Modulus

I = 72,900 in.$^4$, DSC moment of inertia

L = 186.5 in., Total length of DSC

m = 72,000/186.5g = 386/g lb./in.

$\lambda$ = $i\pi$; for lowest natural frequency, i = 1

Substituting yields: $f_1$ = 62.8 Hertz.

The DSC spectral accelerations at this frequency correspond to the zero period acceleration. These seismic accelerations are bounded by those of the ovalling mode frequency that are used in the subsequent stress analysis of the DSC shell.

(ii) DSC Seismic Stress Analysis

With the DSC resting on the support rails inside the HSM, the stresses induced in the DSC shell are calculated due to the 1.0g horizontal and 0.68g vertical seismic accelerations, conservatively increased by a factor of 1.5 to account for the effects of possible multimode excitation. The resulting seismic loads applied to the DSC are 1.5g horizontal and 1.0g vertical, applied as equivalent static loads. The DSC stresses due to the resulting 1.0g vertical acceleration are calculated by factoring the dead load analysis results reported in Section 8.1. For the stress evaluation of the DSC shell due to seismic accelerations in the lateral direction, the equivalent static acceleration of 1.5g is multiplied by 2, based on the conservative assumption that the DSC is supported by only one of the two support rails inside the HSM during the horizontal earthquake. Thus, the DSC shell is qualified to seismic accelerations of 3.0g horizontal and 1.0g vertical. The

DSC shell stresses obtained from the analyses of vertical and horizontal seismic loads are summed absolutely. See Tables 8.2-13 and 8.2-14 for the Level C seismic stress evaluation of the 24P and 52B, respectively. The seismic load combination includes deadweight + pressure + 3g horizontal and 1g vertical.

As stated, in Section 4.2.3.2, an axial retainer is included in the design of the DSC support system inside the HSM to prevent sliding of the DSC in the axial direction during a postulated seismic event. The stresses induced in the DSC shell and bottom cover plate due to the restraining action of this retainer for a horizontal seismic load, applied along the axis of the DSC, are included in the seismic response evaluation of the DSC shell assembly.

The stability of the DSC against lifting off one of the support rails during a seismic event is evaluated by performing a rigid body analysis, using the 0.4g horizontal and 0.17g vertical input accelerations. The factor of 1.5 used in the DSC analysis to account for multimode behavior need not be included in the seismic accelerations for this analysis, as the potential for lift off is due to rigid body motion, and no frequency content effects are associated with this action. The horizontal equivalent static acceleration of 0.40g is applied laterally to the center of gravity of the DSC. The point of rigid body rotation of the DSC is assumed to be the center of the support rail, as shown in Figure 8.2-1. The applied moment acting on the DSC is calculated by summing the overturning moments. The stabilizing moment, acting to oppose the applied moment, is calculated by subtracting the effects of the upward vertical seismic acceleration of 0.17g from the total weight of the DSC and summing moments at the support rail. Since the stabilizing moment calculated below is greater than that of the applied moment, the DSC will not lift off the DSC support structure inside the HSM.

Referring to Figure 8.2-1, the margin of safety associated with DSC lift off is calculated as follows:

$$M_{am} = yF_H \qquad (8.2\text{-}19)$$

and

$$M_{sm} = (F_{v1} - F_{v2})x \qquad (8.2\text{-}20)$$

Where: $M_{am}$ = The applied seismic moment

$M_{sm}$ = The stabilizing moment

All other variables are defined in Figure 8.2-1.

Substituting yields: $M_{am}$ = 1187.3 K-in.

and $M_{sm}$ = 1422.3 K-in.

Thus, the margin of safety (SF) against DSC lift off from the DSC support rails inside the HSM obtained from this bounding analysis is:

$$SF = \frac{M_{sm}}{M_{am}} = 1.2 \qquad (8.12\text{-}21)$$

B. HSM Seismic Evaluation

To evaluate the seismic response of the HSM, a dynamic response spectra analysis of the BWR HSM, which is the more flexible of the HSM modules, is performed. Seismic loads in the horizontal directions are assumed to be resisted by frame and shear wall action of the HSM. Accordingly, the HSM is modeled with plate elements and the horizontal design basis response spectra loads are applied to the model in both horizontal directions. Similarly, the vertical response spectra load is applied to account for vertical seismic effects. Stresses resulting from the horizontal and vertical seismic response spectra include the effects of multimode excitation of the HSM. The results are included in the load combinations with the appropriate strength reduction factors. The factors used for the HSM are presented in Section 3.2.5. The load combination results for normal, off-normal, and accident conditions are presented in Section 8.2.10.

An analysis is also performed to establish the worst case factor of safety against overturning and sliding for a single, free-standing module. This analysis consists of comparing the stabilizing moment produced by the weight of the HSM and DSC, reduced by 17 percent to account for the upward vertical seismic acceleration, against the overturning moment produced by applying the 0.40g load at the centroid of the HSM and DSC. For sliding of the HSM, the horizontal force of 0.40g acceleration is compared against the frictional resisting force of the foundation slab. In this manner, the factor of safety against sliding is established. The concrete coefficient of friction is taken as 0.6 as defined in Section 11.7.4.3 of ACI 318-83 (8.47).

The details of the seismic evaluation of the HSM are described in the paragraphs that follow.

(i) HSM Frequency Analysis

To determine the loaded HSM frequency content, an ANSYS (8.49) finite element model identical to that shown in Figure 8.1-22 is utilized as discussed previously. The lowest horizontal and vertical structural frequencies calculated for a single free standing HSM are 19.1 Hz and 41.3 Hz, respectively. The corresponding horizontal (conservatively) and vertical spectral accelerations are 0.40g and 0.17g.

(ii) HSM Seismic Response Spectrum Analysis

The horizontal and vertical seismic response spectra are applied to the HSM. The horizontal response spectrum is applied in two orthogonal horizontal directions. The response spectra are obtained from Regulatory Guide 1.60 (8.35) at 7% damping, factored by the 0.25g horizontal and 0.17g vertical peak ground accelerations. The horizontal and vertical response spectra utilized in the analysis are shown in Figure 8.2-2. The HSM concrete mass participating in each mode is multiplied by the corresponding spectral acceleration value to determine the applied loads. The mass of the DSC and DSC support structure are also included in the HSM analytical model. The resulting forces and moments in the HSM walls, roof and floor of a single HSM are calculated using the linear finite element modal shown in Figure 8.1-21, and the computer program ANSYS (8.49). The model responses are combined in accordance with Regulatory Guide 1.92 (8.62) using the grouping method for closely spaced modes. The directional responses are then combined by the square root of the sum of the squares (SRSS) method. The combined maximum moments and stress are reported in Table 8.2-3.

(iii) HSM Overturning Due to Seismic

The following conservative analysis is performed to show that a single, free-standing HSM will not overturn due to seismic loads. The HSM stabilizing moment ($M_{st}$) is:

$$M_{st} = Wd = 19{,}959 \text{ K-in.} \qquad (8.2\text{-}22)$$

Where: W and d are as defined in equation 8.2-1.

The seismic overturning moment is:

$$M_{ot} = Wa_vd + Wa_hh = 17{,}076 \text{ K-in.} \qquad (8.2\text{-}23)$$

Where:

$M_{ot}$ = Overturning moment

$a_v$ = 0.40g, Maximum vertical seismic acceleration

$a_h$ = 0.37g, Maximum horizontal seismic acceleration

h = 99.1 in., Vertical height from HSM and DSC center of gravity to base

The result of this analysis indicates that a single free-standing HSM will not overturn during a seismic event. The margin of safety against overturning is 1.17.

(iv) HSM Sliding Due to Seismic

To show that a single free-standing HSM will not slide due to the postulated horizontal and vertical seismic accelerations, the following conservative analysis is performed. The friction force resisting sliding ($F_{s1}$) is:

$F_{s1} = W\mu g = 171.4$ kips (8.2-24)

W = HSM loaded weight = 345 kips

$\mu$ = Coefficient of friction between the HSM concrete walls and the floor slab foundation = 0.6

g = Net downward gravitational force

= (1 - 0.17)g or 0.83g

The applied horizontal seismic force is:

$F_{hs} = Wa_H = 138.0$ kips

Where: $F_{hs}$ = Induced horizontal seismic force

$a_H$ = 0.40g, Horizontal seismic acceleration

The force required to slide the HSM is larger than the resulting lateral seismic force and therefore, the HSM will not slide. The factor of safety against sliding is 1.24.

C. DSC Support Structure Seismic Evaluation

(i) DSC Support Structure Natural Frequency

The lowest structural frequency of the DSC support structure inside the HSM is dominated by the mass of the DSC. The DSC and support structure are included in the HSM analytical model. The dominant horizontal and vertical frequencies of the DSC/DSC support structure are 19.1 Hz and 41.34 Hz, respectively.

(ii) DSC Support Structure, Seismic Response Spectra Analysis

The horizontal and vertical seismic response spectra accelerations are applied to the support structure as previously described for the HSM. The modal summations and directional summations are also the same. For the support frame cross members, the maximum bending stress is 4.1 ksi and the maximum shear stress is 5.27 ksi. Similarly, the maximum stresses in the support rails are 1.19 ksi and 2.01 ksi, respectively. These

compare with Code allowables of 34.1 ksi for bending and 18.1 ksi for shear and, as a result, have a considerable design margin.

The effect of concentrated anchor bolt forces is included in the design of the DSC support structure connection details. Similarly, each connection of the support rails to the support frame cross members is designed for the resulting seismic loads. This condition envelopes all other loading conditions for the individual bolts or structural elements of the DSC support structure.

The stresses in the support frame columns, cross members and rails due to seismic accelerations are included in the subsequent load combination results reported in Section 8.2.10.

(iii) DSC Axial Retainer Analysis

The DSC axial retainer detail, located inside the HSM access opening, is shown on the Appendix E drawings. The retainer bears against the bottom of the DSC shell and transfers the seismic load to the axial retainer.

The clearance between the DSC axial retainer and the DSC is designed for the maximum DSC thermal growth that occurs during the postulated HSM blocked vent case, as discussed in Section 8.2.7.

The DSC will be subjected to maximum seismic accelerations equal to the rigid range spectral acceleration of 0.40g horizontal. The seismic load acting on the axial retainer is computed as follows:

$$P = 1.5W\{S_a-\mu(1-S_\gamma)/\text{Cos}(30)\} \qquad (8.2\text{-}25)$$

Where,

P = seismic load acting on the axial retainer, kips

W = DSC weight, assumed to be 102 kips

$S_a$ = horizontal rigid range spectral acceleration of 0.37g

$S_\gamma$ = vertical rigid range spectra acceleration = 0.17g

$\mu$ = Coefficient of friction between DSC support rail and DSC = 0.25g

1.5 = Impact factor

$$P = (1.5)(102 \text{ kips})\{(0.40g) - (0.25)(0.83)/\text{Cos}30\} = 24.6 \text{ kips}$$

The maximum shear and bending stresses in the DSC axial retainer are 6.2 ksi and 8.1 ksi, respectively. The allowable shear and bending stresses are 23.5 ksi and 44.3 ksi, respectively. Therefore, the DSC axial retainer stresses are within allowable values.

D. Transfer Cask Seismic Evaluation

The effects of a seismic event occurring when a loaded DSC is resting inside the transfer cask are conservatively postulated for two conditions that affect the transfer cask. All other conditions that exist during DSC loading or transport operations are enveloped by the two cases postulated. The first case postulates a fully loaded transfer cask standing vertically in the plant's cask decontamination area during closure of the DSC. For this condition it is required that the transfer cask remain upright. The rigid body horizontal acceleration required to overturn a loaded transfer cask at a minimum gross weight of 190 kips is at least 0.40g. Each licensee shall ensure that the transfer cask is not subjected to accelerations greater than this magnitude while in the plant's decontamination area, or provide sufficient lateral restraint to prevent cask overturning.

The second case postulates a seismic event occurring during transport of a loaded DSC, resting inside the transfer cask, in a horizontal position, secured to the support skid/transport trailer. For the standardized cask this load case is conservatively enveloped by the postulated normal transport load accelerations of ± 0.5g acting in the vertical, axial, and transverse directions, applied simultaneously at the center of gravity of the transfer cask, as specified in Section 8.1.1.8. These accelerations envelop those that would result from a seismic event in the highly unlikely event that a design basis earthquake would occur during transport of the loaded DSC to or from the HSM. Therefore, the calculated stress intensities for the normal transport loads case for the cask structural shell are conservatively used as the standardized cask maximum seismic stresses in the load combination results reported in Section 8.2.10.

The analysis of the OS197 and OS197H casks applies peak amplification factors of 3.5 and 3.3 to the 0.25g and 0.17g peak ground spectral accelerations in the horizontal and vertical directions, respectively. A multimode factor of 1.5 is applied, resulting in accelerations of 1.31g and 0.84g in the horizontal and vertical directions, respectively.

The stabilizing moment to prevent overturning of the cask/trailer assembly due to the 0.25g horizontal and 0.17g vertical seismic ground accelerations is calculated and compared to the dead weight stabilizing moment. The results of this analysis show that there is a factor of safety of at least 2.0 against overturning that ensures that the cask/trailer assembly has sufficient margin for the design basis seismic loading.

8.2.3.3 Accident Dose Calculations

The NUHOMS® system components are conservatively designed and analyzed to withstand the forces generated by a postulated design basis earthquake accident. Hence, there are no dose consequences resulting from an earthquake.

8.2.4 Flood

8.2.4.1 Cause of Accident

Flooding conditions simulating a range of flood types, such as tsunami and seiches as specified in 10CFR72.122(b) are considered. In addition, floods resulting from other sources, such as high water from a river or a broken dam, are postulated as the cause of the accident.

8.2.4.2 Accident Analysis

Since the source of flooding is site specific, the exact source, or quantity of flood water, should be established by the licensee. However, for this generic evaluation of the DSC and HSM, bounding flooding conditions are specified that envelop those that are postulated for most plant sites. As described in Section 3.2, the design basis flooding load is specified as a 50 foot static head of water and a maximum flow velocity of 15 feet per second. Each licensee should confirm that this represents a bounding design basis for their specific ISFSI site.

A. HSM Flooding Analysis

Since the HSM is open to the atmosphere, external pressure due to flooding is not a design load for the HSM.

The maximum drag force acting on the HSM due to a 15 fps flood water velocity is calculated by the Streeter and Wylie (8.38) correlation:

$$F = \frac{v^2}{2g} C_D A \rho_w = 6{,}600 \text{ lbs./ft. length of HSM} \quad (8.2\text{-}26)$$

Where:

$v$ = 15 fps, Flood water velocity

$C_D$ = 2.0, Drag coefficient for flat plate

$A$ = 15.0 $ft.^2$, HSM area per foot length

$\rho_w$ = 62.4 $lb./ft.^3$, Flood water density

$F$ = Drag force (lb.) per foot length

$$g = 32.2 \text{ ft./s}^2$$

The resulting flood induced pressure loading of 6.6 K/ft. length is assumed to be applied normally to the end module shield wall of a stand-alone HSM. The effects of this loading are less significant than and enveloped by those due to tornado missile loading.

(i) HSM Overturning Analysis

The factor of safety against overturning, for the postulated flooding conditions specified in Section 3.2, is calculated by summing moments about the bottom outside corner of a single, free-standing HSM. The BWR HSM is the most critical configuration and its analysis is presented here. A net weight of 194.7 kips for a loaded HSM plus 52 kips for the upstream end shield wall, including buoyancy effects, is used to calculate the stabilizing moment resisting the overturning moment applied to the HSM by the flood water drag force. A conservative estimate of stabilizing moment is:

$$M_{st} = 194.7 \text{ x } 4.83 \text{ ft.} + 52 \text{ x } 11.2 \text{ ft.} \quad (8.2\text{-}27)$$
$$= 1{,}522 \text{ K-ft.}$$

The maximum drag force due to the postulated water current velocity of 15 fps is derived from Equation 8.2-26 as 6.6 k/ft. acting over the entire height and width of an end shield wall of a single free-standing HSM. Therefore, the overturning moment due to the postulated flood current is:

$$M_{ot} = 6.6 \text{ k/ft. x } 19.83 \text{ ft. x } 7.5 \text{ ft.} \quad (8.2\text{-}28)$$
$$= 982 \text{ K-ft.}$$

The factor of safety (F.S.) against overturning for a single, free-standing HSM due to the postulated design basis flood water velocity is given by:

$$\text{F.S.} = \frac{M_{st}}{M_{ot}} = 1.55$$

(ii) HSM Sliding Analysis

The factor of safety against sliding of a free-standing single HSM due to the maximum postulated flood water velocity of 15 fps is calculated using methods similar to those described above. The BWR HSM is the critical configuration with respect to sliding potential during a flood event. The effective weight of the HSM including the DSC and end shield wall acting vertically downward, less the effects of buoyancy acting vertically upward is 246.7 k. The friction force resisting sliding of the HSM is equal to the product of the net weight of the HSM and DSC and the coefficient of friction for concrete placed against a

roughened concrete surface such as that between the HSM and basemat, which is 0.6 as specified in ACI 349-85 (8.20). Therefore, the force resisting sliding of the HSM is 0.6 x 246.7 or 148 kips. As shown in the previous flooding calculations the drag force acting on a single HSM is 6.6 kips/ft., or 130.9 kips total acting on the side wall of a single HSM, due to a flood velocity of 15 fps. The resulting factor of safety against sliding of a single free standing HSM due to the design basis flood is 1.13.

B. DSC Flooding Analyses

The DSC is evaluated for the design basis fifty foot hydrostatic head of water producing external pressure on the DSC shell and outer cover plates. To conservatively determine design margin which exists for this condition, the maximum allowable external pressure on the DSC shell is calculated for Service Level A stresses using the methodology presented in NB-3133.3 of the ASME Code (8.3). The resulting allowable pressure of 63.6 psi is 2.9 times the maximum external pressure of 21.7 psi due to the postulated fifty foot flood height. Therefore, buckling of the DSC shell will not occur under the worst case external pressure due to flooding.

The DSC shell stresses for the postulated flood condition are determined using the ANSYS analytical model shown in Figure 8.1-14. The 21.7 psig external pressure is applied to the model as a uniform pressure on the outer surfaces of the top cover plate, DSC shell and bottom cover plate. The maximum DSC shell primary membrane stress intensity for the 21.7 psi external pressure is 3.96 ksi which is considerably less than the Service Level C allowable primary membrane stress of 21.7 ksi. The maximum stress in the flat heads of the DSC occurs in the bottom cover plate. The maximum membrane plus bending stress in the top cover plate is 2.38 ksi. This value is considerably less than the ASME Service Level C allowable of 32.6 ksi for primary bending. These stresses are combined with the appropriate loads to formulate load combinations. The resulting total stresses for the DSC are reported in Section 8.2.10.

8.2.4.3 Accident Dose Calculations

The radiation dose due to flooding of the HSM is negligible. The radioactive material inside the DSC will remain sealed in the DSC and, therefore, will not contaminate the encroaching flood water. The minimal amount of contamination that may be on the outside surface of the DSC (see Section 3.3.7.1) is not sufficient to be a radiological hazard if it were to be washed off the DSC outer surface.

8.2.4.4 Recovery

Because of the location and geometry of the HSM vents, it is unlikely that any significant amount of silt would enter an HSM should flooding occur. Any silt deposits would be removed using a pump suction hose or fire hose inserted through the inlet vent to suck the silt out, or produce a high velocity water flow to flush the silt through the HSM inlet vents.

## 8.2.5 Accidental Cask Drop

This section addresses the structural integrity of the standardized NUHOMS® on-site transfer cask, the DSC and its internal basket assembly when subjected to postulated cask drop accident conditions.

### 8.2.5.1 Cause of Accident

#### A. Cask Handling and Transfer Operation

As described in Section 5.0, all handling operations involving hoisting and movement of the on-site transfer cask and DSC are performed inside the plant's fuel handling building. These include utilizing the crane for placement of the DSC into the cavity of the transfer cask, lifting the transfer cask/DSC into and out of the plant's spent fuel pool, and placement of the transfer cask/DSC onto or off of the transport skid/trailer. An analysis of the plant's lifting devices used for these operations, such as the crane and lifting yoke, is needed to address a postulated drop accident for the transfer cask and its contents. The postulated drop accident scenarios should be consistent with those currently addressed in the plant's 10CFR50 licensing basis for handling of a shipping cask. Such postulated accidents are plant specific and should be addressed by the licensee.

Once the transfer cask is loaded onto the transport skid/trailer and secured, it is pulled to the HSM site by a tractor vehicle. A predetermined route is chosen to minimize the potential hazards that could occur during transport. This movement is performed at very low speeds. System operating procedures and technical specification limits defining the safeguards to be provided ensure that the system design margins are not compromised. As a result, it is highly unlikely that any plausible incidents leading to a transfer cask drop accident could occur. Similarly, at the ISFSI site, the transport skid/trailer is backed-up to, and aligned with, the HSM using hydraulic positioning equipment. The transport cask is then docked with, and secured to, the HSM access opening. The loaded DSC is transferred to or from the HSM using a hydraulic ram system. The hold down mechanisms that secure the transfer cask to the transport skid/trailer remain in place at all times during the DSC transport. As a result, there is no reasonable way during these operations for a cask drop accident to occur.

#### B. Cask Drop Accident Scenarios

In spite of the incredible nature of any scenario that could lead to a drop accident for the transfer cask, a conservative range of drop scenarios are developed and evaluated. These bounding scenarios assure that the integrity of the DSC and spent fuel cladding is not compromised. Analyses of these scenarios demonstrate that the transfer cask will maintain the structural integrity of the DSC pressure containment boundary. Therefore, there is no potential for a release of radioactive materials to the environment due to a cask drop. The

range of drop scenarios conservatively selected for design are illustrated in Figure 8.2-3 and include the following cases:

1. A horizontal side drop or slap down from a height of 80 inches.

2. A vertical end drop from a height of 80 inches onto the top or bottom of the transfer cask (two cases).

3. An oblique corner drop from a height of 80 inches at an angle of 30° to the horizontal, onto the top or bottom corner of the transfer cask (two cases).

The height of 80 inches is chosen as this envelopes the maximum vertical height of the transfer cask when secured to the transport skid/trailer assembly. The angle of inclination for the corner drop of 30° represents the maximum possible impact angle that the transfer cask can rotate downward with the transfer cask initially supported horizontally on the transport skid trailer at a height of 80 inches.

C. Cask Drop Accident Load Definitions

The various parameters that are needed to completely define and evaluate the transfer cask impact time history loading associated with each postulated drop accident scenario are presented in Appendix C. In particular, the energy absorbing capacity of the transfer cask is determined, given the mechanical properties of the surface onto which the cask is dropped and the maximum height of the drop. In addition, the maximum decelerations experienced by the DSC and its internals is determined.

In order to form a basis for this generic evaluation, conservative static equivalent deceleration values are established for each cask drop scenario as design criteria for the transfer cask, and DSC. Each licensee should ensure that the physical properties of a postulated drop surface are known, and that the postulated drop heights have been predetermined. This will ensure that the transfer cask and DSC is not subjected to deceleration loads that exceed those used for this generic evaluation.

EPRI Report NP-4830, "The Effects of Target Hardness on the Structural Design of Concrete Storage Pads for Spent Fuel Casks," (8.55) provides expected decelerations for postulated cask side and end drops for typical ISFSIs licensed to 10CFR72 requirements. The report establishes the maximum expected decelerations for a range of surface conditions and drop heights up to 80 inches. For the transfer cask weight and dimensions, the expected maximum decelerations for drops onto a 36 inch thick under-reinforced concrete slab are 59g for an end drop and 49g for a side drop. Corner drops are not explicitly covered in the EPRI report. However, based on the information presented in the document and other supporting calculations delineated in Appendix C, the maximum decelerations for a corner drop are determined to be significantly lower than those for side and end drops. Based on this information, a static equivalent

deceleration of 75g is conservatively chosen as the generic design basis for the postulated horizontal and vertical orientation drop accidents. Similarly, a static equivalent deceleration of 25g is conservatively used for the postulated corner drop accidents. These deceleration magnitudes are established to provide bounding design loads for the DSC, and the transfer cask for primary and secondary slap-down drop conditions.

Cask decelerations of 75g from a vertical end drop or a horizontal side drop accident do not compromise the fuel cladding integrity for spent fuel assemblies typically stored in a NUHOMS® system. As shown by LLNL Report UCID-21246, "Dynamic Impact Effects on Spent Fuel Assemblies," (8.58), B&W 15x15 fuel assemblies will maintain their structural integrity for an end drop deceleration of 147g or a side drop deceleration of 101g, and GE 8x8 fuel assemblies will maintain their structural integrity for an end drop deceleration of 126g or a side drop deceleration of 85g. Of the fuel assemblies investigated, the Westinghouse 17x17 had the lowest axial and side drop capacities of 82g and 63g, respectively. Therefore, the side drop and end drop load magnitude of 75g defined for the NUHOMS® components is comparable to the capacity of the spent fuel assemblies to withstand a postulated drop accident.

D. Cask Drop Surface Conditions

Because of the passive nature of the NUHOMS® system operations and the protective measures taken during transport of the transfer cask to and from the HSM, it is concluded that a postulated cask drop accident is much less plausible during transport operations than those that takes place at the HSM site. Site conditions away from the HSM storage pad will typically be relatively thin (12 inch or less) concrete slabs, asphalt road surfaces or compacted gravel. The target hardness numbers as defined by Reference 8.55 for these surfaces will be small compared with that of a 36 inch thick slab. Therefore, the expected cask decelerations for a cask drop accident will be substantially less than the assumed 75g end drop or side drop, and the 25g corner drop design basis loadings.

Furthermore, the impact of an object as massive and stiff as the transfer cask, will tend to punch through lightly reinforced concrete slabs because of the very high shear stresses induced over small areas. Punching shear failures would be expected to occur for deceleration values ranging from as low as 0.5gs for a corner drop, to 2.6gs for a side drop. Also, it is more likely that the surface conditions at the ISFSI site will be more rigid than those that exist along the designated transport route. For these reasons, the cask drop scenarios postulated and evaluated by site license applicants should focus on conditions that exist at the ISFSI site location.

8.2.5.2 Accident Analysis

A. DSC Horizontal Side Drop Analyses

The principal DSC subassemblies affected by the postulated horizontal cask drop are the basket assembly including the spacer disks and the guide sleeves that contain the spent

fuel assemblies. In this manner, the weight of each fuel assembly is transmitted to the spacer disks. The guide sleeves also serve as guides for the placement and positioning of the spent fuel assemblies.

(i) NUHOMS®-24P DSC Spacer Disk Stress Analysis

The most heavily loaded NUHOMS®-24P spacer disk is evaluated for the 75g side drop condition to demonstrate structural adequacy. For the side drop condition, the spacer disks support the weight of the fuel assemblies, guide sleeve assemblies, and support rod assemblies, as well as their own self-weight. The spacer disks are supported by the canister shell in the region of impact and the canister shell is supported by the transfer cask inner shell. Side drop analyses are performed for 0°, 18.5° and 45° orientations. The ANSYS (8.48) finite element model as shown in Figure 8.2-4, for one half (180°) of a typical DSC spacer disk, is developed to analyze the NUHOMS®-24P spacer disk for the 0° orientation postulated horizontal 75g side drop. Full (360°) spacer disk models are developed for analyses of the 18.5° and 45° drop orientations. The 0° drop orientation corresponds to the drop on the 180° azimuth of the spacer disk such that at the point of impact, the load is equally distributed on the two rails. The 18.5° drop orientation corresponds to the drop on the 161.5° azimuth of the spacer disk, such that the impact point is directly on one cask rail. The 45° drop orientation corresponds to the drop on the 135° azimuth of the spacer disk and is intended to apply maximum bending loads to the spacer disk ligaments. The models include the spacer disk, the canister shell, the inner shell of the transfer cask and associated rails, and the cask lead shielding. The lead shielding material is constrained by the cask outer shell. The cask outer shell is considered as rigid. The spacer disks, canister shell, cask and lead components are modeled using 3-D solid elements. Gap elements are used between the spacer disk, DSC shell and cask liner to accurately capture the interaction of the components. The mass of the PWR fuel assemblies and guide sleeves are applied to the spacer disk ligaments as nodal forces distributed equally on the supporting disk ligaments as illustrated in Figure 8.2-5.

Elastic-plastic analyses of the spacer disk side drop models are performed to account for local yielding of the spacer disk during the side drop events. Classical bilinear plasticity with a tangent modulus equal to 5% of the elastic modulus is used to represent the elastic-plastic material properties of the carbon steel spacer disk and stainless steel DSC shell.

Stress results obtained from the ANSYS analyses are linearized, as appropriate, to allow their categorization into primary membrane and membrane plus bending stress intensities. The controlling NUHOMS®-24P spacer disk stresses for the 0°, 18.5°, and 45° horizontal drop conditions are tabulated in Table 8.2-7.

(ii) NUHOMS®-24P DSC Spacer Disk Stability Analysis

In addition, an ANSYS bifurcation buckling analysis of the entire spacer disk is performed to evaluate the global buckling behavior and stability of the spacer disk. The spacer disk model is based on the 24P side drop model shown in Figure 8.2-4 with the canister, support rod, and cask component elements removed. The spacer disk analytical model permits out-of-plane deformations, and is assumed to be supported both in-plane at the perimeter of the spacer disk that is in contact with the DSC shell, and out-of-plane at the four support rod locations. In addition to the 75g side drop loads, the worst case thermal loads are applied to the spacer disk model. Using the stresses from the side drop and thermal loads analyses, a subspace eigenvalue buckling analysis is performed for each drop orientation. This analysis showed that out-of-plane buckling is the controlling buckling mode for the spacer disk. A factor of safety of 1.99 against collapse of the spacer disk is calculated for the postulated 75g horizontal drop.

(iii) NUHOMS®-24P DSC Spacer Disk Deformations

Spacer disk displacements resulting from the 0°, 18.5° and 45° side drop analyses are reviewed to verify that the maximum relative displacements between opposite sides of the spacer disk openings are smaller than the nominal 0.5 inch gap between the fuel assembly and the guide sleeve. The maximum relative displacement was found to be 0.317 inches. This maximum displacement is sufficiently small to ensure that the fuel assembly integrity is maintained and to permit fuel assembly retrieval from the DSC.

(iv) NUHOMS®-24P DSC Guide Sleeve Analysis

The DSC guide sleeves are evaluated considering a single guide sleeve, modeled as a simple beam with ANSYS beam elements. Bounding side drop orientations of 0° and 45° side drop orientations are considered. Beam sheets and bending stresses are combined to obtain a maximum primary membrane stress intensity in the plate wall of the guide sleeve. The maximum primary membrane stress orientation in the guide sleeve due to postulated horizontal side drop accident is tabulated in Table 8.2-7 The results of the comparison to the primary membrane stress allowable is intensity shown in Table 8.2-15. The calculated stress intensity value is well within ASME Code acceptable limits and no permanent deformation of the guide sleeves will occur.

(v) NUHOMS®-24P DSC Support Rod Analysis

The NUHOMS®-24P basket assembly includes four (4) 3.25 inch support rods. For the 75g side drop the support rods are loaded by their own self weight. The support rods are evaluated using simple beam theory. The maximum support rod stresses due to the side drop occur at the base of the top end cantilever section of the support rod assembly. The maximum bending stress is 5.38 ksi and the maximum shear stress is 0.41 ksi.

(vi) NUHOMS®-52B DSC Horizontal Side Drop Analysis

The analysis of the NUHOMS®-52B DSC for a postulated horizontal cask drop is performed utilizing the same methodology as that described above for the NUHOMS®-24P DSC. The half symmetry 180° analytical model used to analyze the NUHOMS®-52B DSC spacer disk for the postulated 0° horizontal side drop condition is shown in Figure 8.2-7a. The NUHOMS®-52B DSC spacer disk is also analyzed for the postulated 18.5° and 45° side drop conditions using full 360° analytical models, such as the one shown in Figure 8.2-7b. The analyses consider the deadweight of the basket assembly (spacer disks, support rods and spacer sleeves, and neutron absorber poison plates) plus the distributed weight of the fuel assemblies. The mass of BWR fuel assemblies and neutron absorber plates are included in the analytical model as pressures distributed over the bottom and side widths of the spacer disk ligaments and as a function of drop orientation.

The controlling stresses in the NUHOMS®-52B DSC spacer disk for the postulated side drop conditions are tabulated in Table 8.2-8.

The stability analysis of the spacer disk shows that out-of-plane buckling is the controlling buckling mode for the spacer disk. A factor of safety of 2.44 against collapse of the spacer disk is calculated for the postulated 75g horizontal drop.

A review of the spacer disk displacements resulting from the side drop analyses is performed to assess the potential for interference between the fuel assemblies and the spacer disk cut-outs. The maximum relative displacement between opposite corners of the spacer disk cut-out obtained from the spacer disk elastic-plastic analysis is 0.118 inches and occurs at the end of a spacer disk horizontal ligament. This magnitude of deflection is much less than the minimum fuel-spacer disk clearance of 0.5 inches, and is sufficiently small to ensure that the fuel assembly integrity is maintained and to permit fuel assembly retrieval from the NUHOMS®-52B DSC if necessary.

(vii) NUHOMS®-52B DSC Neutron Absorber (Poison) Plate Analysis

The DSC neutron absorber plates (also called poison plates) are evaluated for the postulated horizontal drop load condition using hand calculations based on beam and plate theory. The maximum stresses result from the 75g deceleration load being applied to the plate in the out-of-plane direction. The drop orientations considered in the poison plate side drop analysis are shown in Figure 8.2-13.

The poison plates are fabricated from ASTM A887 Type 304B4 borated stainless steel. The yield strength and ultimate strength of borated stainless steel material are 30.0 ksi and 75.0 ksi, respectively. All other material properties of borated stainless steel plate material are assumed to be the same as those for ASME SA-240, Type 304 stainless steel.

The results of the stress analysis shows that the maximum membrane plus bending stress intensity for the neutron absorber plates is 57.98 ksi. This value is below the ASME Code Level D acceptable limits for primary membrane plus bending stresses.

(viii) DSC Shell Assembly Analysis

The DSC shell assembly is analyzed for the postulated horizontal side drop using the ANSYS 3-D models of the DSC shell assembly discussed in Section 8.1.1.2. Halfsymmetry (180°) models of the top end and bottom end sections of the DSC shell assembly are developed based on the models developed for the end drop shown in Figure 8.1-14a and 8.1-14b. Each model includes one-half of the height of the cylindrical shell. Each of the DSC shell assembly components is modeled using ANSYS solid 3-D elements. The full weight of the DSC is conservatively assumed to drop directly onto a single rail.. Elastic-plastic analyses are performed and stresses are determined for each DSC shell assembly component. The NUHOMS®-24P and NUHOMS®-52B DSC shell stresses in the region of the spacer disks are also analyzed for the postulated horizontal side drop conditions. The NUHOMS®-24P and NUHOMS®-52B spacer disk horizontal side drop ANSYS analytical models described in Section 8.2.5.2A(i) and (vi), respectively, are used for these analyses.

The controlling stresses in the NUHOMS®-24P and NUHOMS®-52B DSC shell assembly components are tabulated in Table 8.2-7 and Table 8.2-8, respectively.

B. On-site Transfer Cask Horizontal Drop Analyses

An analysis is performed to evaluate the transfer cask for a postulated horizontal drop accident with a static equivalent deceleration of 75g's. The structural capacity of the transfer cask neutron shield is neglected for the horizontal drop accident analysis. In reality, the neutron shield subassembly would provide additional energy absorbing capacity that would further reduce the equivalent drop deceleration magnitude. No credit is taken for the energy absorbing capacity of the neutron shield in performing the cask analysis. It is also conservatively assumed for this generic analysis that the cask is rigid.

(i) Cask/DSC Analytical Model

The drop analyses are presented for the standardized, OS197, and OS197H transfer casks. Two ANSYS axisymmetric finite element models are utilized for the standardized transfer cask drop analysis, including; one for the cask top region, and the other for the cask bottom region, as shown in Figure 8.2-9 and Figure 8.2-10. Each of the two analytical models consists of the principal load carrying members of the transfer cask, as well as those that contain a significant mass of material. These include the cask structural shell, the radial lead shielding material, the inner liner, and the cask top or bottom cover plates. The DSC shell, shield plug assemblies and cover plates are also included in the transfer cask analytical models to provide a more accurate means of applying loads, to

evaluate load sharing, and to ensure displacement compatibility between the transfer cask and DSC. The nodal degrees of freedom between the DSC shell and the inner surface of the transfer cask are decoupled in the tangential direction such that the DSC shell can move independently of the cask inner surface in this direction. However, they are coupled in the normal direction such that the DSC outer surface bears on the cask inner surface during a postulated drop accident.

A third model (Figure 8.2-10a) is used to evaluate the OS197 and OS197H transfer casks for DSC loading that is transferred through the cask rails. The cask inner liner and structural shell are modeled using 3-D quadrilateral shell elements. The lead gamma shield is modeled using 3-D brick elements.

The lead gamma shield is assumed to transfer only normal loads at the interface with the inner liner and structural shell. It is also assumed that there is no shear transfer between the lead gamma shield and the cask shells. The coincident nodes on the inner liner, gamma shield, and structural shell are coupled in the radial direction only to model the interface between the lead gamma shield and the cask shells.

(ii) Cask/DSC Loading Application

The loading due to the transfer cask horizontal drop is non-axisymmetric since it is reacted by a portion of the shell circumference. The loading is assumed to be uniform along the length of the cask. In order to apply this non-axisymmetric loading to the axisymmetric standardized cask models shown in Figure 8.2-9 and Figure 8.2-10, the loading is resolved into Fourier harmonics using the ANSYS PREP 6 routine. As shown in Appendix C.3, the first twelve Fourier harmonics are chosen to represent the impact force. These Fourier harmonics, expressed in terms of pressure loading, are applied to the exterior nodes of the impacted surface of the cask structural shell.

The DSC loading of the cask includes the DSC and its internals, factored by the equivalent static deceleration value of 75g. These loads are conservatively applied to the transfer cask inner liner at the spacer disk and end plug locations. As for the cask impact force, this loading acts over a portion of the DSC circumference, and is therefore non-axisymmetric. The loading is resolved into Fourier harmonics and the first eight harmonics are selected for application to the axisymmetric model. This loading assumed that the contact surface along DSC the circumference is similar to that obtained from the spacer disk horizontal drop analysis. This assumption does not have a significant impact on the outcome of the analysis since the stresses arise primarily from bearing.

The cask weight, factored by the deceleration values, is applied to the interior nodes of the cask analytical models with its appropriate harmonic components. The cask weight is assumed to have the same circumferential contact surface as the DSC. A detailed description of load development and application of the loads to the axisymmetric model is provided in Appendix C.3.

For the model of the OS197 and OS197H transfer casks, the load acting on the inner surface of the Cask inner liner due to the accelerated mass of the DSC, fuel, and the cask spacer is modeled as a uniform pressure acting over the inner liner elements in the region of the cask rails (centered at 18.5° on each side of the 180° azimuth). It is assumed the spacer assembly will have a minimal impact on the load distribution. The elements over which the pressure load is applied span an arc of 7.5°. In addition to the contents loading, a 75g side drop vertical acceleration load is also applied to the model.

(iii) Cask Stress Analysis

The enveloped results of the transfer cask analyses for a postulated horizontal drop accident show that the maximum primary membrane stress intensity for the standardized and OS197 transfer cask structural shells is 33.4 ksi (43.1 ksi for the OS197H). Similarly, the maximum primary membrane stress intensity in the standardized or OS197 transfer cask inner liner is 30.6 ksi (39.4 ksi for the OS197H). These stresses are combined with other load cases and compared with the ASME Code Service Level D allowable as described in Section 8.2.10. The calculated transfer cask stresses for the horizontal drop are tabulated in Table 8.2-9, Table 8.2-9a, and Table 8.29b for the standardized, OS197, and OS197H transfer casks, respectively.

(iv) Transfer Cask Collar Analysis

During the postulated horizontal cask drop, the shear forces from the cask lid/collar/DSC top cover are transferred to the cask body by the 3 inch thick shield ring of the cask collar. The maximum calculated shear stress in the shield ring is 0.5 ksi which is a small fraction of the ASME Code Service Level D allowables. The 1-3/4" cask collar to cask top flange bolts are not loaded during this postulated accident.

C. DSC Vertical Drop Analyses

For this drop accident case, the transfer cask is assumed to be oriented vertically and dropped onto a uniform unyielding surface. The vertical cask drop evaluation conservatively assumed that the transfer cask could be dropped onto either the top or bottom surfaces. No credit is taken for the energy absorbing capacity of the cask top or bottom cover plate assemblies during the drop. Therefore, the DSC is analyzed as though it is dropped on to an unyielding surface. The principal components of the DSC and internals affected by the vertical drop are the DSC shell, the inner and outer top cover plates, the shield plugs, the inner and outer bottom cover plates and the basket support rods.

The end drop with the bottom end of the DSC oriented downward is the more credible of the two possible vertical orientations. Nevertheless, an analysis for the DSC top end drop accident is also performed. For a postulated vertical drop, membrane stresses in the DSC shell and local stresses at the cover plate weld region discontinuities are evaluated.

(i) DSC Shell Assembly Stress Analysis

The ANSYS analytical models of the DSC shell assembly as described in Section 8.1.1.2 and shown in Figures 8.1-14a and 8.1-14b are used to determine the vertical end drop accident stresses in the DSC shell, the inner cover plates, the outer cover plates, and the shield plugs. The models consist of 90° quarter symmetry models and include one-half of the height of the cylindrical shell. To capture the maximum stress state in the DSC assembly components, each model was analyzed for end drop loading on the opposite end (i.e., the bottom end model was analyzed for top end drop, and the top end model was analyzed for bottom end drop). In these drop orientations, the end plates are supported at the perimeter by the shell. For the top and bottom end drops, the nodal locations on the impacted end are restrained in the vertical direction. An equivalent static linear elastic analysis is conservatively used for the vertical end drop analyses. Inertia loadings based on forces associated with the 75g deceleration are statically applied to the models. Analyses show that the stresses in the DSC cover plates and shield plugs are low. This occurs since for the bottom end drop, the inner and outer top cover plates are supported by the top shield plug. During a top end drop, the outer top cover plate is assumed to be supported by the unyielding impacted surface and is subjected to a uniform bearing load imposed by the DSC internals. The same is true for the DSC bottom outer cover plate and shield plug for the bottom end drop. The highest stresses occur in the DSC shell and bottom inner cover plate. The maximum stresses in the bottom inner cover plate result from the top end vertical drop condition, in which the bottom inner cover plate is supported only at the edges.. The maximum DSC shell membrane stresses, which occur near the top end of the DSC shell area, result from the accelerated weight of the DSC shell and the bottom end (for top end drop case) or top end (for the bottom end drop case) assemblies.

A summary of the calculated stresses for the main components of the DSC and associated welds is provided in Table 8.2-7 and Table 8.2-8.

(ii) DSC Shell Stability Analysis

The stability of the DSC shell for a postulated vertical drop impact is also evaluated. For Level D conditions, the allowable axial stress in the DSC shell is based on Appendix F of the ASME Code. The maximum axial stress in the DSC shell obtained from the 75g end drop analyses is 9.7 ksi, for both the NUHOMS 24-P DSC and the NUHOMS 52-B DSC. The allowable axial stress is 12.9 ksi. Therefore, buckling of the DSC shell for a 75g vertical deceleration load does not occur.

(iii) 24P DSC Basket Assembly Support Rods and 52B DSC Basket Assembly Support Rods/ Spacer Sleeves Analyses

The DSC basket assembly spacer disk support rods and spacer sleeves are also analyzed for the postulated 75g vertical drop. The support rods extend the full length of the DSC cavity with adequate clearance for differential thermal expansion. The spacer sleeves, applicable only to the NUHOMS-52B® design, enclose the support rods. The principal

functions of the support rods and spacer sleeves are to maintain the position of the spacer disks and to provide support for the imposed vertical loads. The support rods are designed to resist the weight of the spacer disks and the internals supported by the spacer disks (such as oversleeves in the NUHOMS-24P® PWR basket and the neutron absorber plates in the NUHOMS-52B® BWR basket) for the postulated vertical end drop accidents.

The NUHOMS-24P® basket assembly contains four (4) support rods, constructed from SA-479, Type XM-19 stainless steel. The support rods are welded to each of the eight (8) spacer disks of the NUHOMS-24P basket assembly. The NUHOMS-52B basket assembly contains six (6) support rods enclosed by spacer sleeves that are located at each spacer disk span and at each end of the support rods. To maintain basket geometry, the support rods are preloaded in tension, placing each of the spacer sleeves in a state of compressive preload. The NUHOMS-52B support rods and spacer sleeves are constructed of ASME SA-564, Type 630 steel.

The NUHOMS-24P DSC basket assembly support rods are analyzed using the ANSYS model shown in Figure 8.2-14. The analytical model includes 1/4 segment spacer disks to simulate the reaction forces acting on the support rods. The effect of the oversleeves, located between the top two and bottom two spacer disks, are included in the analytical model as additional mass. The support rod is conservatively modeled with a 0.5 inch translational offset from the bottom spacer disk to the top spacer disk. The support rod top end node is modeled as pinned. A linear elastic analysis is performed for the 75g top end vertical drop load. Both, top end and bottom end drop analyses are performed for the 24P and 52B models.

The NUHOMS-52B DSC basket assembly support rods and spacer sleeves are analyzed using the ANSYS model shown in Figure 8.2-15a. The support rods and spacer sleeves support the spacer disks in the axial direction. The inertia of the support rods and spacer sleeves, poison plates and associated support plates is included in the model through material density values specified for these components. Two analysis cases are considered: In the first analysis, the support rods and spacer sleeves have moment continuity through each spacer disk. A second analysis is performed to address the effects of possible loss of support rod preload by releasing the moment continuity at the spacer disk, spacer sleeve interface. Both, top end and bottom end drop analyses are performed for the 24P and 52B models. The support rods and spacer sleeves are evaluated for the 75g end drop as a beam-column system in accordance with the ASME Code, Division III, Appendix F Service Level D criteria for linear type component supports subjected to combined axial compression and bending.

The support rods for the NUHOMS-24P and support rods and spacer sleeves for the NUHOMS-52B are evaluated to the Level D allowable stress limits and criteria of ASME Code Subsection NF and Appendix F. Axial forces and bending moments acting on the support rods due to the 75g drop are obtained from the 90° spacer disk and support rod models. Allowable axial and bending stresses are evaluated for each span and axial plus

bending interaction ratios are calculated. The worst case interaction ratio under the 75g bottom drop analysis case is calculated for the NUHOMS -24P and NUHOMS-52B support rods, and the results are presented in Table 8.2-15 and Table 8.2-16. Since all interaction ratios are less than 1.0, buckling of the support rods as a result of postulated end drop accidents is not a concern.

(iv) NUHOMS®-52B DSC Neutron Absorber (Poison) Plate Stability Analysis

The neutron absorber plates are non-structural safety related items that need only support their own weight and remain in position for criticality control. The plates are supported along the edges at the spacer disks location. The neutron absorber plates are restrained from axial translation only at the top spacer disk. The vertical bottom end drop will result in axial tension stresses on the plate. The vertical top end drop will result in compression stresses on the plate. Both, bottom end and top end drop conditions are evaluated.

For the bottom end drop, the poison plate is represented by a vertical beam fixed at the top with a weight at the bottom equal to the weight of the poison plate. The maximum membrane stress in the plate resulting from the 75g vertical drop is listed in Table 8.2-8.

The maximum membrane stress in the poison plates due to the postulated vertical end drop is well below the yield strength of the borated stainless steel material.

For the top end drop, a linear elastic buckling analysis of the poison plate is performed using the neutron absorber plate model shown in Figure 8.2-12, which conservatively accounts for a range of initial eccentricities. The geometry of the analytical model is modified to reflect initial eccentricities due to the worst case dimensional tolerance stack-up of size and location tolerances of the spacer disks. . A unit top end vertical drop acceleration is applied to the analytical model. A factor of safety of 1.32 against collapse of the neutron absorber plate is calculated for the postulated 75g vertical drop.

The elastic buckling analysis results show that the plates will not buckle due to the postulated vertical top end drop. Therefore, the neutron absorber plates will remain in position following the postulated vertical end drop accident.

(v) NUHOMS®-24P DSC Spacer Disk Stress Analysis

The NUHOMS®-24P DSC spacer disks are analyzed for the vertical end drop using the NUHOMS®-24P DSC quarter symmetry spacer disk assembly ANSYS model described previously and shown in Figure 8.2-14. A quarter symmetry model is used since the spacer disks exhibit symmetry along two horizontal axes. The spacer disks are modeled using shell elements and the support rods are modeled using beam elements. The spacer disk is supported in the longitudinal direction by the support rods. The spacer disks support their own inertial load and the inertial load of the over sleeves where applicable. The model is analyzed for top-end 75g drop and bottom-end 75g drop loadings. Since

the model is linear, the results of the 75g accident end drop conditions are scaled by the ratio of 1/75 to obtain the normal 1g dead load condition. The model includes the support rods discussed in Section (iii) above. The resulting maximum spacer disk stresses are tabulated in Table 8.2-7.

(vi) NUHOMS®-52B DSC Spacer Disk Stress Analysis

The NUHOMS®-52B DSC spacer disks are analyzed for the vertical end drop using the NUHOMS®-52B DSC quarter symmetry spacer disk assembly ANSYS model described previously and shown in Figure 8.2-15a and Figure 8.2-15b. Both, the interior spacer disks and the top spacer disk are modeled with ANSYS plastic shell elements. The inertia of the spacer disks are included by specification of material density properties. The models include the support rods and spacer sleeves in their preloaded condition. The support rods and spacer sleeves are modeled using elastic beam elements. The support rods and spacer sleeves support the spacer disk in the axial direction. The 90°model is used for the analysis of top and bottom end 75g drop accident cases. Two variations of this 90° model are developed: The first model addresses moment continuity of the spacer sleeves through each spacer disk to represent the preloaded configuration of the support rods. The second model addresses the effects of the loss of preload of the support rods on the spacer disks. The spacer disk stresses and potential interferences between the fuel assemblies and the spacer disk fuel assembly opening are checked by releasing the moment continuity at the spacer disk, spacer sleeve interface. Linear elastic equivalent static analyses are performed for the 75g vertical end drop static acceleration load. The resulting maximum spacer disk stresses are tabulated in Table 8.2-8.

D. On-site Transfer Cask Vertical Drop Analysis:

A vertical drop onto the bottom surface of the transfer cask is highly unlikely. A drop onto the transfer cask top surface is even more unlikely. At no time during the NUHOMS® system operations, outside the fuel/reactor building, is the transfer cask in a vertical orientation. The transfer cask remains secured to the transport trailer skid in a horizontal position at all times, except for handling operations inside the plant's fuel/reactor building that are not formally covered by this 10CFR72 SAR.

All conceivable scenarios leading to a drop accident onto the transfer cask bottom surface are highly remote, with the most probable postulated to occur in the plant's fuel handling building. A drop onto the transfer cask top surface, is not possible even during placement or removal from the skid/transport trailer. However, both of these vertical drop orientations are conservatively postulated for the transfer cask with specific analyses performed to confirm the structural integrity of the transfer cask and the loaded DSC resting in the cask cavity.

(i) Transfer Cask Analysis Methodology

The ANSYS axisymmetric finite element models used to perform these analyses are described in Section 8.2.5.2. The loadings due to the postulated vertical drops are applied to the transfer cask analytical models in a symmetric manner. The individual models of the top and bottom cask regions shown in Figure 8.2-9 and Figure 8.2-10 are used for these analyses. The respective top or bottom impacted surface of the transfer cask is assumed to be uniformly supported vertically and the 75g equivalent static decelerations are applied to the models.

(ii) Transfer Cask Stress Analysis

The resulting primary membrane and membrane plus bending stresses due to the postulated end drop are tabulated in Table 8.2-9, Table 8.2-9a, and Table 8.2-9b for the standardized, OS197, and OS197H transfer casks, respectively. For the top end drop analysis, the stresses in the cover plates are relatively small since they arise primarily from bearing of the DSC and its contents on the cask top cover plate. The most critical vertical drop direction for the transfer cask top region is the bottom end drop, since this produced the maximum bending stress in the top cover plate. The maximum (enveloped between the standardized and OS197 casks) primary membrane plus bending stress in the cover plate is 28.6 ksi (36.8 ksi for the OS197H transfer cask). The maximum local membrane stresses in the cask structural shell and inner liner are 9.6 ksi and 12.9 ksi, respectively (12.9 ksi for OS197H transfer cask). Similarly for the standardized transfer cask bottom region, the most critical drop direction is the top end drop producing a maximum primary membrane plus bending stress of 26.1 ksi in the cask bottom end plate (28.6 ksi and 34.8 ksi for the OS197 and OS197H transfer cask, respectively). These stresses are well below the appropriate ASME Code Service Level D allowables.

(iii) Transfer Cask Collar Analysis

During the postulated vertical end drop, the maximum compressive stress in the cask collar is 13 ksi and the maximum membrane stress intensity is 26.2 ksi. These stresses are well within the ASME Code Service Level D allowables.

E. On-site Transfer Cask/DSC Corner Drop Analyses

The possibility of a drop onto the top or bottom end corners of the transfer cask is extremely remote due to the limited cask handling operations of the NUHOMS® system, as discussed previously. Nevertheless, for this generic evaluation, a cask corner drop is conservatively postulated to occur onto a concrete surface with an equivalent static deceleration of 25g. The orientation of the drop is shown in Figure 8.2-3 as occurring at 30° to the horizontal. This is the largest drop orientation angle that can occur as the center of gravity of the cask passes beyond the back end of the transport trailer and pitches downward. The derivation of this load definition is contained in Appendix C.2.

It is probable that the cask support skid would remain firmly attached to the cask and would absorb considerable energy upon impact, thus reducing the transfer cask deceleration. In addition, this would further reduce the angle of the impact and the drop height. The combined support skid and transfer cask would act as a substantial energy absorbing mechanism thus significantly reducing the effects of impact loads on the DSC and the spent fuel assemblies. Also, for the postulated case of the cask sliding forward, the cask and skid may initially impact the tractor vehicle, prior to pitching onto the ground, with significant reductions in the resulting impact velocity and the energy imparted to the transfer cask and its contents.

(i) Cask/DSC Analysis Methodology

The combined transfer cask/DSC ANSYS linear elastic axisymmetric models used in the side drop and the end drop analyses as shown in Figure 8.2-9 and Figure 8.2-10, are used for the corner drop analyses. The postulated transfer cask corner drop accident results in a very complex loading function because it involves both symmetric and asymmetric load components in both the vertical and horizontal directions. The analysis involved the development of the impact force and the content loading and applying these loads to the axisymmetric model as Fourier harmonics. A complete description of the load development and application of the loads to the ANSYS models is provided in Appendix C.2.

(ii) Cask/DSC Stress Analysis

The resulting local primary membrane and primary bending stresses in the transfer cask due to both the postulated top and bottom corner drop analysis are tabulated in Table 8.2-9, Table 8.2-9a, and Table 8.2-9b for the standardized, OS197, and OS197H transfer casks, respectively. The resulting stresses in the DSC due to a cask corner drop are evaluated and found to be enveloped by those calculated for the 75g end and side drop analyses. As seen from the results, the DSC and transfer cask stress intensities are within the appropriate ASME Code Service Level D allowable limits.

(iii) Transfer Cask Collar Analysis

During the postulated oblique corner drop, the shear forces from the cask lid/DSC/collar are transferred to the cask body by the 3 inch thick shield ring of the cask collar. The tensile forces associated with the corner drop are transferred from the cask collar to the cask body by 16, 1-3/4-inch diameter bolts. The maximum calculated collar membrane stress intensity is 3.2 ksi and the maximum bolt stress is 74.3 ksi. These stresses are well within the ASME Code Service Level D allowables.

8.2.5.3 Loss of Neutron Shield

This accident conservatively postulates loss of neutron shield on the OS197 transfer cask.

8.2.5.3.1 Cause of Accident

The design basis cask drop analyses show that all components important to safety, including the transfer cask, the DSC and its internal basket assembly, maintain their structural integrity. Complete loss of solid neutron shield material is not a credible event. For this conservative generic analysis, it is assumed that the transfer cask neutron shield is breached as a result of a postulated drop accident, and the shielding effects are lost. The thermal effects of this accident are not considered for the solid neutron shield case because complete loss of solid neutron shield material is not postulated. The effect on the cask, DSC, and fuel temperature is bounded by the results of 100°F ambient case described in Section 8.1.3.3.

For the case of a liquid neutron shield, a complete loss of neutron shield was evaluated at the 100°F ambient condition with full solar load. It is conservatively assumed that the neutron shield jacket is still present but all the liquid is lost. The maximum DSC shell, cask inner shell, cask outer shell, cask neutron shield jacket temperatures are 520°F, 393°F, 384°F, and 238°F respectively. The DSC shell temperatures and hence fuel cladding temperature are bounded by the HSM plugged vent case shown in Table 8.1-26. Accident thermal conditions, such as loss of the liquid neutron shield, need not be considered in the load combination evaluation. Rather the peak stresses resulting from accident thermal conditions must be less than the allowable fatigue stress limit for 10 cycles from the appropriate fatigue design curves in Appendix I of the ASME Code. Similar analyses of other NUHOMS® transfer casks have shown that fatigue is not a concern. Therefore, these stresses in a transfer cask with a liquid neutron shield need not be evaluated for the accident condition.

8.2.5.3.2 Accident Dose Calculations for Loss of Neutron Shield

The effect of this will increase the cask surface contact dose from 552 mrem/hour to 2128 mrem/hour. The only potential off-site dose consequences would be additional direct and air scattered radiation if the accident are to occur sufficiently close to the site boundary. It is assumed that eight hours would be required to either recover the neutron shield or to add temporary shielding while arranging recovery operations. As a result, it is estimated that on-site workers at an average distance of fifteen feet would receive an additional dose rate of 310 mrem/hr.

Off-site individuals at a distance of 2000 feet would receive an additional dose of 0.04 mrem for the assumed eight hour exposure. This increase is well within the limits of 10CFR72 for an accident condition. Also, this does not preclude handling operations for recovery of the cask and its contents. Water bags or other neutron absorbing material could be wrapped around the cask to reduce the surface dose to an acceptable limit for recovery operations thus minimizing exposure of personnel in the vicinity. The actual local and off-site dose rates, recovery time and operations needed to retrieve the cask, and

the required actions to be performed following the event depend upon the severity of the event and the resultant cask and trailer/skid damage.

8.2.5.4 Recovery

For drop heights of less than fifteen inches the transfer cask will be loaded back onto the transfer skid/ trailer and moved to the HSM. The DSC will then be transferred to the HSM in the normal manner described previously. For drop heights greater than fifteen inches the transfer cask and contents will be returned to the plant's fuel/reactor building. There the DSC will be inspected for damage, and the DSC opened and the fuel removed for inspection, as necessary. Removal of the transfer cask top cover plate may require cutting of the bolts in the event of a corner drop onto the top end. This operation will take place in the decontamination pit after recovery of the transfer cask. Removal of the DSC cover plates and shield plug assembly are described in Section 5.0.

Following recovery of the transfer cask and unloading of the DSC, the transfer cask will be inspected, repaired and tested as appropriate prior to reuse.

For drop heights approaching the design basis conditions, it may be necessary to develop a special sling/lifting apparatus to move the transfer cask from the drop site to the fuel pool. This may require several weeks of planning to ensure all steps are correctly organized. During this time, additional blankets can be added to the transfer cask to minimize on-site exposure to site operations personnel. The transfer cask will be roped off to ensure the safety of the site personnel.

8.2.6 Lightning

8.2.6.1 Postulated Cause of Event

The likelihood of lightning striking the HSM and causing an off-normal condition is not considered to be a credible event. Lightning protection system requirements are site specific and depend upon the frequency of occurrences of lightning storms in the proposed ISFSI location and the degree of protection offered by other grounded structures in the proximity of the HSMs. The addition of simple lightning protection equipment, required by plant criteria, to HSM structures (i.e., grounded handrails, ladders, etc.) is considered a miscellaneous attachment and is acceptable as per Note 9 of the General Arrangement drawing (Dwg. No. NUH-03-6008).

8.2.6.2 Analysis of Effects and Consequences

Should lightning strike in the vicinity of the HSM the normal storage operations of the HSM will not be affected. The current discharged by the lightning will follow the low impedance path offered by the surrounding structures. Therefore, the HSM will not be damaged by the heat or mechanical forces generated by current passing through the

higher impedance concrete. Since the HSM requires no equipment for its continued operation, the resulting current surge from the lightning will not affect the normal operation of the HSM.

Since no off-normal condition will develop as the result of lightning striking in the vicinity of the HSM, no corrective action would be necessary. Also, there would be no radiological consequences.

### 8.2.7 Blockage of Air Inlet and Outlet Openings

This accident conservatively postulates the complete blockage of the HSM ventilation air inlet and outlet openings on the HSM side walls.

#### 8.2.7.1 Cause of Accident

Since the NUHOMS® HSMs are located outdoors, there is a remote probability that the ventilation air inlet and outlet openings could become blocked by debris from such unlikely events as floods and tornados. The NUHOMS® design features such as the perimeter security fence and the redundant protected location of the air inlet and outlet openings reduces the probability of occurrence of such an accident. Nevertheless, for this conservative generic analysis, such an accident is postulated to occur and is analyzed.

#### 8.2.7.2 Accident Analysis

The structural consequences due to the weight of the debris blocking the air inlet and outlet openings are negligible and are bounded by the HSM loads induced for a postulated tornado (Section 8.2.2) or earthquake (Section 8.2.3).

The thermal effects of this accident result from the increased temperatures of the DSC and the HSM due to blockage of the ventilation air inlet and outlet openings. The heat generated in the DSC is conservatively assumed to be contained entirely within the DSC and HSM throughout this postulated accident. The spacing of the adjacent HSMs is assumed to be unaffected and the HSM front and roof birdscreens are assumed to be open to ambient. The accident duration is assumed to be five days, at which time the air inlet and outlet opening obstructions would be cleared by site personnel and natural circulation air flow restored to the HSM.

Based on previous NUHOMS® system design experience, it is concluded that heat-up of the spent fuel, DSC and HSM are limited by the heat up of the HSM. The spent fuel assemblies and the DSC quickly rise in temperature to the level required to radiate and conduct the 24 kW of decay heat to the HSM internal surfaces. However, the HSM surface heat up is limited by the heat up of the entire HSM. Because the heat up rate of the HSM is much lower than that of the DSC, or the spent fuel, the DSC can be assumed to be at steady state at any instant in time and transferring 24 kW of heat to the HSM. The HSM internal surface

temperatures are limited by the heat up of the total quantity of concrete behind the surface. Therefore, applying a constant heat flux to the HSM concrete and calculating the time dependent temperature distributions through the concrete, the surface temperature of the concrete as a function of time is obtained. Using the calculated HSM surface temperatures, the maximum DSC and fuel cladding temperatures are determined.

A thermal transient analysis of the HSM for the blocked vent condition is performed using a control volume model of the HSM internal air space and the surrounding concrete walls, roof, and floor. The first law of thermodynamics is used to obtain an energy balance equation that is solved using a forward finite differencing scheme with a sufficiently small time step to ensure the accuracy of the solution. The initial conditions for the analysis correspond to the steady state temperatures calculated for the off-normal analysis cases with an ambient temperature of 125°F. The heat source included in the analysis is the 24 kW decay heat rejected from the surface of the DSC. Technical Specification 1.3.1 of CoC 1004, permits blockage of all vents for a period of 40 hours. At the end of 40 hours, it is assumed that corrective actions would be completed and natural circulation air flow restored to the HSM. However, to be conservative, the solution is carried out to five days. The change in temperature with time after vent opening blockage for the HSM roof interior surface is shown in Figure 8.2-16.

At the end of the five days, the maximum HSM inside surface is 479°F. The concrete temperature transient results are used to calculate the DSC shell transient temperatures. The same model of the DSC in HSM cases described in Section 8.1.3 is used. All the convection boundary conditions on the interior of HSM are deleted to simulate complete blockage of all inlet and outlet vents. The conductivity of the basket material is conservatively assumed to be that of fuel. The effective density and specific heat of the homogenized basket material and fuel are used. The maximum DSC surface temperature is 640°F at the end of 40 hours in the blocked vent transient. Using the HEATING7 models of the DSC and its internals described in Section 8.1.3, the maximum fuel cladding temperatures for this case are calculated to be 871°F (466°C) for the PWR fuel and 905°F (485°C) for the BWR fuel. The fuel clad temperature at the start of the blocked vent transient for the 125°F extreme ambient temperature case are calculated to be less than 720°F (382°C) for the PWR fuel and 743°F (395°C) for the BWR fuel. The maximum fuel clad temperature as a function of time is expected to vary linearly between these two temperature values. The resulting temperatures are well below the fuel cladding short term temperature limit of 570°C.

These temperatures are below the levels that safety impairing damage would occur to the HSM or DSC. ACI 349 (8.20) imposes a maximum upper limit of 350°F for concrete temperatures for accident or other short term conditions. As shown in Figure 8.2-16, the HSM concrete temperatures exceed 350°F sometime after 40 hours for a blocked vent transient. Hence, the NUHOMS® Technical Specification 1.3.1 requires a daily inspection of the HSM air inlets and outlets. The short time exposure of the DSC and the spent fuel assemblies to the elevated temperatures will not cause any damage or result in the release of radioactivity. The maximum DSC internal pressure during this event is 12.1 psig for the PWR fuel and 10.0 psig for the BWR fuel (assuming that no fission and fill gas is released).

If the fission and fill gases are released from 100% of the spent fuel rods from all assemblies, the DSC internal pressures would be 58.7 psig (PWR) and 31.1 psig (BWR) as shown in Tables 8.1-6 and 8.1-7, assuming the 30% of fission gases and 100% of fuel rod fill gas is released. The design basis pressure considered for this accident analysis of the DSC is 60 psig.

The thermal-induced stresses for the blocked vent case are calculated using the HSM structural models shown in Figure 8.1-23 and 8.1-24 as discussed in Section 8.1.1.5, paragraphs C and E. The resulting elastic forces and moments are modified to account for the concrete cracked section properties in accordance with ACI 349 Appendix A, and combined with the calculated forces and moments from other loads.

8.2.7.3 Accident Dose Calculations

There are no off-site dose consequences as a result of this accident. The only significant dose increase is that related to the recovery operation where it is conservatively estimated that the on-site workers will receive an additional dose of no more than one man-rem during the eight hour period it is estimated may be required for removal of the debris from the air inlet and outlet openings in HSM.

8.2.7.4 Recovery

Debris removal is all that is required to recover from a postulated blockage of the HSM ventilation air inlets and outlets. Cooling will begin immediately following removal of the debris from the inlets and outlets. The amount and nature of debris can vary, but even in the most extreme case, manual means or readily available equipment can be used to remove debris.

The debris is conservatively assumed to remain in place for 40 hours as described in Section 8.2.7.2. The last eight hours of this period are assumed to be the time required to completely remove all debris and the natural circulation air flow to be restored.

8.2.8 DSC Leakage

The DSC shell is designed as a pressure retaining containment boundary to prevent leakage of contaminated materials, as discussed in Section 8.1.1.1, paragraph B. The analyses of normal, off-normal, and accident conditions have shown that no credible conditions can breach the DSC shell or fail the double seal welds at each end of the DSC. However, for this conservative generic evaluation, a total and complete instantaneous leak from the DSC is postulated.

This event postulates an instantaneous release directly to the environment of 30% of all fission gasses contained in all the spent fuel rods in each fuel assembly. This accident

conservatively assumes that all spent fuel rods are ruptured and that concurrent DSC leakage occurs. All other components of the NUHOMS® system remain intact.

8.2.8.1 Cause of Accident

There is no credible event that could result in the rupture of any spent fuel rods concurrent with leakage from the DSC due to the passive nature of the NUHOMS® system, and the various design features that ensure that the integrity of the DSC shell containment pressure boundary and spent fuel cladding are maintained. Nevertheless, for this conservative generic evaluation of the NUHOMS® system, this accident assumes that the spent fuel rods and the DSC are ruptured due to an event of unspecified origin.

8.2.8.2 Accident Analysis

There are no structural or thermal consequences resulting from the DSC leakage accident described above. The radiological consequences of this accident are described in Section 8.2.8.3.

8.2.8.3 Accident Dose Calculations

The postulated accident assumes that one DSC is ruptured and that all the spent fuel rod cladding fails simultaneously such that the fission gasses in the spent fuel assemblies including 30% of the Kr-85, 10% of the noble gases other than Kr-85 (primarily H-3), and 10% of the radioactive iodine are instantaneously released to the atmosphere. The whole body dose and skin dose at 1000 feet from the storage site under the worst meteorological conditions were calculated and are listed in Table 8.2-10. From this table it is seen that the resultant accident dose is well within the 10CFR72.106 limit, which restricts the maximum whole body or organ dose beyond the owner controlled area from any design basis accident to be less than five rem. Doses (on-site and off site) must be assessed on a site specific basis by the licensee. Table 8.2-10 shows that typical site boundary doses are below the 10CFR72 limits.

8.2.9 Accident Pressurization of DSC

This accident addresses the consequences of accidental pressurization of the DSC.

8.2.9.1 Accident Analysis

The bounding internal pressurization of the DSC for this conservative generic evaluation is postulated to result from cladding failure of the spent fuel, and the consequent release of spent fuel rod fill gas and free fission gas. Fission gas release fractions are not so easily estimated however. A recent report on ISFSI facility evaluations (8.43) uses a release fraction of 8% as a nominal case and 30% as an upper bound.

For design purposes, and as a means of providing over pressure protection for the DSC, it is conservatively assumed that all fuel rods in the DSC suffer cladding failure, as discussed in Section 8.1.1.1, paragraph B. It is further assumed that the fission gas release fraction is 30%. For the PWR (BWR: noted parenthetically) DSC, this results in release of 13,050 $in.^3$ (BWR: 4,700 $in.^3$) of fission gas per assembly (interpolated from the data provided in Reference 8.42) The limiting postulated accident for DSC pressurization is the HSM blocked vent condition for 5 days. As shown in Table 8.1-6 (BWR: Table 8.1-7) the maximum DSC internal pressure with the fission and fill gas release is 58.7 psig (BWR: 31.1 psig). The stress analysis of the DSC shell assembly for an internal pressure of 60.0 psig is described in Section 8.1.1.1.

Maximum 24P DSC internal pressure for accident conditions when storing fuel with BPRAs is presented in Appendix J.

8.2.9.2 Accident Dose Calculations

There are no dose consequences as the result of the accidental pressurization of the DSC.

8.2.10 Load Combinations

The load categories associated with normal operating conditions, off-normal conditions and postulated accident conditions are described and analyzed in previous sections. The load combination results for the NUHOMS® components important to safety are presented in this section. Fatigue effects on the transfer cask and the DSC are also addressed in this section.

8.2.10.1 DSC Load Combination Evaluation

As described in Section 3.2, the stress intensities in the DSC at various critical locations for the appropriate normal operating condition loads are combined with the stress intensities experienced by the DSC during postulated accident conditions. It is assumed that only one postulated accident event occurs at any one time. The DSC load combinations summarized in Table 3.2-6 are expanded in Table 8.2-24. Since the postulated cask drop accidents are by far the most critical, the load combinations for these events envelope all other accident event combinations. Table 8.2-11 through Table 8.2-16 tabulate the maximum stress intensity for each component of the DSC calculated for the enveloping normal operating, off-normal, and accident load combinations. For comparison the appropriate ASME Code allowables are also presented in these tables.

8.2.10.2 DSC Fatigue Evaluation

Table 8.2-11 through Table 8.2-16 present the calculated enveloping normal, off-normal and accident stress intensities for the DSC components. Fatigue effects on the DSC are addressed using the criteria contained in NB-3222.4 of the ASME Code (Reference 8.3).

Fatigue effects need not be specifically evaluated provided the six criteria contained in NB-3222.4(a) are met. As demonstrated in Appendix C.4.1, an evaluation using these six criteria is performed to show that the ASME Code fatigue requirements are satisfied for the DSC.

8.2.10.3 Transfer Cask Load Combination Evaluation

As described in Section 3.2, the transfer cask calculated stresses due to normal operating loads are combined with the appropriate calculated stresses from postulated accident conditions at critical stress locations. It is assumed that only one postulated accident can occur at a time. Also, since the postulated drop accidents produce the highest calculated stresses, the load combination of dead load plus drop accident envelopes the stresses induced by other postulated accident scenarios. The maximum calculated stress intensities for the transfer cask normal operating, off-normal, and accident load combinations are tabulated in Table 8.2-21 through Table 8.2-23b.

Fatigue effects on the transfer cask are addressed using the criteria provided in NC-3219.2 of the ASME Code (Reference 8.3). As described in Appendix C.4.2, the code specified criteria given in this section are evaluated relative to the transfer cask to demonstrate that fatigue requirements are satisfied.

8.2.10.4 HSM Load Combination Evaluation

The maximum bending moments and shear forces induced in the HSM for the individual normal and off-normal loads are listed in Table 8.1-19. Similarly, the maximum moments and shears induced in the HSM for the individual accident loads are listed in Table 8.2-3. As described in Section 3.2.5.1, the load combination procedure of Section 6.17.3.1 of ANSI 57.9 (8.2) is used to combine the factored normal operation, off normal, and postulated accident loadings imposed on the reinforced concrete HSM. Many of the general event combinations, shown in Table 3.2-5, are enveloped by others that contain the same load factors with additional applied load cases.

The governing calculated bending moments and shears for each load combination are tabulated in Table 8.2-18. The tabulated results represent the bounding shears and moments for either the single free-standing HSM or an array of HSMs. For comparison, the ultimate moment and shear capacity of the HSM for the controlling load combinations are also shown in Table 8.2-18. Comparison of the reported bending moment and shear for each load combination with the corresponding ultimate capacity shows that the design strength of the HSM is greater than the strength required for the most critical load combination.

8.2.10.5 Thermal Cycling of the HSM

As stated earlier, the largest mean daily change of temperature in the United States of 45°F occurs in Reno, Nevada. Because of the massive concrete sections used in the HSM

a period of approximately one week is needed to obtain steady temperatures and a steady state thermal gradient. For conservatism it is assumed that the 45°F maximum daily change could produce a steady state gradient every day for 50 years, for a total of 18250 thermal cycles. The maximum moment caused by the worst case steady state normal operating thermal loads is 284 k-in. This loading is 31% of the minimum ultimate strength. Assuming this load amplitude is cycled daily, and referring to the S-N curve of Figure 6-46 of reference 8.22, the number of cycles before failure that occur is greater than 10,000,000. Since this value is far greater than the postulated worst case 18,250 cycles, thermal cycling has a negligible effect on the HSM reinforced concrete.

8.2.10.6 DSC Support Structure Load Combination Evaluation

The applicable loads for the DSC support structure inside the HSM include the DSC and support assembly dead weight, seismic loads, and DSC handling loads. Three load combinations are evaluated. Load Combination one consists of the DSC plus the support structure dead weight, plus the DSC handling loads for a typical normal operating load case.. Load Combination two includes the dead weight of the support structure plus DSC handling loads in the jammed condition representing an off-normal loading. The third load combination includes the total dead weight plus design basis seismic loads for an accident event. The resulting maximum stresses are compared to AISC code allowables are shown in Table 8.2-19.

The same load combinations are used for the DSC support structure connecting elements. The maximum support loads for the design basis load combinations are shown in Table 8.2-20. All end connection components are designed to meet the AISC Code requirements for these design loads. The structural steel design is based on the requirements of the AISC code, and the embedments are designed in accordance with the requirements of ACI 349-85.

**Table 8.2-1 __**
**Postulated Accident Loading Identification**

| Accident Load Type | Section Reference | NUHOMS® Component Affected | | | | |
|---|---|---|---|---|---|---|
| | | DSC Shell Assembly | DSC Internal Basket | DSC Support Structure | HSM | On-Site Transfer Cask |
| Loss of Adjacent HSM Shielding Effects | 8.2.1 | (radiological consequence only) | | | | |
| Tornado Wind | 8.2.2 | | | | X | X |
| Tornado Missiles | 8.2.2 | | | | X | X |
| Earthquake | 8.2.3 | X | X | X | X | X |
| Flood | 8.2.4 | X | | | X | |
| Accident Cask Drop | 8.2.5 | X | X | | | X |
| Loss of Cask Neutron Shield | 8.2.5 | | | | | X |
| Lightning | 8.2.6 | | | | X | |
| Blockage of HSM Air Inlets and Outlets | 8.2.7 | X | X | X | X | |
| DSC Leakage | 8.2.8 | (radiological consequence only) | | | | |
| DSC Accident Internal Pressure | 8.2.9 | X | | | | |
| Load Combinations | 8.2.10 | X | X | X | X | X |

**Table 8.2-2**
**Comparison of Total Dose Rates for HSM with and without Adjacent HSM Shielding Effects**

| Distance (meters) from Nearest HSM Wall, 2x10 Array | Normal Case Dose Rate[1] (mrem/hr) | Accident Case Dose Rate[1] (mrem/hr) |
|---|---|---|
| 10 | 9.0 | 18 |
| 100 | 0.2 | 0.4 |
| 500 | $2.1 \times 10^{-3}$ | $4.2 \times 10^{-3}$ |
| 1000 | $1.5 \times 10^{-4}$ | $3.0 \times 10^{-4}$ |

(1) Air scattered plus direct radiation.

**Table 8.2-3**
**Maximum HSM Reinforced Concrete Bending Moments and Shear Force for Accident Loads**

| Structural Section | Force[5] Component | HSM Internal Forces (kip/ft., in.-k/ft.)[1] | | | | |
|---|---|---|---|---|---|---|
| | | Tornado Winds | Tornado[3] Missile | Seismic | Flooding | Blocked Vents Thermal[2] |
| Floor Slab | Shear | 3.54 | 8.68 | 1.15 | 3.31 | 2.74 |
| | Moment | 21.98 | 54.11 | 6.63 | 23.08 | 36.7 |
| Side Wall | Shear | 8.72 | 25.0[4] | 7.74 | 9.53 | 8.,64 |
| | Moment | 68.85 | 118.48 | 15.89 | 65.95 | 266.3 |
| Front Wall | Shear | 2.45 | 38.21 | 15.53 | 2.15 | 17.87 |
| | Moment | 74.16 | 644.65 | 36.67 | 55.03 | 485.84 |
| Rear Wall | Shear | 1.61 | 11.14 | 1.41 | 0.81 | 8.65 |
| | Moment | 15.17 | 36.06 | 5.01 | 13.34 | 169.8 |
| Roof Slab | Shear | 2.40 | 35.05 | 0.93 | 0.96 | 3.22 |
| | Moment | 54.89 | 521.51 | 6.02 | 48.09 | 305.8 |

(1) Maximum loads shown are irrespective of location.

(2) Maximum moments are calculated using cracked section properties.

(3) The maximum shear on the HSM rear shield wall for the DBT missile is 487.5 kips. The shield wall capacity for punching shear is calculated based on ACI-349 Section 11.11.2.1, and is 1598 kips.

(4) The maximum shear due to tornado missile is the maximum stress d/2 from the back wall inner face.

(5) Out-of-plane shears and moments.

**Table 8.2-4**

**Deleted**

**Table 8.2-5**

**Deleted**

**Table 8.2-6**

**Deleted**

**Table 8.2-7**
**Maximum NUHOMS®-24P DSC Stresses for Drop Accident Loads**

| DSC Components | Stress Type | Calculated Stress (ksi) [3] | |
|---|---|---|---|
| | | Vertical | Horizontal |
| DSC Shell | Primary Membrane | 10.29 | 28.92 |
| | Membrane + Bending | 25.17 | 46.17 |
| Inner Top Cover Plate | Primary Membrane | 1.57 | 33.70 |
| | Membrane + Bending | 1.86 | 51.83 |
| Outer Top Cover Plate | Primary Membrane | 1.57 | 36.51 |
| | Membrane + Bending | 2.19 | 51.90 |
| Inner Bottom Cover Plate | Primary Membrane | 7.59 | 39.40 |
| | Membrane + Bending | 25.70 | 40.50 |
| Outer Bottom Cover Plate | Primary Membrane | 1.57 | 23.86 |
| | Membrane + Bending | 2.27 | 34.71 |
| Spacer Disks | Primary Membrane | 2.80 | 45.59 |
| | Local Membrane | N/A | 61.02 |
| | Membrane + Bending | 49.61 | 61.02 |
| Support Rods | Compression + Bending Stress Interaction Ratio[3] | 0.94 | N/A |
| | Bending Stress | N/A | 5.38 |
| Guide Sleeves | Axial<br>Bending | 3.47<br>N/A | N/A<br>16.00 |
| Top Cover Plate Weld[4] | Primary | 0.97 | 25.26 |
| Bottom Cover Plate Weld[4] | Primary | 10.67 | 12.58 |

(1) Values shown are maximums irrespective of location.
(2) DSC was also included in corner drop analysis for cask, however, stresses for above cases are enveloping.
(3) For vertical drop case, axial plus bending stress interaction ratio is given for the support rods.
(4) Envelope of inner and outer cover plate weld. Stress values include 10 psig internal pressure

**Table 8.2-8**
**Maximum NUHOMS®-52B DSC Stresses for Drop Accident Loads**

| DSC Components | Stress Type | Calculated Stress (ksi) | |
|---|---|---|---|
| | | Vertical | Horizontal |
| DSC Shell | Primary Membrane | 10.0 | 28.92 |
| | Membrane + Bending | 23.64 | 43.29 |
| Inner Top Cover Plate | Primary Membrane | 1.27 | 33.70 |
| | Membrane + Bending | 1.85 | 51.83 |
| Outer Top Cover Plate | Primary Membrane | 1.27 | 36.51 |
| | Membrane + Bending | 2.16 | 51.90 |
| Inner Bottom Cover Plate | Primary Membrane | 7.10 | 39.40 |
| | Membrane + Bending | 25.34 | 40.50 |
| Outer Bottom Cover Plate | Primary Membrane | 1.27 | 23.86 |
| | Membrane + Bending | 2.35 | 34.71 |
| Spacer Disks | Primary Membrane | 16.3 | 39.80 |
| | Local Membrane | N/A | 54.50 |
| | Membrane + Bending | 61.4 | 60.6 |
| Support Rods | Axial | 23.3 | 32.60 |
| | Bending | 27.87 | 8.18 |
| Spacer Sleeves | Axial<br>Bending | 26.68<br>59.0 | 5.79<br>3.00 |
| Neutron Absorber Plates | Axial<br>Bending | 3.48(3)<br>N/A | N/A<br>57.98 |
| Top Cover Plate Weld(4) | Primary | 0.91 | 25.26 |
| Bottom Cover Plate Weld(4) | Primary | 10.44 | 12.58 |

(1) Values shown are maximums irrespective of location.
(2) DSC was also included in corner drop analysis for cask, however, stresses for above cases are enveloping.
(3) The factor of safety against buckling is 1.32.
(4) Envelope of inner and outer cover plate weld. Stress values include 10 psig internal pressure

**Table 8.2-9**
**Maximum Standardized Transfer Cask Stresses for Drop Accident Loads**

| Transfer Cask Components | Stress Type | Stress (ksi)[1] | | |
|---|---|---|---|---|
| | | Vertical | Horizontal | Corner[2] |
| Cylindrical Structural Shell | Primary Membrane | 9.6 | 3.8 | 5.1 |
| | Membrane + Bending | 10.2 | 15.5 | 15.3 |
| Top Cover Plate | Primary Membrane | 25.2 | 5.8 | 3.0 |
| | Membrane + Bending | 25.2 | 5.8 | 15.5 |
| Bottom End Plate | Primary Membrane | 26.1 | 5.8 | 0.0 |
| | Membrane + Bending | 26.1 | 5.8 | 36.4 |
| Transfer Cask Collar | Primary Membrane | 26.2 | 12.2 | 2.3 |
| | Membrane + Bending | 26.2 | 12.2 | 3.2 |

(1) Values shown are maximums irrespective of location

(2) DSC was also included in corner drop analysis. DSC stresses for this case are enveloped by those for horizontal and vertical drop loads shown in Tables 8.2-7 and 8.2-8.

**Table 8.2-9a**
**Maximum OS197 Transfer Cask Stresses for Drop Accident Loads**

| Transfer Cask Components | Stress Type | Stress (ksi)[1] | | |
|---|---|---|---|---|
| | | Vertical | Horizontal | Corner[2] |
| Cylindrical Structural Shell | Primary Membrane | 9.6 | 33.4 | 6.3 |
| | Membrane + Bending | 9.6 | 39.9 | 19.1 |
| Top Cover Plate | Primary Membrane | 28.6 | 6.9 | 3.7 |
| | Membrane + Bending | 28.6 | 6.9 | 19.4 |
| Bottom End Plate | Primary Membrane | 27.0 | 6.9 | 0.0 |
| | Membrane + Bending | 27.0 | 6.9 | 45.5 |

(1) Values shown are maximums irrespective of location

(2) DSC was also included in corner drop analysis. DSC stresses for this case are enveloped by those for horizontal and vertical drop loads shown in Tables 8.2-7 and 8.2-8.

**Table 8.2-9b**
**Maximum OS197H Transfer Cask Stresses for Drop Accident Loads**

| Transfer Cask Components | Stress Type | Stress (ksi)[1] | | |
|---|---|---|---|---|
| | | Vertical | Horizontal | Corner[2] |
| Cylindrical Structural Shell | Primary Membrane | 9.6 | 43.1 | 8.1 |
| | Membrane + Bending | 9.6 | 51.5 | 24.7 |
| Top Cover Plate | Primary Membrane | 36.8 | 8.8 | 4.8 |
| | Membrane + Bending | 36.8 | 8.8 | 24.9 |
| Bottom End Plate | Primary Membrane | 34.8 | 8.8 | 0.0 |
| | Membrane + Bending | 34.8 | 8.8 | 58.6 |

(1) Values shown are maximums irrespective of location.

(2) DSC was also included in corner drop analysis. DSC stresses for this case are enveloped by those for horizontal and vertical drop loads shown in Tables 8.2-7 and 8.2-8.

**Table 8.2-10**
**Dose at 300m from ISFSI Site Due to Release from Postulated DSC Rupture**

| Dose Type | X /Q[(1)] (Sec./m$^3$) | Dose (Rem) |
|---|---|---|
| Whole Body | 5.0E-3 | 0.22 |
| Skin | 5.0E-3 | 6.7 |

(1) Taken from Reg. Guide 1.4 Ground Level Release Data.

**Table 8.2-11**
**NUHOMS®-24P DSC Enveloping Load Combination Results for Normal and Off-Normal Loads (ASME Service Levels A and B)**

| DSC Components | Stress Type | Controlling Load Combination [1] | Stress (ksi) | |
|---|---|---|---|---|
| | | | Calculated | Allowable [2] |
| DSC Shell | Primary Membrane | UL-5, UL-6 | 15.18 | 18.7 |
| | Membrane + Bending | LD-2 | 21.27 | 26.3 |
| | Primary + Secondary | LD-1 | 43.06 | 54.3 |
| Inner Bottom Cover Plate | Primary Membrane | LD-2 | 16.64 | 19.3 |
| | Membrane + Bending | LD-2 | 27.14 | 29.0 |
| | Primary + Secondary | LD-1 | 35.30 | 54.3 |
| Outer Bottom Cover Plate | Primary Membrane | UL-5, UL-6 | 13.81 | 18.7 |
| | Membrane + Bending | UL-5, UL-6 | 25.37 | 28.1 |
| | Primary + Secondary | LD-1 | 35.61 | 54.3 |
| Inner Top Cover Plate | Primary Membrane | TR-5 | 3.52 | 17.5 |
| | Membrane + Bending | DD-2 | 12.07 | 26.3 |
| | Primary + Secondary | TR-4 | 31.64 | 54.3 |
| Outer Top Cover Plate | Primary Membrane | TR-7 | 4.66 | 17.5 |
| | Membrane + Bending | TR-7 | 11.46 | 26.3 |
| | Primary + Secondary | TR-3 | 27.66 | 54.3 |
| Spacer Disk | Primary Membrane | TR-2, TR-6 | 8.84 | 18.7 |
| | Membrane + Bending | TR-1, TR-5 | 12.43 | 28.05 |
| | Primary + Secondary | DD-2 | 63.25 | Note (5) |

See Table 8.2-17 for notes.

**Table 8.2-12**
**NUHOMS®-52B DSC Enveloping Load Combination Results for Normal and Off-Normal Loads (ASME Service Levels A and B)**

| DSC Components | Stress Type | Controlling Load Combination [1] | Stress (ksi) | |
|---|---|---|---|---|
| | | | Calculated | Allowable [2] |
| DSC Shell | Primary Membrane | UL-5, UL-6 | 15.13 | 19.3 |
| | Membrane + Bending | LD-2 | 20.43 | 26.3 |
| | Primary + Secondary | LD-1 | 42.03 | 54.3 |
| Inner Bottom Cover Plate | Primary Membrane | LD-2 | 14.71 | 17.5 |
| | Membrane + Bending | LD-2 | 23.98 | 26.3 |
| | Primary + Secondary | LD-1 | 34.90 | 54.3 |
| Outer Bottom Cover Plate | Primary Membrane | UL-5, UL-6 | 13.77 | 19.3 |
| | Membrane + Bending | UL-5, UL-6 | 25.30 | 29.0 |
| | Primary + Secondary | LD-1 | 34.29 | 54.3 |
| Inner Top Cover Plate | Primary Membrane | TR-5 | 3.11 | 17.5 |
| | Membrane + Bending | DD-2 | 12.07 | 26.3 |
| | Primary + Secondary | TR-3 | 33.39 | 54.3 |
| Outer Top Cover Plate | Primary Membrane | TR-7 | 4.45 | 17.5 |
| | Membrane + Bending | TR-7 | 10.75 | 26.3 |
| | Primary + Secondary | TR-3 | 28.44 | 54.3 |
| Spacer Disk | Primary Membrane | TR-1, TR-5 | 14.2 | 18.7 |
| | Membrane + Bending | TR-4, TR-8 | 25.9 | 28.1 |
| | Primary + Secondary | DD-2 | 83.6 | Note 5 |

See Table 8.2-17 for notes.

**Table 8.2-13**
**NUHOMS®-24P DSC Enveloping Load Combination Results for Accident Loads (ASME Service Level C)**

| DSC Components | Stress Type | Controlling Load Combination [1] | Stress (ksi) | |
|---|---|---|---|---|
| | | | Calculated | Allowable[2] |
| DSC Shell | Primary Membrane | UL-7[7] | 20.81 | 22.4 |
| | Membrane + Bending | UL-7[7] | 29.80 | 33.7 |
| Inner Bottom Cover Plate | Primary Membrane | UL-7[7] | 12.59 | 22.4 |
| | Membrane + Bending | UL-7[7] | 16.63 | 33.7 |
| Outer Bottom Cover Plate | Primary Membrane | UL-7[7] | 19.25 | 22.4 |
| | Membrane + Bending | UL-7[7] | 34.23 | 35.0 |
| Inner Top Cover Plate | Primary Membrane | HSM-8 | 7.85 | 21.7 |
| | Membrane + Bending | HSM-4[7] | 18.12 | 32.6 |
| Outer Top Cover Plate | Primary Membrane | HSM-8 | 7.97 | 21.7 |
| | Membrane + Bending | HSM-4[7] | 30.41 | 32.6 |
| Spacer Disk | Primary Membrane | | Note 6 | Note 6 |
| | Membrane + Bending | | Note 6 | Note 6 |

See Table 8.2.17 for notes.

**Table 8.2-14**
**NUHOMS®-52B DSC Enveloping Load Combination Results for Accident Loads (ASME Service Level C)**

| DSC Components | Stress Type | Controlling Load Combination [1] | Stress (ksi) | |
|---|---|---|---|---|
| | | | Calculated | Allowable [2] |
| DSC Shell | Primary Membrane | UL-7[7] | 20.81 | 23.2 |
| | Membrane + Bending | UL-7[7] | 29.87 | 34.8 |
| Inner Bottom Cover Plate | Primary Membrane | UL-7[7] | 12.59 | 23.2 |
| | Membrane + Bending | UL-7[7] | 16.74 | 34.8 |
| Outer Bottom Cover Plate | Primary Membrane | UL-7[7] | 19.25 | 23.2 |
| | Membrane + Bending | UL-7[7] | 34.21 | 36.0 |
| Inner Top Cover Plate | Primary Membrane | HSM-8 | 6.57 | 22.4 |
| | Membrane + Bending | HSM-4[7] | 18.12 | 33.7 |
| Outer Top Cover Plate | Primary Membrane | HSM-4[7] | 7.60 | 22.4 |
| | Membrane + Bending | HSM-4[7] | 30.41 | 33.7 |
| Spacer Disk | Primary Membrane | HSM-7<br>HSM-8 | 14.3 | 28.1 |
| | Membrane + Bending | HSM-7<br>HSM-8 | 31.1 | 42.2 |

See Table 8.2.17 for notes.

**Table 8.2-15**
**NUHOMS®-24P DSC Enveloping Load Combination Results for Accident Loads (ASME Service Level D)[3]**

| DSC Components | Stress Types | Controlling Load Combination [1] | Stress (ksi) | |
|---|---|---|---|---|
| | | | Calculated | Allowable[2] |
| DSC Shell | Primary Membrane | TR-11 | 32.4 | 44.5 |
| | Membrane + Bending | TR-11 | 49.7 | 57.2 |
| Inner Bottom Cover Plate | Primary Membrane | TR-11 | 39.40 | 44.5 |
| | Membrane + Bending | TR-11 | 40.50 | 57.2 |
| Outer Bottom Cover Plate | Primary Membrane | TR-11 | 23.86 | 44.5 |
| | Membrane + Bending | UL-8 | 57.0 | 59.0 |
| Inner Top Cover Plate | Primary Membrane | TR-11 | 33.70 | 44.5 |
| | Membrane + Bending | TR-11 | 51.83 | 57.2 |
| Outer Top Cover Plate | Primary Membrane | TR-11 | 36.51 | 44.5 |
| | Membrane + Bending | HSM-6 | 55.2 | 59.0 |
| Spacer Disk | Primary Membrane | TR-11 | 45.59 | 49.0 |
| | Local Membrane | TR-11 | 61.02 | 63.0 |
| | Membrane + Bending | TR-11 | 58.98 | 63.0 |
| Support Rods[4] | Axial/Bending Stress Interaction Ratio | TR-9, TR-10 | 0.94 | 1.0 |
| Guide Sleeves | Shear + Bending Stress | TR-11 | 16.0 | 38.9 |
| Top Cover Plate Welds | Primary | TR-11 | 25.26 | 26.7 |
| Bottom Cover Plate Welds | Primary | TR-11 | 12.58 | 26.7 |

See Table 8.2-17 for notes.

**Table 8.2-16**
**NUHOMS®-52B DSC Enveloping Load Combination Results for Accident Loads (ASME Service Level D) [3]**

| DSC Components | Stress Types | Controlling Load Combination [1] | Stress (ksi) | |
|---|---|---|---|---|
| | | | Calculated | Allowable[2] |
| DSC Shell | Primary Membrane | TR-11 | 32.4 | 44.5 |
| | Membrane + Bending | TR-11 | 46.8 | 57.2 |
| Inner Bottom Cover Plate | Primary Membrane | TR-11 | 39.40 | 44.5 |
| | Membrane + Bending | TR-11 | 40.50 | 57.2 |
| Outer Bottom Cover Plate | Primary Membrane | TR-11 | 23.86 | 44.5 |
| | Membrane + Bending | UL-8 | 57.0 | 59.0 |
| Inner Top Cover Plate | Primary Membrane | TR-11 | 33.70 | 44.5 |
| | Membrane + Bending | TR-11 | 51.83 | 57.2 |
| Outer Top Cover Plate | Primary Membrane | TR-11 | 36.51 | 44.5 |
| | Membrane + Bending | HSM-6 | 55.2 | 59.0 |
| Spacer Disk | Primary Membrane | TR-11 | 39.8 | 49.0 |
| | Membrane + Bending | TR-11 | 60.6 | 63.0 |
| Support Rods[4] | Axial +Bending Stress Interaction Ratio | TR-9, TR-10 | 0.43 | 1.0 |
| Spacer Sleeves[4] | Axial +Bending Stress Interaction Ratio | TR-9, TR-10 | 0.78 | 1.0 |
| Neutron Absorber Plates | Membrane + Bending | TR-11 | 57.98 | 59.0 |
| Top Cover Plate Welds | Primary | TR-11 | 25.26 | 26.7 |
| Bottom Cover Plate Welds | Primary | TR-11 | 12.58 | 26.7 |

See Table 8.2-17 for notes.

**Table 8.2-17**
**DSC Enveloping Load Combination Table Notes**

(1) See Table 3.2-6 and 8.2-24 for load combination nomenclature.

(2) See Table 3.2-9 for allowable stress criteria. Material properties were obtained from Table 8.1-3 at a design temperature of 500°F or as noted in the supporting calculations.

(3) In accordance with the ASME Code, thermal stresses need not be included in Service Level D load combinations.

(4) Compressive stress allowable of the support rods and spacer sleeves is based upon the criteria specified in Subsection NF and Appendix F of the ASME Code.

(5) Evaluated per ASME NB-3228.5 for components with stresses greater than $3.0S_m$.

(6) Service Level C load conditions are not explicitly evaluated for the 24P spacer disks. The seismic loads for the spacer disks are bounded by the handling loads which are evaluated to Level A/B criteria.

(7) Includes a conservative internal pressure of 41 psig. Actual pressure is less than 11 psig for the 24P DSC and less than 10 psig for the 52B DSC.

**Table 8.2-18**
**HSM Enveloping Load Combination Results**

| Load[1] Combination | Loading Combination Description | Governing Load[2][5] | | Capacities | |
|---|---|---|---|---|---|
| | | $V_{max}$ (k/ft.) | $M_{max}$ (k-in./ft.) | $V_c$ (k/ft.)[4] | $M_u$ (k-in./ft.) |
| 1 | 1.4D + 1.7L | 19.09 | 214.96 | 40.5 | 881.00 |
| 2 | 1.4D + 1.7L + 1.7H | 19.09 | 214.96 | 40.5 | 881.00 |
| 3 | 0.75(1.4D + 1.7L + 1.7H + 1.7T + 1.7W) | 16.61 | 355.00 | 22.90 | 881.00 |
| 4 | 0.75(1.4D + 1.7L + 1.7H + 1.7T) | 22.53 | 304.00 | 40.50 | 881.00 |
| 5 | D + L + H + T + E | 27.53 | 347.77 | 40.50 | 881.00 |
| 6 | D + L + H + T + F | 9.67 | 148.57 | 22.90 | 881.00 |
| 7[6] | D + L + H + $T_a$[3] | 28.93 | 533.00 | 38.40 | 788.00 |
| 8 | D + L + H + T + WT | 42.73 | 681.63 | 44.00 | 881.00 |

D = Dead Weight
F = Flood Induced Loads
L = Live Load
$T_a$ = Off-normal or Accident Condition Thermal Load
WT = Tornado Wind and Missile Load
E = Earthquake Load
H = Lateral Soil Pressure Load,
T = Normal Condition Thermal Load
W = Design Basis Wind Load

(1) Load combinations are based on ANSI-57.9 as shown in Table 3.2-5.

(2) Loads reported have minimum margin to design capacity.

(3) Thermal accident load ($T_a$) is based on -40°F ambient with air inlets and outlets blocked (See Section 8.1.2.2) for either 40 hours or 5 days (Results of these two blocked vent cases are enveloped).

(4) The shear capacity $V_c$ is calculated using Equation 11-3 of ACI 349-85.

(5) Results of load combinations 3 through 7 are based on cracked section. Others based on uncracked sections.

(6) Material properties taken at 479°F for load combination 7.

**Table 8.2-19**
**DSC Support Structure Enveloping Load Combination Results**

| Component | Load Combination | Calculated Stress | | | | Interaction (Calc/ Allowable) | Allowable Shear Stress (ksi) |
|---|---|---|---|---|---|---|---|
| | | Axial (ksi) | Strong Axis Bending (ksi) | Weak Axis Bending (ksi) | Shear (ksi) | | |
| Column | Normal Operation $DW_s + DW_c + HL_f + T_n$ | 3.11 | 2.85 | 4.10 | 0.24 | 0.55 | 18.1 |
| | Off-Normal Operation $DW_s + HL_j$ | 2.9 | 0.72 | 3.9 | 0.22 | 0.37 | 19.1 |
| | Accident $DW_s + DW_c + HL_f +$ DBE $+ T_n$ | 6.6 | 4.2 | 4.4 | 0.51 | 0.87 | 18.1 |
| | Accident $DW_s + DW_c + T_a$ | 3.9 | 10.9 | 12.6 | 0.7 | 0.96 | 15.3 |
| Cross Beam | Normal Operation $DW_s + DW_c + HL_f + T_n$ | 1.06 | 3.81 | 6.85 | 3.81 | 0.53 | 18.1 |
| | Off-Normal Operation $DW_s + HL_j$ | 0.12 | 1.7 | 6.1 | 6.5 | 0.31 | 19.1 |
| | Accident $DW_s + DW_c + HL_f +$ DBE $+ T_n$ | 1.87 | 7.04 | 9.25 | 14.63 | 0.88 | 18.1 |
| | Accident $DW_s + DW_c + T_a$ | 2.59 | 8.4 | 20.6 | 7.1 | 0.96 | 15.3 |

**Table 8.2-19**
**DSC Support Structure Enveloping Load Combination Results**

(Concluded)

| Component | Load Combination | Calculated Stress | | | | Interaction (Calc/ Allowable) | Allowable Shear Stress (ksi) |
|---|---|---|---|---|---|---|---|
| | | Axial (ksi) | Strong Axis Bending (ksi) | Weak Axis Bending (ksi) | Shear (ksi) | | |
| Rail | Normal Operation $DW_s + DW_c + HL_f + T_n$ | 1.31 | 2.39 | 10.97 | 2.61 | 0.65 | 18.1 |
| | Off-Normal Operation $DW_s + HL_j$ | 6.5 | 6.58 | 9.3 | 3.74 | 0.93 | 19.1 |
| | Accident $DW_s + DW_c + HL_f +$ DBE $+T_n$ | 2.35 | 3.86 | 15.87 | 6.07 | 0.70 | 18.1 |
| | Accident $DW_s + DW_c + T_a$ | 1.1 | 4.8 | 34.6 | 3.3 | 0.39 | 15.3 |

Key: $DW_s$ = Dead Weight Support Assembly, DBE = Seismic Loads,
$HL_j$ = Off-Normal Handling Loads-Jammed, $T_n$ = Normal Thermal,
$DW_c$ = Dead Weight Canister, $T_a$ = Accident Thermal
$HL_f$ = Normal Loads Friction,

(1) Maximum stresses reported irrespective of location.

(2) Allowable stresses taken at 270°F for all combinations with $T_n$, taken at 100°F for combination with $HL_j$, taken at 570°F for combination with $T_a$

(3) Allowables for $DW_s + DW_c + HL_f + T_n$ increased by 50%, $DW_s + DW_c + HL_f$ +DBE + $T_n$ increased by 60%, allowables for $HL_j$ increased by 33%, and $DW_s + DW_c + T_a$ increased by 70% in accordance with ANSI/ANS 57.9.

**Table 8.2-20**
**DSC Support Structure Enveloping Load Combination Results**
**Support Member End Connection Loads**

| Load Combination | Maximum End Loads | | | | | |
|---|---|---|---|---|---|---|
| | Support Column | | | Lateral Brace | | |
| | Axial (k) | Shear (k) | Bending (in.-k) | Axial (k) | Shear (k) | Bending (in.-k) |
| Normal Operations $DW_s + DW_c + HL_f + T_n$ | 20.42 | 0.9 | 37.3 | 14.5 | 0.0 | 0.3 |
| Off-Normal Operations $HL_j$ | 19.0 | 0.8 | 35.5 | 1.9 | 0.0 | 0.0 |
| Accident $DW_s + DW_c + HL_f + DBE + T_n$ | 43.5 | 0.9 | 40.1 | 26.3 | 0.0 | 0.51 |
| Accident $DW_s + DW_c + T_a$ | 25.7 | 2.6 | 114.8 | 38.3 | 0.0 | 0.0 |

Key: $DW_s$ = Dead Weight Support Assembly,
$HL_j$ = Off-Normal Handling Loads-Jammed,
$DW_c$ = Dead Weight Canister,
$HL_f$ = Normal Loads Friction,
DBE = Seismic Loads,
$T_n$ = Normal Thermal,
$T_a$ = Accident Thermal

**Table 8.2-21**
**Standardized Transfer Cask Enveloping Load Combination Results for Normal and Off-Normal Loads (ASME Service Levels A and B)**

| Transfer Cask Component | Stress Type | Controlling Load Combination[1] | Stress (ksi) | |
|---|---|---|---|---|
| | | | Calculated | Allowable[2] |
| Structural Shell | Primary Membrane | A4 | 1.2 | 21.7 |
| | Membrane + Bending | A4 | 5.0 | 32.6 |
| | Primary + Secondary | A4 | 61.9 | 65.1 |
| Top Cover Plate | Primary Membrane | A1 | 0.2 | 21.7 |
| | Membrane + Bending | A4 | 7.1 | 32.6 |
| | Primary + Secondary | A4 | 20.2 | 65.1 |
| Bottom End Plate | Primary Membrane | A1 | 0.2 | 21.7 |
| | Membrane + Bending | A4 | 15.6 | 32.6 |
| | Primary + Secondary | A4 | 30.3 | 65.1 |

(1) See Table 3.2-7 for load combination nomenclature.

(2) See Table 3.2-11 for allowable stress criteria. Material properties were obtained from Table 8.1-3 at a design temperature of 400°F.

**Table 8.2-21a**
**OS197 Transfer Cask Enveloping Load Combination Results for Normal and Off-Normal Loads (ASME Service Levels A and B)**

| Transfer Cask Component | Stress Type | Stress (ksi) | |
|---|---|---|---|
| | | Calculated[1] | Allowable[2] |
| Structural Shell | Primary Membrane | 1.8/7.9[4] | 21.7 |
| | Membrane + Bending | 14.0/19.5[4] | 32.6 |
| | Primary + Secondary | 25.4/41.4[4] | 65.1 |
| Top Cover Plate | Primary Membrane | 0.56 | 21.7 |
| | Membrane + Bending | 4.2 | 32.6 |
| | Primary + Secondary | 10.8 | 65.1 |
| Bottom End Plate | Primary Membrane | 0.56 | 21.7 |
| | Membrane + Bending | 7.2 | 32.6 |
| | Primary + Secondary | 14.0 | 65.1 |

(1) The load combination for Levels A and B is dead weight plus thermal plus handling loads.

(2) See Table 3.2-11 for allowable stress criteria. Material properties for all components except the cask structural shell were obtained from Table 8.1-3 at a design temperature of 400°F. The cask structural shell allowables are based on a temperature of 250°F.

(3) Allowable stress values and calculated stress intensities are tabulated for the stainless steel cover plate.

(4) The leftmost stress value listed is for locations remote from the trunnions, while the rightmost stress value occurs in the region of the trunnions.

**Table 8.2-21b**
**OS197 Transfer Cask Enveloping Load Combination Results for Normal and Off-Normal Loads (ASME Service Levels A and B)**

| Transfer Cask Component | Stress Type | Stress (ksi) | |
|---|---|---|---|
| | | Calculated[1] | Allowable[2] |
| Structural Shell | Primary Membrane | 2.1/9.45[4] | 20.0 |
| | Membrane + Bending | 14.9/21.8[4] | 30.0 |
| | Primary + Secondary | 25.1/46.8[4] | 60.0 |
| Top Cover Plate | Primary Membrane | 0.7 | 18.7 |
| | Membrane + Bending | 5.3 | 28.1 |
| | Primary + Secondary | 11.2 | 56.1 |
| Bottom End Plate | Primary Membrane | 1.2 | 18.7 |
| | Membrane + Bending | 8.6 | 28.1 |
| | Primary + Secondary | 14.6 | 56.1 |

(1) The load combination for Levels A and B is dead weight plus thermal plus handling loads.

(2) See Table 3.2-11 for allowable stress criteria. Material properties for all components except the cask structural shell were obtained from Table 8.1-3 at a design temperature of 400°F. The cask structural shell allowables are based on a temperature of 250°F.

(3) Allowable stress values and calculated stress intensities are tabulated for the stainless steel cover plate.

(4) The leftmost stress value listed is for locations remote from the trunnions, while the rightmost stress value occurs in the region of the trunnions.

**Table 8.2-22**
**Standardized Transfer Cask Enveloping Load Combination Results for Normal and Off-Normal Loads (ASME Service Levels A and B)**

| Transfer Cask Component | Stress Type | Controlling Load Combination[1] | Stress (ksi) | |
|---|---|---|---|---|
| | | | Calculated | Allowable[2] |
| Structural Shell | Primary Membrane | A4 | 1.2 | 21.7 |
| | Membrane + Bending | A4 | 5.0 | 32.6 |
| | Primary + Secondary | A4 | 61.9 | 65.1 |
| Top Cover Plate | Primary Membrane | A1 | 0.2 | 21.7 |
| | Membrane + Bending | A4 | 7.1 | 32.6 |
| | Primary + Secondary | A4 | 20.2 | 65.1 |
| Bottom End Plate | Primary Membrane | A1 | 0.2 | 21.7 |
| | Membrane + Bending | A4 | 15.6 | 32.6 |
| | Primary + Secondary | A4 | 30.3 | 65.1 |

(1) See Table 3.2-7 for load combination nomenclature.

(2) See Table 3.2-11 for allowable stress criteria. Material properties were obtained from Table 8.1-3 at a design temperature of 400°F.

**Table 8.2-22a**
**OS197 Transfer Cask Enveloping Load Combination Results for Normal and Off-Normal Loads (ASME Service Levels A and B)**

| Transfer Cask Component | Stress Type | Stress (ksi)[1] | |
|---|---|---|---|
| | | Calculated | Allowable[2] |
| Structural Shell | Primary Membrane | 1.6/7.0[4] | 20.0 |
| | Membrane + Bending | 12.4/17.3[4] | 30.0 |
| | Primary + Secondary | 22.6/36.8[4] | 60.0 |
| Top Cover Plate[3] | Primary Membrane | 0.5 | 18.7 |
| | Membrane + Bending | 3.7 | 28.1 |
| | Primary + Secondary | 9.6 | 56.1 |
| Bottom End Plate | Primary Membrane | 0.5 | 18.7 |
| | Membrane + Bending | 6.4 | 28.1 |
| | Primary + Secondary | 12.4 | 56.1 |

(1) The load combination for Levels A and B is dead weight plus thermal plus handling loads.

(2) See Table 3.2-11 for allowable stress criteria. Material properties for all components except the cask structural shell were obtained from Table 8.1-3 at a design temperature of 400°F. The cask structural shell allowables are based on a temperature of 250°F.

(3) Allowable stress values and calculated stress intensities are tabulated for the stainless steel cover plate.

(4) The lower stress value listed is for locations remote from the trunnions, while the higher stress value occurs in the region of the trunnions.

**Table 8.2-22b**
**OS197H Transfer Cask Enveloping Load Combination Results for Accident Loads (ASME Service Level C)**

| Transfer Cask Component | Stress Type | Stress (ksi)[1] | |
|---|---|---|---|
| | | Calculated[1] | Allowable[2] |
| Structural Shell | Primary Membrane | 2.1/9.45[4] | 20.0 |
| | Membrane + Bending | 14.9/21.8[4] | 30.0 |
| Top Cover Plate[3] | Primary Membrane | 0.7 | 18.7 |
| | Membrane + Bending | 5.3 | 28.1 |
| Bottom End Plate | Primary Membrane | 1.2 | 18.7 |
| | Membrane + Bending | 8.6 | 28.1 |

(1) The load combination for Levels A and B is dead weight plus thermal plus handling loads.

(2) See Table 3.2-11 for allowable stress criteria. Material properties for all components except the cask structural shell were obtained from Table 8.1-3 at a design temperature of 400°F. The cask structural shell allowables are based on a temperature of 250°F.

(3) Allowable stress values and calculated stress intensities are tabulated for the stainless steel cover plate.

(4) The leftmost stress value listed is for locations remote from the trunnions, while the rightmost stress value occurs in the region of the trunnions.

**Table 8.2-23**
**Standardized Transfer Cask Enveloping Load Combination Results for Accident Loads (ASME Service Level C)**

| Transfer Cask Component | Stress Type | Controlling Load Combination[1] | Stress (ksi) | |
|---|---|---|---|---|
| | | | Calculated | Allowable[2] |
| Structural Shell | Primary Membrane | C1 | 1.7 | 26.0 |
| | Membrane + Bending | C1 | 9.1 | 39.1 |
| Top Cover Plate | Primary Membrane | C1 | 0.2 | 26.0 |
| | Membrane + Bending | C1 | 14.0 | 39.1 |
| Bottom End Plate | Primary Membrane | C1 | 0.1 | 26.0 |
| | Membrane + Bending | C1 | 31.0 | 39.1 |

(1) See Table 3.2-7 for load combination nomenclature.

(2) See Table 3.2-11 for allowable stress criteria. Material properties were obtained from Table 8.1-3 at a design temperature of 400°F.

**Table 8.2-23a**
**OS197 Transfer Cask Enveloping Load Combination Results for Accident Loads (ASME Service Level C)**

| Transfer Cask Component | Stress Type | Stress (ksi) | |
|---|---|---|---|
| | | Calculated[1] | Allowable[2] |
| Structural Shell | Primary Membrane | 3.4/8.1[4] | 24.0 |
| | Membrane + Bending | 27.6/19.5[4] | 36.0 |
| Top Cover Plate[3] | Primary Membrane | 0.56 | 22.4 |
| | Membrane + Bending | 4.5 | 33.7 |
| Bottom End Plate | Primary Membrane | 1.1 | 22.4 |
| | Membrane + Bending | 15.4 | 33.7 |

(1) The load combination for Level C include dead weight, thermal, handling and seismic loads.

(2) See Table 3.2-11 for allowable stress criteria. Material properties for all components except the cask structural shell were obtained from Table 8.1-3 at a design temperature of 400°F. The cask structural shell allowables are based on a temperature of 250°F.

(3) Allowable stress values and calculated stress intensities are tabulated for the stainless steel cover plate.

(4) The lower stress value listed is for locations remote from the trunnions, while the higher stress value occurs in the region of the trunnions.

**Table 8.2-24**
**Standardized Transfer Cask Enveloping Load Combination Results for Accident Loads (ASME Service Level D)**

| Transfer Cask Component | Stress Type | Controlling Load Combination[1] | Stress (ksi) | |
|---|---|---|---|---|
| | | | Calculated | Allowable[2] |
| Structural Shell | Primary Membrane | D1 | 9.7 | 49.0 |
| | Membrane + Bending | D3 | 15.6 | 70.0 |
| Top Cover Plate | Primary Membrane | D1 | 25.4 | 49.0 |
| | Membrane + Bending | D1 | 25.4 | 70.0 |
| Bottom End Plate | Primary Membrane | D1 | 26.3 | 49.0 |
| | Membrane + Bending | D2 | 37.7 | 70.0 |

(1) See Table 3.2-7 for load combination nomenclature.

(2) See Table 3.2-11 for allowable stress criteria. Material properties were obtained from Table 8.1-3 at a design temperature of 400°F.

**Table 8.2-24a**
**OS197 Transfer Cask Enveloping Load Combination Results for Accident Loads**
**(ASME Service Level D)**

| Transfer Cask Component | Stress Type | Stress (ksi) | |
|---|---|---|---|
| | | Calculated[1] | Allowable[2] |
| Structural Shell | Primary Membrane | 33.4 | 48.0 |
| | Membrane + Bending | 39.9 | 68.5 |
| Top Cover Plate[3] | Primary Membrane | 28.6 | 44.9 |
| | Membrane + Bending | 28.6 | 64.4 |
| Bottom End Plate | Primary Membrane | 27.0 | 44.9 |
| | Membrane + Bending | 45.5 | 64.4 |

(1) The load combination for Level D include dead weight, thermal, handling and cask drop loads.

(2) See Table 3.2-11 for allowable stress criteria. Material properties for all components except the cask structural shell were obtained from Table 8.1-3 at a design temperature of 400°F. The cask structural shell allowables are based on a temperature of 250°F.

(3) Allowable stress values and calculated stress intensities are tabulated for the stainless steel cover plate.

## Table 8.2-25
## Expanded Load Combinations for DSC Analyses

| | | Horizontal DW | | Vertical DW | | Internal | External | Thermal | Lifting | Other | Service |
|---|---|---|---|---|---|---|---|---|---|---|---|
| | | DSC | Fuel | DSC | Fuel | Pressure[9] | Pressure | Condition | Loads | Loads | Level |
| FUEL LOADING LOAD CASES | | | | | | | | | | | |
| FL-1 | DSC/Cask Filling | -- | -- | Cask | -- | -- | Hydrostatic | 100°F Cask | -- | -- | A |
| FL-2 | DSC/Cask Filling | -- | -- | Cask | -- | Hydrostatic | Hydrostatic | 100°F Cask | -- | -- | A |
| FL-3 | DSC/Cask Xfer | -- | -- | Cask | -- | Hydrostatic | Hydrostatic | 100°F Cask | -- | -- | A |
| FL-4 | Fuel Loading | -- | -- | Cask | X | Hydrostatic | Hydrostatic | 100°F Cask | -- | -- | A |
| FL-5 | Xfer to Decon | -- | -- | Cask | X | Hydrostatic | Hydrostatic | 100°F Cask | -- | -- | A |
| FL-6 | Inner Cover Plate Welding | -- | -- | Cask | X | Hydrostatic | Hydrostatic | 100°F Cask | -- | -- | A |
| FL-7 | Fuel Deck Seismic Loading | -- | -- | Cask | X | Hydrostatic | Hydrostatic | 100°F Cask | -- | Note 10 | C |
| DRAINING AND DRYING LOAD CASES | | | | | | | | | | | |
| DD-1 | DSC Blowdown | -- | -- | Cask | X | Hydrostatic + 20 psi | Hydrostatic | 100°F Cask | -- | -- | A |
| DD-2 | Vacuum Drying | -- | -- | Cask | X | 0 psia | Hydrostatic + 14.7 psi | 100°F Cask | -- | -- | A |
| DD-3 | Helium Backfill | -- | -- | Cask | X | 12 psi | Hydrostatic | 100°F Cask | -- | -- | A |
| DD-4 | Final Helium Backfill | -- | -- | Cask | X | 5.0 psi | Hydrostatic | 100°F Cask | -- | -- | A |
| DD-5 | Outer Cover Plate Welding | -- | -- | Cask | X | 5.0 psi | Hydrostatic | 100°F Cask | -- | -- | A |
| TRANSFER TRAILER LOADING | | | | | | | | | | | |
| TL-1 | Vertical Xfer to Trailer | | | Cask | X | 11.0 psi[18] | -- | 0°F Cask | -- | -- | A |
| TL-2 | " | | | Cask | X | 11.0 psi[18] | -- | 100°F Cask | -- | -- | A |
| TL-3 | Laydown | Cask | X | | | 11.0 psi[18] | -- | 0°F Cask | -- | -- | A |
| TL-4 | " | Cask | X | | | 11.0 psi[18] | -- | 100°F Cask | -- | -- | A |

| | | Horizontal DW | | Vertical DW | | Internal | External | Thermal | Handling | Other | Service |
|---|---|---|---|---|---|---|---|---|---|---|---|
| | | DSC | Fuel | DSC | Fuel | Pressure[9] | Pressure | Condition | Loads | Loads | Level |
| TRANSFER TO / FROM ISFSI | | | | | | | | | | | |
| TR-1 | Axial Load - Cold | Cask | X | -- | -- | 11.0 psi[18] | -- | 0°F Cask | 1g Axial | -- | A |
| TR-2 | Transverse Load - Cold | Cask | X | -- | -- | 11.0 psi[18] | -- | 0°F Cask | 1g Transverse | -- | A |
| TR-3 | Vertical Load - Cold | Cask | X | -- | -- | 11.0 psi[18] | -- | 0°F Cask | 1g Vertical | -- | A |
| TR-4 | Oblique Load - Cold | Cask | X | -- | -- | 11.0 psi[18] | -- | 0°F Cask | ½g Axial + ½g Trans + ½g Vert | -- | A |
| TR-5 | Axial Load - Hot | Cask | X | -- | -- | 11.0 psi[18] | -- | 100°F Cask | 1g Axial | -- | A |
| TR-6 | Transverse Load - Hot | Cask | X | -- | -- | 11.0 psi[18] | -- | 100°F Cask | 1g Transverse | -- | A |
| TR-7 | Vertical Load - Hot | Cask | X | -- | -- | 11.0 psi[18] | -- | 100°F Cask | 1g Vertical | -- | A |
| TR-8 | Oblique Load - Hot | Cask | X | -- | -- | 11.0 psi[18] | -- | 100°F Cask | ½g Axial + ½g Trans + ½g Vert | -- | A |
| TR-9 | 75g Top End Drop | -- | -- | Note 1 | | 60 psi[11] | -- | 100°F Cask[2] | -- | 75g TED | D |
| TR-10 | 75g Bottom End Drop | -- | -- | Note 1 | | 60 psi[11] | -- | 100°F Cask[2] | -- | 75g BED | D |
| TR-11 | 75g Side Drop | Note 1 | | -- | -- | 60 psi[11] | -- | 100°F Cask[2] | -- | 75g Side Drop | D |

Notes:

1. 75g drop acceleration includes gravity effects. Therefore, it is not necesary to add an additional 1.0g load.
2. For level D events, only the maximum temperature case is considered. (Thermal stresses are not limited for Level D events and maximum temperatures give minimum allowables).
3. Flood load is an external pressure equivalent to 50 ft. of water.
4. BV = HSM Vents are blocked
5. At temperatures over 100°F, a sunshade is required over the Transfer Cask. Temperatures for these cases are enveloped by the 100°F (without sunshade) case.
6. This pressure assumes release of the fuel cover gas and 30% of the fission gas. Since unloading requires the HSM door to be removed, the pressure and temperatures are based on the normal (unblocked vent) condition. Pressure is applied to the inner pressure boundary.
7. This pressure assumes release of the fuel cover gas and 30% of the fission gas. Although unloading requires the HSM door to be removed, the pressure and temperatures are conservatively based on the blocked vent condition. Pressure is applied to the outer pressure boundary.

Notes continued on following page...

## Table 8.2-25
## Expanded Load Combinations for DSC Analyses
(concluded)

| HSM LOADING | Horizontal DW DSC | Horizontal DW Fuel | Vertical DW DSC | Vertical DW Fuel | Internal Pressure[9] | External Pressure | Thermal Condition | Handling Loads | Other Loads | Service Level |
|---|---|---|---|---|---|---|---|---|---|---|
| LD-1 Normal Loading - Cold | Cask | X | -- | -- | 11.0 psi[18] | -- | 0°F Cask | +80 Kip | -- | A |
| LD-2 Normal Loading - Hot | Cask | X | -- | -- | 11.0 psi[18] | -- | 100°F Cask | +80 Kip | -- | A |
| LD-3 | Cask | X | -- | -- | 11.0 psi[18] | -- | 125°F w/shade[5] | +80 Kip | -- | A |
| LD-4 Off-Normal Loading - Cold | Cask | X | -- | -- | 11.0 psi[18] | -- | 0°F Cask | +80 Kip | -- | B |
| LD-5 Off-Normal Loading - Hot | Cask | X | -- | -- | 11.0 psi[18] | -- | 100°F Cask | +80 Kip | -- | B |
| LD-6 | Cask | X | -- | -- | 11.0 psi[18] | -- | 125°F w/shade[5] | +80 Kip | -- | B |
| LD-7 Accident Loading | Cask | X | -- | -- | 11.0 psi[18] | -- | 125°F w/shade[5] | +80 Kip | -- | B |
| HSM STORAGE | | | | | | | | | | |
| HSM-1 Off-Normal Storage | HSM | X | -- | -- | 11.0 psi[18] | -- | -40°F HSM | -- | -- | B |
| HSM-2 Normal Storage | HSM | X | -- | -- | 11.0 psi[18] | -- | 0°F HSM | -- | -- | A |
| HSM-3 Off-Normal Storage | HSM | X | -- | -- | 11.0 psi[18] | -- | 125°F HSM | -- | -- | B |
| HSM-4 Off-Normal Temp. + Failed Fuel | HSM | X | -- | -- | 11.0 psi[18] | -- | 125°F HSM | -- | Failed Fuel | C |
| HSM-5 Blocked Vent Storage | HSM | X | -- | -- | 60 psi[8,12] | -- | 125°F HSM/BV[4] | -- | -- | D |
| HSM-6 B. V. + Failed Fuel Storage | HSM | X | -- | -- | 60 psi[8,13] | -- | 125°F HSM/BV[4] | -- | Failed Fuel | D |
| HSM-7 Earthquake Loading - Cold | HSM | X | -- | -- | 11.0 psi[18] | -- | 0°F HSM | -- | Seismic | C |
| HSM-8 Earthquake Loading - Hot | HSM | X | -- | -- | 11.0 psi[18] | -- | 100°F HSM | -- | Seismic | C |
| HSM-8a Earthquake Loading - FF | HSM | X | -- | -- | 11.0 psi[17, 18] | -- | 100°F HSM | -- | EQ + FF | C |
| HSM-9 Flood Load (50' $H_2O$) - Cold | HSM | X | -- | -- | 0 psi | 22 psi | 0°F HSM | -- | Flood[3] | C |
| HSM-10 Flood Load (50' $H_2O$) - Hot | HSM | X | -- | -- | 0 psi | 22 psi | 100°F HSM | -- | Flood[3] | C |

| HSM UNLOADING | Horizontal DW DSC | Horizontal DW Fuel | Vertical DW DSC | Vertical DW Fuel | Internal Pressure[9] | External Pressure | Thermal Condition | Handling Loads | Other Loads | Service Level |
|---|---|---|---|---|---|---|---|---|---|---|
| UL-1 Normal Unloading - Cold | HSM | X | -- | -- | 11.0 psi[18] | -- | 0°F HSM | -60 Kip | -- | A |
| UL-2 Normal Unloading - Hot | HSM | X | -- | -- | 11.0 psi[18] | -- | 100°F HSM | -60 Kip | -- | A |
| UL-3 | HSM | X | -- | -- | 11.0 psi[18] | -- | 125°F w/shade | -60 Kip | -- | A |
| UL-4 Off-Normal Unloading - Cold | HSM | X | -- | -- | 11.0 psi[18] | -- | 0°F HSM | -60 Kip | -- | B |
| UL-5 Off-Normal Unloading - Hot | HSM | X | -- | -- | 11.0 psi[18] | -- | 100°F HSM | -60 Kip | -- | B |
| UL-6 | HSM | X | -- | -- | 11.0 psi[18] | -- | 125°F w/shade | -60 Kip | -- | B |
| UL-7 Off-Norm. Unloading-FF/Hot[6,16] | HSM | X | -- | -- | 11.0 psi[18] | -- | 100°F HSM | -80 kip | -- | C |
| UL-8 Accident Unloading - FF/Hot[7,16] | HSM | X | -- | -- | 60 psi[7,8,15] | -- | 100°F HSM | -80 kip | -- | D |

| DSC Unloading/Reflood | Horizontal DW DSC | Horizontal DW Fuel | Vertical DW DSC | Vertical DW Fuel | Internal Pressure | External Pressure | Thermal Condition | Handling Loads | Other Loads | Service Level |
|---|---|---|---|---|---|---|---|---|---|---|
| RF-1 DSC Reflood | -- | -- | Cask | X | 20.0 psi (max) | Hydrostatic | 100°F Cask | -- | -- | B |

Notes (continued):

8. This pressure is applied to the outer pressure boundary.
9. Unless noted otherwise, pressure is applied to the inner pressure boundary.
10. Fuel deck seismic loads are assumed enveloped by handling loads.
11. Actual pressure during this event is the normal condition pressure of 10.0 psi.
    Maximum off-normal in-cask pressure (10% failed fuel, 100°F ambient) is less than 11 psi.
12. This is an enveloping pressure, actual pressure under blocked vent conditions (no failed fuel) is less than 11 psig.
13. This is an enveloping pressure, actual pressure under 125°F blocked vent conditions with failed fuel is less than 60 psig.
14. Not Used
15. This is an enveloping pressure, based on 100% failed fuel and 125°F blocked HSM vent conditions.
16. Load Cases UL-7 and UL-8 envelop loading cases where the insertion loading of 80 kips is considered with an accident pressure (the insertion force is opposed by internal pressure).
17. This pressure is based on two accidents occuring simultaneously (failed fuel+seismic).
18. This is an enveloping pressure. Actual off-normal pressure (10% failed fuel) is less than 11 psi for the 24P DSCs and less than 10 psi for the 52B DSCs This envelops the normal pressure of 10 psi.

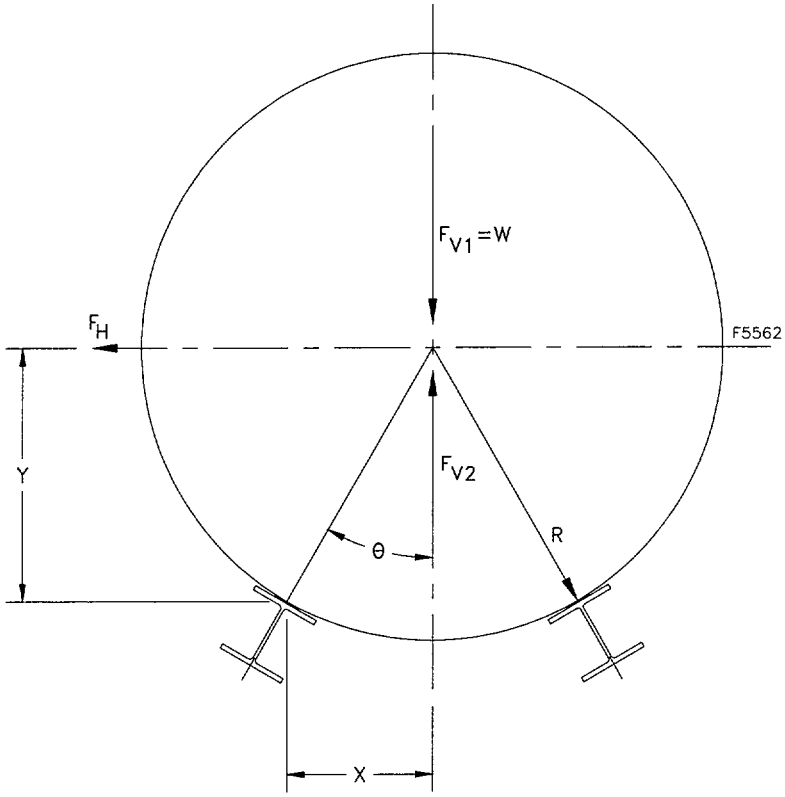


WHERE:

R = 33.625 in., DSC outer radius
θ = 30°
X = R Sin θ = 16.8 in.
Y = R Cos θ = 29.1 in.
$F_{V1}$ = W = 102,000 lb., weight of DSC
$F_{V2}$ = W(0.17g) = 17,340 lb., upward vertical seismic load
$F_H$ = W(0.40g) = 40,800 lb., horizontal seismic load

**Figure 8.2-1**
**DSC Lift-Off Evaluation**

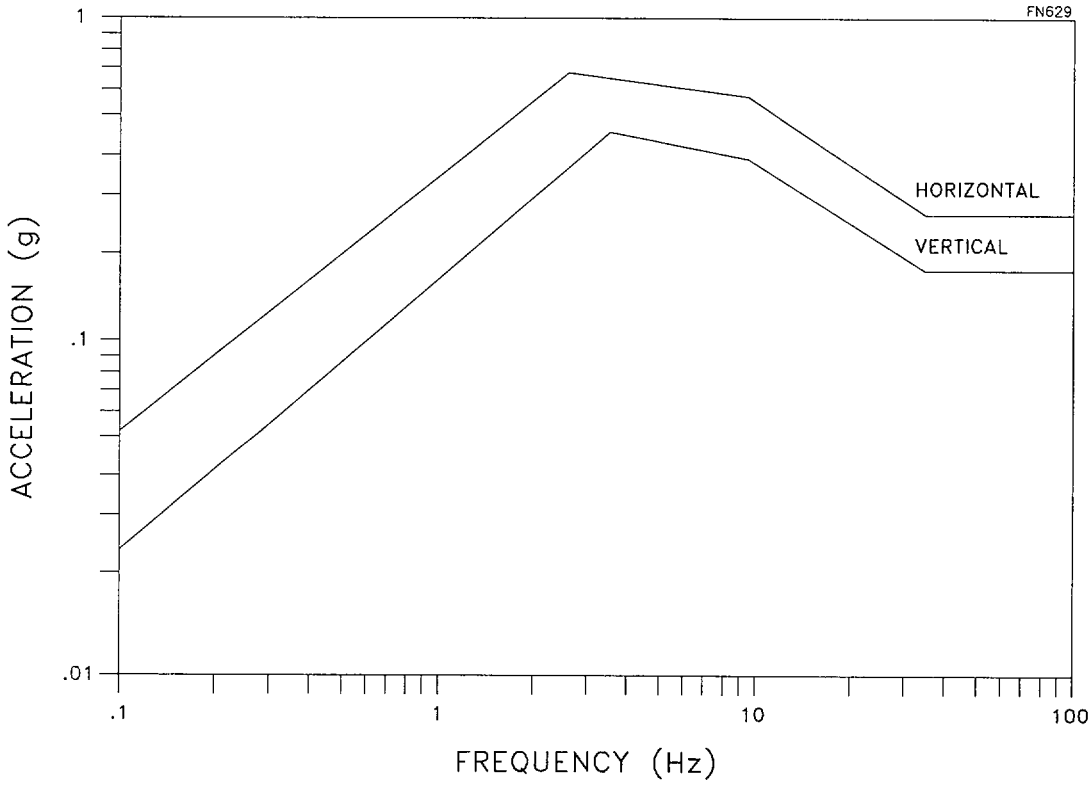


NOTE:

THE RESPONSE SPECTRA SHOWN ARE OBTAINED FROM REGULATORY GUIDE 1.60, BASED ON 7% DAMPING, FRACTORED BY 0.25g PEAK HORIZONTAL AND 0.17g PEAK VERTICAL GROUND ACCELERATIONS.

**Figure 8.2-2**
**Design Seismic Response Spectra**

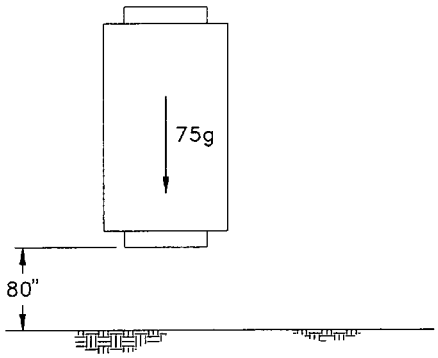


END DROP
(TOP OR BOTTOM)

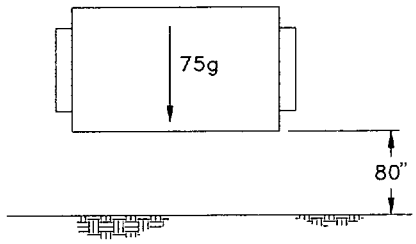


SIDE DROP

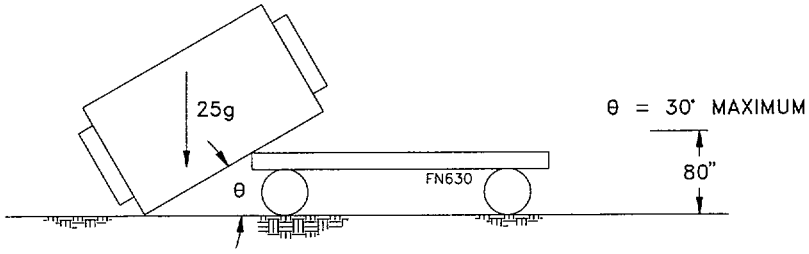


CORNER DROP
(TOP OR BOTTOM)

**Figure 8.2-3**
**Transfer Cask Postulated Drop Accident Scenarios**

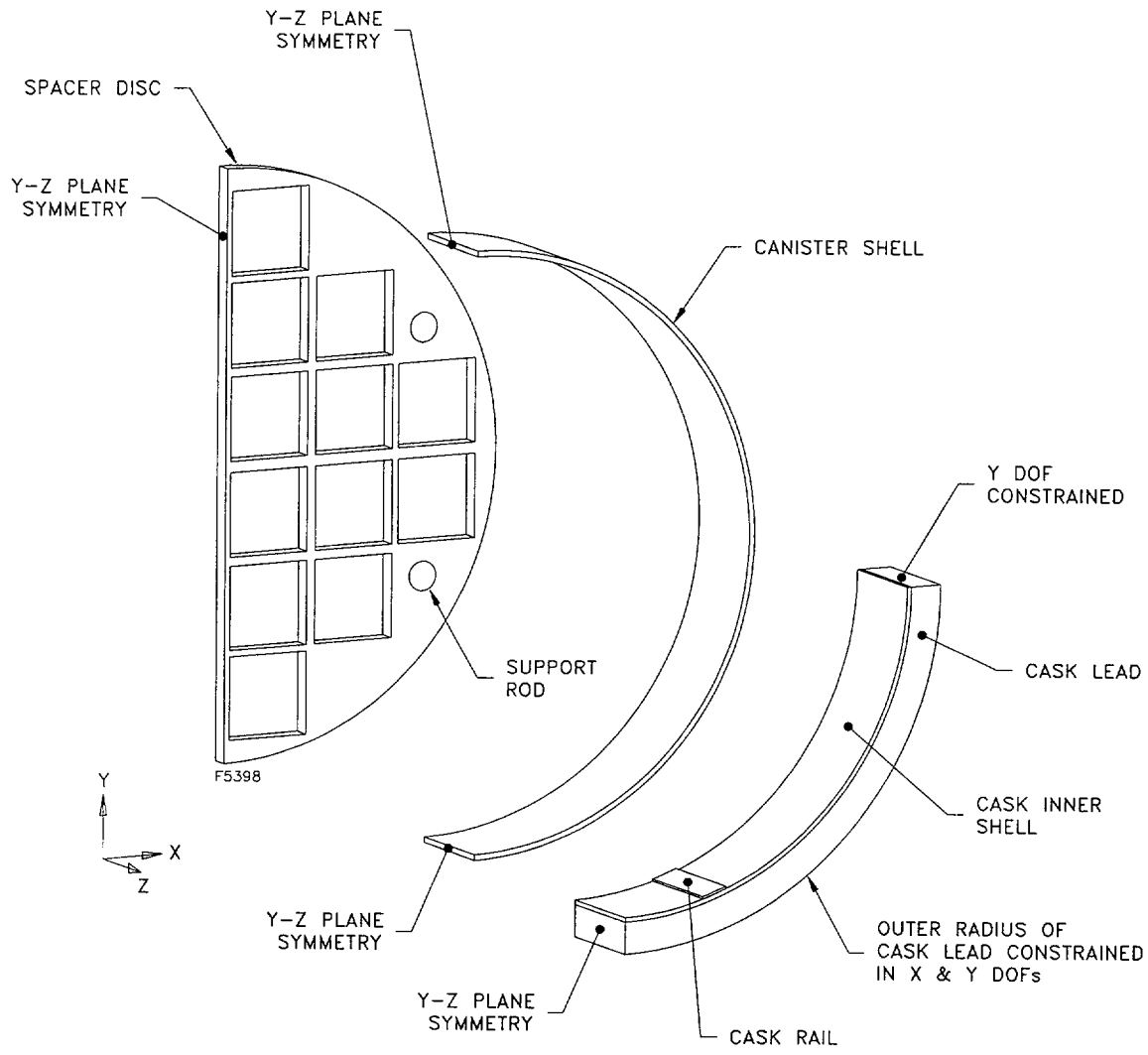


**Figure 8.2-4**
**NUHOMS®-24P DSC Spacer Disk Horizontal Side Drop Analytical Model**

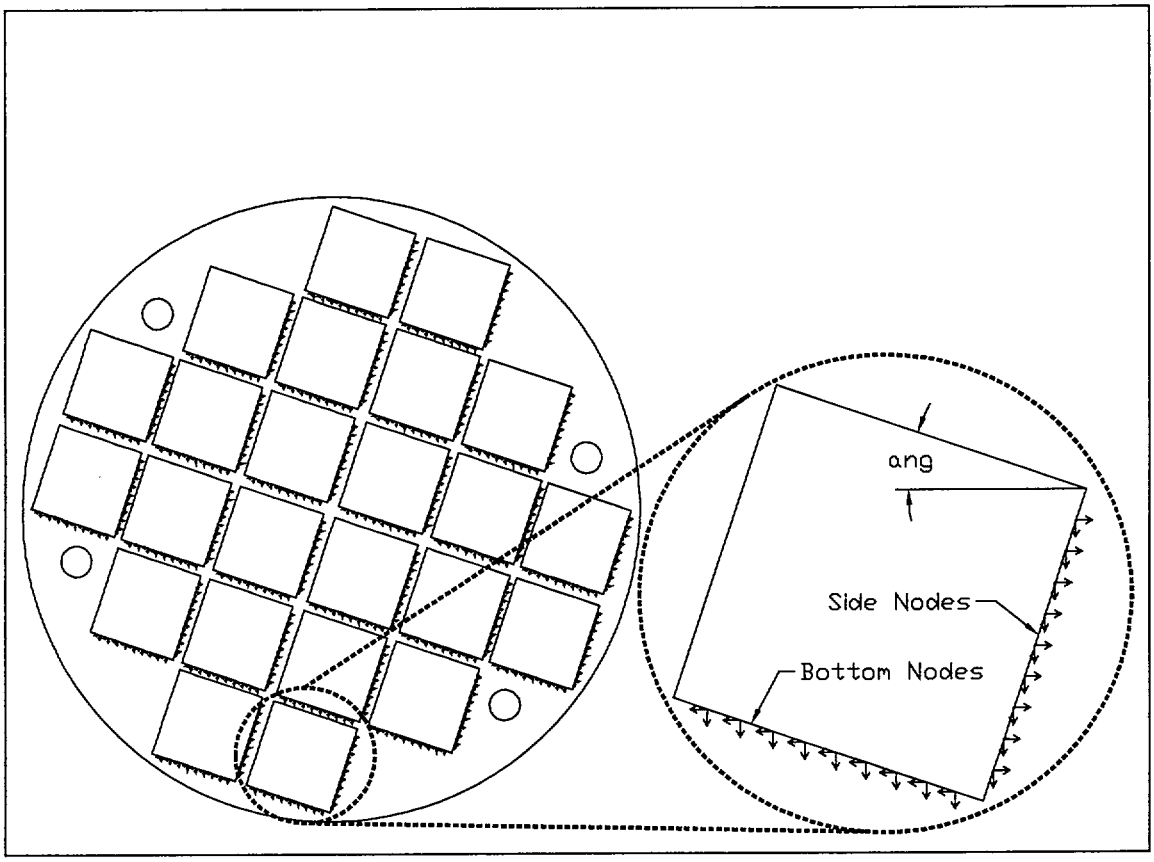


**Figure 8.2-5**
**NUHOMS®-24P DSC Spacer Disk Loading for Horizontal Drop Accident**

**Figure 8.2-6**

**Deleted**

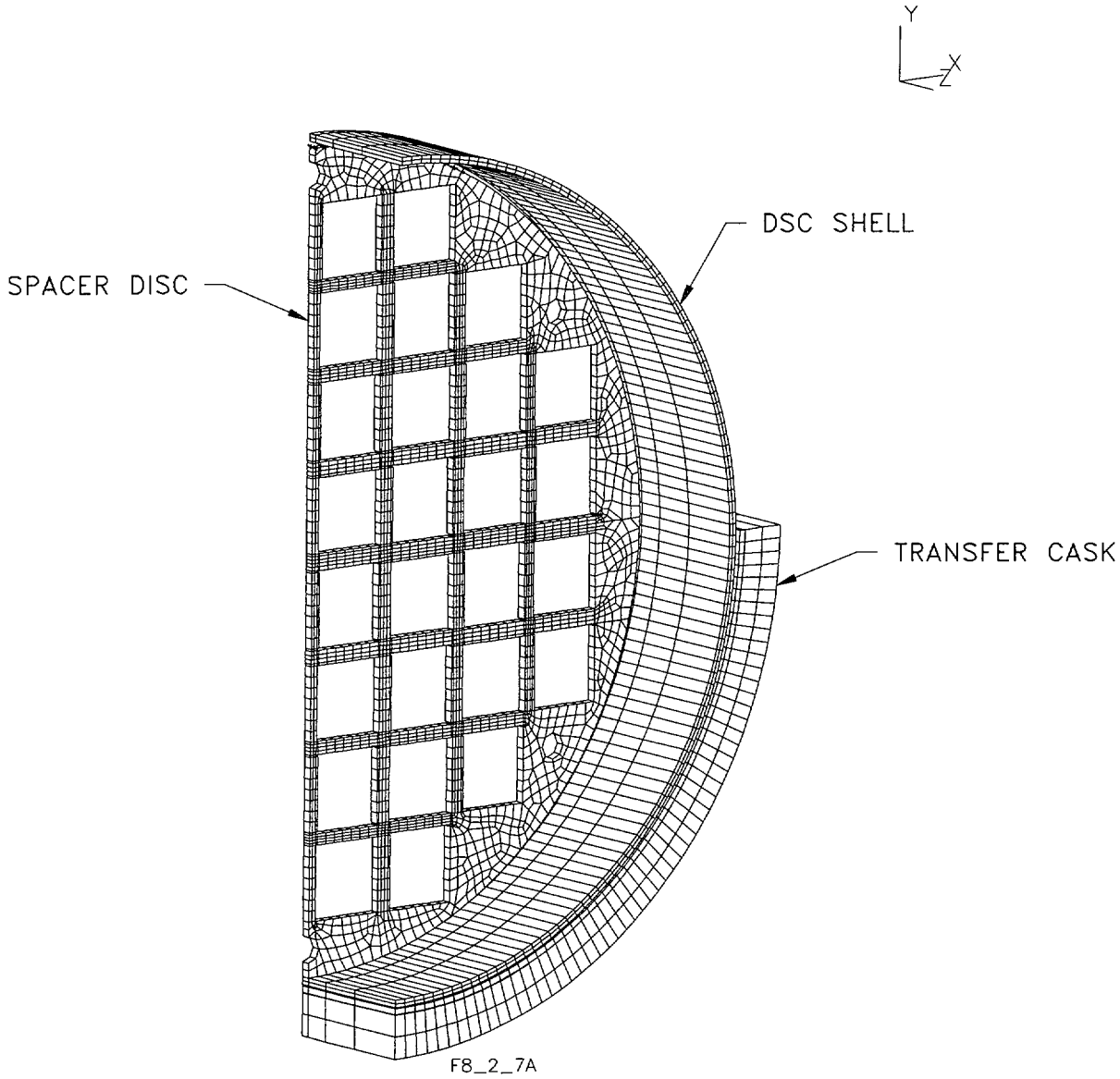


**Figure 8.2-7a**
**NUHOMS®-52B DSC 180° Spacer Disk Side Drop Analytical Model**

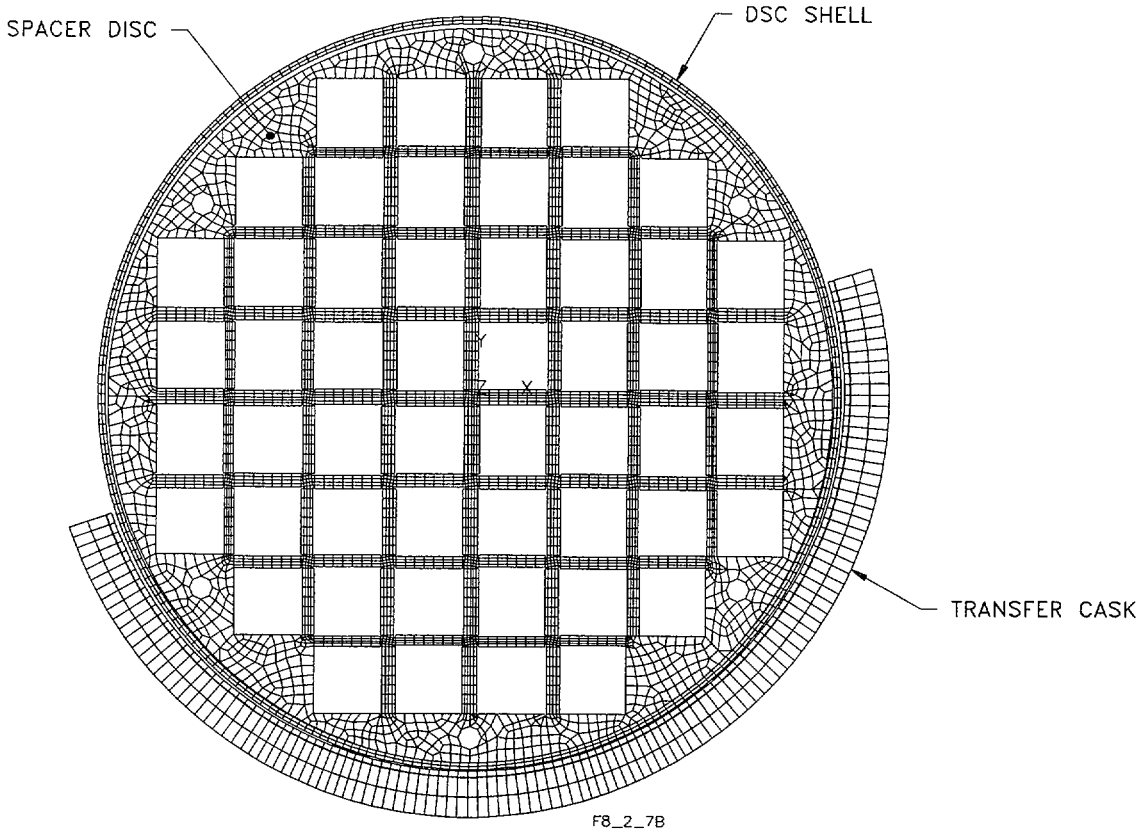


**Figure 8.2-7b**
**NUHOMS®-52B DSC 360° Spacer Disk Side Drop Analytical Model**

**Figure 8.2-8**

**Deleted**

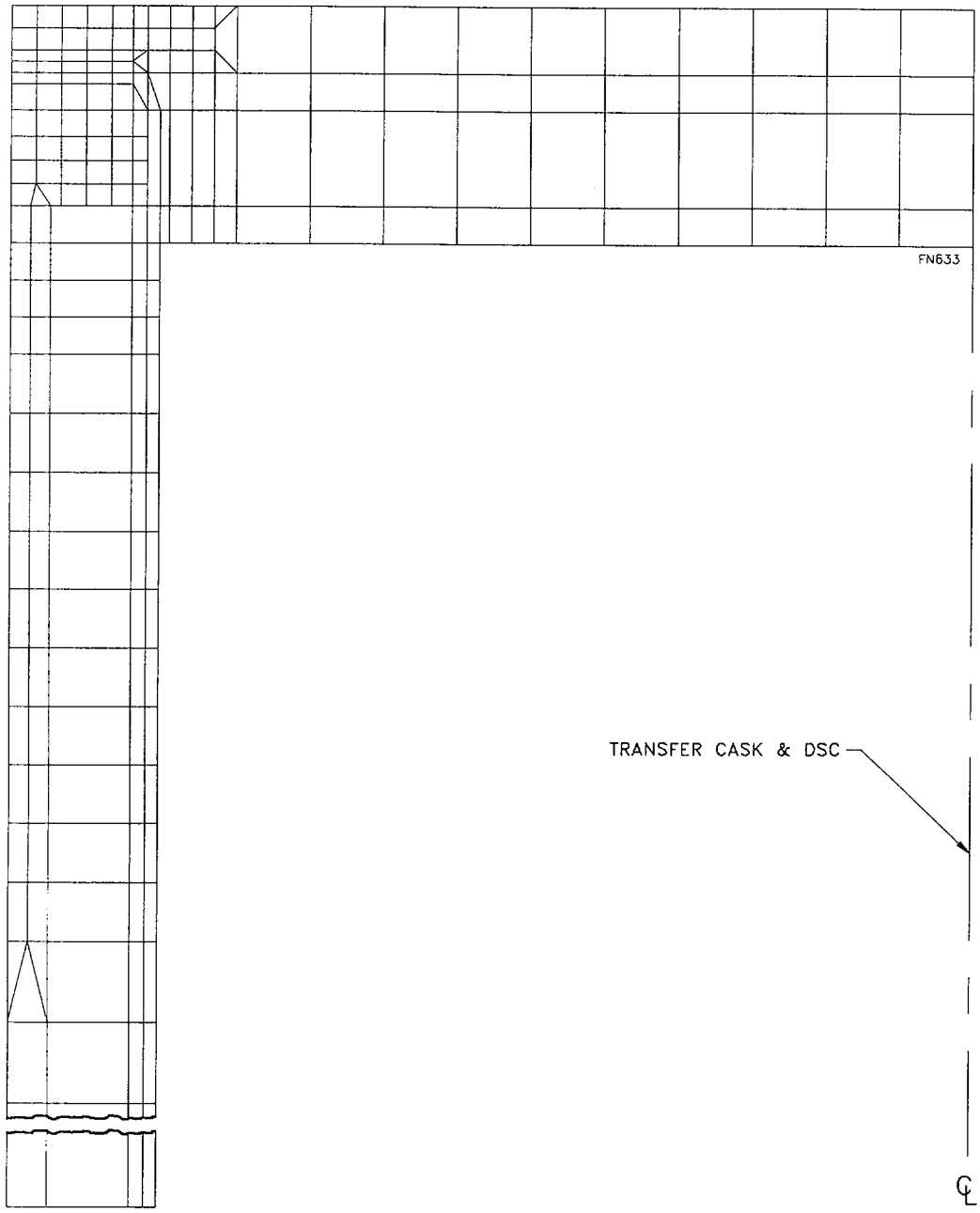


**Figure 8.2-9**
**Transfer Cask and DSC Top Drop Model**

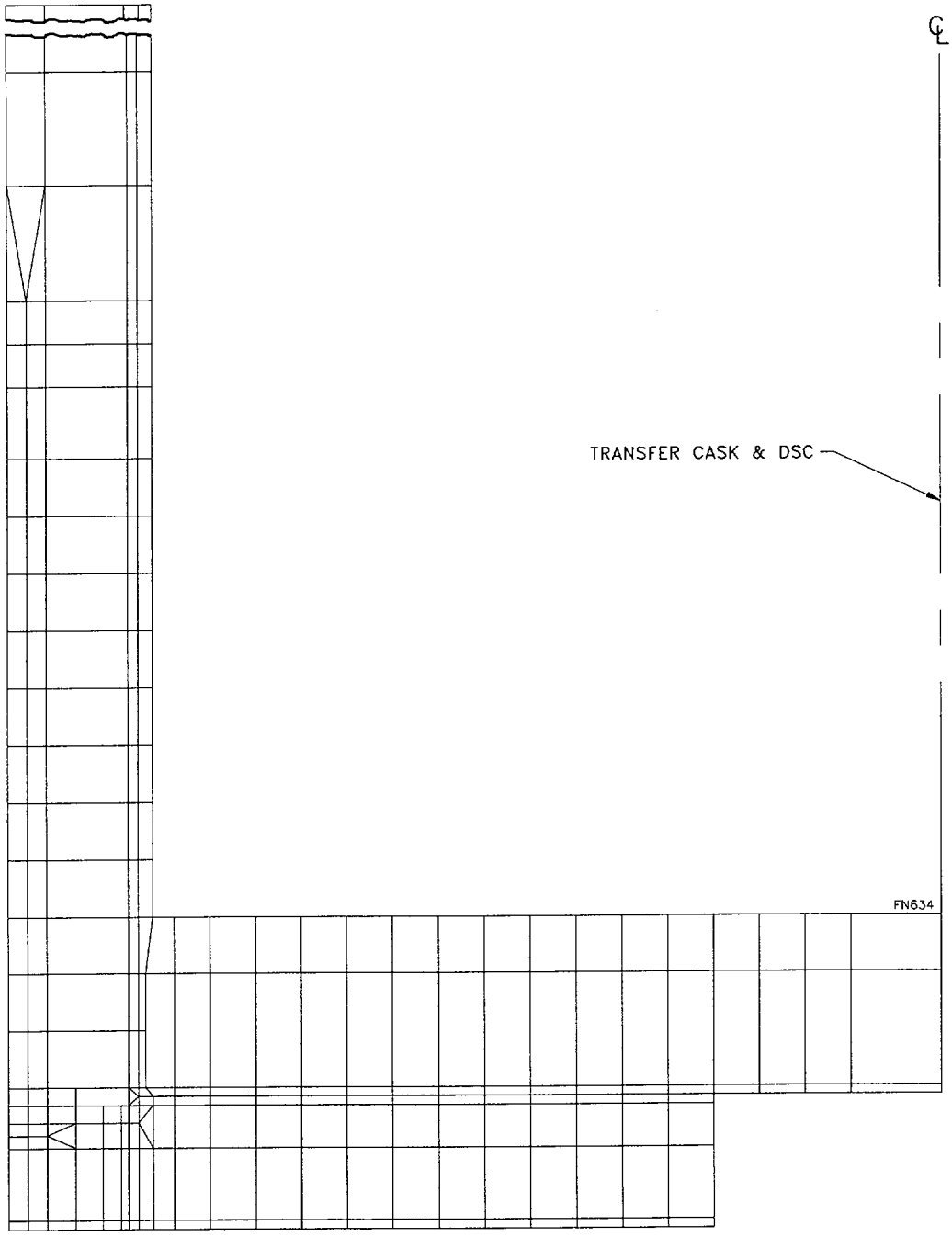


**Figure 8.2-10**
**Transfer Cask and DSC Bottom Drop Model**

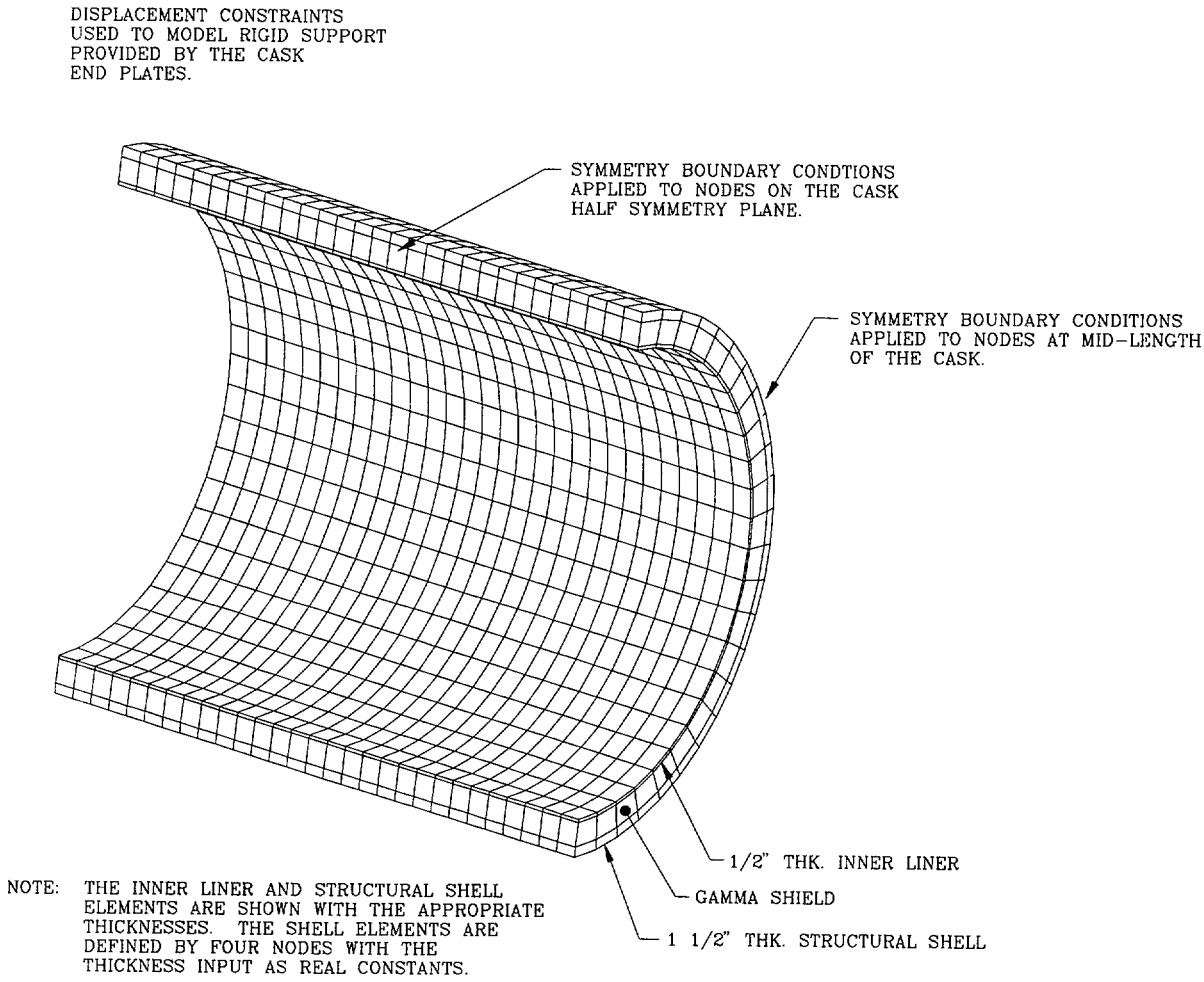


**Figure 8.2-10a**
**OS197 and OS197H Transfer Cask Side Drop Model**

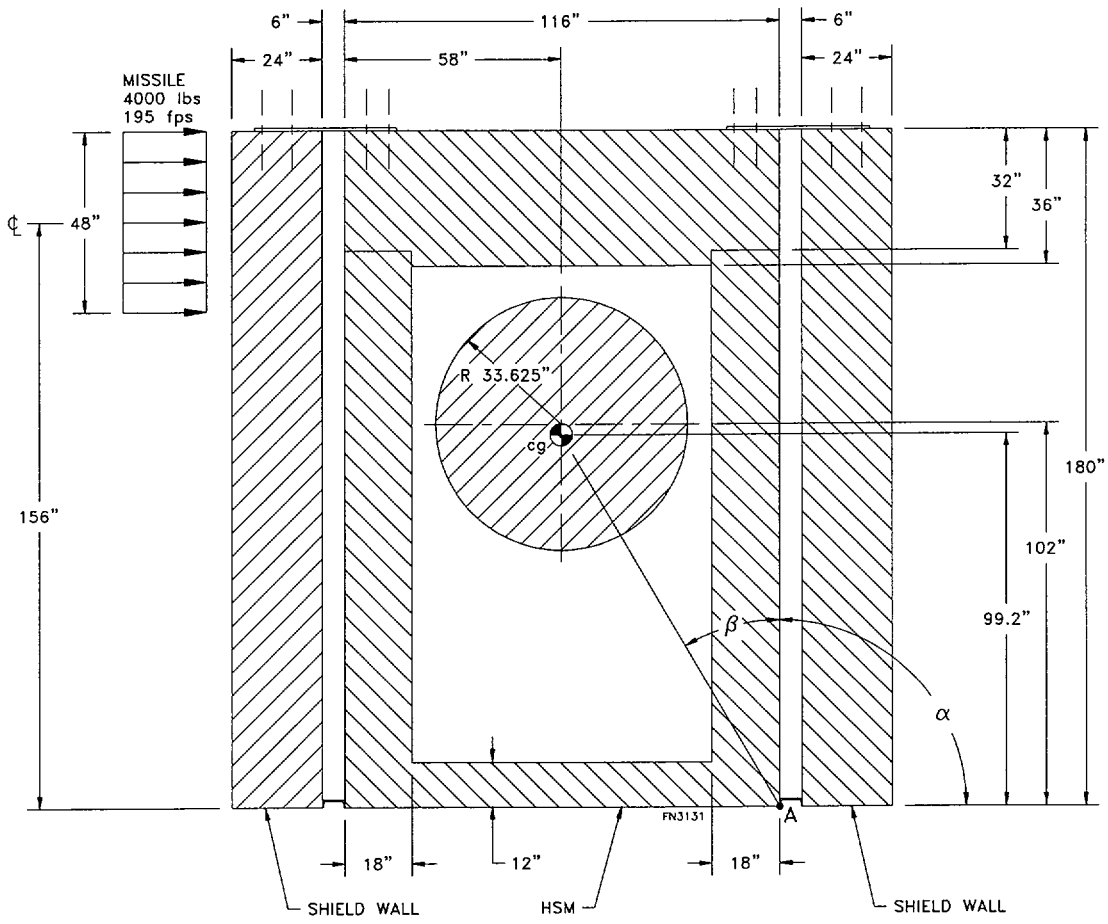


$\alpha$ = Angle of rotated module

**Figure 8.2-11**
**Tornado Missile Impact Model**

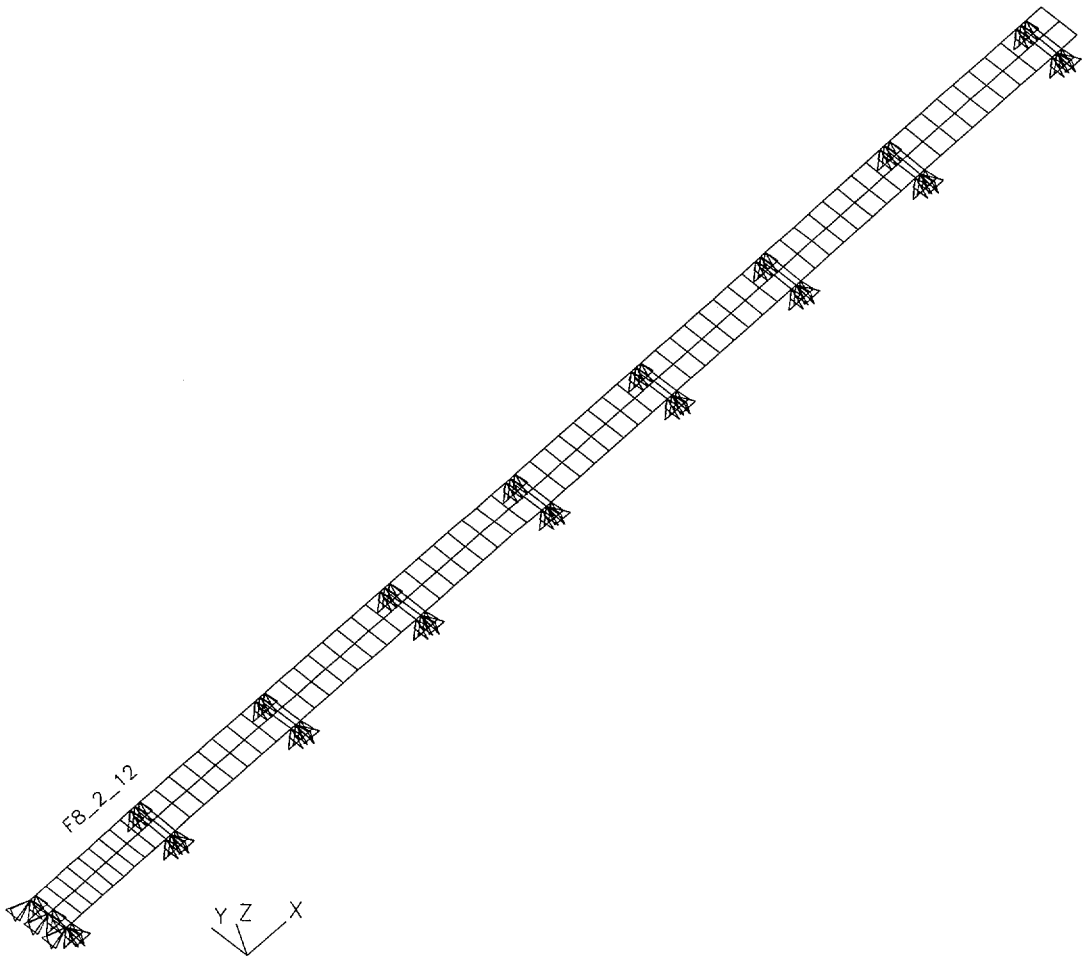


**Figure 8.2-12**
**NUHOMS®-52B DSC Neutron Absorber Plate Analytical Model for Top End Drop**

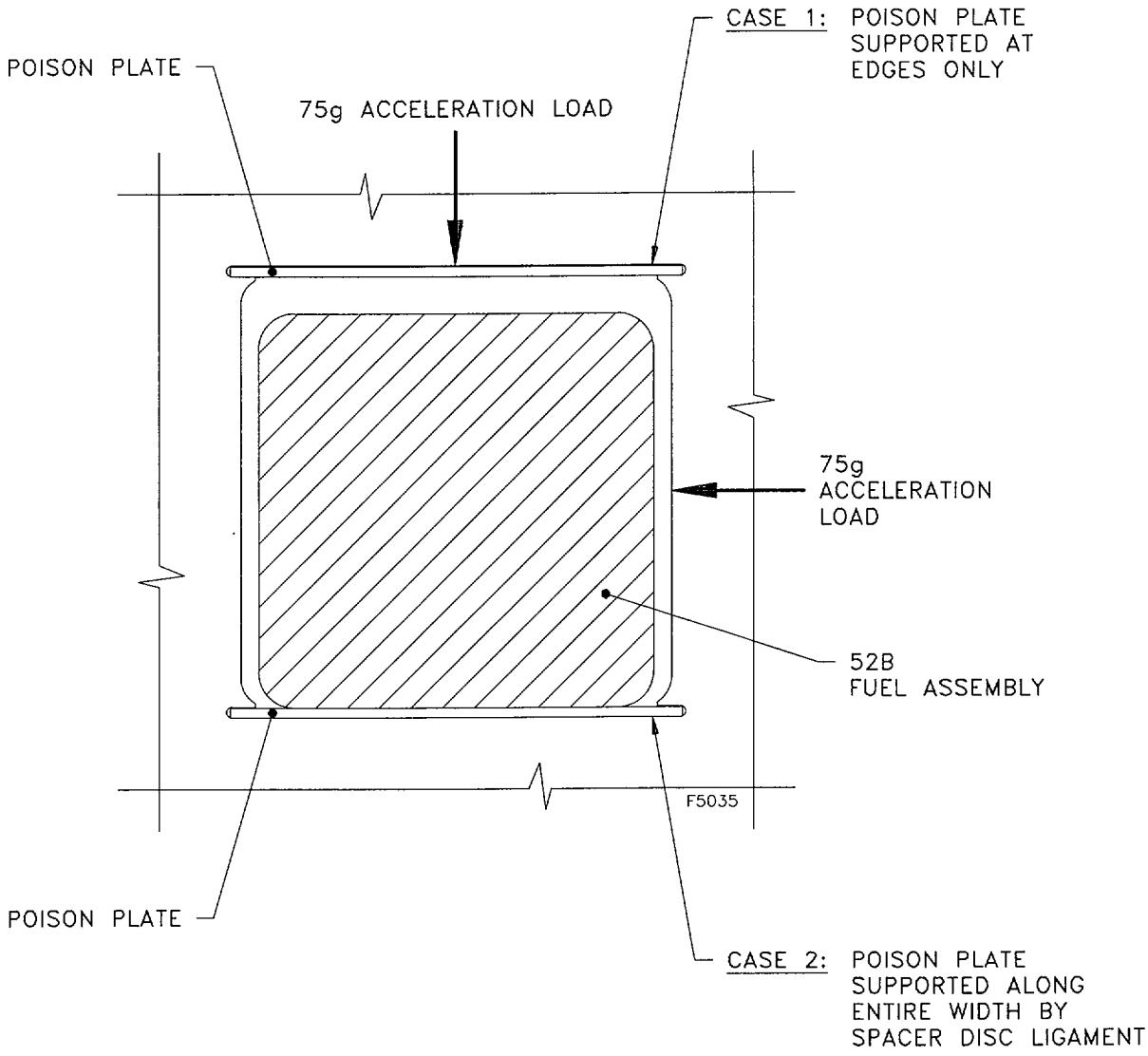


**Figure 8.2-13**
**NUHOMS®-52B DSC Neutron Absorber Plate Horizontal Side Drop Load Conditions**

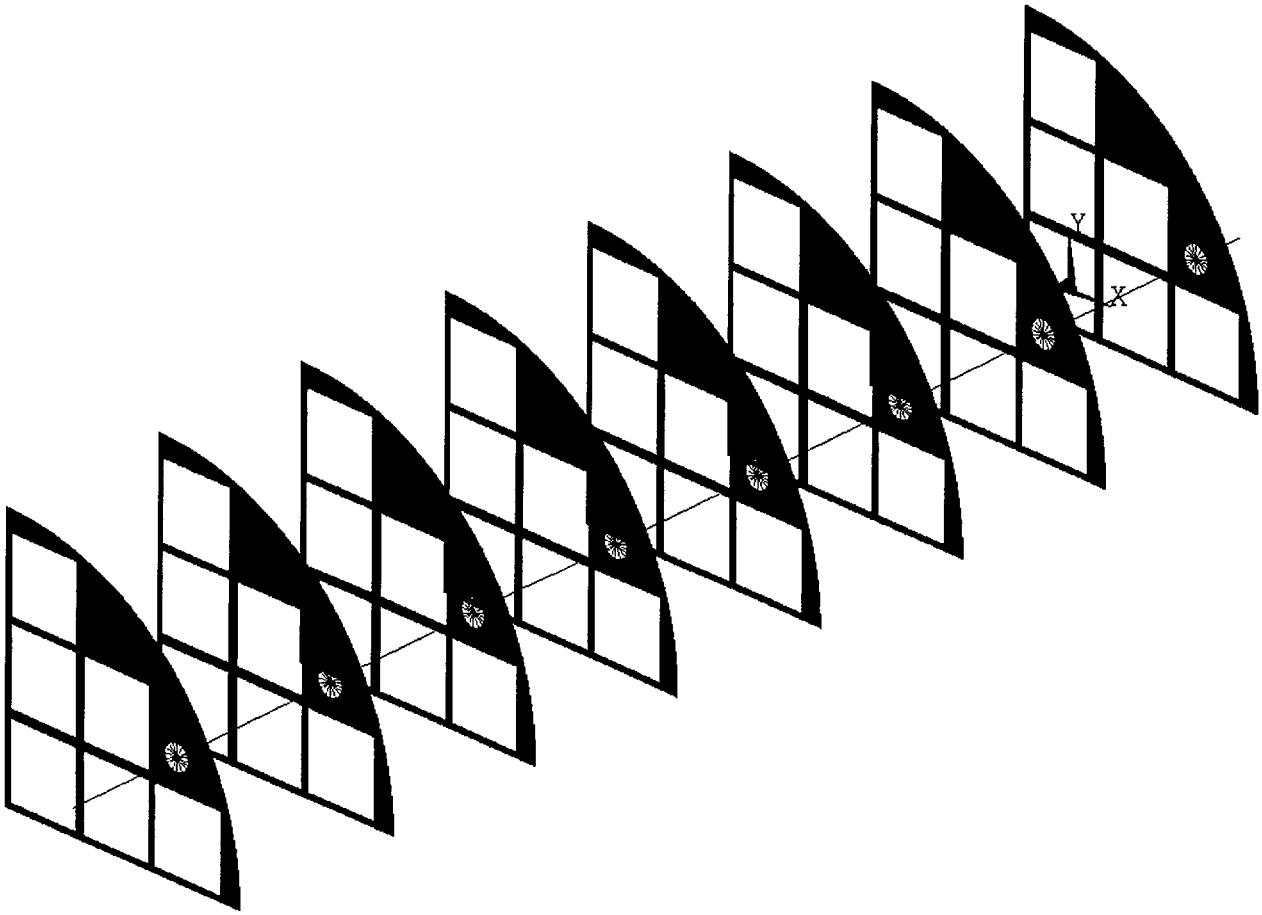


**Figure 8.2-14**
**NUHOMS®-24P Support Rod Vertical End Drop Analytical Model**

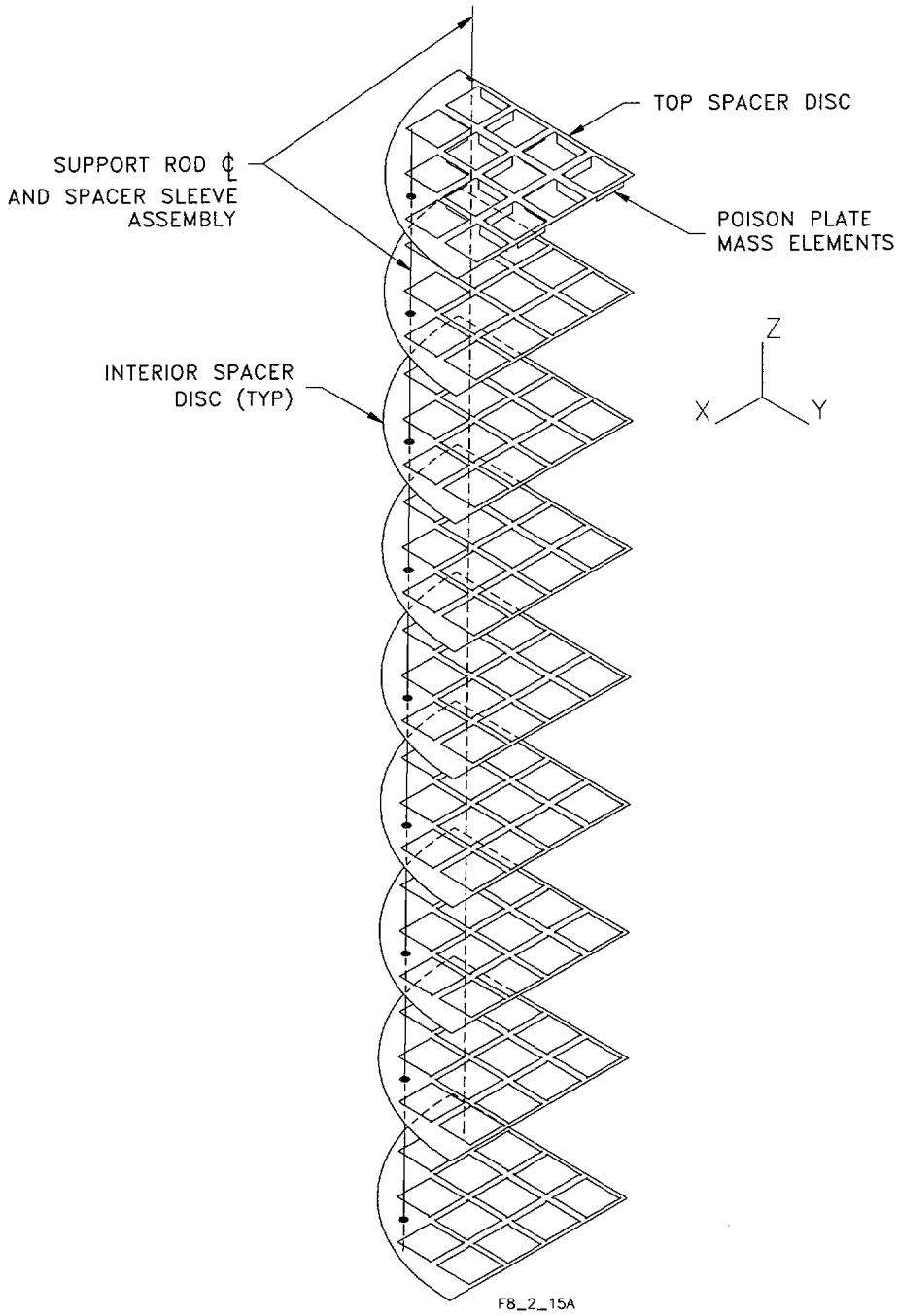


**Figure 8.2-15a**
**NUHOMS®-52B DSC Basket Assembly 90° Model Vertical End Drop Analytical Model**

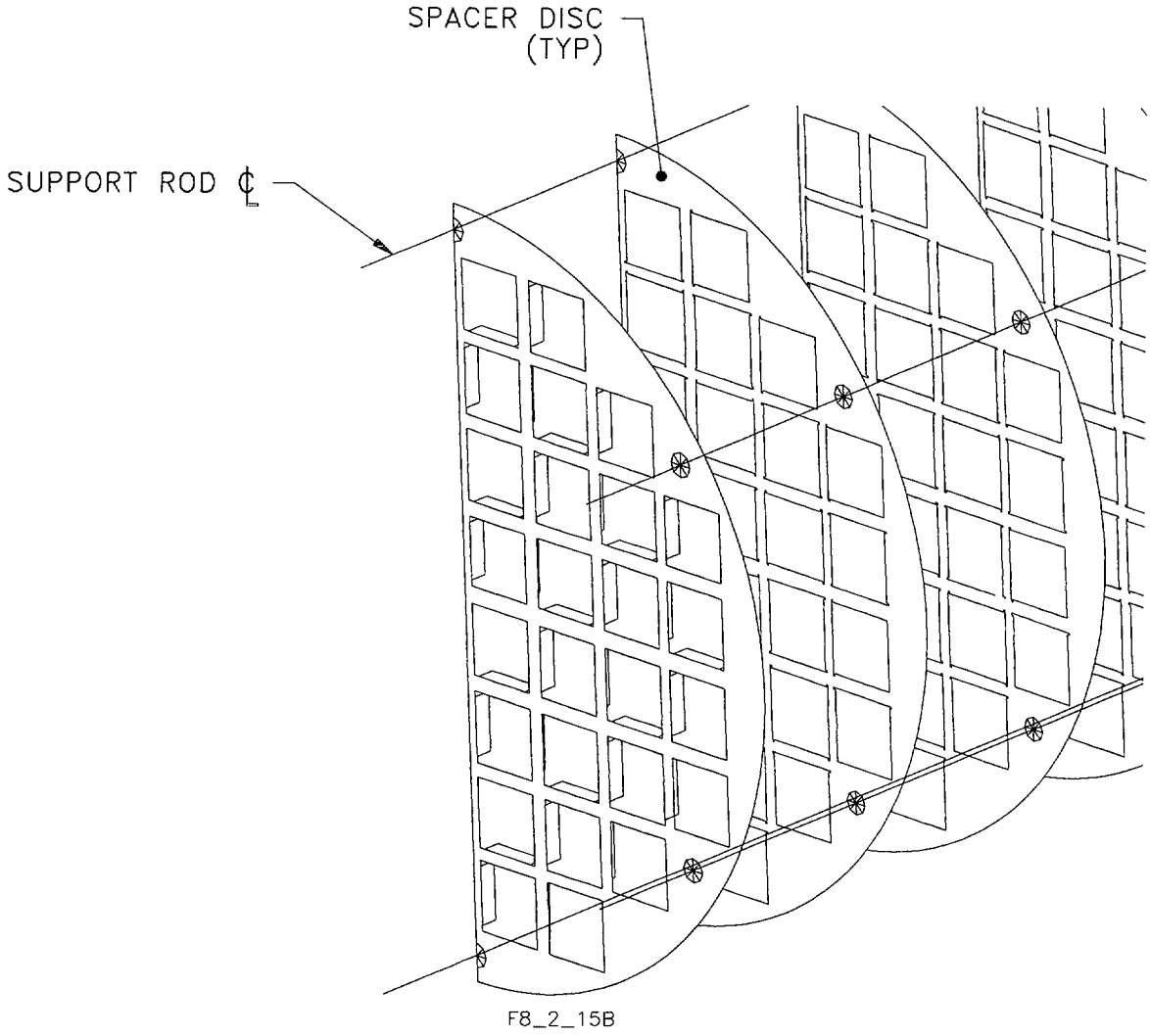


**Figure 8.2-15b**
**NUHOMS®-52B DSC Basket Assembly 180° Model Vertical End Drop Analytical Model**
**(Finite element mesh not shown for clarity.)**

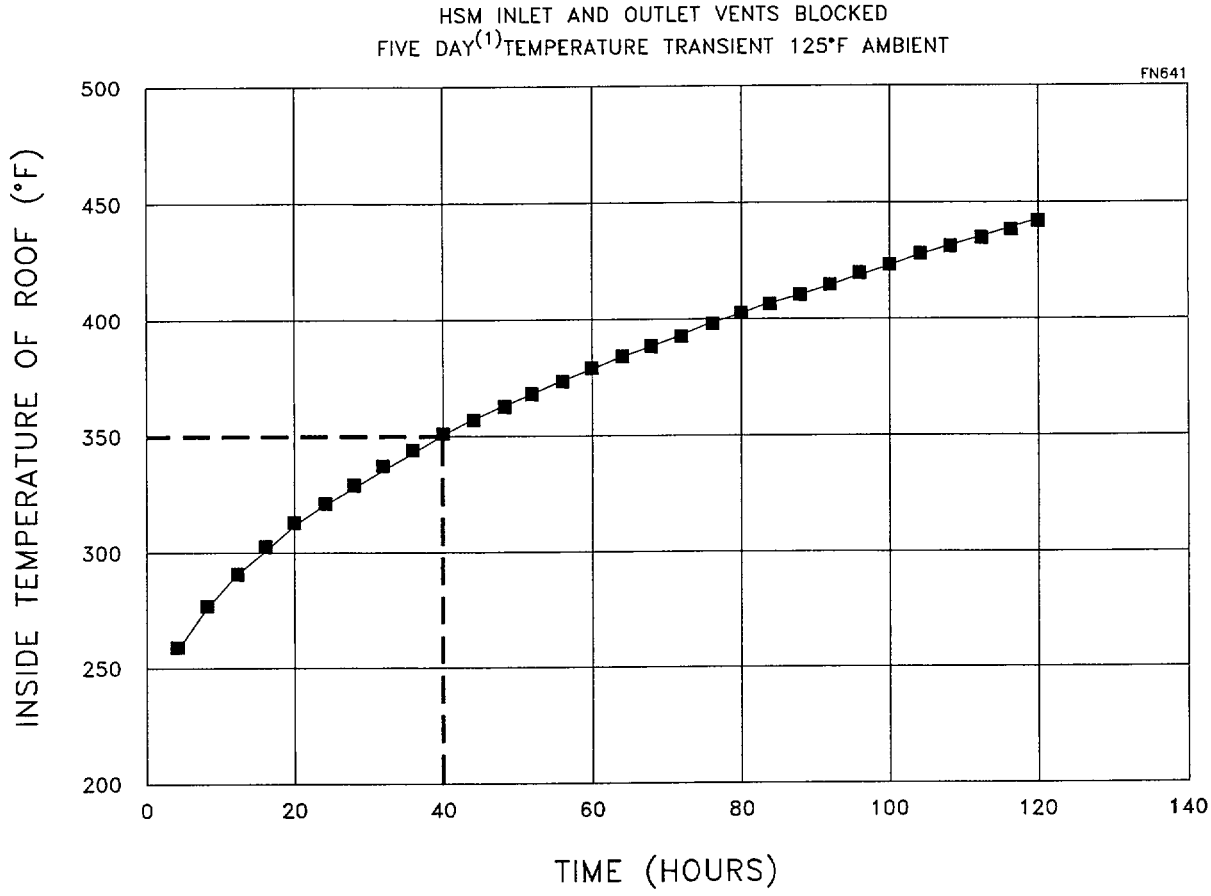


(1) THE DURATION OF HSM VENT BLOCKAGE TRANSIENT IS LIMITED BY NUHOMS® TECHNICAL SPECIFICATIONS TO A MAXIMUM OF 40 HOURS.

**Figure 8.2-16**
**HSM Roof Internal Concrete Temperatures Following Vent Blockage**

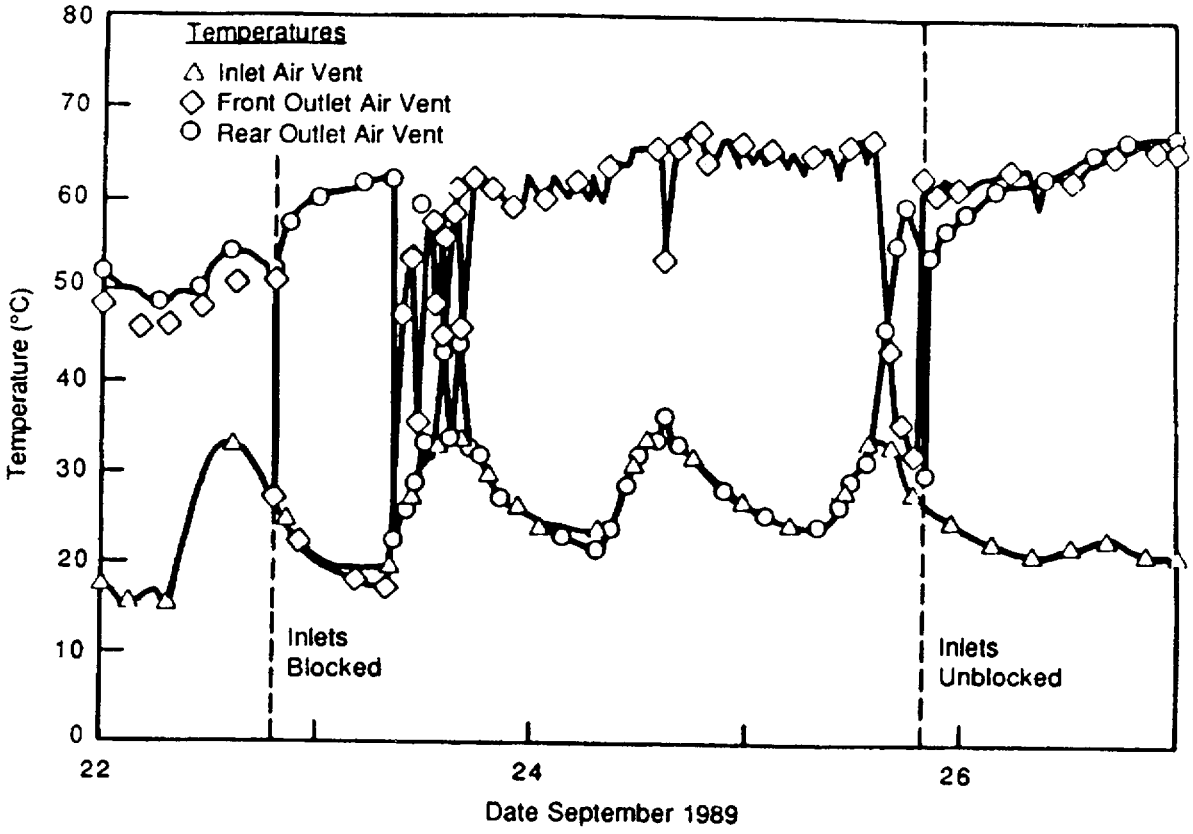


**Figure 8.2-17**
**Temperature Performance of the NUHOMS® System During the Electrically Heated Tests**

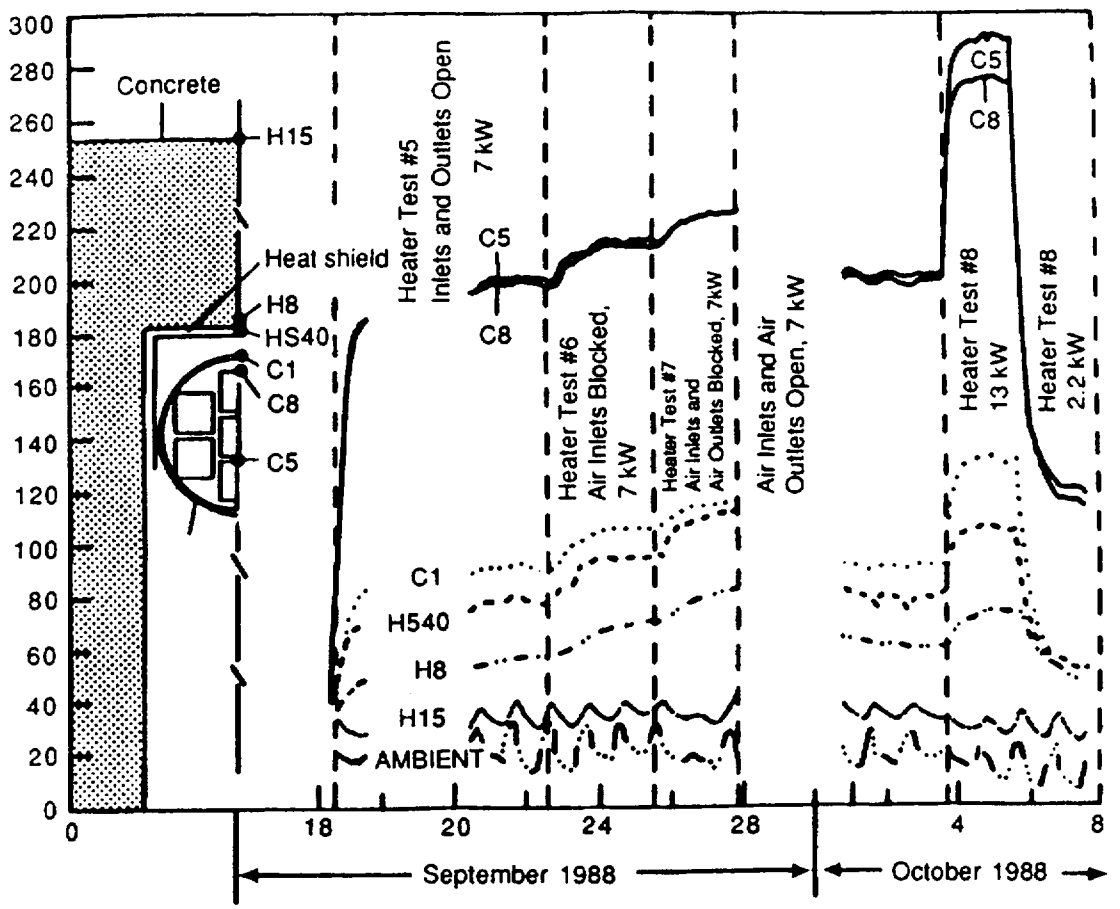


**Figure 8.2-18**
**Effect of Blocking the Inlet and Outlet Air Vents**

## 8.3 Site Characteristics Affecting Safety Analysis

All site characteristics affecting the safety analysis of the standardized NUHOMS® system are noted throughout this SAR where they apply.

## 8.4 References


8.1 U.S. Nuclear Regulatory Commission (U.S. NRC), "Standard Format and Content for the Safety Analysis Report for an Independent Spent Fuel Storage Installation (Dry Storage)," Regulatory Guide 3.48 (Task FP-029-4), (October 1981).

8.2 American National Standard, "Design Criteria for an Independent Spent Fuel Storage Installation (Dry Storage Type)," ANSI/ANS 57.9-1984, American Nuclear Society, La Grange Park, Illinois (1984).

8.3 American Society of Mechanical Engineers, ASME Boiler and Pressure Vessel Code, Section III, Division 1, Subsections NB, NC, and Appendixes, 1983 Edition with Winter 1985 Addenda.

8.4 R. E. Bolz and G. L. Tuve, CRC Handbook of Tables for Applied Science, 2nd Edition, Chemical Rubber Co., (1973).

8.5 Scale, Book II, Volume 2, NUREG/CR-0200, ORNL/NUREG/CSD-2.

8.6 DELETED

8.7 Handbook of Chemistry and Physics, 55th Edition CRC Press, pages E15, E16, 883-8156, D144.

8.8 J.A. Buchholz, Scoping Design Analyses for Optimized Shipping Casks Containing 1-, 2-, 3-, 5-, 7-, or 10- year-old PWR Spent Fuel, ORNL/CSD/TM-149, Union Carbide Nuclear Division Published date 1983, page 95.

8.9 DELETED

8.10 DELETED

8.11 N. G. Zoldners: Thermal Properties of Concrete Under Sustained Elevated Temperatures, ACI Publication, paper SP25-1, American Concrete Institute, Detroit, MI (1970).

8.12 DELETED

8.13 DELETED

8.14 "AEC Fuels and Materials Development Program Progress Report, Section on Spectral and Total Emittance Measurements of Accident Zircaloy-4," GEMP-1004, General Electric, page 33.

8.15 Scale, Book V. NUREG/CR-0200 Volumes 1, 2, 3, ORNL/NUREG/CSD-2.

8.16 R. J. Roark and W. C. Young, Formulas for Stress and Strain, Fifth Edition, McGraw-Hill, New York, N.Y., (1975).

8.17 J. F. Harvey, Pressure Component Construction, Design and Materials Application, Van Nostrand Reinhold Co., New York, N.Y., (1974).

8.18 Cybernet Services, STARDYNE User Information Manual, Control Data Corp., Minneapolis, MN, Rev. C, (April 1, 1980).

8.19 U. S. Nuclear Regulatory Commission, "Barrier Design Procedures," Standard Review Plan NUREG-0800, 3.5.3 (Formerly NUREG-75/087) Revision 1, (July 1981).

8.20 American Concrete Institute, Code Requirements for Nuclear Safety Related Concrete Structures and Commentary, ACI 349-85 and ACI 349R-85, American Concrete Institute, Detroit, MI (1980).

8.21 C. Wang and C. G. Salmon, Reinforced Concrete Design, Third Edition, Harper and Row, New York, N. Y., (1979).

8.22 M. Fintel, Handbook of Concrete Engineering, Van Nostrand Reinhold Co., New York, N.Y., (1985).

8.23 Prestressed Concrete Institute, PCI Design Handbook, 2nd Edition, Prestressed Concrete Institute, (1978).

8.24 M. S. Abrams, M. P. Gillen, and D. H. Campbell, Elastic and Strength Properties of Hanford Concrete Mixes at Room and Elevated Temperatures, Construction Technologies Laboratories, Portland Cement Association, Skokie, IL, (1979).

8.25 H. K. Hilsdorf, J. Kropp, and H. J. Koch, "The Effects of Nuclear Radiation on the Mechanical Properties of Concrete", Paper 55-10, Douglas McHenry International Symposium on Concrete and Concrete Structures, American Concrete Institute, Detroit, MI (1978).

8.26 American Nuclear Society, "American National Standard Guidelines on the Nuclear Analysis and Design of Concrete Radiation Shielding for Nuclear Power Plants," ANSI/ANS-6.4-1977, American National Standards Institute, Inc., (1977).

8.27 Peter J. Lunde, Solar Thermal Engineering Space Heating and Hot Water Systems, John Wiley and Sons, New York, N.Y. (1980).

8.28 ASHRAE Handbook 1981 Fundamentals, Fourth Printing 1983, American Society of Heating, Refrigerating and Air-Conditioning Engineers, Inc.

8.29 Conduction of Heat in Solids, Carslaw, H.S., Jaeger, J.C., Oxford at the Clarendon Press, 2 Edition, page 190.

8.30 U.S. Nuclear Regulatory Commission, "Missiles Generated by Natural Phenomena," Standard Review Plan NUREG-0800, 3.5.1.4 (Formerly NUREG-75/087), Revision 2, (July 1981).

8.31 U.S. Atomic Energy Commission, "Design Basis Tornado for Nuclear Power Plants," Regulatory Guide 1.76, (April 1974).

8.32 R. P. Kennedy, Holmes and Narver, Inc.", A Review of Procedures for the Analysis and Design of Concrete Structures to Resist Missile Impact Effects," Nuclear & Systems Sciences Group, Anaheim, California, (September 1975).

8.33 J. R. McDonald, K. C. Mehta, and J. E. Minor, "Design Guidelines for Wind-Resistant Structures," Institute for Disaster Research and Department of Civil Engineering, Texas Tech University, Lubbock, Texas, (June 1975).

8.34 DELETED

8.35 U.S. Atomic Energy Commission, "Design Response Spectra for Seismic Design of Nuclear Power Plants," Regulatory Guide 1.60, Revision 1, (December 1973).

8.36 U.S. Atomic Energy Commission, "Damping Values for Seismic Design of Nuclear Power Plants," Regulatory Guide 1.61, (October 1973).

8.37 R. D. Blevins, Formulas for Natural Frequency and Mode Shape, Van Nostrand Reinhold Co., New York, N.Y., (1979).

8.38 V. L. Streeter and E. B. Wylie, Fluid Mechanics, Sixth Edition, McGraw-Hill, New York, N.Y., (1975).

8.39 DELETED

8.40 National Fire Protection Association, National Fire Codes, No. 78, 1986 Edition.

8.41 DELETED

8.42 Extended Fuel Burnup Demonstration Program, Nuclear Assurance Corporation Final Report, DOE/ET/34014-10, NAC C-8327 (September 1983).

8.43 E. Elias and C. B. Johnson, "Radiological Impact of Clad and Containment Failure in At-Reactor Spent Fuel Storage Facilities," EPRI NP-2716, Project 2062-1, Electric Power Research Institute, (October 1982).

8.44 I. E. Idel'Chik, Handbook of Hydraulic Resistance, Coefficients of Local Resistance and of Friction, the U.S. Atomic Energy Commission and the National Science Foundation, Washington, D.C., 1960.

8.45 American Institute of Steel Construction, Specification for Structural Steel Buildings (1990), Chicago, Illinois.

8.46 M. L. Nicodemus and N. B. Guttman, "Probability Estimates of Temperature Extremes for the Contiguous United States," NUREG/CR-1390 U.S. Nuclear Regulatory Commission, Washington, D.C. (1980).

8.47 American Concrete Institute, Building Code Requirements for Reinforced Concrete (ACI 318-83) ACI, Detroit, MI (1983).

8.48 Swanson Analysis Systems Inc., ANSYS Engineering Analysis System User's Manual, Version 5.3, Swanson Analysis Systems Inc., Pittsburgh, PA.

8.49 DELETED

8.50 DELETED

8.51 Topical Report, "Design of Structures for Missile Impact," BC-TOP-9A Revision 2, September 1974, Bechtel Power Corporation.

8.52 Henry H. Bednar, P.E., Pressure Vessel Design Handbook, Van Nostrand Reinhold Co. (1981).

8.53 American National Standard for Radioactive Materials, "Special Lifting Devices for Shipping Canisters Weighing 10,000 lbs. (4,500 Kg) or More," ANSI N14.6-1986, American National Standards Institute, New York, N.Y. (1987).

8.54 J. L. Mershon et. al., "Local Stresses in Spherical and Cylindrical Shells Due to External Loadings," Welding Research Council Bulletin No. 107, March 1979.

8.55 Electric Power Research Institute, "The Effects of Target Hardness on the Structural Design of Concrete Storage Pads for Spent-Fuel Casks," EPRI Report NP-4830, October 1986.

8.56 F. P. Incropera and D. P. Dewitt, Fundamentals of Heat and Mass Transfer, Second Edition, J. Wiley and Sons Co., 1985.

8.57 Frank Kreith, Principles of Heat Transfer, Third Edition, Harper and Row Publishers.

8.58 Lawrence Livermore National Laboratory, "Dynamic Impact Effects on Spent Fuel Assemblies," Report No. UCID-21246 dated October 20, 1987.

8.59 1987 ASHRAE Handbook, HVAC Systems and Applications, American Society of Heating, Refrigeration and Air-Conditioning Engineering, Inc.

8.60 J. P. Holman, Heat Transfer, Fourth Edition, McGraw Hill Book Company Publishers.

8.61 DELETED

8.62 U. S. Nuclear Regulatory Commission, "Combining Modal Responses and Spatial Components in Seismic Response Analysis," Regulatory Guide 1.92, Revision 1, (February 1976).

8.63 Product Data Sheet-NS-3, BISCO Products, Inc., Elk Grove Village, Illinois.

8.64 Rust, James H., Nuclear Power Plant Engineering, Haralson Publishing Co., 1979.

8.65 Brandes, Eric A., Smithells Metals Reference Book, 6th Edition, Butterworth, 1983.

8.66 "Request for Additional Information Regarding the VECTRA Response to Inspection Report 72-1004/96-207," NRC Docket Number 72-1004, February 28, 1997.

8.67 Swanson Analysis Systems, Inc., ANSYS Engineering Analysis System, User's Manual, Release 5.6.

8.68 TN-32 Dry Storage Cask Topical Safety Analysis Report, Transnuclear Inc.